

Engineering Properties of Lightweight Concrete containing Poly-lactic Acid

Aliakbar Sayadi

A thesis submitted to Auckland University of Technology in fulfilment of
the requirements for the degree of Doctor of Philosophy (PhD)

School of Engineering,
Computer and Mathematical Sciences

2018

CERTIFICATE

I certify that this thesis has not already been submitted for any degree and is not being submitted as part of candidature for any other degree.

I also certify that the thesis has been written by me and that any help that I have received in preparing this thesis, and all sources used, have been acknowledged in this thesis.

Signature of Candidate

ABSTRACT

Lightweight concrete is being used in the construction industry as a building material in its own right. Ultra-lightweight concrete can be applied as a filler and support material for the manufacturing of composite building materials. In the past various techniques have been utilised to reduce the specific weight of concrete like lightweight aggregates, mixing with foam and the inclusion of expanded polystyrene, polyurethane or polyisocyanurate. A novel development is the addition of a bio-degradable polymer into lightweight concrete to reduce specific weight, carbon footprint and negative effects in the case of fire.

This thesis is about the development of a stable and reproducible ultra-lightweight concrete. Expanded poly-lactic acid (EPLA) was used to assess the feasibility of a biodegradable polymer as a lightweight aggregate that will deliver advantages such as eco-friendly concrete and being a non-petroleum polymer aggregate. The properties of EPLA concrete were compared to concrete made with expanded polystyrene (EPS) with similar mix design proportions using ordinary Portland cement (OPC), ground granulated blast-furnace slag (GGBS) and magnesium phosphate cement (MPC). In addition, two types of lightweight aggregate, expanded perlite (EP) and expanded vermiculite, are investigated as fine aggregate in this study.

It was found that chemical reactions of EPLA in the highly alkaline environment of cement causes significant changes in the microstructure of concrete. A large amount of calcium carbonate was found as hydration products of EPLA concrete. Furthermore, EPLA aggregates shrunk and lost their strength, and the rate of degradation was much higher in moist conditions.

This investigation has shown that non-structural grade ultra-lightweight concrete with relative densities of 512.85 to 203.2 kg/m³ can be obtained. The compressive strength of the concretes containing different ratios of EPLA and EPS aggregate varied from 4.62 MPa to 0.28 MPa.

It could be demonstrated that the engineering properties such as density, compressive strength, tensile strength, elastic modulus and thermal conductivity of concretes containing EPLA aggregate decreased compared to EPS concrete. The application of EPLA causes changes in hydration products and increases in concrete porosity, which led to an increase in electrical resistivity and water absorption ratio. The shrinkages of EPLA aggregate and bond

failures at the interface area of EPLA and the matrix caused the EPLA concrete failing in a more brittle way.

Fire resistance has also been investigated as an essential parameter of this ultra-lightweight concrete. The experimental results show that the carbon dioxide production and heat release rate of EPLA concrete is much lower than that of concrete containing EPS. Furthermore, the concrete containing EPLA aggregate shows the lower bond strength compared to EPS concrete when used as filler in composite sections. While the influence of ultra-lightweight concrete on the load carrying capacity of cold-formed beams was minimal, its effect on lateral torsional buckling was significant.

After a comprehensive study on combinations of different binders to eliminate the degradation of EPLA beads in an alkaline environment, magnesium phosphate cement was found as a proper binder for concrete containing EPLA. Another solution to the problem of EPLA degradation was established by coating the EPLA. The experimental results from coated EPLA (CEPLA) show that coating is the best solution in the high alkaline environment.

A set of equations were developed to predict the compressive strength, thermal conductivity, elastic modulus, water absorption, bond strength and load-displacement behaviour of the investigated concretes. In addition, a new method is proposed for the mix design of ultra-lightweight concrete.

ACKNOWLEDGMENTS

The author wishes to express his thanks and appreciation to Prof. Thomas Neitzert for his endless support, valuable advice, constant guidance and supervision of this project. The author also acknowledges the guidance and support of Assoc. Prof. Charles Clifton as second supervisor from the University of Auckland.

DEDICATION

This work is dedicated to my lovely wife for her endless support

TABLE OF CONTENTS

CERTIFICATE	i
ABSTRACT	ii
ACKNOWLEDGMENTS	iv
DEDICATION	v
TABLE OF CONTENT	vi
LIST OF FIGURES	xiv
LIST OF TABLES	xxii
NOTATION	xxv
ABBREVIATIONS	xxviii
CHAPTER 1 INTRODUCTION	1
1.1 General introduction	1
1.2 Problem statement	3
1.3 Purpose and scope of the study	3
1.4 Outline of the thesis	4
CHAPTER 2 LITERATURE REVIEW	6
2.1 Introduction	6
2.2 Lightweight aggregate	6
2.3 Lightweight concrete	7
2.3.1 Perlite lightweight concrete	9
2.3.2 Vermiculite lightweight concrete.....	15
2.3.3 Expanded polystyrene lightweight concrete	21
2.3.3.1 Influence of EPS particles on creep and shrinkages of concrete	26
2.3.3.2 Influence of modified EPS on mechanical properties of concrete.....	28

2.3.3.3	Influence of polymer additives on mechanical behaviour of EPS concrete	30
2.3.3.4	Influence of EPS aggregate size on mechanical properties of concrete	31
2.3.3.5	Influence of fibrous additives on mechanical properties of EPS concrete	32
2.3.3.6	Influence of fly ash on mechanical behaviour of EPS concrete	35
2.3.3.7	Influence of silica fume and rice husk ash on mechanical behaviour of EPS concrete	36
2.3.4	Foamed concrete	38
2.4	Application of lightweight concrete (LWC)	44
2.4.1	LWC as filler of composite structural assemblies (CSAs)	44
2.4.2	LWC as bracing components of cold formed members	48
2.5	Application of Poly-lactic Acid	50
2.6	Research questions	51
 CHAPTER 3 EXPERIMENTAL PROGRAM		53
3.1	Introduction	53
3.2	Raw Materials	53
3.2.1	Binder materials	53
3.2.1.1	Ordinary Portland cement (OPC)	53
3.2.1.2	Calcium oxide (CaO)	54
3.2.1.3	Magnesium oxide	55
3.2.1.4	Ground granulated blast-furnace slag (GGBS)	55
3.2.1.5	Ammonium dihydrogen phosphate	56
3.2.1.6	Borax	56
3.2.2	Aggregates	56
3.2.2.1	Expanded poly-lactic acid	56
3.2.2.2	Expanded polystyrene	56

3.2.2.3	Expanded perlite (EP).....	57
3.2.2.4	Expanded vermiculite (EV)	57
3.2.2.5	Coated EPLA	58
3.2.3	Chemical agents.....	59
3.2.3.1	Superplasticizer.....	59
3.2.3.2	Air entraining agent	59
3.2.3.3	Foam agent.....	59
3.2.3.4	Limelock.....	59
3.2.3.5	Resene X-200.....	60
3.2.4	Steel	60
3.2.4.1	Galvanized steel.....	60
3.2.4.2	Cold-formed profile	61
3.3	Experimental test methods	61
3.3.1	Workability.....	61
3.3.2	Density	62
3.3.3	Compressive strength.....	62
3.3.4	Tensile strength.....	62
3.3.5	Thermal conductivity	63
3.3.6	Electrical resistivity	63
3.3.7	Phase analysis	64
3.3.8	Fire resistance test.....	64
3.3.9	Pull-out test.....	65
3.3.10	Beam test	65
3.4	Proposed mix design method.....	67
3.4.1	Mix design and mix proportion	67
3.4.2	Selection of approximate water-cement ratio (w/c).....	67
3.4.3	Required cement content	68

3.4.4	Example of mix design procedure of perlite concrete	69
CHAPTER 4 VERMICULITE CONCRETE CONTAINING EPLA.....		73
4.1	Introduction	73
4.2	Experimental program.....	73
4.2.1	Mix proportions and procedure	73
4.2.2	Curing regimes.....	74
4.2.3	Test method	75
4.3	Results and discussion.....	75
4.3.1	Density	75
4.3.2	Compressive strength and failure modes	77
4.3.3	Splitting tensile strength	82
4.3.4	Thermal conductivity	83
4.3.5	Water absorption.....	85
4.3.6	pH evaluation and concrete carbonation.....	87
4.3.7	Electrical resistivity and setting time.....	91
4.3.8	Exothermic reaction.....	93
4.3.9	Scan Electron Microscopy (SEM) and X-ray Diffraction (XRD) analysis	95
4.4	Conclusions	101
CHAPTER 5 PERLITE CONCRETE CONTAINING EPLA		103
5.1	Introduction	103
5.2	Experimental program.....	103
5.2.1	Materials	103
5.2.2	Mix design and mix proportion	104
5.3	Experimental procedure	105
5.4	Results and discussion.....	106

5.4.1	Workability	106
5.4.2	Density	107
5.4.3	Compressive strength.....	108
5.4.4	Tensile Strength	112
5.4.5	Stress-strain relationship.....	114
5.4.6	Elastic Modulus	116
5.4.7	Water absorption.....	117
5.4.8	Thermal conductivity	119
5.4.9	Setting time and degradation mechanisms of EPLA	122
5.4.10	Fire resistance test.....	126
5.4.11	XRD analysis	129
5.4.12	SEM-EDS analysis	131
5.5	Conclusions	134
 CHAPTER 6 GGBS CONCRETE CONTAINING EPLA.....		137
6.1	Introduction	137
6.2	Experimental procedure	137
6.2.2	Specimen preparation and test methods	137
6.3	Results and discussion	139
6.3.1	Density and compressive strength	139
6.3.2	Thermal conductivity	141
6.3.3	Exothermic reaction.....	142
6.3.4	Fire resistance	143
6.4	Conclusion	147

CHAPTER 7 MAGNESIUM PHOSPHATE CONCRETE CONTAINING EPLA	149
7.1 Introduction	149
7.2 Experimental procedure	150
7.2.1 Materials	150
7.2.2 Specimen preparation and test methods	150
7.3 Results and discussion	152
7.3.1 Density	152
7.3.2 Compressive strength	152
7.3.3 pH assessment	157
7.3.4 Thermal conductivity	159
7.3.5 Exothermic reaction	161
7.3.6 Electrical resistivity	162
7.3.7 Fire resistance	165
7.3.8 Phase analysis	170
7.4 Conclusion	177
CHAPTER 8 PERLITE CONCRETE CONTAINING CEPLA	179
8.1 Introduction	179
8.2 Experimental procedure	179
8.2.1 Materials	179
8.2.2 CEPLA preparation	179
8.2.3 Mix proportion	180
8.2.4 Experimental procedure	181
8.3 Experimental results	181
8.3.1 Density and compressive strength	181
8.3.2 Thermal conductivity	185

8.3.3	Exothermic reaction and electrical resistivity.....	186
8.3.4	Fire resistance	188
8.4	Conclusions	191
 CHAPTER 9 BOND-SLIP BEHAVIOUR OF EPLA CONCRETE		193
9.1	Introduction	193
9.2	Experimental program	193
9.2.1	Materials	193
9.2.2	Mix proportions	194
9.2.3	Test methods.....	195
9.3	Results and discussion	196
9.3.1	Mechanical properties.....	196
9.3.2	Bond stress.....	197
9.3.3	Effect of elastic and inelastic zone on bond stress.....	199
9.3.4	Effect of locking components angle on bond strength	203
9.3.5	Effect of compressive strength on bond stress.....	204
9.3.6	Failure modes.....	205
9.3.7	Bond stress-slip behaviour.....	207
9.3.8	Analytical model of bond stress-slip behaviour	209
9.4	Conclusions	214
 CHAPTER 10 APPLICATION OF LIGHTWEIGHT CONCRETE		215
10.1	Introduction	215
10.2	Experimental program	215
10.2.1	Sample preparation and test set-up.....	215
10.3	Experimental results and discussion	218
10.3.1	Mechanical properties of infill concrete	218

10.3.2	Bending test	219
10.3.2.1	Channel section	219
10.3.2.1.1	Failure modes	219
10.3.2.1.2	Load-displacement response	222
10.3.2.1.3	Load-strain response.....	224
10.3.2.2	Box section.....	226
10.3.2.2.1	Failure modes	226
10.3.2.2.2	Load-displacement behaviour	228
10.3.2.2.3	Load-strain response.....	229
10.3.3	Analytical model.....	231
10.4	Conclusions	237
 CHAPTER 11 CONCLUSIONS AND RECOMMENDATIONS		239
11.1	Introduction	239
11.2	Conclusions	239
11.2.1	Fresh properties of proposed concretes	239
11.2.2	Mechanical properties of proposed concretes.....	241
11.2.3	Thermal properties of proposed concretes.....	242
11.2.4	Electrical properties of proposed concretes	243
11.2.5	Fire resistance of proposed concretes	244
11.2.6	Phase analysis of proposed concretes	245
11.2.7	Bond properties of proposed concretes.....	246
11.3	Design recommendations for proposed concretes	247
11.4	Recommendations for further study	254
	References	255
	List of publications	273

LIST OF FIGURES

Figure 2. 1. Aggregates to produce insulating concrete [100]	10
Figure 2. 2 Effect of expanded perlite aggregate on; (a) thermal conductivity, (b) unit weight, (c) compressive strength, (d) modulus of elasticity, (e) water absorption, (f) capillary coefficient [83].	11
Figure 2. 3 (a) Hydration exothermic rate and (b) hydration heat amount of expanded perlite (EXP) modified cement paste [40].	12
Figure 2. 4 The effect of expanded perlite ratio on thermal conductivity of concrete [87].	13
Figure 2. 5 The influence of pumice (PA), perlite (EPA), silica fume (SF) and fly ash (FA) content on thermal conductivity of concrete; (a) 100% PA, (b) 80% PA+ 20% EPA, (c) 60% PA+ 40% EPA, (d) 40% PA+ 60% EPA [88].	13
Figure 2. 6 The relationship between calcium hydroxide (CH) content and curing time for pastes containing 0, 10 and 20 % of ground WEP [39].	15
Figure 2. 7 Compressive strength of vermiculite concrete with different vermiculite to cement ratios [23].	16
Figure 2. 8 Flexural performance of vermiculite concrete with different vermiculite to cement ratios [23].	17
Figure 2. 9 Thermal conductivity of vermiculite concrete with different vermiculite to cement ratios [23].	17
Figure 2. 10 Pore size distribution of the hardened mortars with different perlite (P) and vermiculite (V) content [91].	18
Figure 2. 11 Relations between engineering properties of vermiculite concrete [24].	19
Figure 2. 12 The relationship between thermal conductivity and the rate of lightweight aggregate added to the matrix; (a) perlite aggregate, (b) vermiculite aggregate [21].	21
Figure 2. 13 Chloride permeability of EPS concretes with variation on EPS ratio where NC, E76, E95, E124, E153, E182 and E220 have the density of 2578, 779, 984, 1304, 1484, 1723 and 2215 kgm ³ [92].	22
Figure 2. 14 The relationship between drying shrinkage and drying time [7].	23
Figure 2. 15 The relationship between foam content and thermal conductivity [102]	24
Figure 2. 16 Compressive strength of EPS foamed concrete for different densities;	25

Figure 2. 17 The relationship between slump flow and EPS volume with variation on water-binder ratio (W/B), nano-SiO ₂ ratio (NS) and Polycarboxylic ether based high range water reducer (HRWR) [65].	25
Figure 2. 18 The shrinkage of modified expanded polystyrene (MEPS) aggregate concrete [70].	27
Figure 2. 19 The relationship between ratio of the dynamic modulus of elasticity (RMDE) and freezing and thawing [108].	29
Figure 2. 20 Effect of freezing-thawing on MEPS concrete, C1: 50% fine MEPS + 50% coarse MEPS aggregate, C2: 25% fine MEPS + 50% coarse MEPS + 25% natural sand, C3: 50% coarse MEPS aggregate + 50% natural sand, C4: 50% fine MEPS and 50% coarse natural aggregate, C5: 25% fine MEPS + 25% coarse MEPS and 25% natural sand + 25% coarse natural aggregate, C6: 5% fine MEPS aggregate + 25% natural sand + 50% coarse natural aggregate [108].	29
Figure 2. 21 The relationship between compressive strength and polymer-cement ratio; (a) effect of drying treatment, (b) effect of curing conditions (7W21D (7 days water cured + 21 days air dried), 1D3W24D (1 day air cured + 3 days water cured + 24 days air cured), 14W14D (14 days water cured + 14 air cured day)) [109].	31
Figure 2. 22 Effect of EPS aggregate size on compressive strength of concrete [110]	32
Figure 2. 23 Load-displacement behaviour of EPS concrete containing WCPP fibre [44].	33
Figure 2. 24 The influence of paper sludge ash (PSA) addition on thermal conductivity of concrete [113].	34
Figure 2. 25 The influence of paper sludge ash (PSA) addition on compressive strength of concrete [113].	35
Figure 2. 26 Effect of EPS volume on compressive strength of concrete containing 50% FA - 50% cement [115].	36
Figure 2. 27 Effects of EPS beads ratio and binder on electrical resistivity of concrete [44].	37
Figure 2. 28 Effect of EPS percentage on water absorption ratio of concrete; PC: Portland cement contained EPS concrete, SF: Silica fume contained EPS concrete, and RHA: Rice husk ash contained [44].	38
Figure 2. 29 The required water content for cement and fly ash [138].	40
Figure 2. 30 The effect of foam content on workability of foamed concrete [102].	41

Figure 2. 31 The effect of foam content on thermal conductivity of foamed concrete [102].	41
Figure 2. 32 The relationship between compressive strength and dry density [133].....	43
Figure 2. 33 The relationship between water absorption and porosity [120].....	43
Figure 2. 34 The relationship between water vapour permeability and dry density [120]. .	43
Figure 2. 35 Load-displacement behaviour of concrete with densities of (a) 800 kgm ³ , (b) 1000 kgm ³ , (c) 1200 kgm ³ [139, 140].	45
Figure 2. 36 Load - slip curves for test bars with (a) rib height of 0.05 in, (b) rib height of 0.10 in [152]......	47
Figure 2. 37 Failure modes of cold formed column; (a) unbraced sample, (b) braced sample (filled with EPS concrete)	49
Figure 2. 38 Effect of PAC bracing on load carrying capacity of a cold-formed beam where I200-15-2300-0-001 and I200-15-2300-WM-001 are the control and sample with bracing component [164].	50
Figure 3. 1 The atomic concentration of ordinary Portland cement (OPC).....	54
Figure 3. 2 Polymer aggregate; (a) Expanded polystyrene (EPS) with relative density of 10kgm ³ ; (b) Expanded poly-lactic acid (EPLA) with relative density of 19kgm ³	56
Figure 3. 3 EDS analysis of expanded perlite (EP).....	57
Figure 3. 4 EDS analysis of expanded vermiculite (EV)	58
Figure 3. 5 Coated poly-lactic acid (CEPLA).....	58
Figure 3. 6 Slump test, (a) true, (b) zero, (c) collapse, (d) shear	61
Figure 3. 7 Giatec SmartBox.....	64
Figure 3. 8 Pull-out test configuration	65
Figure 3. 9 Beam test setup.	66
Figure 4. 1 The relationship between density and expanded poly-lactic acid content.....	77
Figure 4. 2 Bond failure at interfacial transition zone (ITZ) of EPLA-vermiculite concrete.	78
Figure 4. 3 Reaction of EPLA particles when subjected to the alkaline environment of cement; (a) dissolution of EPLA particles, b) carbonation of EPLA concrete	79
Figure 4. 4 Failure modes of concrete; (a) V1 (ADC), (b) V2 (ADC), (c) V3 (ADC), (d) V4 (ADC), (e) V4 (WC)	81

Figure 4. 5 Thermal conductivity of EPLA-vermiculite concrete; (a) effect of EPLA ratio, (b) effect of concrete density.....	84
Figure 4. 6 Time vs. water absorption ratio (%) of vermiculite concrete containing EPLA	87
Figure 4. 7 The degradation of EPLA aggregate and concrete carbonation	88
Figure 4. 8 Carbonation of EPLA concrete.....	89
Figure 4. 9 Analysis of concrete efflorescence	90
Figure 4. 10 The electrical resistivity response of concrete; (a) up to 1day, (b) up to 7 days	93
Figure 4. 11 Exothermic reaction of vermiculite and EPLA-vermiculite concrete, (a) V1, (b) V2, (c) V3, (d) V4, (e) V5.....	95
Figure 4. 12 SEM image of mix V1 at 2.5K magnification.....	96
Figure 4. 13 SEM image of mix V5 after 28 days	97
Figure 4. 14 EDS analysis of proposed concrete; (a) sample V1, (b) sample V5.....	98
Figure 4. 15 SEM image of mix V5 after one year.....	98
Figure 4. 16 XRD analysis of proposed concrete; (a) sample V1, (b) sample V5.....	99
Figure 4. 17 EDS analysis after one year; (a) point 1, (b) point 2, (c) point 3, (d) point 4	100
Figure 5. 1 The workability and slump of proposed concrete, (a) sample PP2, (b) sample PP5.	107
Figure 5. 2 EPLA degradation and bond failure at interfacial transition zone	109
Figure 5. 3 Interfacial transition zone; (a) EPS Concrete, (b) EPLA Concrete - Air Cured, (c) EPLA Concrete – Water Cured.....	110
Figure 5. 4 Degradation of EPLA in alkaline environment	111
Figure 5. 5 Failure modes of concrete cured in a moist condition; (a) mix P1, (b) mix PP4, (c) mix PE4.	112
Figure 5. 6 Failure modes of polymer aggregates; (a) EPS concrete, (b) EPLA concrete.	112
Figure 5. 7 Stress-strain relationship of perlite concrete with different EPLA ratios.....	114
Figure 5. 8 The water absorption ratio vs time of proposed concretes, (a) EPLA concrete, (b) EPS concrete.	118
Figure 5. 9 EPLA shirinkages in alkaine enviroment of cement	119
Figure 5. 10 The correlation between thermal conductivity and concrete density	120
Figure 5. 11 The electrical resistivity response of concrete; (a) up to 1day, (b) up to 5 days	123

Figure 5. 12 EPLA degradation in sodium hydroxide solution (NaOH)	124
Figure 5. 13 Fire resistance of concrete and its failure modes; (a) Perlite concrete (P1), (b) EPLA concrete (PP4), (c) EPS concrete (PE4).....	126
Figure 5. 14 Heat release rate (HRR) response of proposed concretes under 50 kW/m ² external heat flux.....	127
Figure 5. 15 Total heat released (HTR) of proposed concretes.	128
Figure 5. 16 (a) Carbon dioxide and (b) carbone monoxide production curves of proposed concretes during combustion.....	129
Figure 5. 17 XRD Profiles (a) PE4, (b) PP4	131
Figure 5. 18 EDS analysis of sample containing 60% EPS (PE4).....	132
Figure 5. 19 EDS analysis of sample containing 60% EPLA (PP4).....	132
Figure 5. 20 SEM image of mix PE4; (a) at 2.5k magnification, (b) at 5.0k magnification	133
Figure 5. 21 SEM image of mix PP4; (a) at 2.5k magnification, (b) at 5.0k magnification.	134
Figure 6. 1 The influence of GGBS activator on rate of EPLA degradation; (a) PGMC1, (b) PGMC2, (c) PGMC3, (d) PGMC4, (e) PGMC5	140
Figure 6. 2 The exothermic reaction of GGBS concrete.....	143
Figure 6. 3 Fire test results; (a) EPLA concrete, (b) EPS concrete, (c) PGMC 3, (d) EGMC3 3.....	144
Figure 6. 4 Cone calorimeter test results; (a) Heat release rate (HRR), (b) Total heat released (THR).....	145
Figure 6. 5 Cone Calorimeter test results; (a) Carbon dioxide production (CO ₂ P), (b) Carbon monoxide production (COP).....	147
Figure 7. 1 The strength development of magnesium phosphate concrete; (a) PM16-1.0, (b) PM15-1.0, (c) PM13-1.0.	157
Figure 7. 2 The comparison between pH variation of magnesium phosphate concrete and cement-based concrete.	158
Figure 7. 3 Effect of alkaline-based and acid based environment on degradation of EPLA beads, (a) cement based concrete, (b) magnesium phosphate concrete	159

Figure 7. 4 Exothermic reaction of magnesium phosphate concrete, (a) PM13-1.0-05, (b) PM13-1.0-10, (c) PM15-1.0-05, (d) PM15-1.0-10.	162
Figure 7. 5 The electrical resistivity response of magnesium phosphate concrete and EPLA concrete.	163
Figure 7. 6 Fire tests of concrete; (a) EPS concrete, (b) EPLA concrete, (c) Magnesium phosphate concrete	165
Figure 7. 7 The cone calorimeter test results, (a) heat release rate (HRR), (b) total heat released (HTR), (c) carbone monoxide production (COP), (d) carbone dioxide production (CO2P), (e) mass reduction, (f) smoke volume.	168
Figure 7. 8 The EDS analysis of magnesium phosphate concrete after 1 day, (a) PM15-1.0-5, (b) PM15-1.0-10.....	171
Figure 7. 9 The XRD spectra of magnesium phosphate concrete after 1 day of curing, (a) PM15-1.0-5, (b) PM15-1.0-10.	172
Figure 7. 10 EDS results of magnesium phopsate concrete after 3 days of curing (a) PM15-1.0-05, (b) PM15-1.0-10.	173
Figure 7. 11 The XRD spectra of magnesium phosphate concrete after 3 days of curing, (a) PM15-1.0-5, (b) PM15-1.0-10.	174
Figure 7. 12 The EDS results of PM15-1.0-05 at the age of, (a) 28 days, (b) 90 days.....	175
Figure 7. 13 The XRD spectra of sample PM15-1.0-05 after, (a) 28 days, (b) 90 days. ...	176
Figure 8. 1 The preparation of CEPLA aggregate, a) non-coated EPLA, b) coated EPLA180	
Figure 8. 2 EPLA degradation, a) Before subjecting to alkaline environment, b) after subjecting to alkaline environment.	184
Figure 8. 3 The mechanism of calcium carbonate formation at CEPLA aggregate	184
Figure 8. 4 Coated EPLA aggregate and its interfacial bonding.....	185
Figure 8. 5 Exothermic reaction of concrete, a) CEPLA, b) EPLA, c) Perlite.	187
Figure 8. 6 Electrical resistivity response of CEPLA, EPLA and perlite concrete.....	187
Figure 8. 7 Fire resistance of concretes, (a) Perlite concrete, (b) EPLA concrete, (c) EPS concrete, (d) CEPLA concrete.	188
Figure 8. 8 Cone calorimeter tests of proposed concretes, a) HRR, b) THR, c) CO2P, d) COP	190

Figure 9. 1 Patterns of embedded galvanized strips.....	195
Figure 9. 2 Pull out test configuration.....	195
Figure 9. 3 EPLA degradation in alkaline environment of cement; (a) bond failure at ITZ zone, (b) changes in hydration product (more calcium carbonate).....	197
Figure 9. 4 Confinement effect and elastic and inelastic length of embedded strips.....	202
Figure 9. 5 Effects of interlocking patterns on bond strength.....	203
Figure 9. 6 The correlation between bond stress and compressive strength of concrete EPLA, EPS and foamed concrete (FC12 and FC8) [139, 140].....	205
Figure 9. 7 Failure modes of proposed concretes; (a) CPL-Y, (b) CPL-Inverse V, (c) CPE-Y, (d) CPE-Inverse V.....	206
Figure 9. 8 The bond stress-slip behaviour; (a) EPLA concrete, (b) EPS concrete.....	208
Figure 9. 9 The bond stress-slip model for EPS and EPLA concrete.....	210
Figure 9. 10 The comparison between the experimental results, new proposed model and proposed model by Sayadi et al. [140] for EPLA concrete; (a) sample 9R4.9, (b) sample 9R4.9 Bolt, (c) sample Y.....	212
Figure 9. 11 The comparison between the experimental results, new proposed model and proposed model by Sayadi et al. [140] for EPS concrete (a) sample 9R4.9, (b) sample 9R4.9 Bolt, (c) sample Y.....	213
Figure 10. 1 Test setup; (a) cross-section, (b) bending test.....	217
Figure 10. 2 Failure modes of channel sections under bending force, (a) control sample, (b) filled with perlite concrete, (c) filled with EPLA concrete, (d) filled with EPS concrete.....	220
Figure 10. 3 The effect of infill materials on lateral torsional bulking of channel sections.....	221
Figure 10. 4 Load-deflection curves of channel sections subjected to bending.....	222
Figure 10. 5 Load-strain curves obtained from the strain gauges placed at the middle of channel beams; (a) Ref. in X direction, (b) Ref. in Y direction, (c) PC in X direction, (d) PC in Y direction, (e) EPS in X direction, (f) EPS in Y direction, (g) PLA in X direction, (h) PLA in Y direction.....	225
Figure 10. 6 Failure modes of box section beams under bending force.....	226
Figure 10. 7 Failure modes; (a) profile segregation of control sample, (b) bearing failure of composite beam.....	227
Figure 10. 8 Load-deflection curves of box sections subjected to bending.....	228

Figure 10. 9 Load-strain curves obtained from the strain gauges placed at the middle of box beam; (a) Ref. in X direction, (b) Ref. in Y direction, (c) PC in X direction, (d) PC in Y direction, (e) EPS in X direction, (f) EPS in Y direction, (g) PLA in X direction, (h) PLA in Y direction..... 231

Figure 10. 10 Load-displacement model; (a) channel section, (b) box section. 232

Figure 10. 11 The comparison between load-displacement response of proposed model and experimental results of composite channel section beam; (a) PC concrete, (b) PPC concrete, (c) PEC concrete. 235

Figure 10. 12 The comparison between load-displacement response of proposed model and experimental results of composite box section beam; (a) PC concrete, (b) PPC concrete, (c) PEC concrete..... 236

LIST OF TABLES

Table 2. 1 Effect of expanded perlite aggregate (EPA) and curing conditions on capillarity coefficient of concrete [90].	14
Table 2. 2 Mechanical properties of vermiculite lightweight concretes [26].	20
Table 2. 3 Mechanical properties of EPS lightweight concretes [26].	20
Table 2. 4 Thermal conductivity of the lightweight concretes containing EPS and vermiculite concrete [29].	23
Table 2. 5 Slump and fresh density of MEPS aggregate concrete [70].	30
Table 2. 6 Effect of fibre, EPS percentage and binder on water absorption ratio of concrete [44].	37
Table 2. 7 The mechanical and thermal properties of ultra-lightweight foamed concrete [137].	42
Table 2. 8 Effect of polystyrene aggregate concrete (PAC) bracing on ultimate load capacity of a cold formed column.	49
Table 3. 1 The fineness of calcium oxide (CaO)	54
Table 3. 2 Chemical composition of OPC, MgO and CaO	55
Table 3. 3 Chemical composition of GGBS	55
Table 3. 4 Chemical composition of expanded perlite and expanded vermiculite	58
Table 3. 5 Mix proportion of preformed aqueous foam.	59
Table 3. 6 Physical properties of Limelock and X-200	60
Table 3. 7 Comparing the mix design of INPRO and proposed equation.	69
Table 3. 8 Summary of mix design proportions of perlite concrete.	70
Table 3. 9 Summary of mix design proportions of vermiculite concrete.	72
Table 4. 1 Mix proportions of vermiculite and vermiculite-EPLA concrete.	74
Table 4. 2 The fresh and air dried density (ADC) of vermiculite and EPLA-vermiculite concrete.	76
Table 4. 3 Effect of curing conditions on compressive and tensile strength of proposed concrete	80
Table 4. 4 Thermal conductivity of vermiculite concrete containing PLA aggregate	85
Table 4. 5 Water absorption results of proposed concretes.	86

Table 4. 6 pH level variation of water and air cured samples with 70% EPLA (V5).....	88
Table 4. 7 The initial and final setting time of proposed concretes based on electrical resistivity response.....	92
Table 4. 8 The peak temperature of curing vermiculite concrete.....	94
Table 5. 1 Mix proportion of perlite and perlite-PLA concrete	105
Table 5. 2 Effect of EPLA replacement on workability and density of perlite concrete... ..	108
Table 5. 3 Compressive strength of perlite and EPLA-perlite concrete	109
Table 5. 4 The tensile strength of proposed concretes	113
Table 5. 5 The elastic modulus of proposed concretes.....	117
Table 5. 6 The thermal conductivity of proposed concretes	120
Table 5. 7 The initial and final setting time of the control sample and samples containing higher amounts of EPLA based on electrical resistivity response.....	126
Table 5. 8 The time to ignition and flameout of proposed concretes.....	128
Table 6. 1 Mix proportion of magnesium phosphate concrete containing EP and EPLA.	138
Table 6. 2 Density and compressive strength of GGBS concrete containing EPLA and EPS aggregate.....	139
Table 6. 3 Thermal conductivity of proposed concrete.....	142
Table 6. 4 The time to ignition and flameout of proposed concretes.....	145
Table 7. 1 Mix proportions of magnesium phosphate concrete containing EP and EPLA.	151
Table 7. 2 The density and compressive strength of magnesium phosphate concrete.....	155
Table 7. 3 The comparison between thermal conductivity of magnesium phosphate concrete and EPLA concrete.....	160
Table 7. 4 The peak temperature of magnesium phosphate concrete.....	162
Table 7. 5 The initial and final setting time of proposed concretes based on electrical resistivity response.....	164
Table 7. 6 The summary of cone calorimeter test results of magnesium phosphate, EPLA and EPS concrete.....	169
Table 7. 7 The summary of EDS analysis of magnesium phosphate concrete after 1 day.	171

Table 7. 8 The summary of EDS analysis of magnesium phosphate concrete after 3 days.	173
Table 7. 9 The summary of EDS analysis of samples PM-1.0-05 and PM15-1.0-10 after 28 days and 90 days.	176
Table 8. 1 The mix proportions of CEPLA concrete.	181
Table 8. 2 Density of perlite concrete and perlite concrete containing EPLA, EPS and CEPLA.	182
Table 8. 3 The compressive strength of proposed concretes with variation of aggregate types	183
Table 8. 4 The results of thermal conductivity of proposed concretes.	185
Table 8. 5 The ignition and flameout point of proposed concretes.....	190
Table 9. 1 Mix proportions of EPLA and EPS concrete.	194
Table 9. 2 Mechanical properties of EPLA and EPS concrete	196
Table 9. 3 The ultimate and critical bond stress of proposed concretes	198
Table 9. 4 Pull-out test results of embedded strips in EPS and EPLA concrete.....	201
Table 9. 5 Failure modes of proposed concretes.....	206
Table 10. 1 Mix proportions of perlite and perlite-EPLA concrete.	216
Table 10. 2 Mechanical properties of infill materials	219
Table 10. 3 The section weight and maximum load capacity of channel sections	223
Table 10. 4 The section weight and maximum load capacity of box sections.....	229

NOTATIONS

a	Water-cement ratio
A_c	Locking area
A_e	Embedded area
A_s	Cross-section area of cold-formed steel
b	Width of strip
f'_c	Compressive strength of concrete
f_{ca}	Compressive strength of air cured concrete
f_{cf}	Compressive strength of fog cured concrete
f_{cw}	Compressive strength of water cured concrete
f_t	Tensile strength of concrete
f_{ta}	Tensile strength of air cured concrete
f_{tf}	Tensile strength of fog cured concrete
f_{tw}	Tensile strength of water cured concrete
f_u	Ultimate tensile strength
f_y	Yield tensile strength
K	Shape factor
l_e	Elastic length
l_{in}	Inelastic length
m_d	Dry mass
m_w	Wet mass
P_u	Ultimate load capacity
R_c	Concrete resistance
R_{EPLA}	EPLA ratio
R_{EPS}	EPS ratio
$R_{Perlite}$	Perlite ratio

R_s	Resistance
$R_{\text{vermiculite}}$	Vermiculite ratio
RD_{EPLA}	Relative density of expanded poly-lactic acid aggregate
RD_{EPS}	Relative density of expanded polystyrene aggregate
RD_P	Relative density of perlite aggregate
RD_V	Relative density of vermiculite aggregate
RD_X	Relative density of perlite/vermiculite aggregate
t	Time
t_s	Embedded length of strip
τ_u	Ultimate tensile stress
u_e	Elastic bond stress
u_{in}	Inelastic bond stress
V_P	Perlite aggregate volume
V_{PLA}	Volume of poly-lactic acid
V_V	Vermiculite aggregate volume
V_X	Perlite/vermiculite aggregate volume
WA_r	Water absorption ratio
WA_V	Water absorption ratio of vermiculite aggregate
α	Correction factor
β	Correction factor
γ_{concrete}	Concrete density
γ_{EPLA}	EPLA density
γ_{EPS}	EPS density
γ_f	Fresh density of concrete
γ_{Perlite}	Perlite density

$\gamma_{\text{vermiculite}}$	Vermiculite density
δ	Relative displacement
δ_u	Ultimate displacement
μ	Correction factor
φ	Correction factor
ρ_m	Target casting density
σ_s	Electrical conductivity

ABBREVIATIONS

AASHTPO	American Association of State Highway and Transportation Officials
ACI	American Concrete Institute
AE	Air Entraining agent
AISI	American Iron and Steel Institute
APMC	Hydroxypropyl Methylcellulose
AS	Australian Standard
ASTM	American Society for Testing and Materials
BS	British Standard
CEPLA	Coated Expanded Poly-lactic Acid
CFS	Cold Formed Steel
CH	Calcium Hydroxide
COP	Carbon Monoxide Production
CO2P	Carbon Dioxide Production
CSAs	Composite Structural Assemblies
CSH	Calcium Silicate Hydrate
EC	European Commission
EDS	Energy Dispersive X-ray Spectroscopy
EN	European Standard
EP	Expanded Perlite
EPA	Expanded Perlite Aggregate
EPLA	Expanded Poly-lactic Acid
EPS	Expanded Polystyrene
EV	Expanded Vermiculite
FA	Fly Ash
FC	Foamed Concrete
GGBS	Ground Granulated Blast-furnace Slag

GP	General Purpose
HRR	Heat Release Rate
ITZ	Interfacial Transition Zone
JGJ	China Standard
LVDT	Linear Variable Differential Transformer
LWC	Lightweight Concrete
MEPS	Modified Expanded Polystyrene
MPC	Magnesium Phosphate Concrete
NZS	New Zealand Standard
OPC	Ordinary Portland Cement
OPS	Oil Palm Shell
OSB	Orientated Strand Board
PAC	Polystyrene Aggregate Concrete
PC	Perlite Concrete
PCL	Polycaprolactone
PDO	Polydioxanone
PEC	Perlite Expanded-polystyrene Concrete
PGA	Polyglycolic Acid
PHBV	Polyhydroxylvalerate
PLA	Poly Lactic Acid
PP	Polypropylene
PPC	Perlite Expanded Poly-lactic Acid Concrete
PSA	Paper Sludge Ash
PVOH	Poly Vinyl Alcohol
RHA	Rice Husk Ash

SBR	Styrene-butadiene Rubber
SEM	Scanning Electron Microscope
SF	Silica Fume
TC	Thermal Conductivity
THR	Total Heat Released
UEPS	Unexpanded Polystyrene
UPV	Ultrasonic Pulse Velocity
VOCs	Volatile Organic Compounds
WCPP	Waste Carpet Polypropylene
WEP	Waste Expanded Perlite
XRD	X-ray Diffraction

CHAPTER 1

INTRODUCTION

1.1 General introduction

The application of lightweight concrete as structural components track back to the eighteenth century. The use of lightweight concrete provides a substantial improvement in terms of technical and environmental features. The application of lightweight concrete is instrumental to effectively reduce the risk of earthquake damage as the earthquake acceleration and its magnitude is significantly affected by the weight of a structure. The factors such as lower density, higher strength/weight ratio, lower coefficient of thermal conductivity, better fire resistance, improved durability properties, better tensile capacity and sound insulation characteristics are considered as advantages of lightweight concrete compared with normal concrete [1-3]. However, parameters such as bulk specific gravity, unit weight, maximum size and particle shapes, texture surface, strength of lightweight particles, moisture content and water absorption ratio considerably affect negatively the properties of lightweight concrete.

Lightweight concrete is commonly used as sub-base materials like pavement, construction materials such as floating marine structures, cladding panels, composite flooring systems, load-bearing panels, concrete blocks [4], heat preservation, sound insulation materials [3, 5] like interior and exterior partition walls [3], and energy absorbing materials such as fender structures [6-10]. Aerated concrete [11], no-fines concrete [12, 13] and replacement of natural aggregates with lightweight aggregate [14] are the common methods of producing lightweight concrete. Acetated or cellular concrete is obtained by introducing large air voids within a matrix by chemical admixture. No-fines concrete is mostly produced by using a uniform size of coarse aggregate and eliminating the fine aggregate completely from the concrete matrix. The replacement of natural aggregate with lightweight aggregate such as pumice [5], diatomic, volcanic cinder, perlite [15], clay [16], sintered fly ash [17-19], oil palm shell [20], vermiculite [21-27] and expanded polystyrene (EPS) [28, 29] are the most popular ways of producing lightweight concrete. Lightweight aggregates can be classified in five groups of naturally occurring aggregates such as pumice [30-38], basaltic pumice, diatomite, tuff and volcanic cinders; artificially produced aggregate such as expanded perlite

[39, 40], expanded clay [16], expanded shale, expanded slate, and expanded vermiculite [21-27]; artificial by-product aggregate such as pulverized fly ash [41], air-cooled blast furnace slag and expanded slag; industrial by-product aggregate such as expanded polystyrene (EPS) [26], waste glass [42], cenospheres, cork granules, along with broken bricks; and organic aggregate such as oil palm shell (OPS), rice husk saw dust [43, 44], coconut pith [45], saw dust and wood chippings.

Research on EPS concrete and EPS aggregate traces back to 1973 [46-48]. The interest in using expanded polystyrene as lightweight aggregate is evident from the number of researches and data published in this field. The availability of expanded polystyrene in the market and its superior characteristics increased its popularity in the concrete industry. However, the main problem with using EPS as lightweight aggregate is its non-biodegradability.

The demands for environmentally friendly polymers and sustainable materials is increasing lately because of environmental concerns and depletion of petroleum oil. The increase in applications of bio-products in place of petrochemical products leads to a reduction of carbon dioxide emissions and the human footprint on the environment. In order to decrease the influence of petroleum polymer on the environment, and to replace non-renewable oil derived polymers with renewable bio-based resources, several bio-polymer materials were invented and introduced by researchers. Various types of renewable bio-polymers such as Polycaprolactone (PCL), Polyglycolic acid (PGA), Polyhydroxyvalerate (PHBV), Polydioxanone (PDO) and cellulose acetate are commercially available in the market. Petroleum-derived poly vinyl alcohol or PVOH and microorganism-derived poly-lactic acid (PLA) are two types of biodegradable polymers. However, the petroleum-derived polymers are categorized as non-environment friendly polymers because of the emission of greenhouse gases associated with the production process. The production cost of a petroleum-derived polymer mainly depends on the fluctuation of crude oil prices. The production process of microorganism-derived polymers is based on bio-activity of bacteria for transferring agricultural sources into starting products for polymerization [49, 50]. From all the available bio-polymers, poly-lactic acid (PLA) is one of the most widely available and more cost-competitive bio-plastics which is progressively preferred as an alternative for petrochemical polymers like polyethylene, polypropylene and polystyrene. Preliminary tests by Forest Research Scion, an expanded poly-lactic acid (EPLA) manufacturer in New Zealand, proved

that the thermal and mechanical properties of EPLA are comparable with EPS and it can be considered as a good substitution for a petroleum polymer [51-53].

1.2 Problem statement

The disposal of waste petroleum products poses a severe environmental impact. The packaging industries produce millions of tonnes of waste EPS [52]. EPS is non-biodegradable, resistant to photolysis and derived from non-renewable petroleum resources (according to EN 13432) [54]. In addition, pentane emissions during the manufacturing of EPS is another problem, which considerably affects the environment. It has been estimated that volatile organic compounds (VOCs) escaping into the atmosphere amount to 250000 to 300000 t/year. Moreover, increases in oil prices considerably affect polymer product prices. Thus, parameters such as environmental concerns, fluctuation of crude oil prices along with natural gas pricing cause a growing interest in developing materials with more environmentally friendly characteristics.

1.3 Purpose and scope of the study

The purpose of this study is to assess the feasibility of expanded poly-lactic acid lightweight aggregate as a proper substitution for petroleum polymers such as expanded polystyrene. In addition, this project aims to produce a more economical and environmentally friendly ultra-lightweight concrete. Up to now, much of experimental researches concentrate on physical, mechanical and thermal properties of expanded polystyrene concrete, while no information is available on the performance of poly-lactic acid concrete. From all the available biopolymers, poly-lactic acid is one of the most widely available and more cost-competitive bioplastics which is progressively preferred as an alternative for petroleum polymers such as polyethylene, polypropylene and polystyrene due to its eco-friendly profile and performance features. PLA is being introduced as foamed packaging for food applications due to its advantages such as excellent insulation properties, good mechanical properties and its characteristics in terms of heat resistance or flame retardancy [55, 56]. Based on the European standard EN 13432, PLA is considered and categorized as a sustainable and compostable polymer. PLA is produced through ring-opening polymerization of lactide and a dimer of

lactic acid, which is derived from fermented corn starch. Moreover, carbon dioxide (CO₂) as an eco-friendly blowing agent is used for the expansion.

1.4 Outline of the thesis

The thesis consists of eleven chapters, namely: introduction (chapter 1), literature review (chapter 2), experimental program (chapter 3), results (Chapter 4 to chapter 10) and conclusions and recommendations (Chapter 11).

Chapter 1 (Introduction): This chapter gives a general view of lightweight concrete, the problem statement, the scope and objectives of this study.

Chapter 2 (Literature review): This chapter provides a comprehensive review of previous studies on lightweight concrete and its application as filler and bracing material. The literature review comprises of three main sections of literature relating to this study. The first part provides an overview of different types of lightweight aggregates in terms of occurrence and sources. That follows a comprehensive study of different types of concrete namely perlite concrete, vermiculite concrete, EPS concrete, foamed concrete and magnesium phosphate concrete. The last section discusses the application of lightweight concrete as a construction element or filler along with bonding phenomena. Finally research questions for this study are derived from the literature review.

Chapter 3 (Experimental program): This chapter presents the raw materials, which are used to produce concrete at different stages of experiments and a proposed mix design method for ultra-lightweight aggregate. The specific mix design compositions, test preparations and experimental methods will be described as experimental procedures of the following chapters.

Chapter 4 (Vermiculite concrete containing EPLA): This chapter presents the experimental results of vermiculite concrete containing EPLA aggregate. The main content of this chapter is published in "KSCE Journal of Civil Engineering" and "International Journal of Civil and Environmental Engineering" with the title of "Ultra-lightweight Concrete Containing Expanded Poly-lactic Acid as Lightweight Aggregate" and "Assessment of vermiculite concrete containing bio-polymer aggregate", respectively.

Chapter 5 (Perlite concrete containing EPLA): This chapter presents the experimental results of perlite concrete containing EPLA aggregate which comprises of three journal papers titled (1) “Influence of Poly-lactic Acid on the Properties of Perlite Concrete” (Accepted in Construction & Building Materials), (2) “Feasibility of a bio-polymer as lightweight aggregate in perlite concrete” (published in International Journal of Civil and Environmental Engineering) and (3) “A comparative investigation of the engineering properties of perlite concrete containing petroleum and bio-polymer aggregates” (published in International Conference of Architecture and Civil Engineering).

Chapter 6 (GGBS concrete containing EPLA): This chapter presents the experimental results of GGBS concrete containing EPLA aggregate and its results compared with EPS concrete.

Chapter 7 (Magnesium phosphate concrete containing EPLA): This chapter presents the experimental results of magnesium phosphate concrete containing EPLA aggregate.

Chapter 8 (Coated EPLA): This chapter presents the experimental results of novel coated EPLA (CEPLA) as a solution for EPLA degradation in the high alkaline environment of cement.

Chapter 9 (Bond slip behaviour): This chapter presents the results of bond-slip behaviour of concrete. The content and findings of this chapter are published in KSCE Journal of Civil Engineering with the title of “A comparative study on bond stress-slip behaviour of bio- and petrochemical polymer concrete”.

Chapter 10 (Application of lightweight concrete): This chapter presents the bond-slip behaviour of proposed concretes and their performance as bracing components of cold-formed members. The content and results of this chapter is under review by Thin-Walled Structures with the title of "Experimental study on flexural behaviour of cold-formed steel structures filled with bio and petro-chemical polymer lightweight aggregate concrete".

Chapter 11 (Conclusions and recommendations): The overall conclusions of this study are presented. This study is the first comprehensive study of bio-polymer concrete containing expanded poly-lactic acid aggregate and determining most of the mechanical properties, thermal properties, electrical properties and microstructure of the proposed concrete.

CHAPTER 2

LITERATURE REVIEW

2.1 Introduction

This chapter provides a comprehensive review of previous studies of lightweight concrete and its application as filler and bracing materials. The literature review comprises of three main sections of literature relating to this study. The first part covers different types of lightweight aggregates in terms of occurrence and sources. Following that, a detailed study is presented of different types of concrete, namely perlite concrete, vermiculite concrete, EPS concrete, and foamed concrete. The last section discusses the application of lightweight concrete as construction elements or fillers along with bonding phenomena and its parameters. Finally research questions for this study are derived from the literature review.

Up to now, many experimental researches concentrated on physical, mechanical and thermal properties of expanded polystyrene concrete, while no information is available on the performance of poly-lactic acid concrete and its contribution as a lightweight aggregate. Therefore, the polystyrene aggregate concrete is used as reference for concrete containing EPLA due to the similarity in mechanical and thermal properties.

2.2 Lightweight aggregate

Lightweight aggregates in terms of source and occurrence are classified in four types of naturally occurring aggregates, artificially produced aggregates [57], by-product aggregates and organic aggregates. Naturally occurring aggregates such as pumice [30-38], basaltic pumice, diatomite, tuff and volcanic cinders are commonly used as lightweight aggregate and have volcanic origin (lavas) except diatomite, which is a siliceous sedimentary rock. These materials have the capability to produce lightweight concrete with a density range of 1630-1885 kg/m³ and compressive strength of 24-55 MPa.

Artificial lightweight aggregate [57] can be obtained from industrial by-products. Expansion and agglomeration are two common techniques to produce artificial aggregates. The artificial aggregates such as expanded perlite [58], clay [59], shale, slate, and vermiculite [21-27] are produced by expansion methods. Concrete with a density range of 1300-1855 kg/m³ and

correspondent compressive strength of lower than 50 MPa can be produced with expanded artificial aggregates, while these ranges can be slightly higher in terms of density and compressive strength (density range of 1490 to 2000 kg/m³ with compressive strength of up to 60 MPa) when as a by-product artificial aggregates such as pulverized fly ash [41], air-cooled blast furnace slag and expanded slag [60-63] are used. Expanded polystyrene [64, 65], waste glass [42], cenospheres, cork granules, and broken bricks are common industrial by-product aggregates.

The potential use of expanded polystyrene beads (by-products of the packaging industry) as lightweight aggregate is studied by several researchers [65-67]. Concrete with densities and compressive strength ranges of 1000-2000 kg/m³ and up to 35 MPa is achieved when EPS replaces a certain volume of natural aggregates. Concrete made from cenospheres, broken bricks, waste glass and cork granules reached densities of 1090-1415 kg/m³, 1560-1670 kg/m³, 1500-2472 kg/m³ and 1360-1570 kg/m³ along with corresponding compressive strengths of 5-33 MPa, 13-21 MPa, 15-60 MPa and 21-39 MPa, respectively. Agricultural materials such as oil palm shell (OPS) [20], rice husk saw dust [43, 44] and coconut pith [45] along with timber by-products like saw dust and wood chippings are categorized as organic lightweight aggregate. Addition and replacement with agricultural materials causes a considerable reduction in density and unit weight of concrete. Concrete made with rice husk, saw dust and OPS reached densities with ranges of 1110-1145 kg/m³, 1940 kg/m³ and 1760-1900 kg/m³, respectively.

2.3 Lightweight concrete

Structural lightweight concrete provides a vital improvement in terms of technical, economic and environmental aspects [1-3]. Design of lightweight concrete is mostly determined by density and unit weight rather than strength [68, 69]. Lightweight concrete significantly reduces the dead load of structures, the cross-section of structural elements such as columns, beams, braces and foundation sizes. Moreover, longer spans, thinner sections and a better cycling load response can be obtained by using lightweight concrete [70]. Generally, lightweight concrete is instrumental to effectively reduce the risk of earthquake damage as the earthquake acceleration and its magnitude is significantly affected by the weight of a structure.

The factors such as lower density, higher strength/weight ratio, lower coefficient of thermal conductivity, better fire resistance, improved durability properties, better tensile capacity and sound insulation characteristics are considered as advantages of lightweight concrete compared with normal concrete [1-3]. However, parameters such as bulk specific gravity, unit weight, maximum size and particles shape, texture surface, strength of lightweight particles, moisture content and water absorption ratio considerably affect the properties of lightweight concrete. Three common methods are applied: Aerated concrete, no-fines concrete and replacement (partially or totally) of natural aggregates with lightweight aggregate.

Acetated or cellular concrete is obtained by introducing large air voids within a matrix by chemical admixture such as foaming agents or aluminium powder, which increases matrix porosity and decreases the unit weight of concrete. No-fines concrete is mostly produced by using a uniform size of coarse aggregate and eliminating the fine aggregate completely from the concrete matrix. Substituting totally or partially natural lightweight aggregate with lightweight aggregate such as pumice [30-38], diatomic, volcanic cinder, perlite [71], clay [59], sintered fly ash [17-19], oil palm shell, vermiculite and expanded polystyrene is another method to produce lightweight concrete. Generally, the addition of lightweight aggregates results in lower slump value, workability and compacting factor due to a higher water absorption ratio and lower density of lightweight aggregate compared with normal aggregates.

These characteristics of lightweight aggregates cause matrix segregation when higher workability is needed. ACI 302 [72] suggested that the slump value of lightweight aggregate should be limited to ranges of 75-100 mm to avoid segregation of the matrix. However, this problem can be solved by the addition of a water reducer admixture such as superplasticizer. Factors like mix design, water absorption value, specific gravity, and moisture content of lightweight aggregates significantly affect the unit weight of fresh concrete [73]. However, the fresh density of lightweight concrete is due to a higher water absorption value of lightweight aggregates about 100 to 200 kg/m³ higher than its air dry density after 28 days. Inherent strength of aggregates is a factor, which significantly affects the mechanical properties of lightweight concrete. The mechanical properties such as compressive strength, tensile strength, elastic modulus and density of lightweight concrete are much lower than normal concrete (e.g. the elastic modulus is decreased by about 25-50%) and are mainly affected by strength and specification of aggregates. The method of curing is another vital

factor which substantially affects the long term strengths of lightweight concrete [74, 75]. However, lightweight concrete is less sensitive to early curing as a result of the fact that water within porous lightweight aggregate transfers to the mortar to maintain the hydration process at the early stage of curing.

The water-cement ratio considerably affects the mechanical and physical properties of concrete as the water content and its volume directly affects the distance between cement particles and the relative volume of capillarity pores [73, 76, 77].

The design procedure of lightweight concrete is very different to normal concrete. Normal concrete design is based on strength of cement and the water-cement ratio, whereas the design of lightweight concrete is more complex and relies on water absorption value, specific gravity, moisture content, strength, surface texture, porosity and type of lightweight aggregates. Structural lightweight and ultra-lightweight (non-structural) concrete are two forms of lightweight concrete.

According to ACI 213 [78] lightweight concrete in terms of unit weight and compressive strength is categorized in three batches of low density concretes, moderate strength lightweight concretes and structural lightweight concretes. The low density concrete (ultra-lightweight concrete) is mostly used for insulation purposes, while moderate and structural lightweight concretes are used for load bearing walls and structural purposes, respectively. However, these definitions are varied in different codes of practice such as ACI 318 [79], BS 3797 [80], AS 3600 [81] and China standard (JGJ 51) [82]. ACI 318 [79] categorized the concrete with densities lower than 1840 kg/m^3 as lightweight concrete, while BS 3797 [80] defines concrete with air dry densities lower than 2000 kg/m^3 as lightweight concrete. The lightweight concrete with density ranges of $1880\text{-}2100 \text{ kg/m}^3$ and lower than 1950 kg/m^3 are classified as low density concrete in AS 3600 [81] and JGJ 51 [82], respectively.

2.3.1 Perlite lightweight concrete

Perlite is a siliceous volcanic glass, contains 2-5% water and can be expanded about 4-20 times by transforming chemically bound water to vapour when subjected to heat within its softening range (above $870 \text{ }^\circ\text{C}$). The process of expansion leads to a significant reduction in

unit weight of perlite by the formation of numerous pores within an amorphous sintered mass [39].

Expanded perlite (EP) is a high porosity aggregate with low density, low thermal conductivity value and high sound absorption. Expanded perlite is also classified as an artificial pozzolanic material due to its glassy structure along with a high silicon dioxide (SiO₂) and aluminium oxide (Al₂O₃) content [39]. Turkey (43%), Greece (24%), United States (16%) and Japan (7%) are the leaders in producing perlite in the world. Perlite particles are mostly used as bricks, plasters, filling materials, and pipes, as well as for agricultural, medical and chemical purposes. However, perlite is not technically used in concrete yet [83, 84].

A number of experimental and analytical studies have been conducted on the influence of perlite on physical and mechanical properties of fresh and hardened concrete. It has been reported (Figure 2. 1) that expanded perlite is a proper artificial aggregate with potential uses as coarse aggregate to produce lightweight concrete with a density of lower than 800 kg/m³ [85, 86].

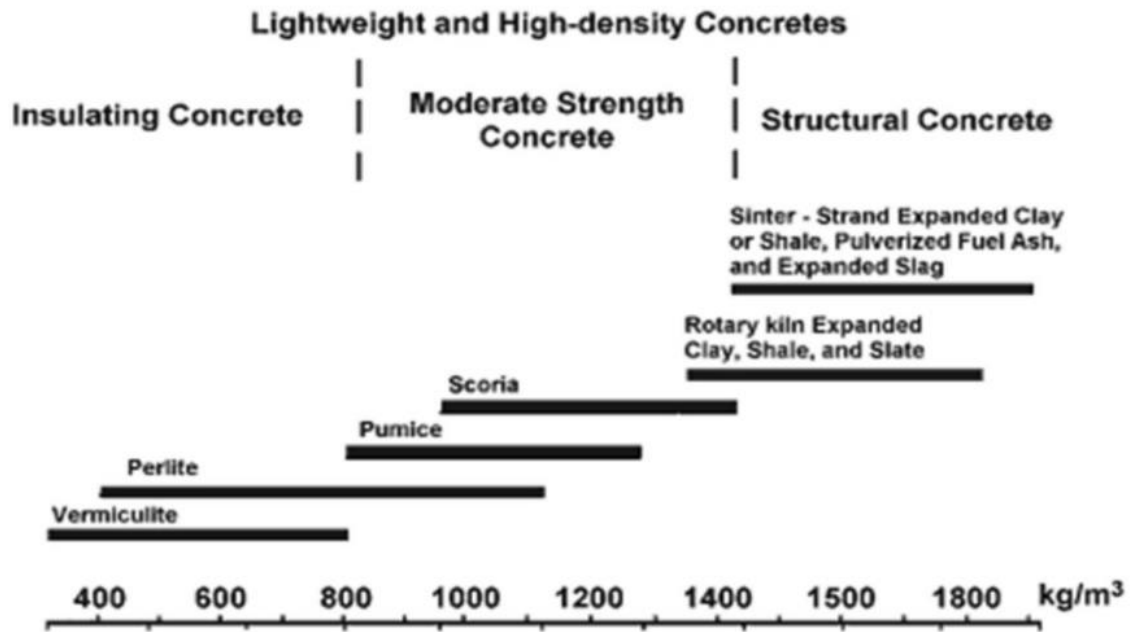


Figure 2. 1. Aggregates to produce insulating concrete [100]

Ozakan et al. [83] have concluded that thermal conductivity (Figure 2. 2a) and unit weight (Figure 2. 2b) of perlite concrete significantly decreased as expanded perlite replaces natural

aggregate. In addition, the same trend was observed in terms of compressive strength (Figure 2. 2c) and elastic modulus (Figure 2. 2d) as the content of expanded perlite is enhanced. However, the loss of elastic modulus was considerable higher than the loss of compressive strength [83]. Moreover, increasing the amount of expanded perlite significantly increased the water absorption (Figure 2. 2e) and sorptivity (Figure 2. 2f).

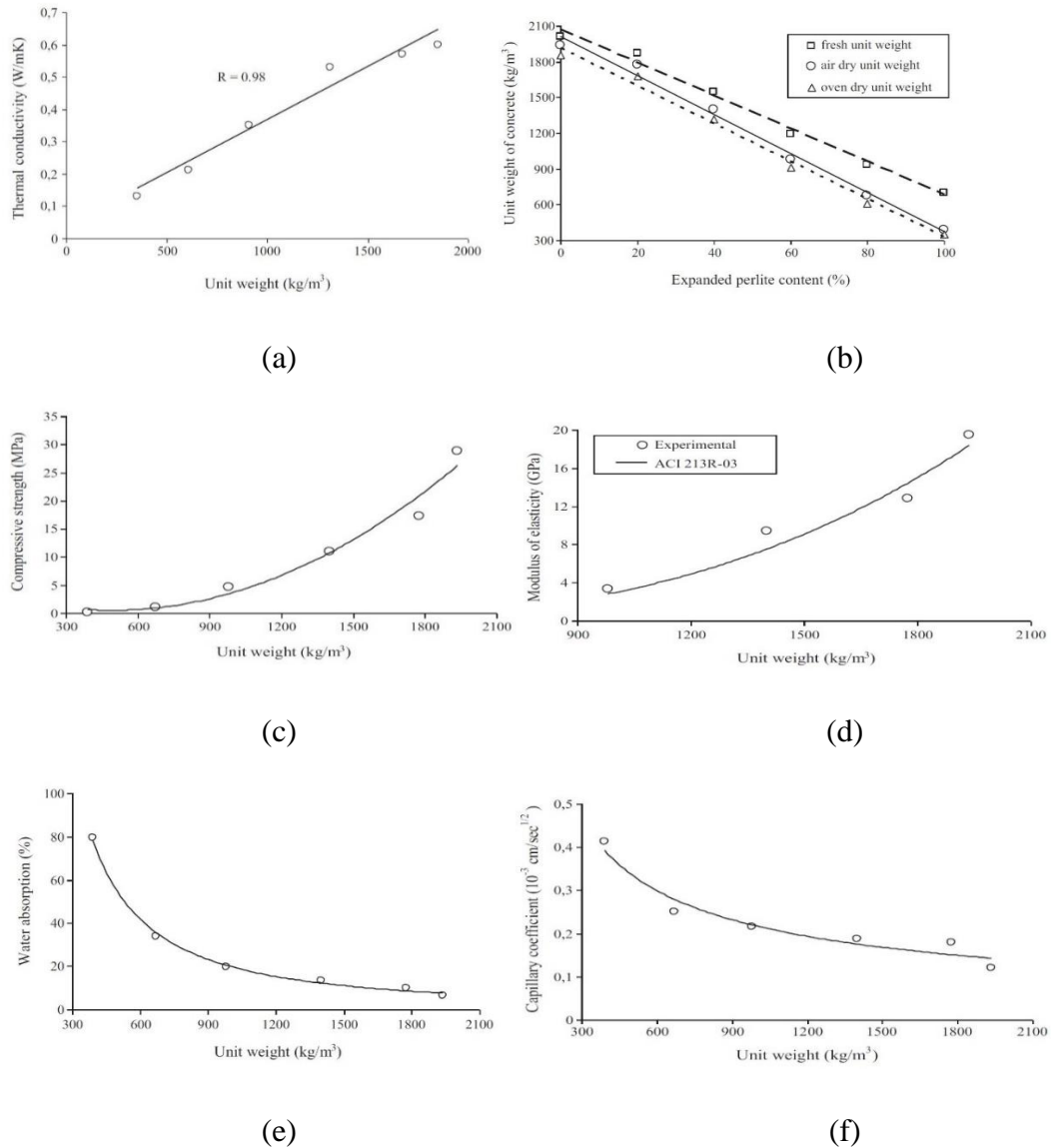
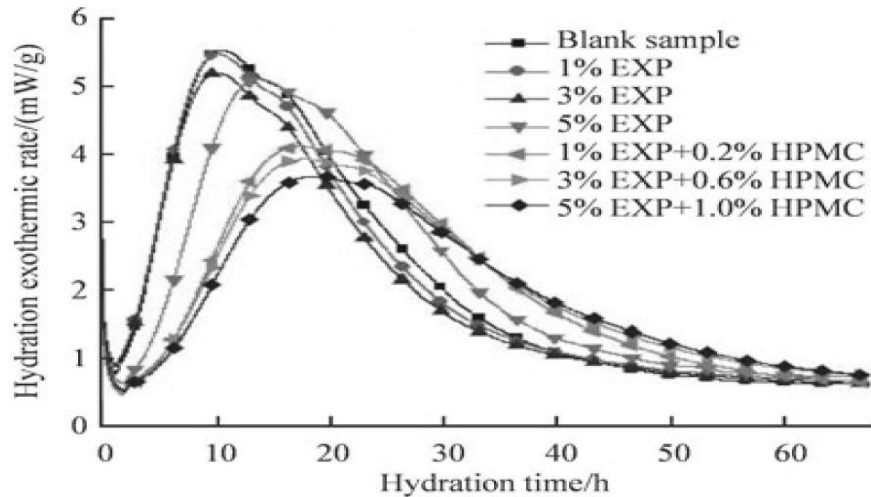


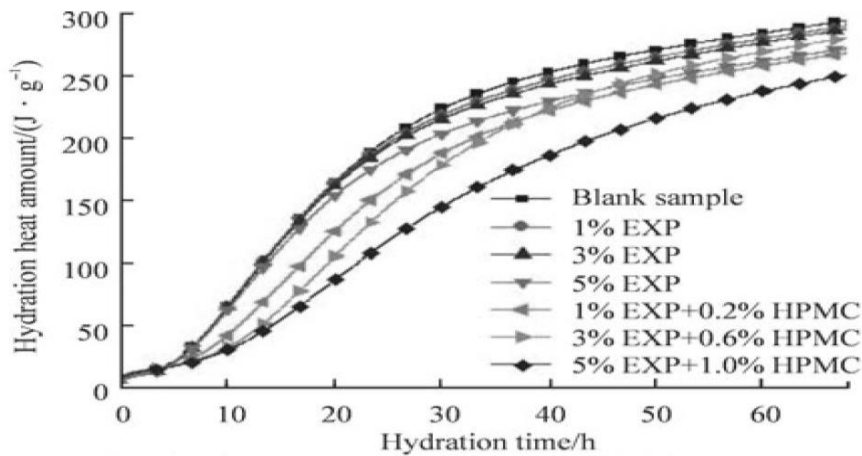
Figure 2. 2 Effect of expanded perlite aggregate on; (a) thermal conductivity, (b) unit weight, (c) compressive strength, (d) modulus of elasticity, (e) water absorption, (f) capillary coefficient [83].

Gurhan et al. [58] have concluded that expanded perlite is capable of being used as a lightweight construction material. Additionally, the effect of expanded perlite and hydroxypropyl methylcellulose (HPMC) on the hydration heat of concrete has been

investigated by Su et al. [40]. They have found that expanded perlite causes a significantly delayed hydration induction period and an acceleration period of cement pastes (Figure 2. 3).



(a)



(b)

Figure 2. 3 (a) Hydration exothermic rate and (b) hydration heat amount of expanded perlite (EXP) modified cement paste [40].

Demirboga and Gül [87] have found that thermal conductivity of concrete is a factor of porosity and increasing the expanded perlite percentage results in a lower thermal conductivity value due to the porous structure of perlite (Figure 2. 4). This trend is observed in another study about the influence of perlite on thermal conductivity [88]. They have found

that perlite brings down the density and thermal conductivity value of the matrix. In addition, they concluded that the thermal conductivity of concrete is a factor of lightweight aggregate content and characteristics of the binder (Figure 2. 5).

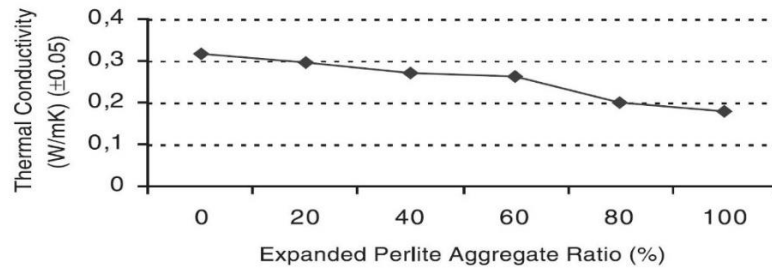


Figure 2. 4 The effect of expanded perlite ratio on thermal conductivity of concrete [87]

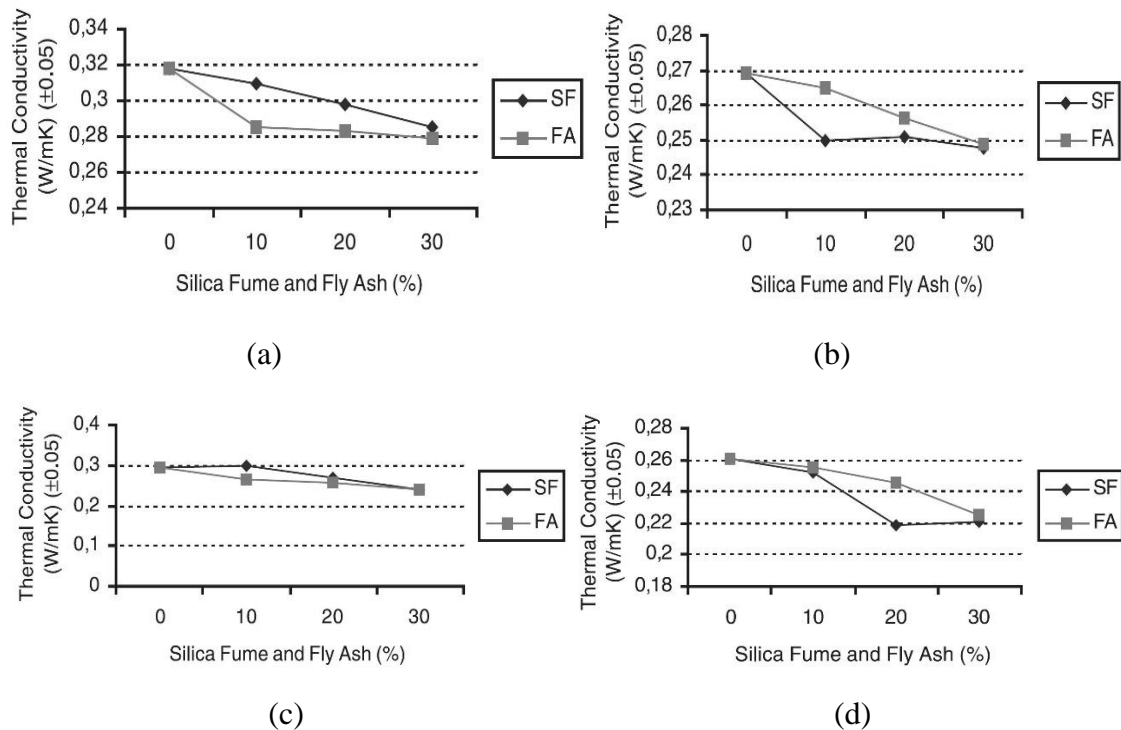


Figure 2. 5 The influence of pumice (PA), perlite (EPA), silica fume (SF) and fly ash (FA) content on thermal conductivity of concrete; (a) 100% PA, (b) 80% PA+ 20% EPA, (c) 60% PA+ 40% EPA, (d) 40% PA+ 60% EPA [88].

Yu et al. [89] found that the addition of perlite powder significantly improved the high-freeze-thaw resistance and fire resistance as well as causes an increase in the alkali silica reaction of the matrix due to the microcrystalline quartz content of perlite, which is mostly chalcedony. Bekir et al. [84] have reported, that the mechanical properties such as dynamic elasticity modulus, compressive strength and tensile strength of concrete increased as the ratio of perlite decreased. Turkmen et al. [90] have found that slump flow is a factor of viscosity and the addition of silica fume increases the cohesiveness of the matrix due to an

increase in the number of solid to solid contact points. The addition of expanded perlite aggregate (EPA) remarkably decreased the unit weight of the matrix mainly due to the fact that EPA has a lower specific gravity compared with normal aggregate. Moreover, they have concluded that the capillarity coefficient of concrete depends on curing time, curing conditions and EPA ratio (Table 2. 1).

Table 2. 1 Effect of expanded perlite aggregate (EPA) and curing conditions on capillarity coefficient of concrete [90].

Curing conditions	Capillarity coefficient					
	Mixtures (%)	Curing time (days)				
		28 days (x10 ⁻⁶)	56 days (x10 ⁻⁶)	90 days (x10 ⁻⁶)	120 days (x10 ⁻⁶)	150 days (x10 ⁻⁶)
CC1 (water)	EPA0	0.45	0.79	0.65	0.40	0.15
	EPA5	0.51	0.76	0.68	0.63	0.20
	EPA10	0.59	0.87	0.64	0.63	0.20
	EPA15	0.64	1.13	0.72	0.66	0.21
CC2 (air)	EPA0	8.94	7.11	4.26	2.07	0.52
	EPA5	9.25	7.17	2.46	1.51	0.35
	EPA10	10.13	7.38	2.62	1.80	0.42
	EPA15	11.71	7.38	2.67	1.96	0.54
CC3 (wet-14 days)	EPA0	0.85	0.92	0.84	0.63	0.20
	EPA5	0.90	0.97	0.97	0.65	0.20
	EPA10	1.06	1.14	1.33	0.72	0.20
	EPA15	1.27	1.20	1.60	0.80	0.20
CC4 (wet sack)	EPA0	0.57	0.63	0.90	0.66	0.20
	EPA5	0.66	0.62	1.05	0.68	0.19
	EPA10	0.71	0.82	1.11	0.71	0.20
	EPA15	0.93	0.88	1.44	0.77	0.20
CC5 (100% RH)	EPA0	0.48	0.59	0.72	0.45	0.22
	EPA5	0.55	0.78	0.88	0.79	0.23
	EPA10	0.56	0.82	1.62	1.04	0.31
	EPA15	0.63	1.46	1.74	1.19	0.31

Kotwica et al. [39] have reported that waste expanded perlite (WEP) significantly decreased the calcium hydroxide (CH) content and increased the amount of hydration products within hardened pastes (Figure 2. 6).

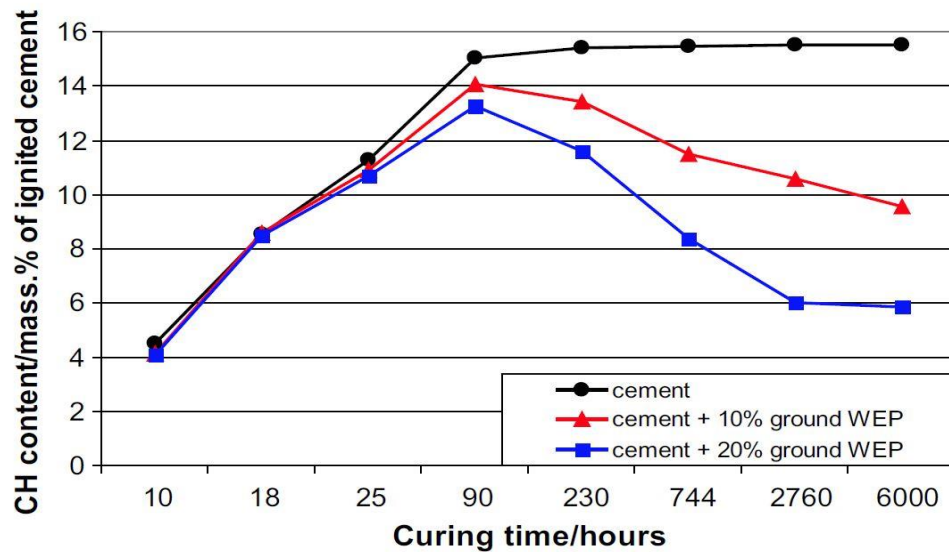


Figure 2. 6 The relationship between calcium hydroxide (CH) content and curing time for pastes containing 0, 10 and 20 % of ground WEP [39].

2.3.2 Vermiculite lightweight concrete

Vermiculite is widely found in South Africa, United States and China. Vermiculite has a platy structure, almost similar to mica and can be expanded 8 to 30 times of its original size when heated rapidly. Temperature and processing time significantly affect the expansion ratio of vermiculite [21-25, 27, 29]. Vermiculite with its advantages, i.e. very low density and thermal conductivity, is known as an appropriate material for different applications in the fields of construction, industry and agriculture. They are insulation concrete, thermal insulation filler, potting soils, soil conditioners, carrier for fertilizer, insecticides and herbicides, different livestock applications, seed germination, ammonia filtering in aquaculture, high-temperature insulation, refractory materials, acoustic panels, fireproofing of steel structures, fireproofing of pipes, roof screeds and floor screeds [23]. The application of vermiculite as lightweight aggregate has been studied by several researchers [21-25, 27, 29].

Fuat et al. [23] have reported that increasing SAE latex-cement (W_p/W_c) and vermiculite-cement (V_v/V_c) ratio decreases the water absorption along with fresh and dry bulk density of mortar. In addition, they have found that the percentage of expanded vermiculite plays a significant role in flexural and compressive strength of the mixture. A lower compressive (Figure 2. 7) and flexural (Figure 2. 8) strength is observed with a higher vermiculite volume. In contrast, the addition of polymer latex improved the flexural strength rather than the compressive strength. In addition, there is a direct relation between the vermiculite-cement (V_v/V_c) ratio, porosity and thermal conductivity as an increase in V_v/V_c ratio results in higher porosity and lower thermal conductivity due to the porous structure of vermiculite (Figure 2. 9).

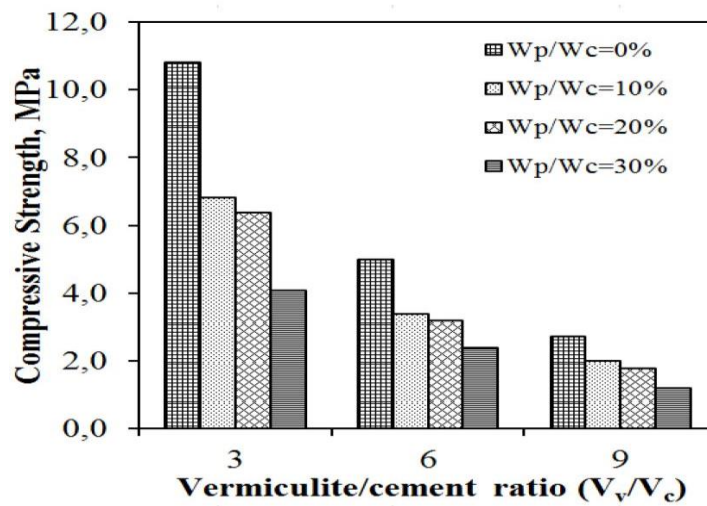


Figure 2. 7 Compressive strength of vermiculite concrete with different vermiculite to cement ratios [23].

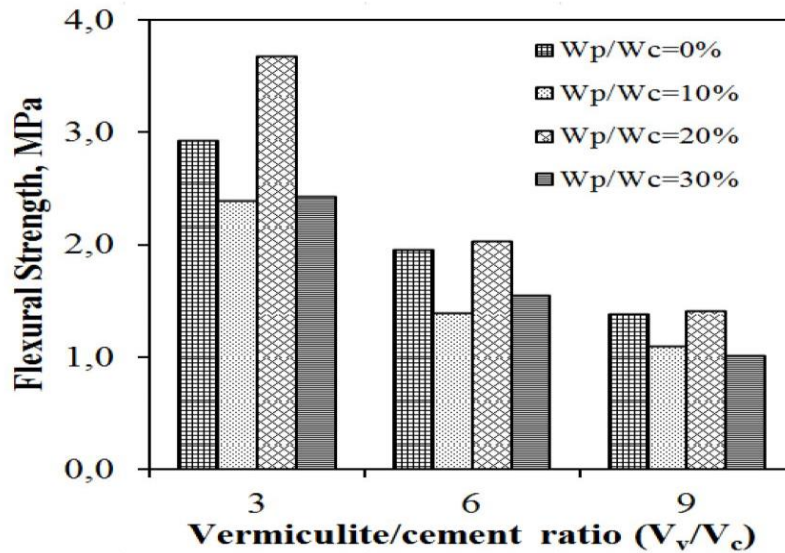


Figure 2. 8 Flexural performance of vermiculite concrete with different vermiculite to cement ratios [23].

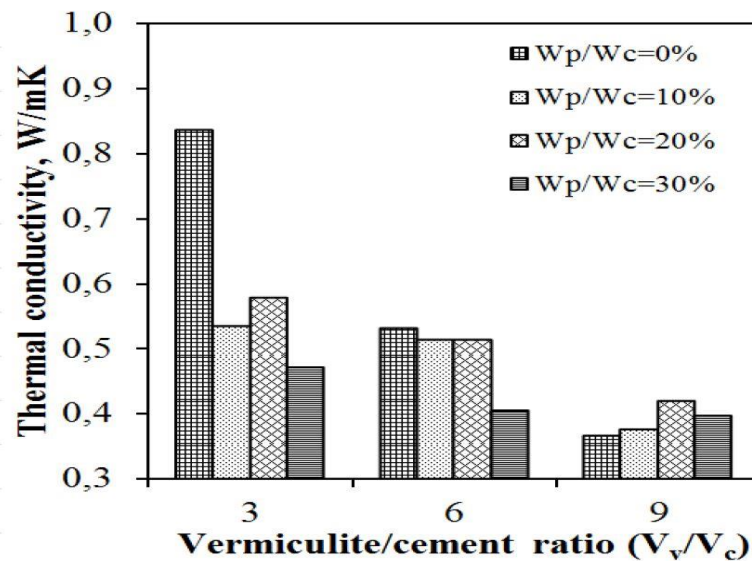


Figure 2. 9 Thermal conductivity of vermiculite concrete with different vermiculite to cement ratios [23].

The test results of Silva et al. [91] demonstrated that the pore size and pore distribution is reasonably different in perlite and vermiculite. They have stated that mortar porosity has a considerable effect on water absorption and mechanical properties of mortar. This phenomenon strongly affects the capillary water absorption of mortar as the coarser voids in the microstructure of perlite mortar cause higher capillarity action while the small pores in

vermiculite mortars do not assure a continuous capillary network (Figure 2. 10). Moreover, vermiculite mortar with its smaller pore size needs less water content and exhibited higher compressive strength along with lower loss of density compared with perlite. In contrast, perlite mortar showed better shrinkage behaviour.

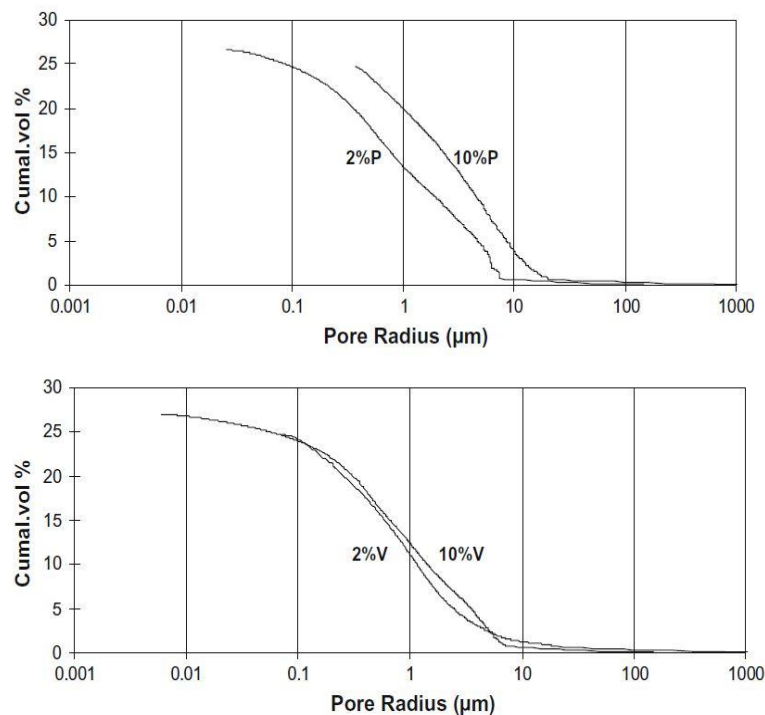


Figure 2. 10 Pore size distribution of the hardened mortars with different perlite (P) and vermiculite (V) content [91].

Koksal et al. [24] have found that increases in the vermiculite-cement ratio of mortar causes higher flow-ability. However, the addition of silica fume imposes an inverse effect on flow-ability of mortar due to the high specific surface area of silica fume. In addition, a higher density is observed when the ratio of silica fume is enhanced at each v/c ratio. Also, it was observed that there is a relation between vermiculite volume, density and compressive strength (Figure 2. 11). Mortar with lower vermiculite content presents a higher density and compressive strength, mainly due to lower porosity. The impact of vermiculite volume and silica fume on porosity and water absorption shows that vermiculite enhanced the porosity and in contrast silica fume decreased this value.

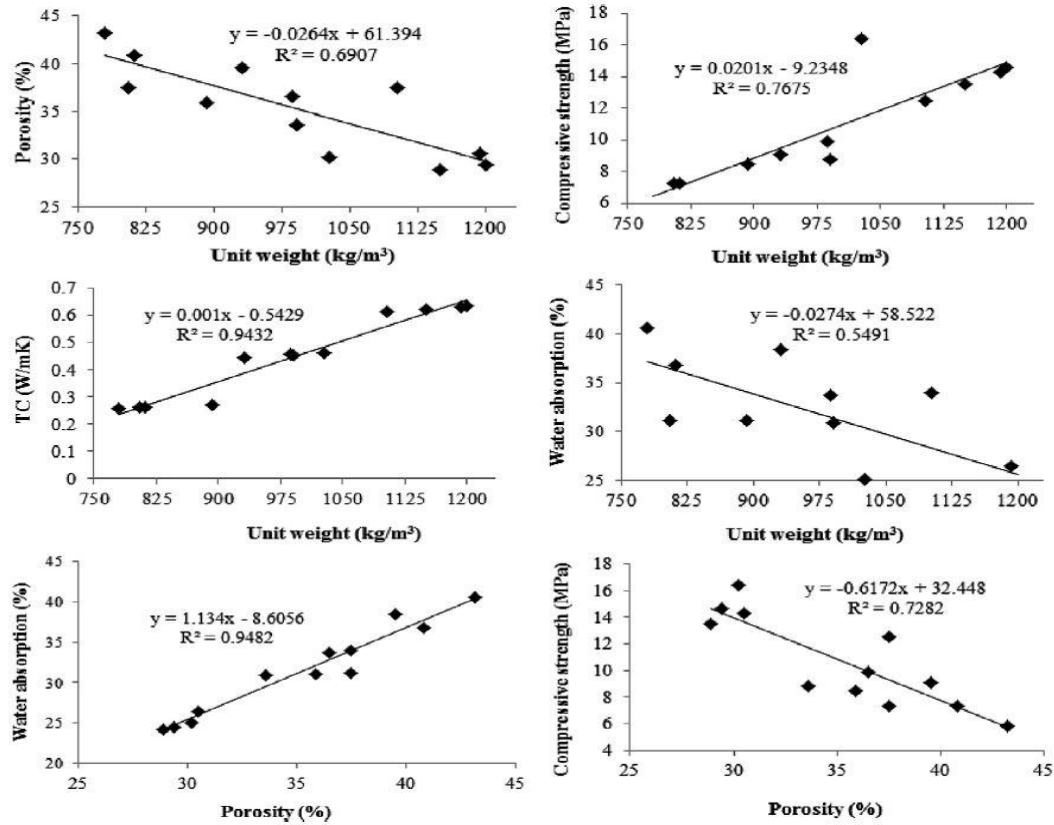


Figure 2. 11 Relations between engineering properties of vermiculite concrete [24].

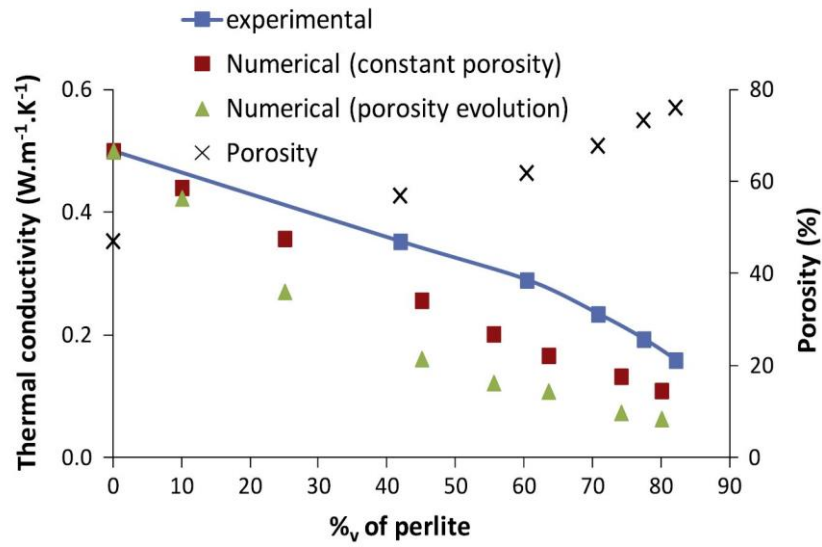
Schackow et al. [26] have reported that a lower amount of vermiculite, EPS and air-entraining agent exhibited higher compressive strength and density (Table 2. 2). However, EPS lightweight concrete shows a higher strength and lower density compared with vermiculite concrete (Table 2. 3). In addition, they have confirmed that a lower thermal conductivity was observed in vermiculite lightweight concrete than in EPS concrete and suggested that EPS and vermiculite lightweight aggregate can be used up to 55% of the matrix volume. Moreover, data from a study conducted by Adidi et al. [21] show that the impact of perlite and vermiculite volume on thermal conductivity of a plaster composite material directly depends on the components ratio. A better thermal insulation is observed in perlite than vermiculite concrete, mainly because perlite particles have greater porosity (Figure 2. 12).

Table 2. 2 Mechanical properties of vermiculite lightweight concretes [26].

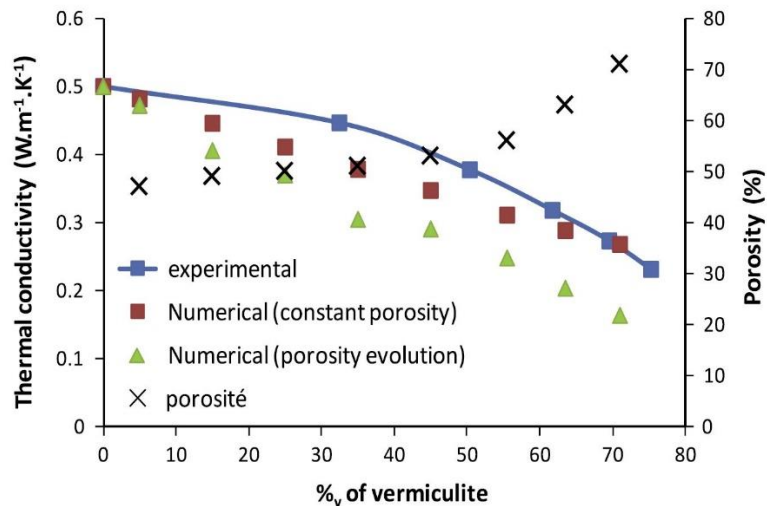
Design mixture	Factors and levels		W/C ratio (weight)	Slump (mm)	CS28 days (MPa)	Density (g/cm ³)	Voids index (%)	Water absorption (%)
	Volume of vermiculite (% of volume of concrete)	Air-entraining agent (% weight)						
V1	55	0.5	0.50	110	13.74 ± 0.64	1.29 ± 0.01	41.49 ± 1.19	33.51 ± 1.69
V2	65	0.5	0.50	33	9.49 ± 1.13	1.18 ± 0.03	45.02 ± 4.95	38.28 ± 5.10
V3	55	1.0	0.60	123	14.80 ± 0.32	1.25 ± 0.02	42.65 ± 2.20	32.03 ± 1.10
V4	65	1.0	0.60	45	6.31 ± 0.35	1.13 ± 0.03	46.21 ± 1.97	41.12 ± 2.84

Table 2. 3 Mechanical properties of EPS lightweight concretes [26].

Design mixture	Factors and levels		W/C ratio (weight)	Slump (mm)	CS28 days (MPa)	Density (g/cm ³)	Voids index (%)	Water absorption (%)
	Volume of EPS (% of volume of concrete)	Air-entraining agent (% weight)						
E1	55	0.5	0.76	125	15.55 ± 0.99	1.25 ± 0.05	36.82 ± 6.8	35.99 ± 4.46
E2	65	0.5	0.76	108	8.43 ± 0.74	1.11 ± 0.03	34.89 ± 5.8	31.73 ± 3.77
E3	55	1.0	1.10	160	11.85 ± 0.77	1.14 ± 0.06	42.04 ± 7.4	39.10 ± 1.48
E4	65	1.0	1.10	110	7.74 ± 0.78	1.07 ± 0.05	42.51 ± 2.40	39.81 ± 0.44



(a)



(b)

Figure 2. 12 The relationship between thermal conductivity and the rate of lightweight aggregate added to the matrix; (a) perlite aggregate, (b) vermiculite aggregate [21].

2.3.3 Expanded polystyrene lightweight concrete

A wide range of lightweight concrete densities can be produced by substituting of a certain ratio of natural aggregate with EPS beads. Research on EPS concrete and EPS aggregate traces back to 1973 [46-48]. The extremely low density and hydrophobic nature of EPS beads constrains the application of EPS concrete. In fact, beads tend to float, because of their low specific weight of $10 - 20\text{kg/m}^3$, when used as lightweight aggregate and cause serious segregation and poor mix distribution in the matrix. Bonding additives such as epoxy resin (aqueous dispersions of polyvinyl propionate) [75, 78, 79], water-emulsified epoxies [8], and chemically treated EPS [7] particles like BST (commercially available in Australia) used to increase the interfacial bonding strength between beads and matrix. It was reported that mineral admixtures such as silica fume [44], fly ash [92] and ground granulated blast furnace slag were used as bonding additives to increase the interfacial bonding strength between beads and matrix and assisted the dispersion of EPS beads in the cement matrix [93]. A significant improvement is observed in terms of chemical attack and corrosion characteristics of concrete when EPS aggregate replaces normal aggregates [92].

Babu et al. [92] reported that the chloride permeability of polystyrene concrete is a factor of EPS volume as increasing the volume of polystyrene causes lower chloride permeability values of about 50-65% less (Figure 2. 13). In addition, EPS concrete has a better stability

against chemical attack which is due to the inert behaviour of EPS aggregate [92]. It has been confirmed and reported that the compressive strength of expanded polystyrene concrete is reduced as a certain amount of EPS beads replaces natural aggregates [7, 14, 26, 44, 67, 92, 94-101].

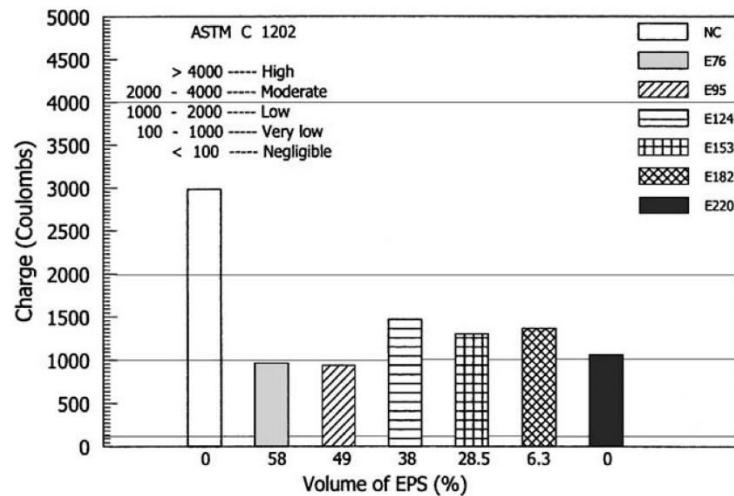


Figure 2. 13 Chloride permeability of EPS concretes with variation on EPS ratio where NC, E76, E95, E124, E153, E182 and E220 have the density of 2578, 779, 984, 1304, 1484, 1723 and 2215 kg/m^3 [92]

The mechanical properties of chemically treated EPS lightweight concrete have been investigated by Ravindrarajah et al. [7]. They have concluded that the water-cement ratio of EPS concrete should be retained as low as possible to obtain the highest compressive strength. Moreover, EPS concrete exhibited acceptable resistance to chemical attack such as calcium hydroxide, sodium sulphate and ammonium sulphate solution, and its resistance to 5% hydrochloric acid enhanced as the water-cement ratio decreased. Also, they have found that a higher compressive strength and tensile strength is obtained with a lower water-cement ratio. In addition, a higher shrinkage value observed by inclusion of EPS aggregate is mainly due to the lower resistance of EPS particles, because of their smooth surface and spherical shape (Figure 2. 14).

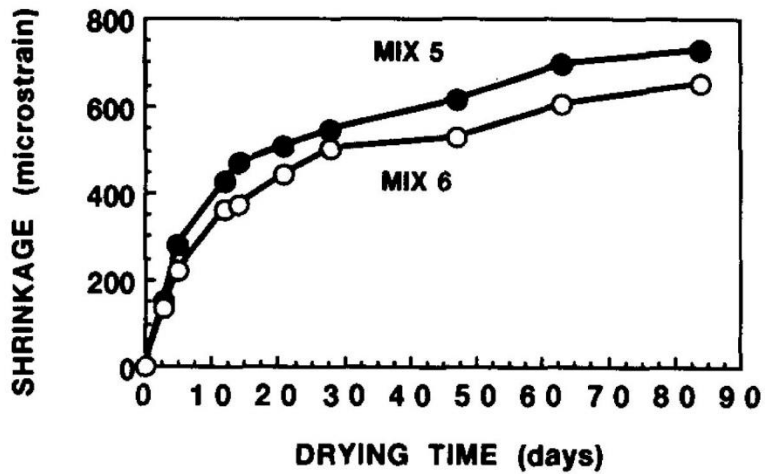


Figure 2. 14 The relationship between drying shrinkage and drying time [7]

Schachow et al. [29] have investigated the differences between mechanical properties of EPS and vermiculite concrete and concluded that air-entraining agent and lightweight aggregate volume directly affect the compressive strength and density of concrete. Lower compressive strength and density is obtained as the volume of EPS and foam is enhanced. This can be explained by lightweight aggregate having a lower specific unit weight along with close to zero strength and the air-entraining agent increases the porosity of concrete, which causes a considerable reduction in the compressive strength of the matrix. Furthermore, vermiculite concrete shows a lower thermal conductivity value than EPS concrete due to higher porosity of vermiculite (Table 2. 4). However, EPS concrete has advantages in terms of its water absorption ratio, which is almost zero, and unit weight, i.e. being lighter than vermiculite.

Table 2. 4 Thermal conductivity of the lightweight concretes containing EPS and vermiculite concrete [29].

Mixture	Volume of lightweight aggregate (% of volume of concrete)	Air-entraining agent (% weight)	Thermal conductivity (W/mK)
V3	55	1.0	0.50
V4	65	1.0	0.34
E3	55	1.0	0.56
E4	65	1.0	0.50

Chen et al. [102] have indicated that the inclusion of foam substantially enhances the slump value of EPS concrete because foam reduces the bulk density of the matrix and increases the volume of the cement paste. In addition, the introduction of foam with its small spherical bubbles acts as ball bearings in the matrix and reduces the internal friction between particles. They have also found that an increase in the volume of foam causes a decrease in compressive strength of concrete (Figure 2. 16). Moreover, they have concluded that thermal and mechanical properties of EPS foamed concrete are a factor of foam content and EPS volume (Figure 2. 15).

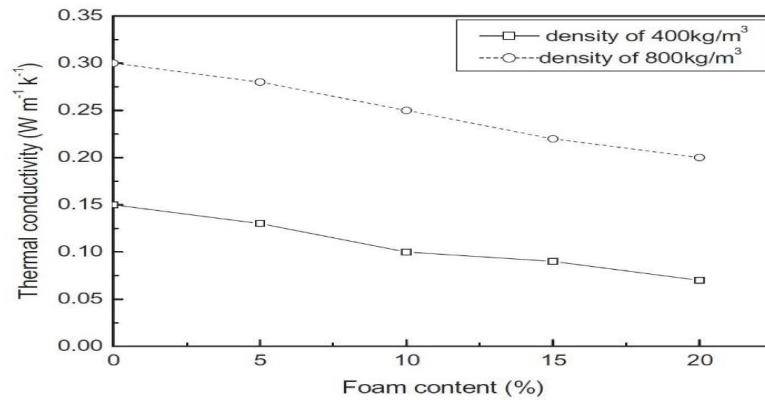
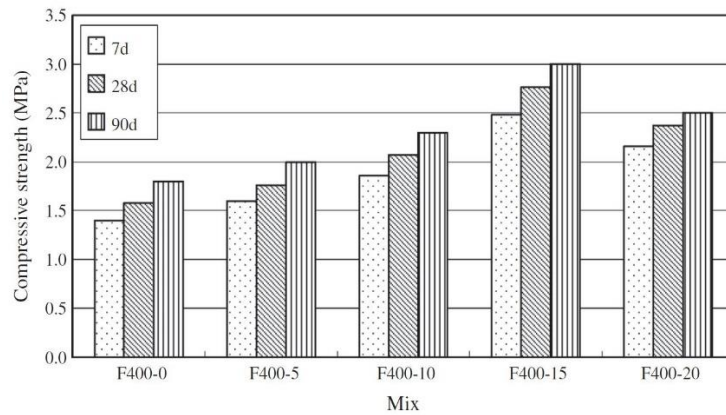
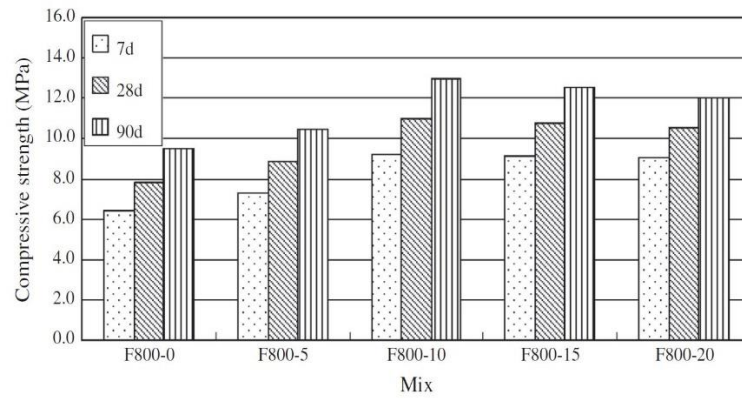


Figure 2. 15 The relationship between foam content and thermal conductivity [102]



(a)



(b)

Figure 2. 16 Compressive strength of EPS foamed concrete for different densities; (a) 400kg/m^3 , (b) 800kg/m^3 [102].

Madandoust et al. [65] have found that the slump flow enhanced, when the volume of expanded polystyrene is increased. The slump flow increased as a result of lower internal friction between cement paste and particles due to the spherical shape, smooth surface and hydrophobic nature of EPS. The addition of nano-SiO₂ decreased the slump flow because nano-SiO₂ has a higher surface area and promotes the packing of particles. This trend causes higher internal friction between the particles of the matrix resultant in a lower slump flow (Figure 2. 17). The influence of nano-SiO₂ is reduced as the volume of EPS particles increased.

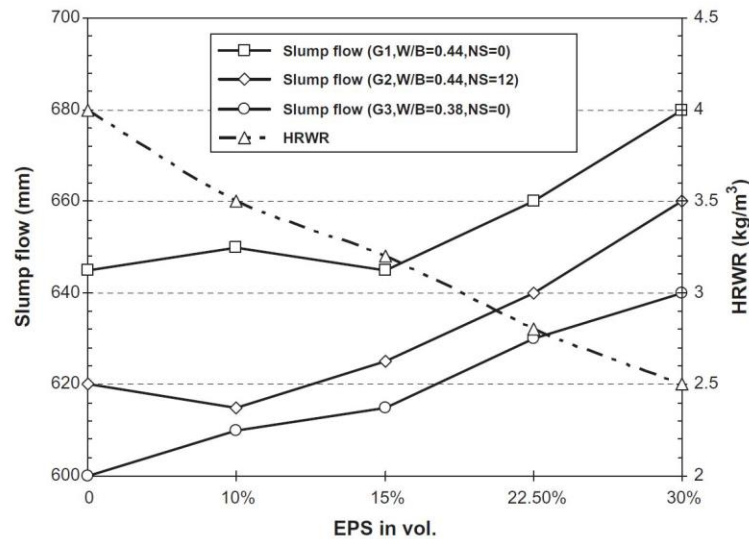


Figure 2. 17 The relationship between slump flow and EPS volume with variation on water-binder ratio (W/B), nano-SiO₂ ratio (NS) and Polycarboxylic ether based high range water reducer (HRWR) [65].

Kan et al. [14] have concluded that the density of lightweight concrete is more sensitive to the slump flow value than the water-cement ratio. A higher compressive strength and density is observed as the cement-EPS ratio is increased. Xu et al. [103] have found that mechanical properties of EPS lightweight concrete are a factor of EPS volume, water-cement ratio, cement content and sand content. However, EPS volume and cement/sand content are the most and least important factor in design of EPS concrete, respectively. The lower degree of compaction and workability obtained with an increase in EPS volume is mainly due to the compressible nature and low unit weight of EPS. Compared with normal concrete, the failure mode of EPS concrete was more gradual. The stress-strain diagram of EPS concrete was almost the same as normal concrete. However, the length of the elastic segment and the slope of the stress-strain curve increased as the volume of EPS decreased.

2.3.3.1 Influence of EPS particles on creep and shrinkages of concrete

Ben Sabaa et al. [64] have reported that the inclusion of EPS aggregate results in a considerable reduction in density, compressive strength, tensile strength and modulus of elasticity of concrete and significantly increased the drying shrinkage and creep of concrete. They have concluded that increases in the volume of EPS results in a higher creep value due to the inability of the low modulus EPS beads to restrain the creep of the cement paste matrix. Another study on creep and shrinkages of EPS concrete [104] shows that the EPS concrete has higher shrinkage values in contrast with normal concrete. They have found that increases in the shrinkage values induce cracking on the surface of concrete, which reduces the life expectancy of concrete. A reduced water absorption was observed for EPS aggregate due to its closed cellular structure and hydrophobic nature [105]. The workability of EPS concrete enhanced as the volume of air content increased. This phenomenon can be attributed to the fact that air bubbles probably act as a fine aggregate with very low surface friction. Whereas, increasing the volume of air results in more voids in the concrete mixture and lower strength [106]. The experimental results from calorimetric tests indicated that the peak temperature increased with a greater volume of EPS particles. Moreover, they have found that EPS concrete shows a greater shrinkage than normal concrete due to the negligible elastic module and the smooth surface of aggregates which results in less resistance to the shrinkage process.

The differences in shrinkage values at the later age were negligible between normal and EPS concrete.

Demirboga et al. [70] have found that cement content, cement quality and the degree of restraint by aggregate is significantly affiliated with the shrinkage value of concrete. The normal concrete with its hard, dense aggregate exhibits a lower shrinkage as a result of the cement being restrained by the rigidity of aggregate, while low density aggregate like modified expanded polystyrene (MEPS) offers lower hindrance to shrinkage of the cement paste due to the less restraint force. It is worth to note that the ratio of MEPS aggregate remarkably affects the shrinkage value. They have found that the sample with 100% MEPS (aggregate volume) exhibits almost 2.35 times greater shrinkage than the sample with 25% MEPS (Figure 2. 18).

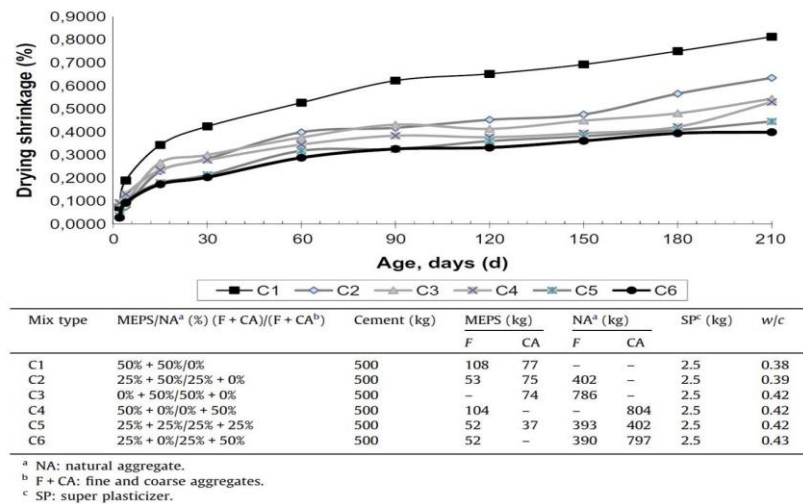


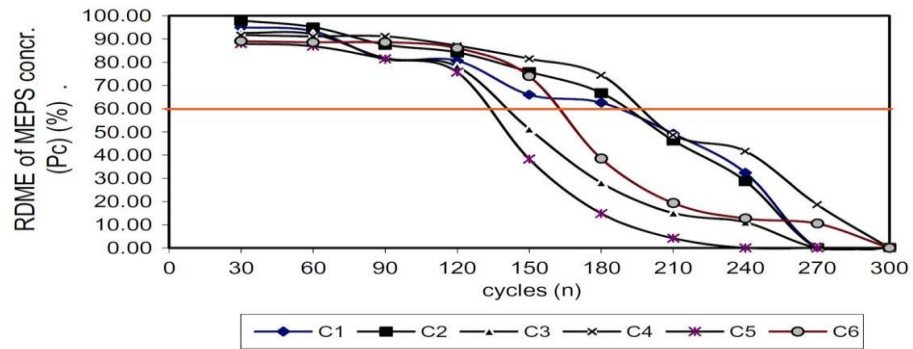
Figure 2. 18 The shrinkage of modified expanded polystyrene (MEPS) aggregate concrete [70].

Chen et al. [96] have reported the volume and properties of EPS particles significantly affect the value of shrinkage and an increase in the volume of polystyrene results in a higher shrinkage value. Compared with normal concrete, concrete containing polystyrene offers higher shrinkage at the initial stage, while this value was minimal at the later stage. They have found that an increase in the volume fraction of EPS causes higher strain shrinkage due to the lower hindrance of EPS beads to the shrinkage of the paste. The degree of restraint by the aggregate and the volumetric proportion of paste in the mix are considerable factors affecting the shrinkage of concrete. The higher drying shrinkage strain of EPS concrete of up

to $1.125e^{-4}$ indicates a disadvantage of this material compared with normal concrete with a shrinkage strain of $6.32e^{-5}$.

2.3.3.2 Influence of modified EPS (MEPS) on mechanical properties of concrete

In order to increase the mechanical properties of EPS concrete and to eliminate the segregation problem contributed to the inclusion of EPS particles a modification method was proposed by researchers [70, 94, 102, 107]. A significant improvement in terms of mechanical properties was obtained as waste EPS particles were exposed to a temperature of 130°C for 15min [107]. They have indicated that the surface of modified expanded polystyrene was harder than unmodified particles. The water absorption value of MEPS was much lower than available lightweight aggregate such as perlite and vermiculite. Kan et al. [108] have reported that strength of concrete considerably depends on the strength of aggregate. The near zero strength of EPS particles leads to the lower strength of EPS concrete contrary to the natural aggregate with higher compressive strength. The workability of concrete decreased as the MEPS particles replaced natural aggregate because coarse MEPS introduced a larger number of pores and a lower compaction value. With an identical concrete density, MEPS concrete shows a 40% higher compressive strength compared with vermiculite or perlite aggregate concrete and exhibits better freeze-thaw resistance and thermal insulation (Figure 2. 19 and Figure 2. 20). A higher ultrasonic pulse velocity (UPV) value is observed for MEPS concrete as the volume of modified polystyrene aggregate is reduced.



Mix type	MEPS/NA ^a (%) (F + CA)/(F + CA ^b)	Cement (kg)	MEPS (kg)		NA ^a (kg)		SP ^c (kg)	w/c
			F	CA	F	CA		
C1	50% + 50%/0%	500	108	77	-	-	2.5	0.38
C2	25% + 50%/25% + 0%	500	53	75	402	-	2.5	0.39
C3	0% + 50%/50% + 0%	500	-	74	786	-	2.5	0.42
C4	50% + 0%/0% + 50%	500	104	-	-	804	2.5	0.42
C5	25% + 25%/25% + 25%	500	52	37	393	402	2.5	0.42
C6	25% + 0%/25% + 50%	500	52	-	390	797	2.5	0.43

^a NA: natural aggregate.
^b F + CA: fine and coarse aggregates.
^c SP: super plasticizer.

Figure 2. 19 The relationship between ratio of the dynamic modulus of elasticity (RMDE) and freezing and thawing [108].

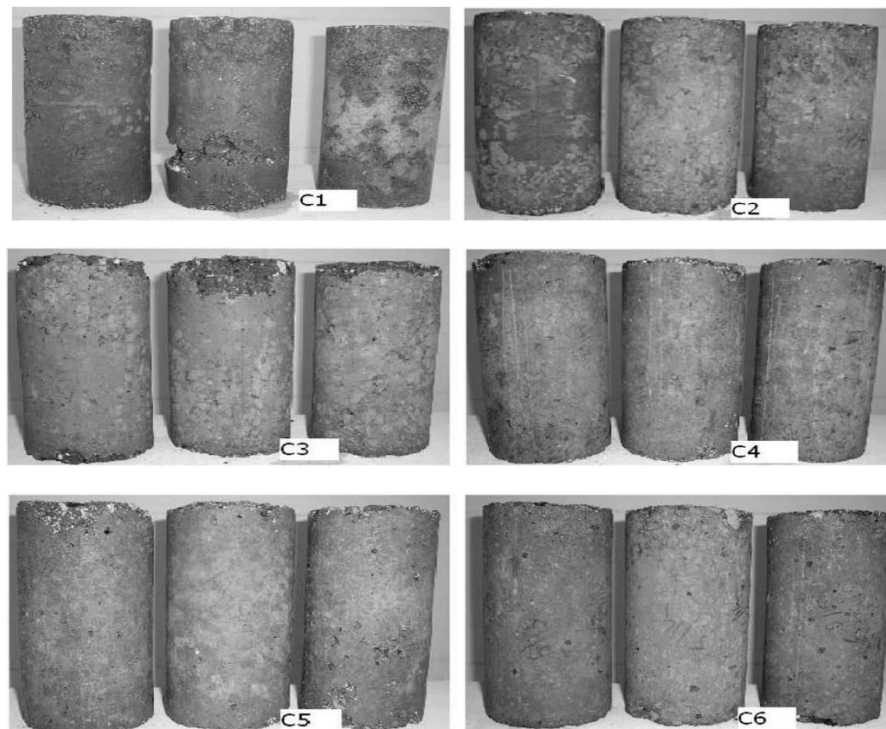


Figure 2. 20 Effect of freezing-thawing on MEPS concrete, C1: 50% fine MEPS + 50% coarse MEPS aggregate, C2: 25% fine MEPS + 50% coarse MEPS + 25% natural sand, C3: 50% coarse MEPS aggregate + 50% natural sand, C4: 50% fine MEPS and 50% coarse natural aggregate, C5: 25% fine MEPS + 25% coarse MEPS and 25% natural sand + 25% coarse natural aggregate, C6: 5% fine MEPS aggregate + 25% natural sand + 50% coarse natural aggregate [108].

Demirboga et al. [70] have investigated the influence of a modification method on thermal and shrinkage properties of expanded polystyrene concrete. They have found that increasing the volume of EPS particles leads to a reduction of workability and a harsh matrix was obtained mainly due to the shape of modified crushed EPS through the melting process and the lower density of EPS particles (

Table 2. 5).

Table 2. 5 Slump and fresh density of MEPS aggregate concrete [70].

Mix type	MEPS/NA ^a (%) (F+CA)/(F+CA ^b)	Cement (kg)	MEPS (kg)		NA ^a (kg)		SP ^c (kg)	w/c	Fresh density (kg/m ³)	Slump values (mm)
			F	CA	F	CA				
C1	50% + 50%/0%	500	108	77	-	-	2.5	0.38	876	25
C2	25% + 50%/25% + 0%	500	53	75	402	-	2.5	0.39	1229	30
C3	0% + 50%/50% + 0%	500	-	74	786	-	2.5	0.42	1572	30
C4	50% + 0%/0% + 50%	500	104	-	-	804	2.5	0.42	1621	30
C5	25% + 25%/25% + 25%	500	52	37	393	402	2.5	0.42	1596	40
C6	25% + 0%/25% + 50%	500	52	-	390	797	2.5	0.43	1956	50

^a NA: natural aggregate.

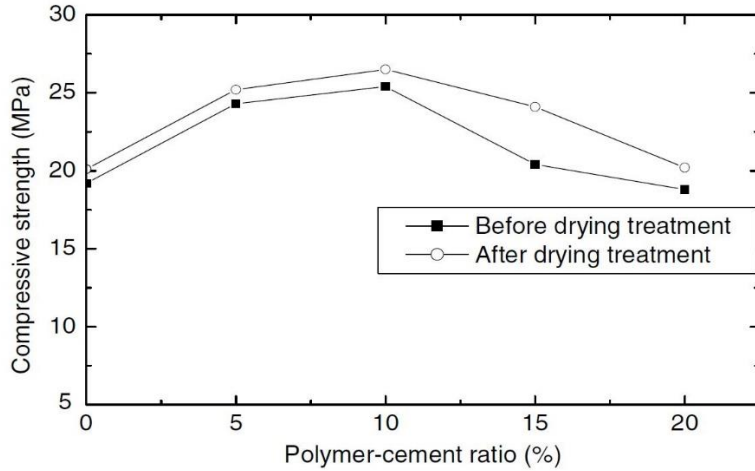
^b F+CA: fine and coarse aggregates.

^c SP: super plasticizer.

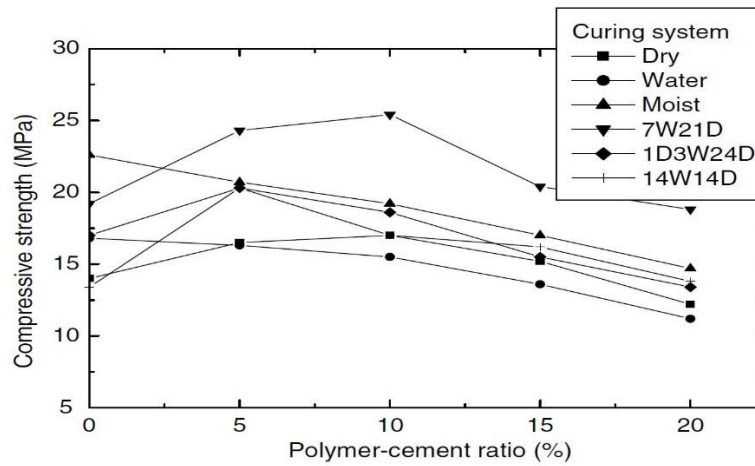
2.3.3.3 Influence of polymer additives on mechanical behaviour of EPS concrete

Chen et al. [109] have investigated an addition of styrene-butadiene rubber (SBR) latex resulting in higher interfacial bonding between EPS beads and cement paste due to a formation of SBR films in the cement matrix. A higher compressive strength of polymer modified EPS concrete was achieved with a 5-10% polymer-cement ratio. Whereas, a lower strength was observed as a higher cement-polymer ratio of 15% was added to the matrix. A significant improvement in compressive strength was observed with seven days water curing and twenty-four days dry curing. They have found that the water curing at the initial period enables the complete hydration of the cement matrix while the solidification of SBR latex takes place during dry curing in the later stage, as SBR latex is an aqueous polymer dispersion preferring dehydration and solidification under a dry condition. The dry curing condition reveals a low compressive strength as a result of insufficient strength development of the cement matrix. Dry treatment, i.e. the specimens were put into an oven for 24h at 80°C before testing, significantly increased the compressive and flexural strength of the polymer-modified EPS concrete as a results of the fact that dry treatment is the proper method for the

solidification of SBR latex. They have also found that increasing the amount of SBR latex was an effective way for an improvement in the strength of EPS concrete (Figure 2. 21).



(a)



(b)

Figure 2. 21 The relationship between compressive strength and polymer-cement ratio; (a) effect of drying treatment, (b) effect of curing conditions (7W21D (7 days water cured + 21 days air dried), 1D3W24D (1 day air cured + 3 days water cured + 24 days air cured), 14W14D (14 days water cured + 14 air cured day)) [109].

2.3.3.4 Influence of EPS aggregate size on mechanical properties of concrete

Researchers agreed that the compressive strength of concrete was increased with a smaller size EPS aggregate and concluded that the stress distribution within the matrix significantly

relies on the aggregate's elastic modulus and EPS particle size [98, 100]. Le Roy et al. [110] reported that the use of a larger EPS size contributed to decreased compressive strength of concrete (Figure 2. 22). They have confirmed that the rupture mechanism of EPS concrete is different from normal aggregate and this was attributed to the low modulus of elasticity of EPS beads and the fact that a stress concentration occurs in the vicinity of the aggregate. Daneti et al. [111] have investigated the relationship between aggregate size, compressive strength and moisture migration characteristics of concrete containing un-expanded polystyrene (UEPS). The compressive strength of concrete was decreased with an increase in UEPS particle size. It was also observed that the inclusion of UEPS aggregate results in a sudden and brittle failure. Compared with UEPS concrete, it is interesting to note that EPS concrete was more capable of retaining the load after failure without full fragmentation. Furthermore, the interfacial bonding strength between the polystyrene particles and the matrix was much higher in EPS particles than UEPS particles. It is worth to note that most of EPS aggregates sheared off along the failure plan while no damage was observed in UEPS aggregates. Miled et al. [99, 100] have concluded that the impact of aggregate size on the elastic modulus of concrete was minimal.

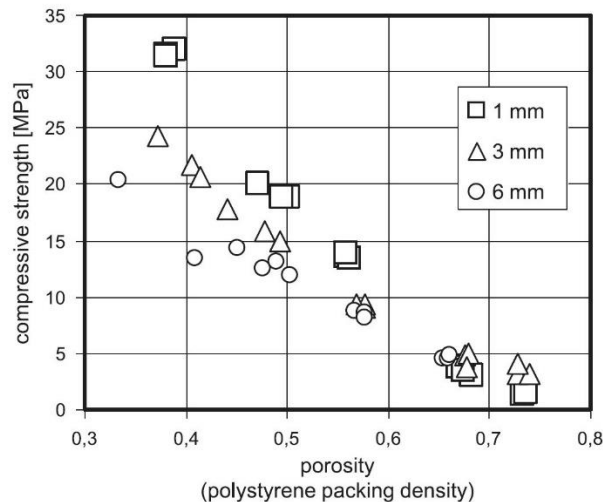


Figure 2. 22 Effect of EPS aggregate size on compressive strength of concrete [110]

2.3.3.5 Influence of fibrous additives on mechanical properties of EPS concrete

Chen et al. [93] found significant improvements in the mechanical properties of EPS concrete when steel fibres were used as an additive in the matrix. The drying shrinkage and

compressive strength of EPS concrete was reduced in the presence of steel fibres. Chen et al. [96] have reported that a considerable improvement in terms of interfacial bond, workability and ductility was obtained by replacing a certain amount of steel with polypropylene (PP) fibres. This phenomenon can be attributed to the formation of a network structure within the matrix which eliminates the sedimentation of EPS particles [112]. In addition, the fibres strangely affect the slump flow rather than the slump because of a holding effect of fibres and a reduction of surface bleeding of concrete. A higher compressive strength was obtained when a combination of steel and PP fibres was introduced to the matrix. The benefits of waste carpet polypropylene (WCPP) have been studied by Sadrmomtazi et al. [44]. The influence of WCPP fibres was more apparent in the tensile strength rather than the compressive strength and a minor development of greater toughness of concrete was observed with the inclusion of PP fibres (Figure 2. 23).

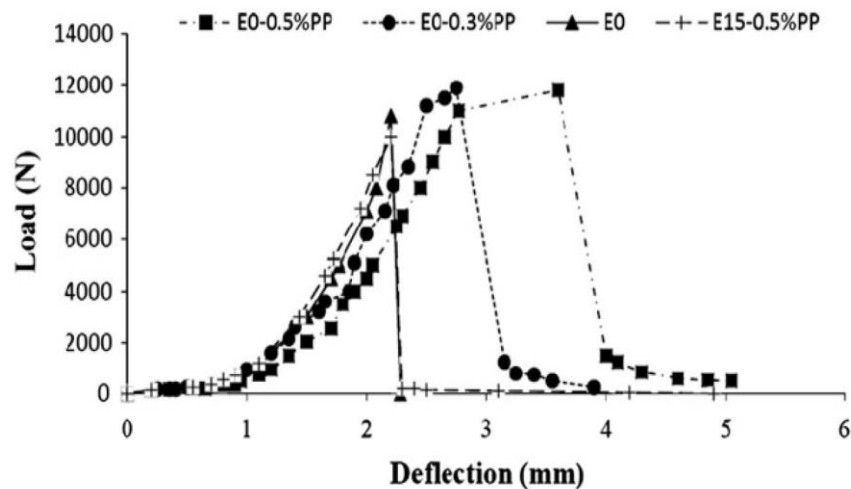


Figure 2. 23 Load-displacement behaviour of EPS concrete containing WCPP fibre [44].

Bing et al. [112] carried out an investigation of the influence of PP fibres on the drying shrinkage of EPS concrete. It was found that the inclusion of steel fibres, silica fumes (SF) and fly ash caused an improvement in mechanical properties of EPS concrete [8, 66, 93]. Ferrandiz-Mas et al. [113] have explored the influence of paper sludge ash and polystyrene aggregate on mechanical and thermal properties of lightweight mortar. The thermal conductivity (TC) of lightweight mortar was significantly decreased as paper sludge ash

(PSA) and EPS was used (Figure 2. 24). Furthermore, the application of ground EPS leads to a higher reduction of compressive strength rather than EPS powder and control mortars (Figure 2. 25).

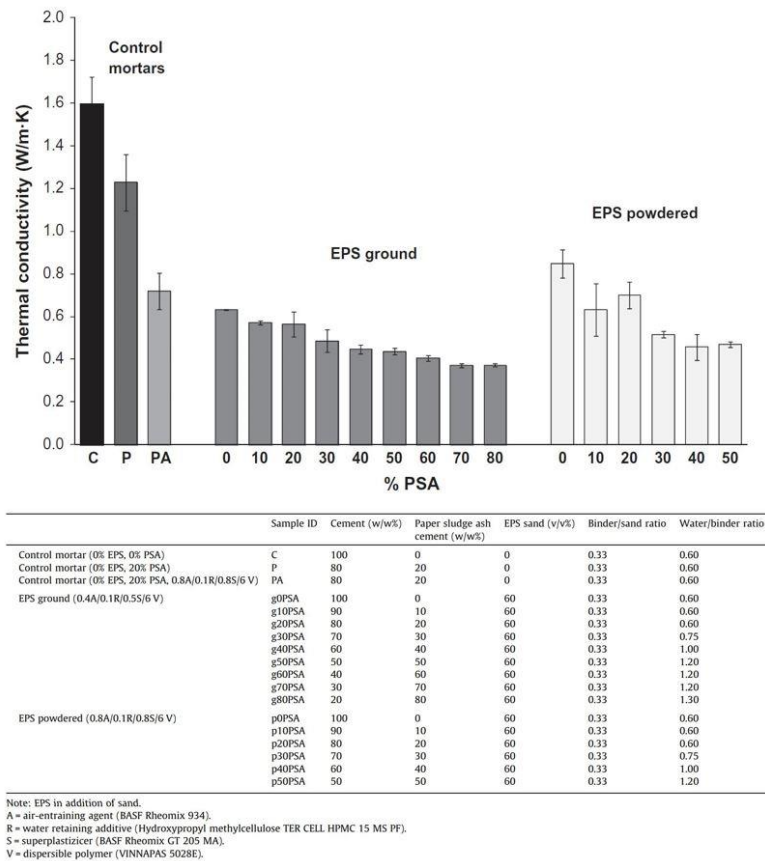


Figure 2. 24 The influence of paper sludge ash (PSA) addition on thermal conductivity of concrete [113].

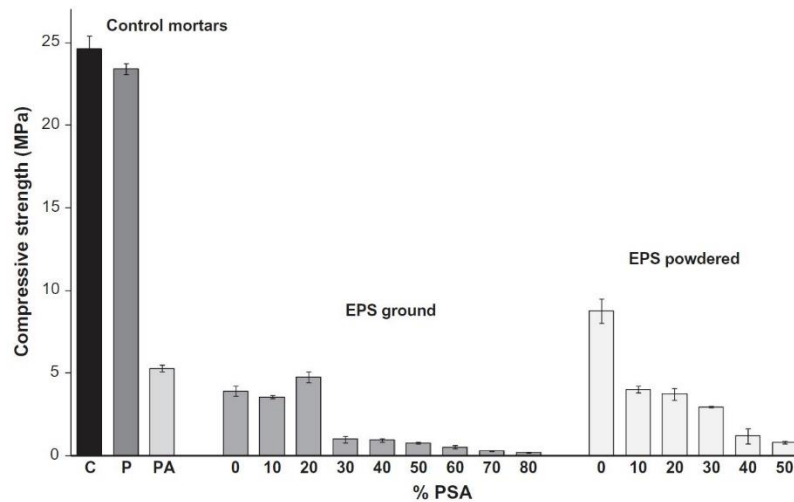


Figure 2. 25 The influence of paper sludge ash (PSA) addition on compressive strength of concrete [113].

2.3.3.6 Influence of fly ash on mechanical behaviour of EPS concrete

Compressive strength of lightweight concrete is a factor of aggregate strength. Partial replacement of natural aggregate with polystyrene aggregate causes a considerable reduction of compressive strength, unit weight and E-modulus of concrete. Moreover, the drying shrinkage and creep value of concrete was enhanced in the presence of EPS aggregate [66, 106, 114]. The inclusion of fly ash (FA) causes a continuing gain in compressive strength up to 90 days. However, a lower early compressive strength was obtained through the presence of FA, due to the slow pozzolanic reactivity of fly ash. Several studies have indicated that the inclusion of FA causes a higher workability and eliminates the segregation of fresh EPS concrete. However, Herki et al. [115] have concluded and reported that an increase in FA volume results in lower workability due to the higher amount of carbon content in fly ash, which demands for more mixing water. They have reported that the addition of FA as a partial replacement of Portland cement resulted in a lower absorption value, better chemical resistance and lower corrosion rate. A significant improvement in binding capacity, pore structure and impermeability of concrete was obtained as fly ash replaced 50% of cement content. A decrease in compressive strength was observed (Figure 2. 26) with a higher amount of EPS and fly ash due to the surface area of very fine particles leading to weakening of the interfacial zone between the aggregate and the cement paste. A similar study on mechanical properties of EPS concrete containing fly ash has been done by Badu et al. [66].

They have found that the hydrophobic nature of EPS can be compensated by using fly ash as a bonding additive.

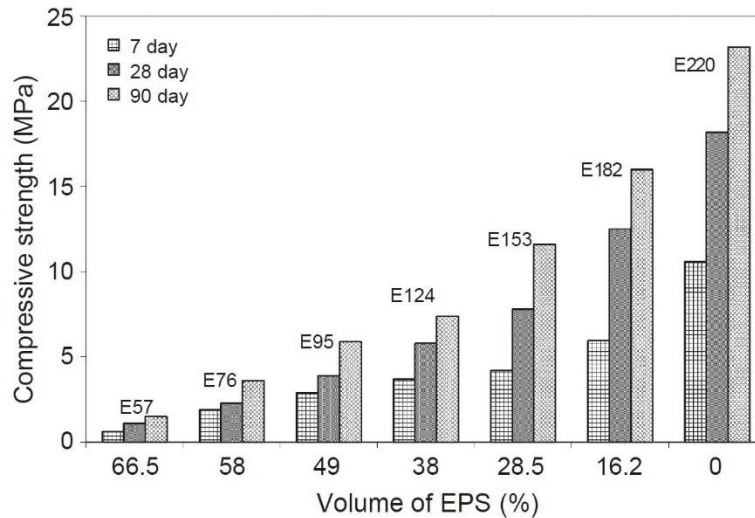


Figure 2. 26 Effect of EPS volume on compressive strength of concrete containing 50% FA - 50% cement [115].

2.3.3.7 Influence of silica fume and rice husk ash on mechanical behaviour of EPS concrete

Several researchers have studied the effectiveness of silica fume (SF) on mechanical properties of expanded polystyrene concrete [8, 44, 112]. The findings revealed that the inclusion of SF resulted in an improved absorption value and reduced flow value [112]. The strength of concrete appears to decrease with an increase in the volume of EPS. Sadrumontazi et al. [44] also carried out a study on partially replacing Portland cement with SF in EPS concrete. It was reported that the increase in replacement ratio results in an improvement in terms of strength increment rate at the initial ages of concrete. The interfacial bond strength between EPS aggregate and cement paste and compressive strength increase with the inclusion of SF. The inclusion of silica fume imposes the inverse effect on compressive strength as the volume of EPS reached up to the 60%. Furthermore, a higher electrical resistivity level was observed in samples containing larger EPS volumes. This trend was much stronger in samples made by silica fume and rice husk ash compared to normal concrete (Figure 2. 27).

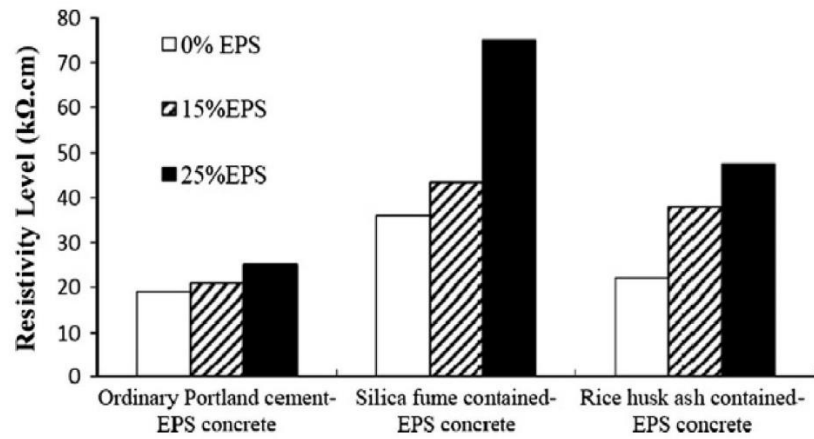


Figure 2. 27 Effects of EPS beads ratio and binder on electrical resistivity of concrete [44].

Sadrumontazi et al. [44] have found that the water absorption value of polystyrene concrete was increased as a higher volume of EPS replaced normal aggregate (Table 2. 6). They have concluded that the higher amount of micro-cracks between the elements of the matrix and hydrophobicity of EPS spheres resulted in higher porosity and water absorption. In addition, a significant increment rate in terms of water absorption and porosity of concrete was obtained when PP fibres are used (Figure 2. 28).

Table 2. 6 Effect of fibre, EPS percentage and binder on water absorption ratio of concrete [44].

Description	Fiber percentage	EPS percentage				
		0	10	25	40	55
Ordinary portland cement-EPS concrete	0	4.87	5.64	6.79	8.7	11.05
	0.1	4.92	5.65	6.77	8.78	11.14
	0.3	5.03	5.68	6.83	8.83	11.16
	0.5	5.21	5.78	6.92	8.85	11.31
	1	5.32	5.86	6.96	8.89	11.45
	Average	5.07	5.722	6.854	8.81	11.222
Silica fume contained-EPS concrete	0	4.27	6.14	6.14	8.55	10.43
	0.1	4.31	6.15	6.2	8.59	10.59
	0.3	4.35	6	6.25	8.67	10.51
	0.5	4.42	6.6	6.38	8.7	10.68
	1	4.49	6.83	6.49	8.73	10.81
	Average	4.368	6.344	6.292	8.648	10.604
Rice husk ash contained-EPS concrete	0	6.95	7.98	8.7	11.76	11.6
	0.1	7.16	8.21	8.81	11.68	11.81
	0.3	7.35	8.29	8.79	11.81	11.8
	0.5	7.62	8.39	8.92	11.92	11.91
	1	7.64	8.46	9.21	11.92	12.12
	Average	7.344	8.266	8.886	11.818	11.848

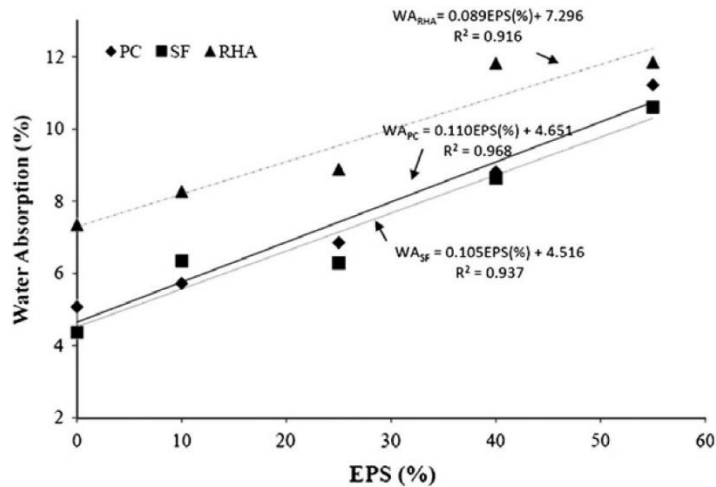


Figure 2. 28 Effect of EPS percentage on water absorption ratio of concrete; PC: Portland cement contained EPS concrete, SF: Silica fume contained EPS concrete, and RHA: Rice husk ash contained [44].

Sadrmomtazi et al. [44] have used rice husk ash (RHA) as partial cement replacement in EPS concrete and reported a considerable reduction of compressive strength due to the slow pozzolanic activity of RHA. However, this variation was minimal at the later stage of hardening as the differences between compressive strength of EPS and RHA EPS concrete were minor. The flexural strength of polystyrene concrete is decreased with an increase in EPS and rice husk ash (RHA) volume. The mechanical, durability and porosity characteristic of polystyrene concrete was improved by the incorporation of silica fume, while RHA imposes an inverse effect. In addition, the electrical resistivity of concrete was increased in the presence of SF and RHA.

2.3.4 Foamed concrete

Foamed concrete can be produced by a pre-foaming method or mixed foaming method [116]. Mortar or cement paste foamed concrete (air-entraining concrete) is categorised as lightweight concrete due to the existence of larger amounts of homogeneous air-voids inside the matrix through a suitable foaming agent. This method causes high flow-ability, lower unit weight, minimal consumption of aggregate and reduced thermal conductivity. The factors such as foam agent specification, foam preparation method, material characteristics, mix design method, foam concrete production and its performance in fresh and hardened

state are significantly important for the design of foamed concrete [117]. Increasing the early strength of foamed concrete along with a reduction in setting time is obtained by using calcium sulfoaluminate cement [118], high alumina cement [118], and rapid hardening Portland cement [119]. Substitution of fly ash (30-70%) [119, 120] with ground granulated blast furnace slag (10-50%) [121] significantly reduces the hydration heat, cost and increases the consistency of the mixture, whereas silica fume of up to 10% substantially improves the strength of foamed concrete [122]. The density and unit weight of foamed concrete was reduced by the addition of lime [123], oil palm shell [120], fly ash [124, 125], chalk [126], crushed concrete [126], silica fume [127], expanded polystyrene [67, 102], Lytag fines, foundry sand [128] and quarry finer [128] as fine aggregate.

Proportioning and preparation of foamed concrete needs special consideration as a lower water content causes the bubbles to break along with a stiff mixture, while segregation of bubbles occurs with a higher water content [129]. ASTM C 796-97 [130] and ACI 523-1975 [131] provide a method for calculation of foamed volume with known water-cement ratio and density, while Kearsely and Mostert [124] proposed an equation based on mixture composition for estimating the foam volume and cement content. The mechanical properties of foamed concrete and its behaviour are directly influenced by the water-cement ratio, sand-cement ratio, type of foaming agent, water content, cement content, foam volume, ingredients characteristics, mixing method, curing method, pore formation method and void diameter [117, 129, 132-137]. The compressive strength of foamed concrete enhances with an increase in density of the concrete and is decreased with increasing the diameter of voids. Thus, the strength of foamed concrete mainly depends on (a) water-cement ratio and (b) air-cement ratio.

Kearsley and Mostert [138] proposed a mix design method for foamed concrete containing high volumes of fly ash. They have concluded that the required water content can be obtained by using a flow table test (Figure 2. 29) and found that the compressive strength of foamed concrete is a factor of concrete density, while the influence of cement and fly ash content on strength development of foamed concrete was minimal. Furthermore, the effect of void content appears to counteract the influence of the water-cement ratio on compressive strength of concrete (Eq. 2.1 and Eq. 2.2).

$$\rho_m = x + x \left(\frac{w}{c} \right) + x \left(\frac{a}{c} \right) + x \left(\frac{s}{c} \right) + x \left(\frac{a}{c} \right) \left(\frac{w}{a} \right) + x \left(\frac{s}{c} \right) \left(\frac{w}{s} \right) + RD_f V_f \quad (2.1)$$

$$1000 = \frac{x}{RD_c} + x \left(\frac{w}{c} \right) + \frac{x \left(\frac{a}{c} \right)}{RD_a} + \frac{x \left(\frac{s}{c} \right)}{RD_s} + x \left(\frac{a}{c} \right) \left(\frac{w}{a} \right) + x \left(\frac{s}{c} \right) \left(\frac{w}{s} \right) + V_f \quad (2.2)$$

Where,

ρ_m is the target casting density (kg/m^3)

x is the cement content (kg/m^3)

$\frac{w}{c}$ is the water/cement ratio

$\frac{a}{c}$ is the ash/cement ratio

$\frac{s}{c}$ is the sand/cement ratio

$\frac{w}{a}$ is the water/ash ratio

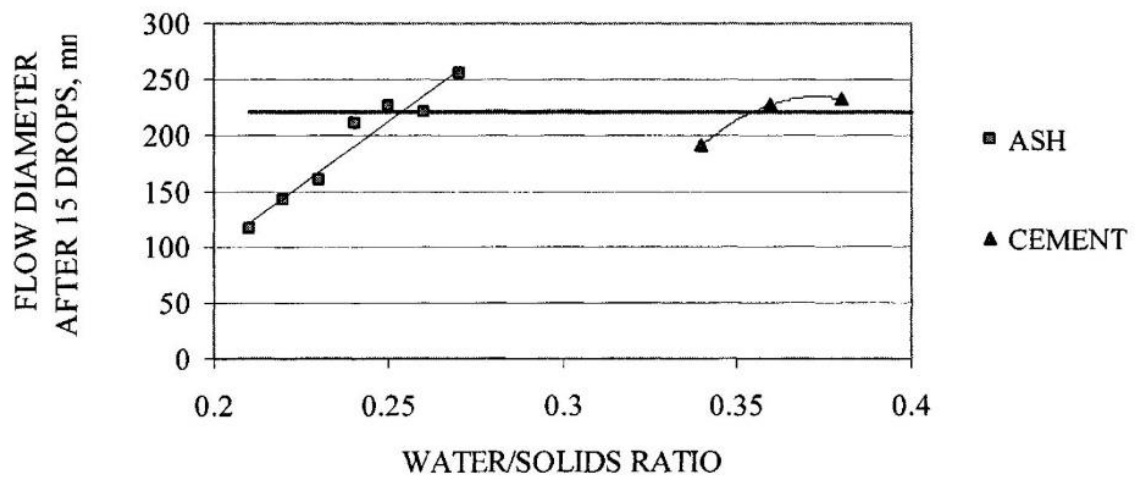


Figure 2. 29 The required water content for cement and fly ash [138].

Hilal et al. [132] investigated the influence of different additives on the strength development and microstructure of foamed concrete by a variation of air-void size and shape parameters. They have found that the additives lead to an increase in void numbers and foam strength as a result of the formation of smaller void sizes and the prevention of air-voids merging. In addition, the application of superplasticizer improves the air structure when combined with additives. Chen and Liu [102] investigated the influence of foam content on mechanical and thermal properties of EPS concrete. They have found that an adequate amount of foam content leads to a significant improvement on workability and reduces the floating problem of EPS aggregate (Figure 2. 30). Furthermore, the replacement of EPS beads with foam

causes an increase in mechanical properties of foamed concrete. They have suggested that the optimum foam content is about 10-15% of total volume. Also, the EPS foam concrete exhibited a ductile behaviour and higher energy absorption capacity compared to normal concrete. Regarding thermal properties, a significant reduction in thermal conductivity of concrete was observed with the incorporation of foam and EPS aggregate (Figure 2. 31).

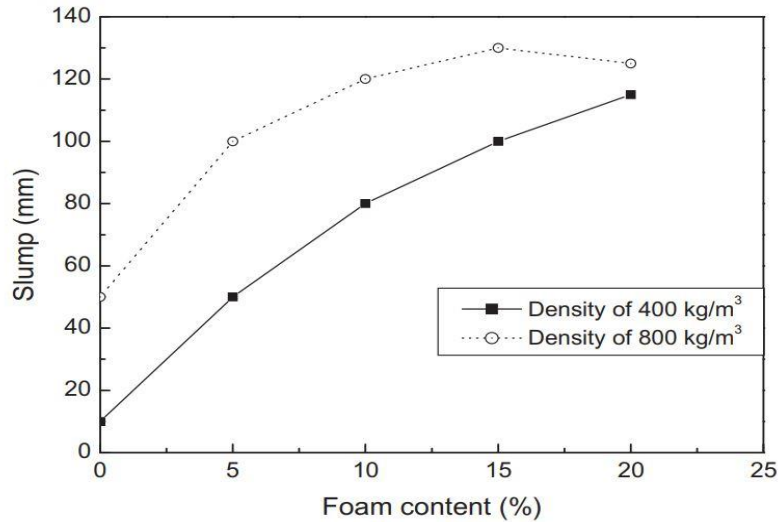


Figure 2. 30 The effect of foam content on workability of foamed concrete [102].

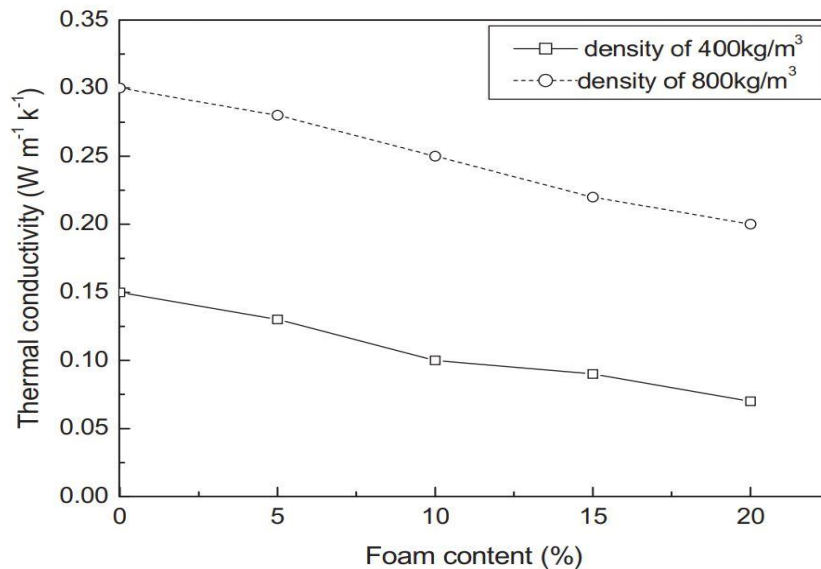


Figure 2. 31 The effect of foam content on thermal conductivity of foamed concrete [102].

Zhihua et al. [137] studied the preparation and characterisation of ultra-lightweight foamed concrete at the density ranges of 150-300 kg/m³. They have found that a significant

improvement in mechanical properties of concrete was obtained using the appropriate amount of polycarboxylate superplasticiser and ultrafine blast furnace slag powder (Table 2. 7). The surface dusting phenomenon of ultra-lightweight foamed concrete was controlled by using polypropylene (PP) fibres and styrene-acrylate emulsion. The application of organic silicone waterproofing agent and styrene-acrylate emulsion leads to a noticeable improvement in water resistance of foamed concrete.

Table 2. 7 The mechanical and thermal properties of ultra-lightweight foamed concrete [137].

No.	Target density kg/m ³	Compressive strength (MPa)			Thermal conductivity (W/mK), at 28 d age	Water absorption (%), at 28 d age
		3 d	7 d	28 d		
1	300	0.66	0.91	1.10	0.071	6.6
2	250	0.57	0.78	0.95	0.062	7.0
3	200	0.45	0.63	0.78	0.057	7.6
4	150	0.33	0.46	0.57	0.050	8.3

The effect of a high volume fly ash content on mechanical properties of foamed concrete was studied by Kearsley and Wainwright [119]. They have concluded that the density of concrete is a critical factor that affects the compressive strength of foamed concrete after 28 days and 1 year, and the influence of fly ash content and its replacement ratio with cement was minimal. Also, it was found that the replacement of cement with a high percentages of fly ash has a minor effect on the long-term compressive strength of foamed concrete. In another study, Kearsley and Wainwright [133] investigated the relationship between foamed concrete porosity and compressive strength (Figure 2. 32). They also developed mathematical models to describe the correlation between porosity and strength development of foamed concrete. It was found that the compressive strength of foamed concrete is a factor of concrete porosity and its ages. Kearsley and Wainwright [120] have also reported that the porosity of foamed concrete mainly depends on dry density and the influence of the fly ash type and the content was insignificant. The water absorption of foamed concrete is about twice that of cement paste concrete with the same water-cement ratio (Figure 2. 33), and the impact of an air entraining agent was minimal. They found that the water absorption ratio of concrete was increased with an increase in concrete porosity and foam content. In addition, they have found that the water vapour permeability enhanced with an increase in concrete porosity and

the same trend was observed as the ash/cement ratio increased. However, the significance of the ash/cement ratio and concrete porosity on vapour permeability of foamed concrete was more notable in low density foamed concrete (Figure 2. 34).

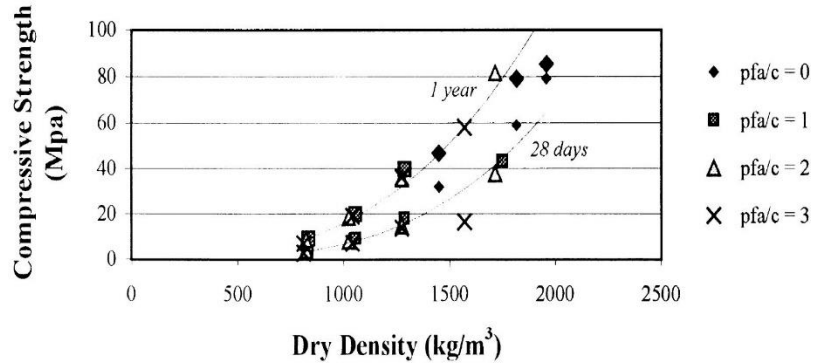


Figure 2. 32 The relationship between compressive strength and dry density [133].

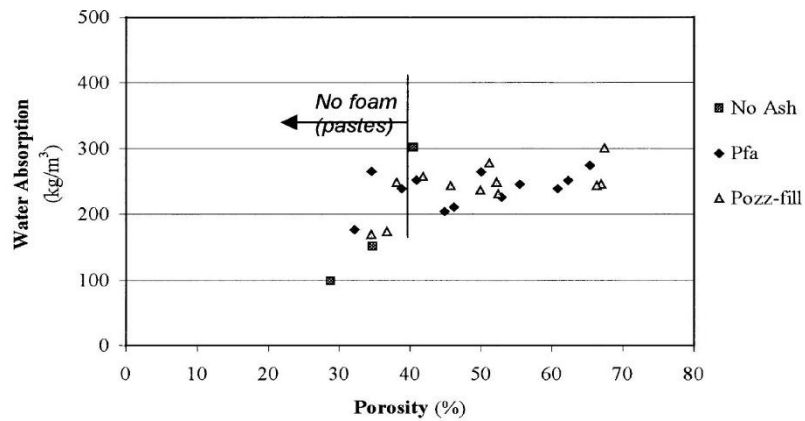


Figure 2. 33 The relationship between water absorption and porosity [120].

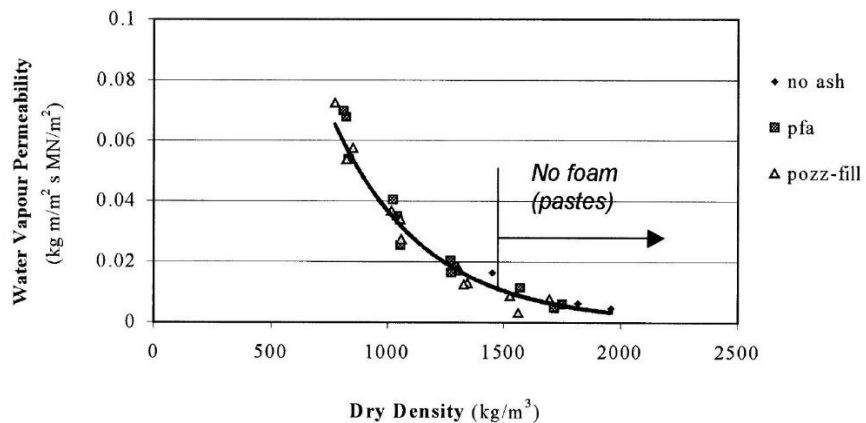
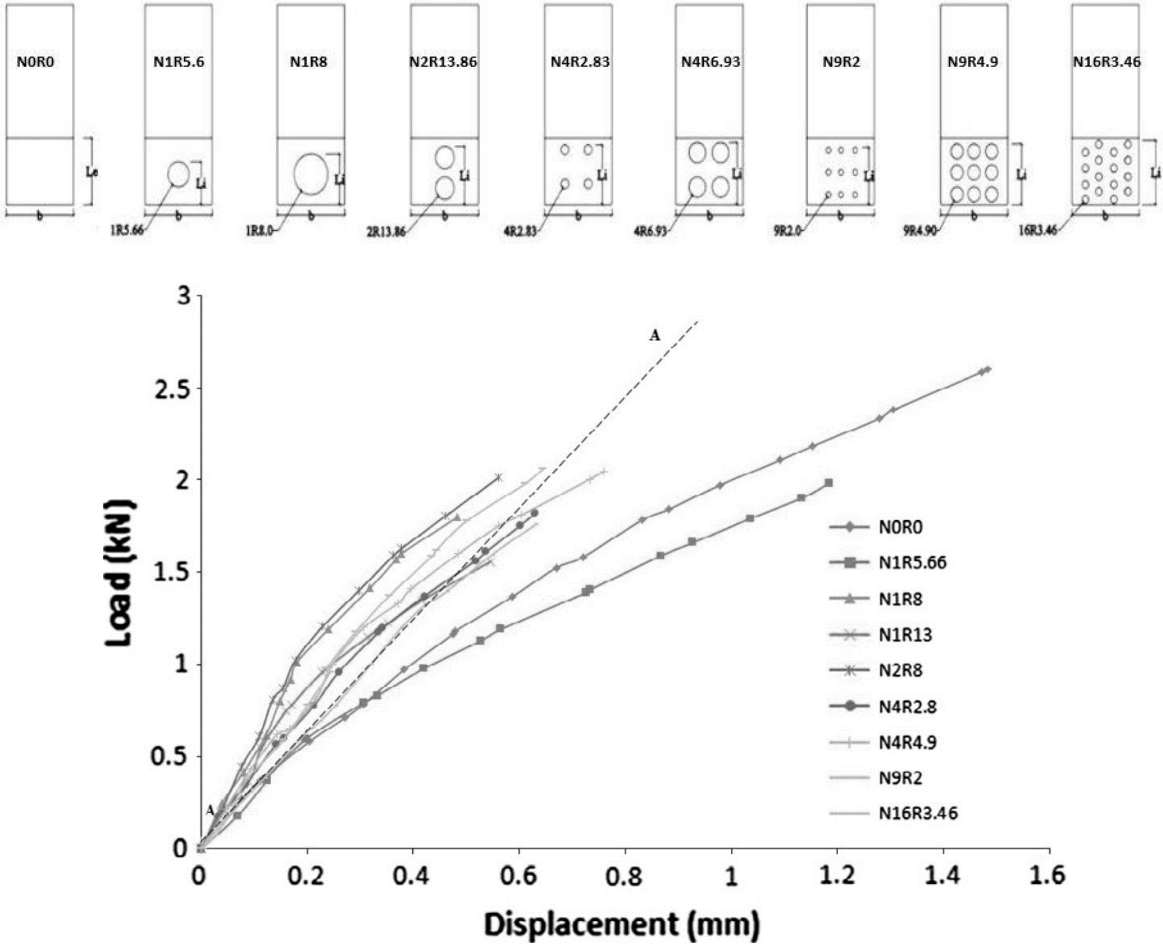


Figure 2. 34 The relationship between water vapour permeability and dry density [120].

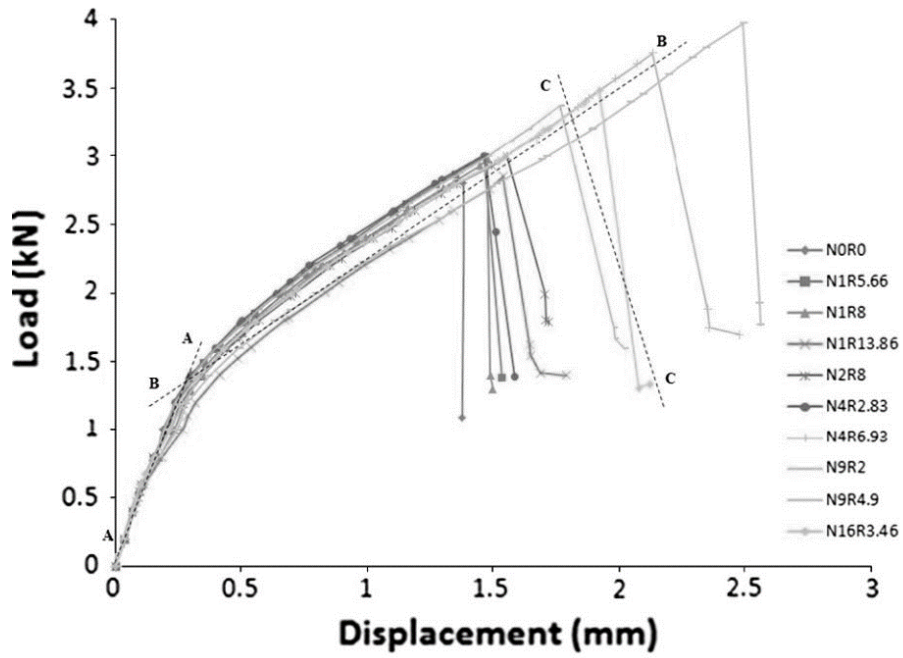
2.4 Application of lightweight concrete (LWC)

2.4.1 LWC as filler of composite structural assemblies (CSAs)

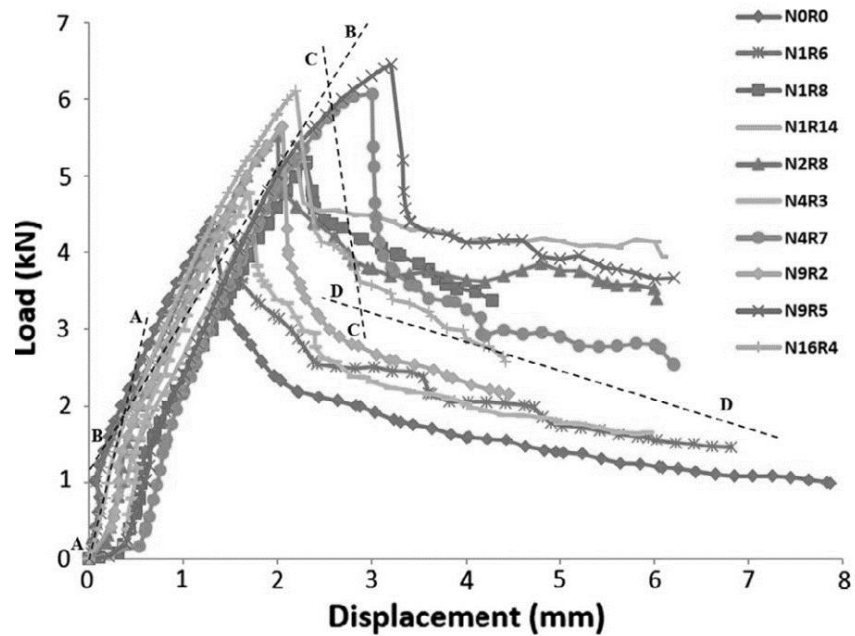
Composites structural assemblies (CSAs) consist of a settable filler such as lightweight concrete embedded in light gauge steel components which are mostly used as roof and wall panels [139, 140]. The performance of CSA panels significantly depends on the thickness of components and mechanical properties of infill materials [140]. A higher tensile capacity was observed in embedded elements with a larger thickness due to the bearing and interlocking action of components [139]. Moreover, it was found that the parameters such as elastic and inelastic length of embedded elements, the locking area in the elastic and inelastic zone, locking patterns of integrated components and compressive strength of infill materials directly affect the bond properties of embedded strips (Figure 2. 35) [139, 140].



(a)



(b)

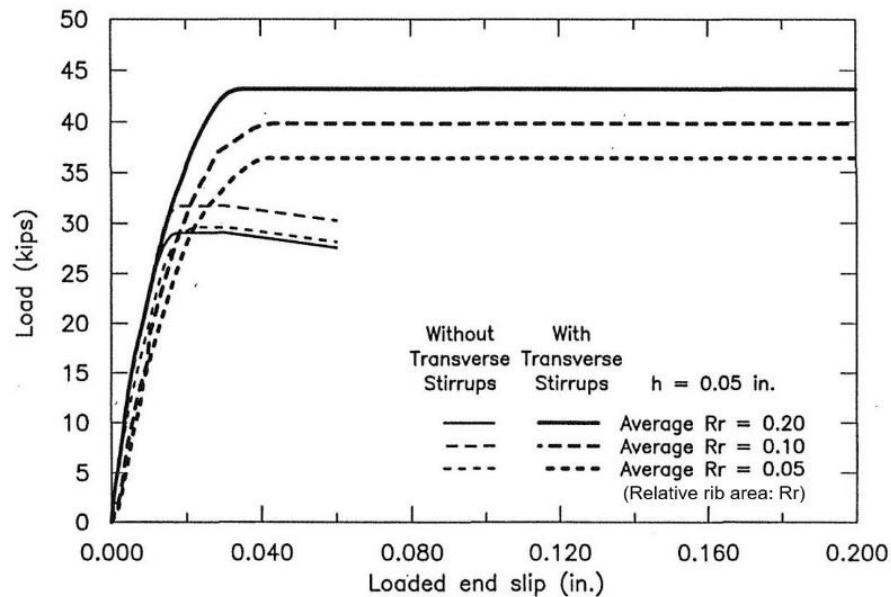


(c)

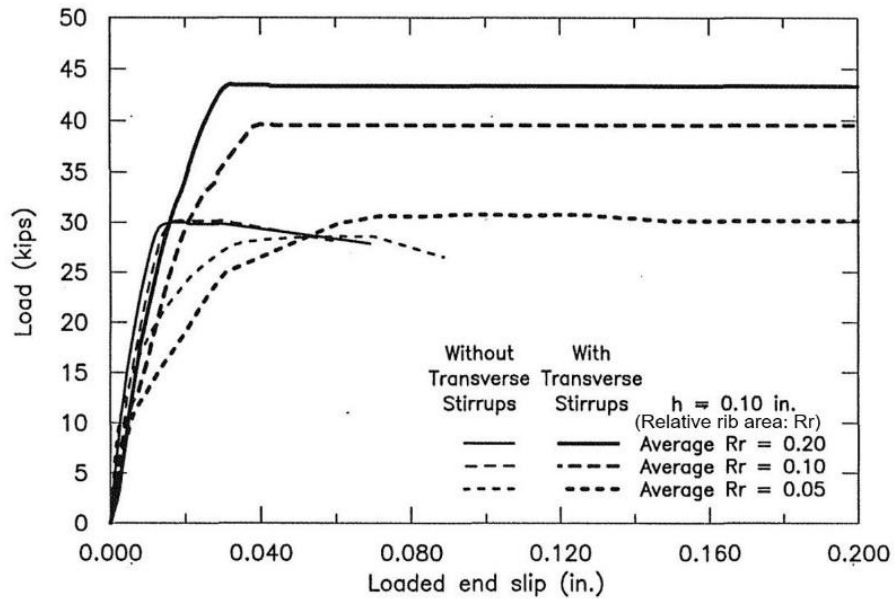
Figure 2. 35 Load-displacement behaviour of concrete with densities of (a) 800kg/m^3 , (b) 1000kg/m^3 , (c) 1200kg/m^3 [139, 140].

The interaction between the components of a matrix significantly relies on their bond strength. The degree of bond strength between the components of a composite matrix is attributed to a wide range of factors [141]. The literature contains many investigations about

rebars embedded into concrete. The bond mechanisms of a composite matrix and its strength depend on the magnitude of shear stress generated by chemical adhesion, friction and mechanical interlocking between the embedded rebar and the matrix [142, 143]. The resisting force associated with chemical adhesion breaks down at very small displacements between the embedded bar and the surrounding concrete of 0.48-1.03 MPa compressive strength [144]. The surface friction, which is up to 35% of the resisting force [145, 146], and mechanical interlocking between ribs and adjacent concrete keys are the main factors contributing to the resisting force [146]. Thus, the bond strength of a composite matrix is initially caused by the mechanical interlocking between the ribs and the concrete keys. At the ultimate stage, slippage occurs as shear cracks propagate at the interface zone of concrete and ribs as a result of a large bearing stress around the ribs [147]. It has been confirmed that the concrete strength [185-189], steel strength, concrete cover thickness [148, 149], transverse reinforcement, bar spacing [150], bar size [142], bar features (Figure 2. 36) [150-152], yield strength of embedded bar [141], bar casting position [153], confinement [154] and elastic and inelastic segment length [142, 143] substantially affect the magnitude of the bond strength.



(a)



(b)

Figure 2.36 Load - slip curves for test bars with (a) rib height of 0.05 in, (b) rib height of 0.10 in [152].

The mechanical characteristics of concrete affect the magnitude of bond stress as the development of micro cracks and transferring the shear force between the components of the matrix are attributed to the tensile stresses of concrete [148]. Moreover, increasing the compressive strength of concrete results in higher bond stress developed over the length of a spliced bar and affects the modes of bond failure [149]. Several equations are proposed by researchers to estimate bond stress at yield and ultimate stage [145, 155]. The bond stress over the length of an embedded bar for concrete with a compressive strength lower than 55 MPa is the square root of its compressive strength ($f_c^{1/2}$) [145], whereas the bond stress for unconfined and confined concrete with a compressive strength higher than 55 MPa is $f_c^{1/4}$ and $f_c^{3/4}$, respectively [155, 156]. The thickness of concrete significantly affects the bond stress due to the fact that a higher thickness is resulting in a higher confinement pressure [142].

The effects of embedded bar geometry [150], rib bearing area [157, 158], and rib face angle [156] have been studied by several researchers [150, 159]. The features of an embedded bar rib and its interlocking mechanism considerably affect the bond strength as a result of the significance of the mechanical interlocking on the bond strength [152, 158]. Test results show that a reduction in rib face angle results in lower bond strength along with less concrete

crushing at the interface of the steel bar and surrounding concrete [150]. Confinement is a significant technique to enhance the bond strength of an embedded bar [143]. Other researchers show that increasing confinement pressure and controlling the spread of splitting cracks by transvers reinforcement [8], spiral reinforcement [155, 160], shear bolts [143], aluminium tube [161], steel pipe [143, 155, 160, 162], square hollow section, and fibre reinforced polymer (FRP) [142] significantly enhance the bond strength of an embedded bar and change the modes of failure.

Splitting and pull-out failure are two modes of bond failure [145]. The mode of failure changes from pull-out to splitting failure when the concrete cover and bar spacing is inadequate, i.e. insufficient confinement. In this case, cracks tend to propagate under the radial component of the rib bearing forces parallel to the embedded bar resulting in early bond failure [145]. The load-slip relation of concrete is an important factor in the design of concrete structures and the understanding of the mechanism of bond and its parameters are significant. Pull-out, beam-end, beam anchorage and splice test are four types of standard tests for estimating the bond behaviour between the components of a composite matrix. The pull-out test is useful in assessing the load-slip relationship of reinforcing bars, however this method only applies a tensile load and does not reflect the state of stress in a composite matrix in use. In a recent study, Sayadi et al. [139, 140] proposed a bond stress-slip model for embedded galvanised strips in foamed concrete and concluded that the compressive strength of foamed concrete, pattern configuration of embedded strip and strips thickness are the main factors that affect the failure modes and tensile capacity.

2.4.2 LWC as bracing components of cold formed members

The demand for lightweight and cost-effective structures is increasing rapidly. Cold-formed steel (CFS) elements are one form of fast and efficient construction methods. The research of cold-formed structures tracks back to the middle of the 20th century [163]. Up to now, a number of experiments have been done to assess the stability behaviour of cold-formed members under different load conditions and to support standardized formulae [163-168]. The AISI S100-07 [169], AS/NZS 4600 [170] and EC-EN 1993-1-3 [171] are design codes for CFS elements in the USA, Australia/New Zealand, and Europe, respectively. The cold-formed steel members are used as main load-bearing structures in residential and commercial

construction [168]. Self-drilling screws join the sheathing and CSF members at connection points. The research of the influence of braced cold-formed members shows that failure modes changed from global to local deformation (Figure 2. 37) and led to a significant increase in load carrying capacity of CFS members (Table 2. 8) [164, 165].

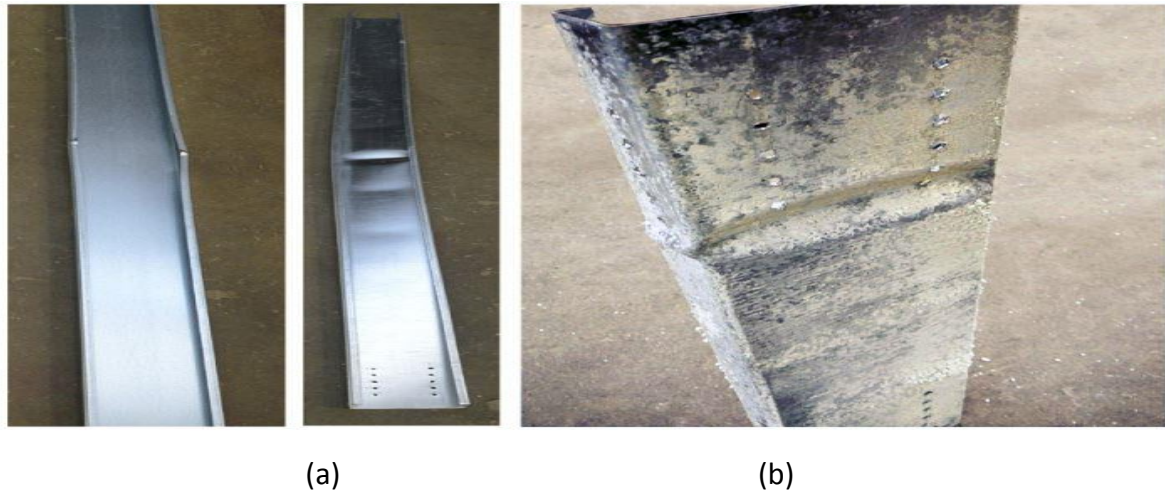


Figure 2. 37 Failure modes of cold formed column; (a) unbraced sample, (b) braced sample (filled with EPS concrete)

Table 2. 8 Effect of polystyrene aggregate concrete (PAC) bracing on ultimate load capacity of a cold formed column.

specimen type	Number of specimens ^a	Ultimate load [kN]			Increment [%]	
		Unbraced - 0	Braced - A	Braced - X	Braced - A	Braced - X
C90-10-300	3/3/2	27.34	38.93	40.26	42	47
C90-10-600	3/2/3	27.34	37.80	37.44	38	37
C90-10-2000	3/3/3	17.76	34.44	33.57	94	89

^a Numbers correspond to specimens without PAC mixture, with mixture A, and mixture X, respectively.

Hegyí and Dunai [164] have reported that filling the steel core of CFS members with polystyrene aggregate concrete (PAC) increases the load carrying capacity and changes their failure mode (Figure 2. 38). They also showed that the primary beneficial influence of the infill material was its bracing action. The research on U-section CFS members reveals that local phenomena were the main failure modes and found that the influence of sheathing on the local buckling of the web was insignificant but causes an increase of 80% in load capacity

as a result of its impact on overall buckling [172]. In addition, they have found the increment rate is a factor of the specimens' properties.

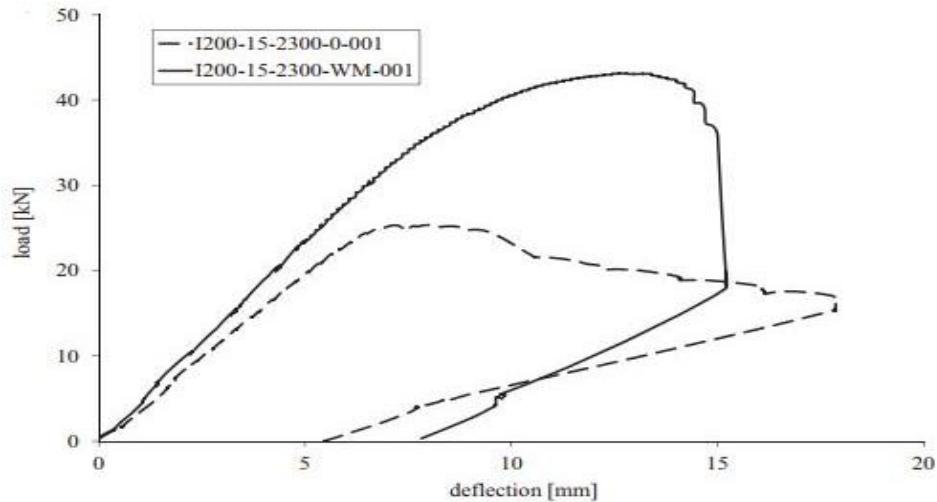


Figure 2. 38 Effect of PAC bracing on load carrying capacity of a cold-formed beam where I200-15-2300-0-001 and I200-15-2300-WM-001 are the control and sample with bracing component [164].

The shear performance of enclosed panels was studied by Pan and Shan [173]. They have reported that the influence of the infill material on the structural behaviour of the panel was notable and affects the structural stiffness. In addition, they observed a 46% greater stiffness in samples filled with orientated strand board (OSB) compared to gypsum board.

2.5 Application of Poly-lactic Acid

In recent years, the research on improvements of PLA has progressed considerably, while no literature has been published on application of poly-lactic acid as lightweight aggregate. Poly-lactic acid (PLA) is categorized as a biodegradable polymer and known as the most popular bio-degradable polymer among the other polymers. PLA was discovered in the 1800s when Pelouze condensed lactic acid through a distillation process of water to form low-molecular-weight PLA. However, the purification cost of the proposed method to produce a high purity PLA was not viable at a larger scale. Many efforts have been done to form a cost

effective PLA. Generally, PLA can be obtained from the fermentation of dextrose by bacteria, where dextrose is derived from plant starch.

Various types of renewable bio-polymers such as Polycaprolactone (PCL), Polyglycolic acid (PGA), Polyhydroxyvalerate (PHBV), Polydioxanone (PDO) and cellulose acetate are commercially available. Petroleum-derived poly vinyl alcohol or PVOH and microorganism-derived poly-lactic acid (PLA) are two types of biodegradable polymers. However, the petroleum-derived polymers are categorized as non-environmental friendly polymers because of the emission of greenhouse gases associated with the production and degradation process. The production cost of a petroleum-derived polymer mainly depends on the fluctuation of crude oil prices. The production process of microorganism-derived polymers is based on bio-activity of bacteria to transfer agricultural sources into starting products for polymerization [49, 50]. From all the available bio-polymers, poly-lactic acid (PLA) is one of the widely available and more cost-competitive bio-plastics which is progressively preferred as an alternative for current petrochemical polymers like polyethylene, polypropylene and polystyrene. Preliminary tests by Forest Research Scion, an expanded poly-lactic acid (EPLA) manufacturer in New Zealand, proved that the thermal and mechanical properties of EPLA are comparable with EPS and it can be considered as a good substitution for a petroleum polymer [51-53].

2.6 Research questions

For the past several decades, the incorporation of expanded polystyrene as a lightweight aggregate has been extensively studied due to its interesting mechanical and thermal properties, while no information is available on the performance of concrete containing a bio-polymer. In this work, expanded poly-lactic acid is applied as a substitution for a petrochemical polymer and as a basis for a comprehensive study on the performance of EPLA concrete. From the description of the state of the art of lightweight concretes in the literature review the following research questions are created:

- 1- Is it possible to replace EPS with a more environmentally friendly aggregate in lightweight concrete?
- 2- What are the properties and characteristics of a lightweight concrete containing a biopolymer aggregate?
- 3- What is the optimum mixture of materials for a stable and reproducible ultra-lightweight concrete with the inclusion of EPLA beads and a target density of 200 to 300 kg/m³?
- 4- What are quantifiable potential advantages of the developed material in terms of mechanical and thermal behaviour such as fire and thermal insulation compared with existing ultra-lightweight concretes?
- 5- What kind of modifications are required to increase the stability of EPLA beads in the alkaline environment of cement? What are the optimum process conditions for such a material?
- 6- What kind of modifications at the interface of sandwich panels are required to increase the bond strength between embedded components and ultra-lightweight concrete?

CHAPTER 3

EXPERIMENTAL PROGRAM

3.1 Introduction

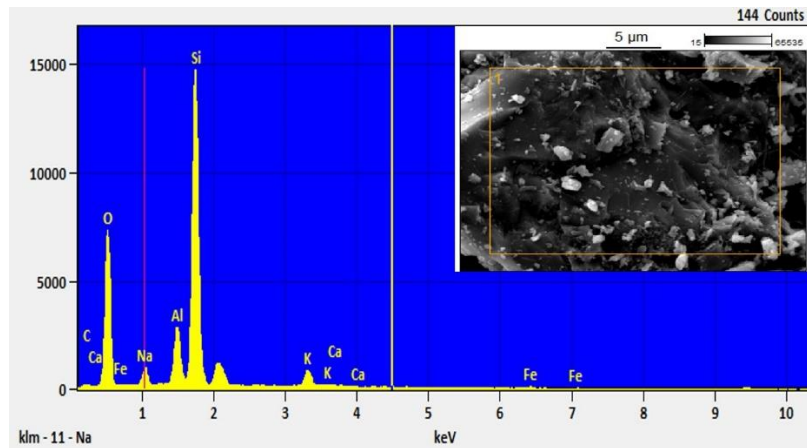
This chapter presents the raw materials used to produce concrete at different stages of experiments along with test preparations and experimental methods. In addition, a new method is proposed for the mix design of ultra-lightweight aggregate concrete. The detailed mix design compositions will be described as experimental procedures of each chapter. The combination of materials such as Portland cement, magnesium oxide (MgO), calcium oxide (CaO), and ammonium dihydrogen phosphate are used as binder in this study. Also, five types of lightweight aggregate, i.e. expanded perlite (EP), expanded vermiculite (EV), expanded polystyrene (EPS), expanded poly-lactic acid (EPLA) and coated expanded poly-lactic acid (CEPLA) are used as aggregates. The concrete samples are prepared in seven groups of foamed concrete, EPLA-vermiculite concrete, EPLA-perlite concrete, EPS-perlite concrete, EPLA-perlite magnesium phosphate concrete and CEPLA-perlite concrete. The chapter also describes the common test methodologies and equipment employed in the experimental program to investigate mechanical properties, thermal properties, electrical properties, fire resistance, bond properties, flexural performance and phase analysis.

3.2 Raw Materials

3.2.1 Binder materials

3.2.1.1 Ordinary Portland cement (OPC)

The ordinary Portland cement used throughout this study was EverSure type GP complying with the requirement of the New Zealand standard NZS3122:2009 [174] and having 3, 7 and 28-days compressive strengths of 34.1, 45.0 and 62.8 MPa, respectively. The relative density and specific surface area of cement were 3.11 and 340 m²/kg. The atomic concentration and chemical composition of Portland cement are presented in Figure 3. 1 and Table 3. 2.



	Atom %									
	C	O	Mg	Na	Al	Si	K	Ca	Fe	Ti
OPC	-	41.95	1.63	0.04	6.27	9.08	0.15	37.33	3.23	0.32

Figure 3. 1 The atomic concentration of ordinary Portland cement (OPC).

3.2.1.2 Calcium oxide (CaO)

A fine calcium oxide powder with specific gravity and loose bulk density of 3.25 g/ml and 920 kg/m³ supplied by Omya UK is used as activator for ground granulated blast-furnace slag in this study. The fineness of calcium oxide and chemical composition are presented in Table 3. 1 and Table 3. 2.

Table 3. 1 The fineness of calcium oxide (CaO)

Calcium oxide (CaO)	Fineness (%)			
	> 250μm	> 180μm	> 125μm	> 45μm
	95.5	0.5	0.5	0.8

3.2.1.3 Magnesium oxide

A commercial magnesium oxide with a purity of 95% is used as activator for GGBS and ammonium dihydrogen phosphate. The magnesium oxide had a specific gravity of 3.65 kg/m^3 . The chemical composition of magnesium oxide is presented in Table 3. 2.

Table 3. 2 Chemical composition of OPC, MgO and CaO

	Chemical Composition (%)		
	OPC	MgO	CaO
SiO₂	22.8	1.73	0.5
Al₂O₃	4.2	0.16	-
Fe₂O₃	2.3	0.81	0.5
CaO	64.8	1.63	95.5
MgO	1.0	95.5	0.8
Na₂O	0.19	-	-
K₂O	0.49	-	-
SO₃	0.42	-	-
P₂O₂	-	0.17	-
LOI	3.1	-	-

3.2.1.4 Ground granulated blast-furnace slag (GGBS)

Ground Granulated Blast Furnace Slag (Slag Powder) with a specific gravity and fineness specific surface of 2.90 and $453 \text{ m}^2/\text{kg}$ is used in this study. The GGBS had an initial and final setting time of 312 and 385 min. The GGBS was supplied from EnGro Co. of South Korea. The chemical composition of GGBS is presented in Table 3. 3.

Table 3. 3 Chemical composition of GGBS

	Chemical composition (%)						
	CaO	SiO₂	Al₂O₃	Fe₂O₃	S	MgO	MnO
GGBS	30-50	30-40	7-17	0.1-1.8	0-2.0	2-14	0-1.0

3.2.1.5 Ammonium dihydrogen phosphate

Ammonium dihydrogen phosphate ($\text{NH}_4\text{H}_2\text{PO}_4$) with a specific gravity of 1.87 kg/m^3 is used to react with magnesium oxide (MgO) and to provide an acid-based reaction.

3.2.1.6 Borax

Sodium tetraborate decahydrate with the commercial name of Glitz Green Borax is used as retarder for magnesium phosphate cement.

3.2.2 Aggregates

3.2.2.1 Expanded poly-lactic acid

An expanded poly-lactic acid (EPLA) beads with a bulk density of 19 kg/m^3 and an average diameter of 5.5 mm was used as coarse aggregate (Figure 3. 2). The EPLA beads were obtained from Forest Research Scion, a crown research institute in New Zealand.

3.2.2.2 Expanded polystyrene

As shown in Figure 3. 2, a commercially available polystyrene beads with an average diameter and bulk density of 6.5 mm and 10.0 kg/m^3 were used as lightweight aggregate for foamed concrete and perlite/vermiculite concrete, respectively.

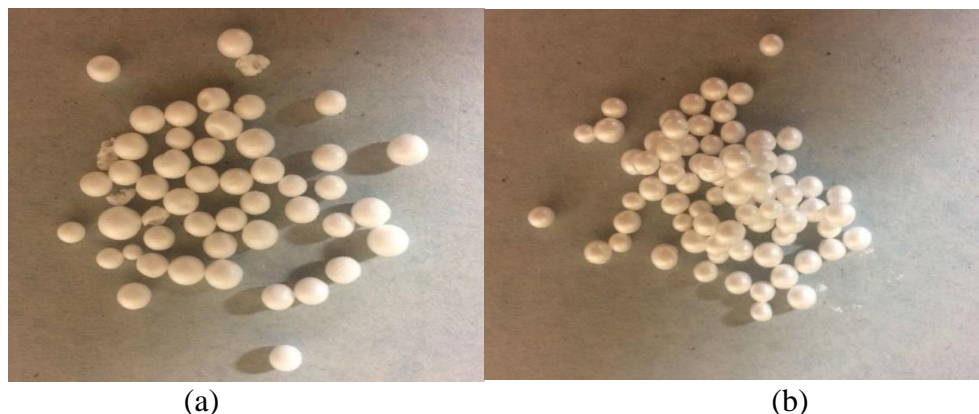


Figure 3. 2 Polymer aggregate; (a) Expanded polystyrene (EPS) with relative density of 10 kg/m^3 ; (b) Expanded poly-lactic acid (EPLA) with relative density of 19 kg/m^3 .

3.2.2.3 Expanded perlite (EP)

A commercially available expanded perlite C400 with a nominal size, relative density, and water absorption ratio of 0 - 4 mm, 121 kg/m³, and 2.23, supplied by INPRO, New Zealand was used as fine aggregate throughout this study. An ultrafine expanded perlite with the commercial name of F100 with a nominal size of 0-1mm is used as a coating material for EPLA. The atomic concentration and chemical composition of expanded perlite (C400) are presented in Figure 3. 3 and Table 3. 4, respectively.

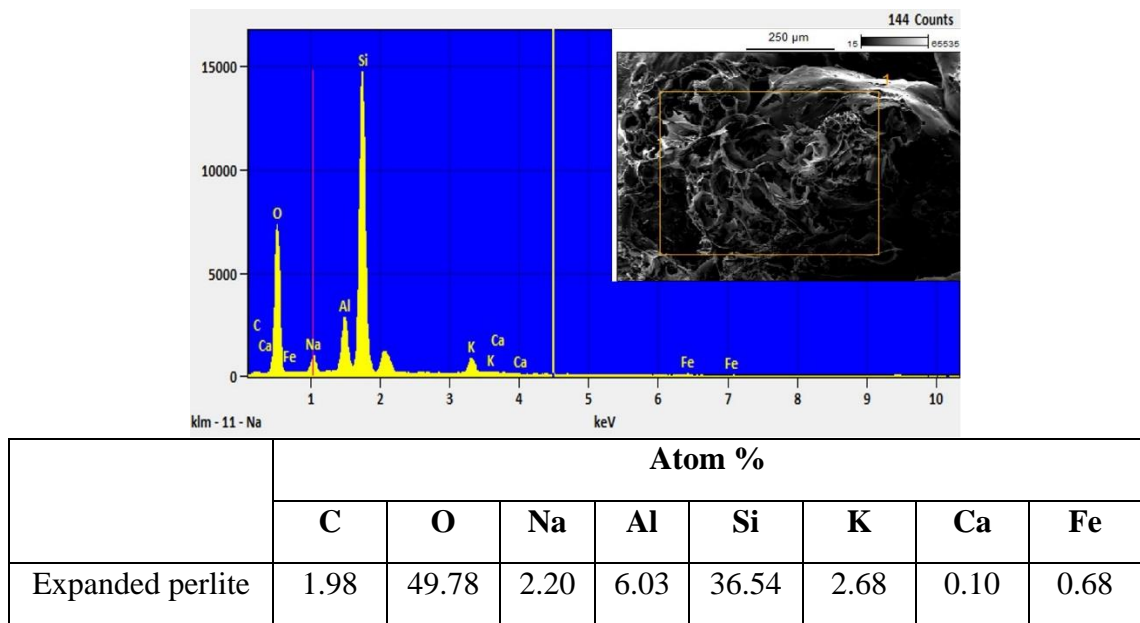


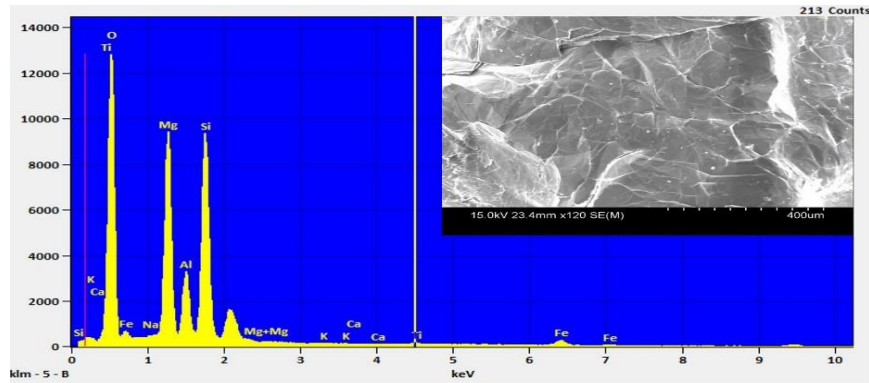
Figure 3. 3 EDS analysis of expanded perlite (EP).

3.2.2.4 Expanded vermiculite (EV)

Expanded vermiculite (Grade 2) with nominal size, specific gravity and water absorption ratio of 1- 4mm, 94.5 kg/m³ and 3.64 is used as a fine aggregate. The expanded vermiculite was supplied by INPRO, New Zealand. The atomic concentration and chemical composition of expanded vermiculite is presented in Table 3. 4 and Figure 3. 4. Table 3.4 also contains the atomic concentration of the expanded perlite.

Table 3. 4 Chemical composition of expanded perlite and expanded vermiculite

	Chemical Composite (%)							
	SiO ₂	Al ₂ O ₃	Fe ₂ O ₃	CaO	MgO	Na ₂ O	K ₂ O	TiO ₂
Expanded Perlite	74.0	14.0	1.0	1.3	0.3	3.0	4.0	0.1
Expanded Vermiculite	42.3	11.9	10.2	6.6	23.4	0.2	4.4	0.8



	Atom %								
	O	Mg	Na	Al	Si	K	Ca	Fe	Ti
Expanded Vermiculite	56.54	16.67	0.13	4.68	17.69	0.0	0.0	1.84	0.42

Figure 3. 4 EDS analysis of expanded vermiculite (EV)

3.2.2.5 Coated EPLA

Coated EPLA (CEPLA) is manually produced by coating of EPLA with a combination of X-200 paint and Limelock paint from Resene, New Zealand, as well as expanded perlite (F100). The specific gravity of coated EPLA was in the range of 210-220 kg/m³ (Figure 3. 5).



Figure 3. 5 Coated poly-lactic acid (CEPLA)

3.2.3 Chemical agents

3.2.3.1 Superplasticizer

Superplasticizer (Sikament HE200) with a dosage of 5 ml per kg of binder was used to increase the workability of concrete.

3.2.3.2 Air-entraining agent

An air-entraining agent (water-soluble liquid based on a synthetic chemical blend) with a specific gravity of 1.01 kg/L was used to secure good compaction, prevent the segregation, eliminate the shrinkage of vermiculite and perlite aggregate and increase the workability of concrete. The air-entraining agent (AE) was supplied by Sika NZ with a commercial name of Sika Air Mix.

3.2.3.3 Foam agent

In order to provide stable foam for lightweight foamed concrete, a high performance foaming agent (Quick-Foam) along with a specific viscosifier (QUICK-GEL) from Baroid IDP were used as the main components of the foam. The mix proportion of water, foaming agent and viscosifier is shown in Table 3. 5.

Table 3. 5 Mix proportion of preformed aqueous foam.

	Water (Litres)	QUICK-GEL Viscosifier (kg)	QUICK-FOAM Foaming agent (% by volume)
Mud-Mist Foam	1000	30	0.3-1.0

3.2.3.4 Limelock

A limelock paint with the commercial name of Resene Limelock from Resene New Zealand is used to eliminate the chemical reactivity of EPLA beads with free lime in the cementitious substance. The Limelock paint was used as the first coating layer of CEPLA aggregate. The physical properties of Limelock is presented in Table 3. 6.

3.2.3.5 Resene X-200

Acrylic weathertight membrane paint is used as an anti-carbonate paint in this study. The X-200 paint is applied as second layers of coating materials for CEPLA aggregate. The X-200 is supplied by Resene New Zealand. The physical properties of X-200 paint is presented in Table 3. 6.

Table 3. 6 Physical properties of Limelock and X-200

	Physical properties	
	Limelock	X-200
Vehicle type	100% acrylic	Pure acrylic
Pigmentation	Titanium dioxide	Titanium dioxide/mineral and fibre reinforcement
Solvent	water	water
Dry time	30 min at 18°C	1 hour at 18°C
Absorption resistance	Very good	Very good
Chemical resistance	Good	Very good
Heat resistance	Thermoplastic	Thermoplastic
Solvent resistance	Good	Good
Durability	Excellent	Excellent

3.2.4 Steel

3.2.4.1 Galvanized steel

Hot-dip galvanized strips (G250) with a thickness of 0.75mm were prepared from GALVSTEEL produced by New Zealand Steel with a yield, f_y and ultimate, f_u strength of 250 MPa and 320 MPa, respectively.

3.2.4.2 Cold-formed profile

A hot-dip zinc-coated steel (G550) rolled into C-sections was used with a thickness of 0.75mm and a yield and tensile strength of 577 MPa and 642 MPa, respectively. Framacad Ltd., New Zealand, supplied the steel profiles.

3.3 Experimental test methods

3.3.1 Workability

The characteristics and consistency of fresh concrete is determined by the slump test as per ASTM C143/C143M [175]. This test utilises a frustum shaped mould with the base diameter, top diameter and height of 100 mm, 200 mm and 305 mm, respectively. The mould is filled with fresh concrete and compacted at three layers of equal volume with a tamping rod. Based on ASTM C143, it is called true slump when concrete remains intact and holds a symmetric shape (Figure 3. 6). Although, a slump value of 50-75 mm is suggested for lightweight concrete, a slump range of 200-220 mm is adopted for this study based on visual observations and trial tests to obtain acceptable compaction and workability. In addition, no segregation was observed at this range of slump values for the proposed concretes.

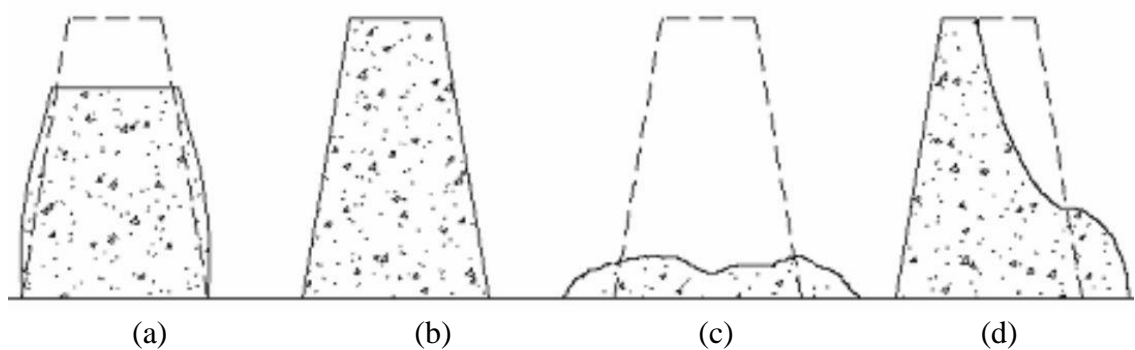


Figure 3. 6 Slump test, (a) true, (b) zero, (c) collapse, (d) shear

3.3.2 Density

The density of concrete is determined as per ASTM C567 [176] with a 100x200 mm (diameter x height) standard cylinders. The densities of samples are measured in fresh and air-dried conditions.

3.3.3 Compressive strength

The compressive strength tests were carried out on 100x200 mm (diameter x height) standard cylinders as per ASTM C495 [177]. The Instron® with 100 kN capacity is used. The compressive strength of concrete samples were measured in displacement control mode with a constant crosshead speed of 0.05 mm/min. The cylinders were demoulded and then cured with designated curing methods and ages. Also, the strain-stress curved is used to determine the elastic modulus of concrete.

3.3.4 Tensile strength

Splitting tensile strength tests were done as per ASTM C496 [178] on 100x200 mm (diameter x height) standard cylinders. The splitting tensile strength test includes applying load to induce transverse tension. Two stiff parallel plates are positioned and distribute the compressive stress perpendicular to the cylinder diameter. The applied stress causes tensile stress along the vertical plane. It worth to note that the same crosshead speed is used (1.0 mm/min) to evaluate the tensile capacity of concrete. The splitting tensile stress is calculated using the following equations (Eq. 3.1).

$$f_t = \frac{2P}{\pi DL} \quad (3.1)$$

Where, P is the applied load (N), D is the sample diameter (mm), L is the length of sample (mm).

3.3.5 Thermal conductivity

Prisms of $200 \times 200 \times 40$ mm were cast for thermal conductivity tests and an Anacon TCA-8 thermal conductivity analyser was used for k-factor measurements. The specimens were contacted by a cold and a hot plate with a diameter of 10 cm, which are kept at temperatures of 37°C and 10°C , respectively. The TCA-8 automatically measures the thickness of the sample and combines the reading with the heat-flow measurement to yield a direct digital readout of thermal conductivity [179]. Further samples were prepared with a prism size of $70 \times 20 \times 20$ mm for studying the thermal conductivity with a Mathis Instruments TC-30 tester.

3.3.6 Electrical resistivity

The electrical resistivity of concrete was measured using a compact wireless device, Giatec SmartBox as per AASHTO TP 95-11 [180] (Figure 3. 7). The parameters such as electrical resistivity and exothermic reaction were measured. The following procedure was followed to determine the shape factor (K) and electrical resistivity.

- 1) A standard cylinder of 100×200 mm is filled with a standard solution of known electrical conductivity (σ_s)
- 2) The standard cylinder is then inserted into the SmartBox and the resistance is measured (R_s).
- 3) The shape factor can be calculated by the following equation (Eq. 3.2).

$$K = \frac{R_s}{\sigma_s} \quad (3.2)$$

Where, σ_s is the electrical conductivity of the standard solution, R_s is measured resistance by SmartBox.

- 4) At the second stage, the standard cylinder was filled with the investigated concrete and the resistance of concrete was measured (R_C).
- 5) The electrical resistivity can be determined by dividing the investigated concrete resistance (R_C) by the obtained shape factor (K) as described in following equation (Eq. 3.3).

$$\sigma_C = \frac{R_C}{K} \quad (3.3)$$

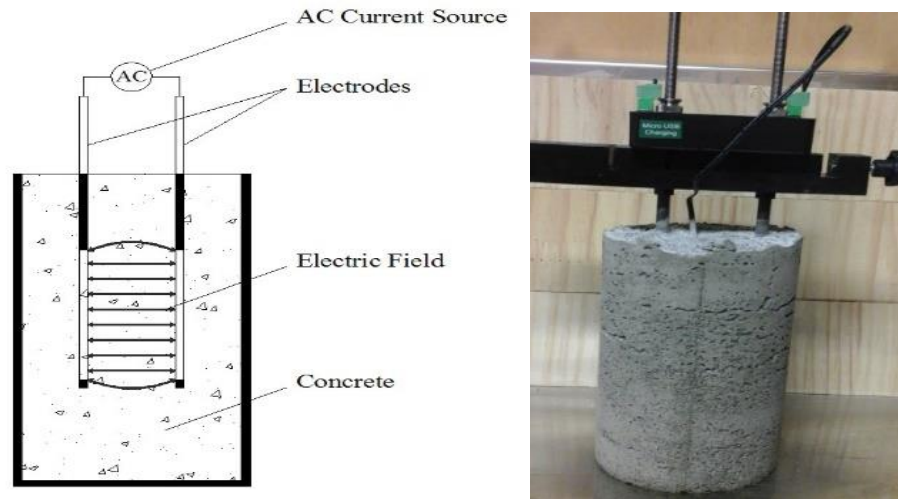


Figure 3. 7 Giatec SmartBox

3.3.7 Phase analysis

A powder X-ray Diffraction System (XRD) was used to reveal the crystalline phases of the hardened cement paste. A powder XRD pattern was collected for each sample using a PANalytical's Empyrean Powder X-ray diffractometer equipped with a Cu anode X-ray tube using mono-chromatid Cu $K\alpha$ X-rays at operating voltage and current of 45kV/40mA. All XRD data were collected from $2\theta = 10^\circ \sim 80^\circ$ with a step size of 0.0131° [181]. A Hitachi SU-70 Scanning Electron Microscope (SEM) was used to study the microstructure of the hydrated cement-paste materials. In order to stop the hydration process of concrete at different stages of curing, the samples were immersed in acetone for 3 days followed by a vacuum oven for 1 day at a temperature of 35°C [182].

3.3.8 Fire resistance test

Cone calorimeter tests were performed to assess the fire reaction properties of the proposed concretes as per ASTM E1354 [183]. A square (100 x 100 mm) concrete sample with a thickness of 10 mm was exposed to a 50 kW/m^2 heat flux using a cone calorimeter from FTT, East Grinstead, UK.

3.3.9 Pull-out test

Galvanized steel strips are positioned in the middle of specimens and embedded 50 mm into concrete. Due to the narrow thickness of steel strips and eccentricity of loads that cause a bending of the galvanized strips, the conventional pull-out test method is not suitable for testing these steel strips [179]. Thus, a testing mechanism was designed that would eliminate the influence of undesirable effects of either bending and/or twisting the steel strips during tests. The test were therefore conducted with a universal testing machine equipped with a testing rig and a freely adjustable ball-joint. Moreover, four M10 bolts were embedded and fixed to a plate at the bottom of the foamed concrete sample to hold the specimens and to avoid any eccentricity through loading. The applied load and displacements were measured and recorded until the extraction of the steel strip. The configuration of the test setup is shown in Figure 3. 8.

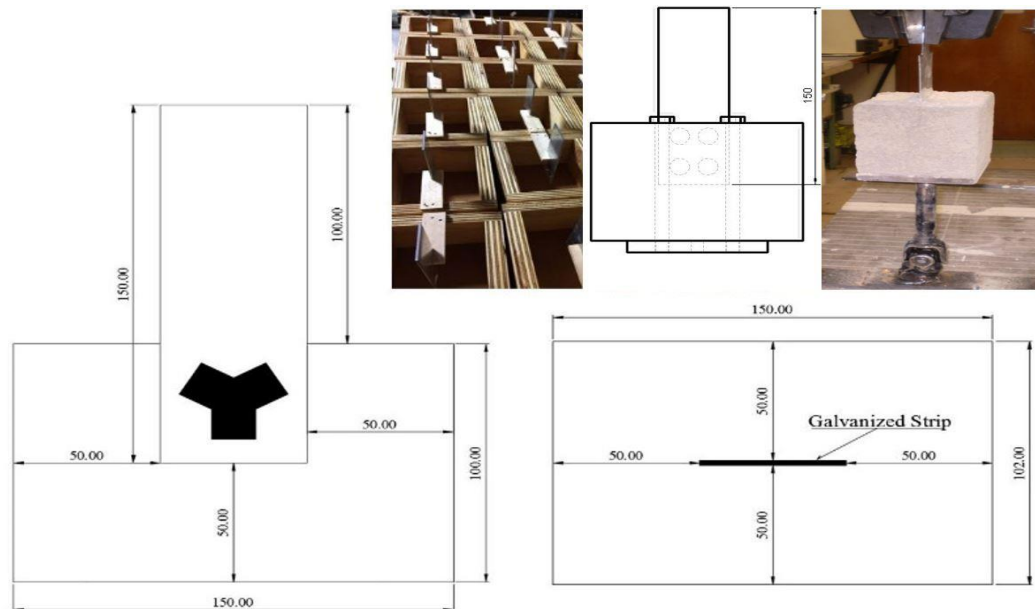


Figure 3. 8 Pull-out test configuration

3.3.10 Beam test

A quasi-static bending tests was conducted to evaluate the flexural performance of the proposed concretes. An Instron machine with 100 kN capacity is used at a load ratio of 0.05 mm/min. The total length of the beams was 1000 mm for all samples with a constant

moment region length of 300 mm. The schematic test setup of the quasi-static bending is shown in Figure 3. 9. The two load transferring points were placed at a distance of 300 mm and 600 mm from the support to provide a constant moment region between the applied point loads. The side surface of the beams at the middle span was equipped with two strain gauges. The strain gauges were mounted longitudinally (S.G.x) and tangentially (S.G.y). A linear variable differential transformer (LVDT) was used to assess the beam deflection at mid-span. The load was applied at a displacement rate of 0.1 mm/s until it reached the maximum load carrying capacity and experienced the unloading stage where excessive deformation took place (Figure 3. 9).

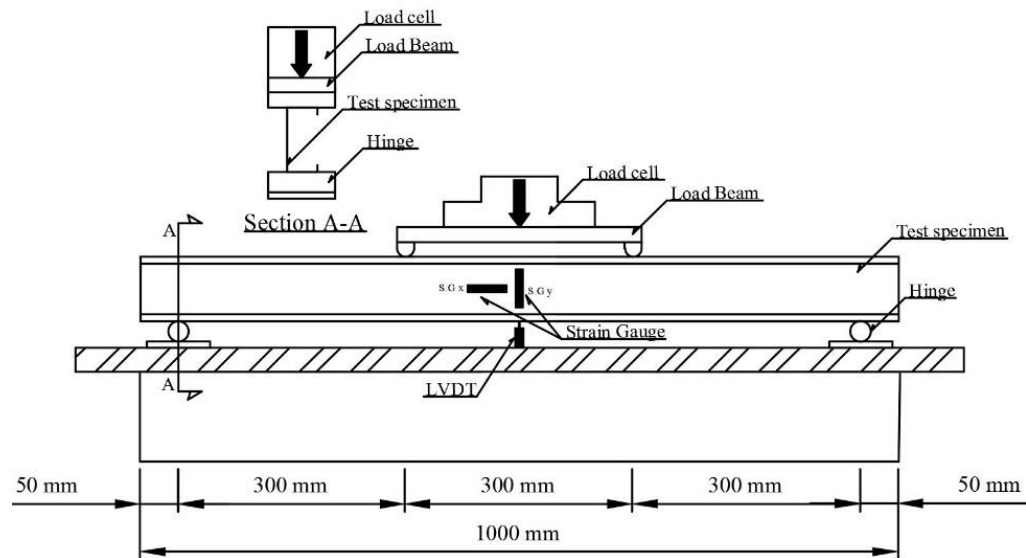


Figure 3. 9 Beam test setup

3.3.11 Beam test

The samples were dried and ground into powder form for pH measurements and then 2 g of powdered samples were dissolved in 10 g of distilled water. After an hour of mixing, the solids were filtered through vacuum and the pH was measured by using a Horiba pH meter with an accuracy of ± 0.01 .

3.4 Proposed mix design method

3.4.1 Mix design and mix proportion

Mix design of ultra-lightweight concrete is more complicated than normal concrete as it mostly depends on characteristics of lightweight aggregate and its absorption value. The variation of the degree of water absorption is the most significant difficulty of a lightweight concrete mix design due to the complexity of measuring saturated and surface-dry bulk specific gravity of lightweight aggregate [184]. There exists no specific mix design for the mix proportions of ultra-lightweight concrete. However, ACI 211.2 [185] provides design charts and tables for lightweight concrete based on the volumetric and weight method, but the provided guideline is limited to a compressive strength of 20.7 MPa which is much higher than mechanical properties of ultra-lightweight concrete. The factors such as density, cement content and water-cement ratio substantially affect the mechanical properties of ultra-lightweight concrete. For this reasons, a mix design procedure and set of equations are proposed to estimate the proper water-cement ratio and cement content by knowing the required density of concrete [22]. It is worth to note that the provided equations are only valid for perlite and vermiculite concrete and have not been applied to other lightweight concretes. The following equations are derived based on a mathematical model by considering relevant parameters [22, 186].

3.4.2 Selection of approximate water-cement ratio (w/c)

The water-cement ratio is the most important factor of concrete in both fresh and hardened states. Also, this ratio directly affects the rheology, mechanical properties, permeability and durability of concrete. This mix design equation for a required water-cement ratio is designed based on the target density of lightweight concrete (Eq. 3.4 and Eq. 3.5).

Perlite Concrete:

$$\frac{w}{c} = a = \frac{0.76\gamma^{0.0001\gamma}}{0.0001\gamma\gamma^{0.5}} \quad (3.4)$$

Vermiculite concrete:

$$\frac{w}{c} = a = \frac{0.77\gamma^{0.0001\gamma}}{0.0001\gamma\cdot\gamma^{0.5}} + 0.25WA_r \quad (3.5)$$

Where γ is density of concrete (kg/m^3), a is water-cement ratio, WA_r is water absorption ratio of vermiculite aggregate.

3.4.3 Required cement content

The cement content of lightweight concrete directly affects the density and mechanical properties of concrete. The following equation (Eq. 3.6) has been developed to estimate the required cement content by knowing the target density and water-cement ratio (Eq. 3.4 and Eq. 3.5). It is worth to note that K is a constant value of 117 and 211 for perlite and vermiculite concrete, respectively.

$$\begin{cases} 1000 = \frac{(\frac{\gamma}{a})^{0.5}}{RD_c \cdot RD_x} C + \frac{Ka(\frac{a}{\gamma})^{0.5}}{RD_x} C + 10aV_x \\ \gamma = \frac{1}{10a} C + aC + RD_x V_x \end{cases} \quad (3.6)$$

Where γ is density of concrete (kg/m^3), a is water-cement ratio, C is cement content (kg/m^3), RD_c is relative density of cement, RD_x is relative density of perlite / vermiculite aggregate, V_p is perlite / vermiculite aggregate volume (m^3).

The accuracy of the proposed equations and guideline is compared with a provided mix design proportion of a local company in New Zealand, INPRO. The proposed equations are designed based on the parameters concrete density, cement content, the relative density of cement and relative density of perlite (Table 3. 7).

Table 3. 7 Comparing the mix design of INPRO and proposed equation

Density (kg/m ³)	Provided mix design (INPRO Co.)		Proposed Equation	
	W/C	Cement Content (kg/m ³)	W/C	Cement Content (kg/m ³)
576	0.79	376	0.79	376
488	0.96	301	0.95	300.5
432	1.07	252	1.10	252
352	1.43	188	1.42	189

3.4.4 Examples of mix design procedure of perlite and vermiculite concrete

Based on mix trial tests of mix compositions of perlite and vermiculite concrete, the optimum density with relatively adequate cement content was observed in a mix proportion with a density of 432 kg/m³ as no segregation with perfect compaction was obtained at this amount of cement content. The following mix design procedures are examples of mix designs with a relative density of 432 kg/m³.

Example 1: Ultra-lightweight perlite concrete is required to have a specific density of 432kg/m³, so to determine the required water-cement ratio, cement content, perlite content and water content the following steps needs to be done.

Step 1: Determination of water-cement ratio

Target density = 432 kg/m³

From Eqn. (3.1) w/c is obtained as:

$$\frac{w}{c} = a = \frac{0.76\gamma^{0.0001\gamma}}{0.0001\gamma \cdot \gamma^{0.5}}$$

$$\frac{w}{c} = a = \frac{0.76(432)^{0.0001(432)}}{0.0001(432) \cdot (432)^{0.5}} = 1.1$$

The obtained water cement ratio is the summation of effective water-cement ratio and required water content for saturating the perlite aggregate at a slump value of 220 mm.

Step 2: Determination of cement content

From Eqn. (3.3) cement content is obtained as:

Where,

$RD_p = 0.135$ (Relative density of perlite aggregate)

$RD_c = 3.11$ (Relative density of cement)

$$\begin{cases} 1000 = \frac{(\frac{Y}{a})^{0.5}}{RD_c \cdot RD_p} C + \frac{Ka(\frac{a}{Y})^{0.5}}{RD_p} C + 10aV_p \\ \gamma = \frac{1}{\gamma^{10a}} C + aC + RD_p V_p \end{cases}$$

$$\begin{cases} 1000 = \frac{(\frac{432}{1.1})^{0.5}}{(3.11) \cdot (0.135)} C + \frac{117(1.1)(\frac{1.1}{432})^{0.5}}{0.135} C + (10 * 1.1 * V_p) \\ 432 = 432 \frac{1}{10 * 1.1} C + 1.1C + 0.135V_p \end{cases}$$

$C = 251.86 \sim 252.0$

Step 3: Determination of water content

Where, $\frac{w}{c} = 1.1$ and $C = 252.0 \text{ kg/m}^3$

The required water content is $w = 277.2 \text{ kg/m}^3$

Step 4: Determination of perlite content

The perlite content is equal to the density of the perlite aggregate, 135 kg/m^3 .

The resulting mix proportions of perlite concrete with a relative density of 423 kg/m^3 are represented in Table 3. 8.

Table 3. 8 Summary of mix design proportions of perlite concrete

	Mix proportion (kg/m ³)			
	Target density	Cement content	Water content	Perlite content
Perlite concrete	432.0	252.0	277.5	135.0

Example 2: Ultra-lightweight vermiculite concrete is also required to have a specific density of 432 kg/m³. To determine the required water-cement ratio, cement content, vermiculite content and water content the following steps needs to be done.

Step 1: Determination of water-cement ratio

From Eqn. (3.2) w/c is obtained as:

Target density = 432kg/m³

$$\frac{w}{c} = a = \frac{0.77\gamma^{0.0001\gamma}}{0.0001\gamma \cdot \gamma^{0.5}} + 0.25WA_r$$

$$\frac{w}{c} = a = \frac{0.77(432)^{0.0001(432)}}{0.0001(432) \cdot (432)^{0.5}} + 0.25(3.64) = 2.02$$

The obtained water cement ratio is the summation of effective water-cement ratio and required water content for saturating the vermiculite aggregate at the slump value of 220 mm.

Step 2: Determination of cement content

From Eqn. (3.3) cement content is obtained as:

Where,

RD_p = 0.0945 (Relative density of vermiculite aggregate)

RD_c = 3.11 (Relative density of cement)

$$\begin{cases} 1000 = \frac{(\frac{\gamma}{a})^{0.5}}{RD_c \cdot RD_p} C + \frac{Ka(\frac{a}{\gamma})^{0.5}}{RD_p} C + 10aV_p \\ \gamma = \frac{1}{\gamma^{10a}} C + aC + RD_p V_p \end{cases}$$

$$\begin{cases} 1000 = \frac{(\frac{432}{2.02})^{0.5}}{(3.11) \cdot (0.0945)} C + \frac{211(2.02)(\frac{2.02}{432})^{0.5}}{0.0945} C + (10 * 2.02 * V_p) \\ 432 = 432 \frac{1}{10 * 2.02} C + 2.02C + 0.0945V_p \end{cases}$$

$$C = 252.13 \sim 252.0$$

Step 3: Determination of water content of perlite concrete

Where, $\frac{w}{c} = 2.02$ and $C = 252.0 \text{ kg/m}^3$

The required water content is $w = 509.0 \text{ kg/m}^3$

Step 4: Determination of vermiculite content

The vermiculite content is equal to the density of vermiculite aggregate, 94.5 kg/m³.

The resulting mix proportions of vermiculite concrete with relative density of 423 kg/m³ are presented in Table 3. 9.

Table 3. 9 Summary of mix design proportions of vermiculite concrete

	Mix proportion (kg/m³)			
	Target density	Cement content	Water content	Perlite content
Vermiculite concrete	432.0	252.0	509.0	94.5

CHAPTER 4

VERMICULITE CONCRETE CONTAINING EPLA

4.1 Introduction

This chapter is about the possibility of producing ultra-lightweight concrete by using a biopolymer aggregate. Expanded poly-lactic acid and expanded vermiculite are added as aggregate to produce a biopolymer concrete. In total, five concrete mixtures are designed with varying EPLA and EV contents. The cement content and effective water-cement ratio are kept constant. The EV aggregate was replaced with 20%, 40%, 60% and 80% EPLA aggregate. Three types of curing conditions were used. The mechanical properties, thermal properties as well as electrical properties of biopolymer concrete were assessed and analysed. The microstructure of the concrete was assessed after 28-days and one year. It was found that the properties of EPLA concrete are mainly influenced by the volume of EPLA and the curing conditions. The chemical reactivity of EPLA significantly changes the hydration products of concrete and causes concrete carbonation as well as the conversion of hydration products to more calcium carbonate. However, in the long-term investigation after a year more calcium silicate hydrate (C-S-H) gel was found. Furthermore, EPLA aggregates shrunk and lost their strength in the alkaline environment of cement.

4.2 Experimental program

4.2.1 Mix proportions and procedure

Five mixes with varying EV/EPLA ratio were prepared based on the proposed equations 3.5 and 3.6. The mix design was targeted to attain a density of 500 kg/m³ for the sample with 100% vermiculite (V1). The sample with 100% vermiculite is used as a reference for EPLA-vermiculite concrete, and in other mixtures, vermiculite was partially substituted with EPLA aggregate at 20% (V2), 40% (V3), 60% (V4) and 80% (V5) by volume. The effective water-cement ratio is kept at 0.45 (Eq. 3.5) and the cement content is fixed at 323.5 kg/m³ (Eq. 3.6). The EPLA and cement were blended in a rotary mixer for about 1 min. Before adding

water, an appropriate amount of air entraining agent was mixed with the required amount of water and then 70% of the mixed water (water + air entraining agent) were added to the cement-EPLA mixture and mixed for 3 min. The vermiculite aggregate was slowly added to the mixture followed by the remaining water for 2 min, due to the sensitivity of vermiculite aggregate to the mixing processes and to avoid the compaction of vermiculite aggregate during mixing, which causes a higher density. The mix proportions of the proposed concrete are shown in Table 4. 1.

Table 4. 1 Mix proportions of vermiculite and vermiculite-EPLA concrete.

Mix No.	Mix proportion (kg/m ³)							
	w/c	EV/EPLA ratio (Vol.)	C	W	EV	EV Vol. (m ³)	EPLA	EPLA Vol. (m ³)
V1	0.45	-	323.5	557.1	113.1	1	0	0
V2	0.45	4	323.5	474.8	90.5	0.8	8.7	0.2
V3	0.45	1.5	323.5	392.5	67.8	0.6	17.4	0.4
V4	0.45	0.67	323.5	310.2	45.2	0.4	26.2	0.6
V5	0.45	0.25	323.5	227.8	22.6	0.2	34.9	0.8

C: cement, W: water, w/c: effective water-cement ratio, EV: expanded vermiculite.

4.2.2 Curing regimes

In order to assess the influence of curing conditions on mechanical properties of EPLA-vermiculite concrete, the samples were cured under three different curing conditions. The following is a brief explanation of the different curing regimes:

- (a) Air drying curing (ADC): The specimens were kept in the laboratory environment with a temperature of 20 ± 2 ° C after demoulding for a period of 28 days and 56 days.
- (b) Water curing (WC): The specimens were immersed in tap water for the whole curing period (28 days and 56 days) at a temperature of 20 ± 2 ° C.
- (c) Fog curing (FC): the specimens were kept in a fog room for a period of 28 days and 56 days.

4.2.3 Test method

The density and compressive strength tests were carried out on 100x200 mm (diameter x height) standard cylinders as per ASTM C567 [176] and ASTM C495 [177], respectively. The cylinders were demoulded and then cured according to the mentioned curing methods and times. A Hitachi SU-70 scanning electron microscope (SEM) was used to investigate the microstructure of raw materials and the hydrated cement-paste materials. A powder X-ray diffraction system was used to reveal the crystalline structure of the hardened cement paste. The electrical resistivity of concrete was measured with a compact wireless device, Giatec SmartBox as per AASHTO TP 95-11 [180]. Prisms of 200x200x40 mm size were used for studying the thermal conductivity of EPLA-vermiculite concrete. The thermal conductivity value of concrete was assessed and analyzed with an Anacon TCA-8 thermal conductivity analyzer. The readings were taken after 24 h, 3 days, 7 days, 14 days and 28 days. The proposed samples were immersed in water at room temperature for 1 hour, 24 hours and 72 hours. The water absorption was calculated with the following equation (Eq. 4.1). It is worth to note that the average results of three specimens were considered to evaluate the engineering properties of proposed concrete.

$$W_A = \frac{m_d - m_w}{m_w} * 100 \quad [4.1]$$

Where, W_A is the water absorption ratio (%), m_d is the dry mass (g), m_w is the wet mass (g).

4.3 Results and discussion

4.3.1 Density

Table 4. 2 shows the test results for the fresh, demoulded and air dried densities of all mixes. The fresh and air dried densities of concrete varied from 808.50 to 532.5 kg/m³ and 512.8 to 414.5 kg/m³, respectively. The highest density was observed in the sample with 100% vermiculite aggregate. The decrease in air dried density of samples with an EV/EPLA ratio of 4.0, 1.5, 0.67 and 0.25 was 3.4, 11.0, 15.8 and 19.7%, respectively. This could be attributed to the lower relative density of EPLA, which is 43.5 kg/m³ compared to 94.5 kg/m³ for

EV. However, an increase in EV/EPLA ratio results in a significant reduction in workability and degree of compaction of concrete due to an increase in surface area caused by the EPLA aggregate. In addition, the differences between demoulded and air dried density of concrete decreased as the volume of EPLA increased mainly due to the hydrophobic nature of EPLA aggregate. These differences were 208.67, 191.0, 124.43, 106.93 and 89.24 kg/m³ for samples containing 0, 20, 40, 60 and 80% EPLA, respectively. The dry density of vermiculite and EPLA vermiculite concrete can be obtained by the following equations 4.2 and 4.3.

$$\gamma_f = -1.402V_{PLA} + 521.92 \quad [4.2]$$

$$\gamma_d = -3.5716V_{PLA} + 795.16 \quad [4.3]$$

Where, γ_f is fresh density of concrete (kg/m³), γ_d is dry density of concrete (kg/m³), V_{PLA} is poly-lactic acid volume (m³).

Table 4. 2 The fresh and air dried density (ADC) of vermiculite and EPLA-vermiculite concrete.

Mix No.	Density (kg/m ³)		
	Fresh	Demoulded	ADC
V1	808.50	721.52	512.85
V2	720.65	689.21	498.22
V3	631.52	583.56	459.13
V4	578.34	541.43	434.50
V5	532.50	503.75	414.51

As shown in Figure 4. 1, the density of concrete can be decreased by substituting vermiculite with EPLA beads. Thus, the application of a polymer aggregate can be a solution to decrease the absorption ratio of concrete containing a high absorbent aggregate such as vermiculite or perlite aggregate. Furthermore, the application of a bio-polymer as an eco-friendly aggregate can be counted as another advantage of using polymer aggregate in the construction industry.

These types of concrete mostly are used as infill materials for metalcraft insulated panel systems. Such a reduction in density of concrete causes a considerable decrease in overall weight of a structure and stresses generated in structural elements during static and seismic loads.

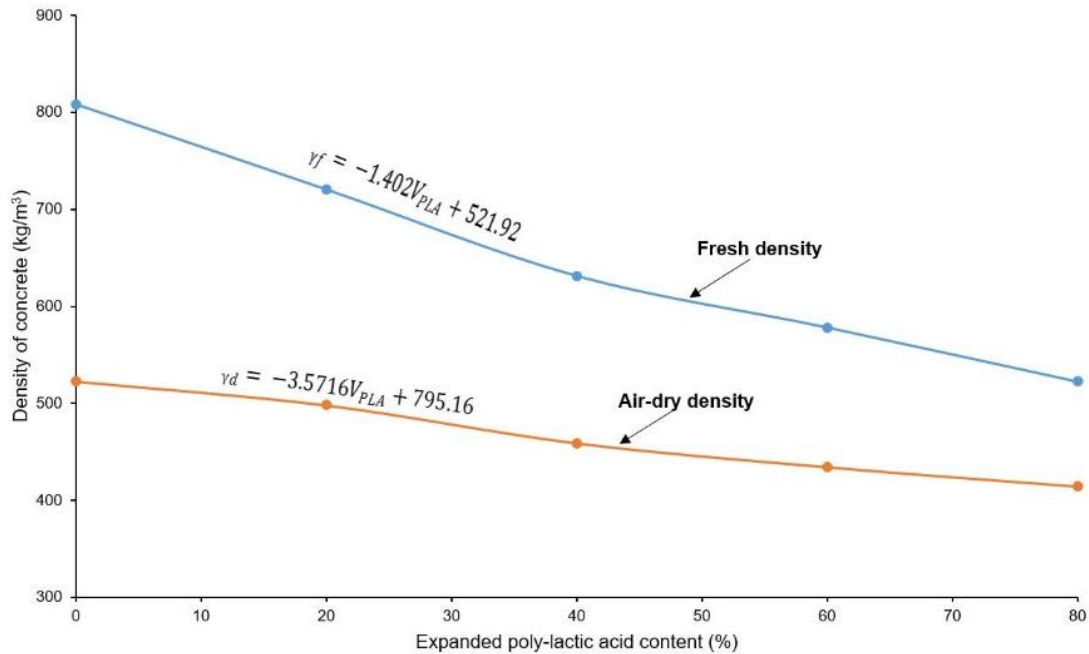


Figure 4. 1 The relationship between density and expanded poly-lactic acid content.

4.3.2 Compressive strength and failure modes

Table 4. 3 shows the compressive strength of the proposed vermiculite concrete under different curing conditions and replacement of EV with EPLA. The curing of concrete plays a significant role in the performance and strength development of concrete. ACI [187] has suggested that the concrete should be kept in a moist environment for at least the first seven days. The experimental results show that the changes of curing conditions caused an inverse effect on compressive strength of EPLA concrete and a significant reduction in its strength. This change in strength development can be attributed to the alkaline reactivity of bio-polymer aggregate with alkaline components of cement.

The air cured samples show a higher compressive strength compared to the corresponding water and fog cured samples after 28 and 56 days. Compared with air-cured samples (28 days) the compressive strength of samples with an EV/EPLA ratio of 4.0, 1.5, 0.67 and 0.25

was decreased by 10%, 12%, 22% and 25% along with 16%, 15%, 31% and 34% for sample cured in fog and water condition, respectively. However, the continued moist curing causes a gradual increase in strength development of mix V1. The strength increased 4% and 7% as the fog and water curing is applied. The highest and lowest compressive strength is observed in samples V1 and V5 with the 28 days (water cure) corresponding strength of 0.92MPa and 0.28MPa, respectively. This phenomenon can be attributed to the fact that the penetration of fresh cement into the open pores of vermiculite aggregate resulted in a higher interfacial bond between the components of the matrix. Whereas, the weaker bond interface between EPLA beads and matrix was observed due to alkaline reactivity and shrinkage of EPLA beads (Figure 4. 2).

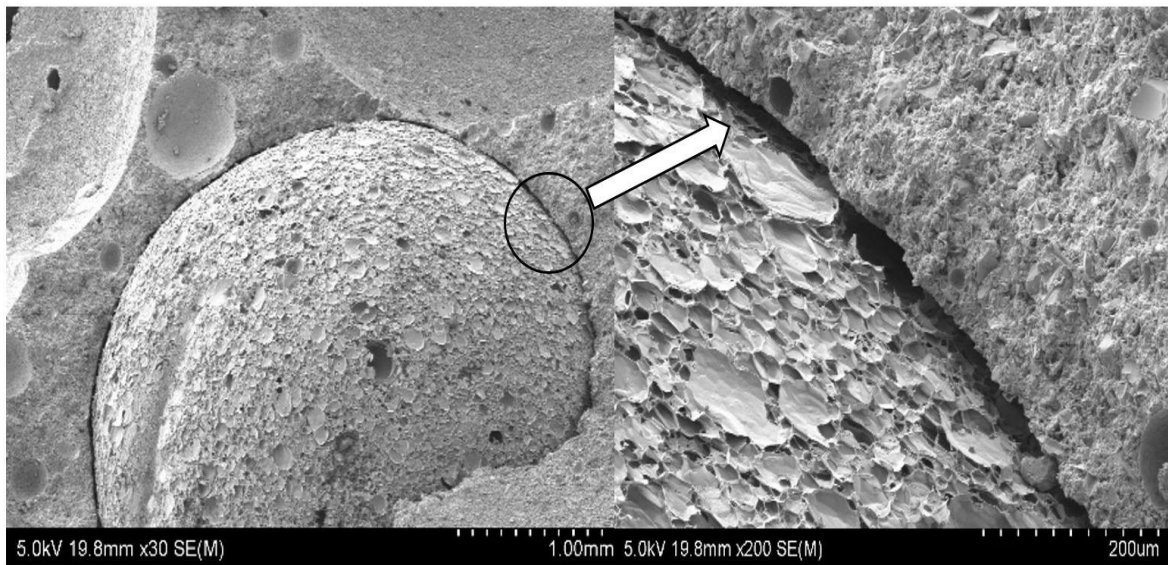
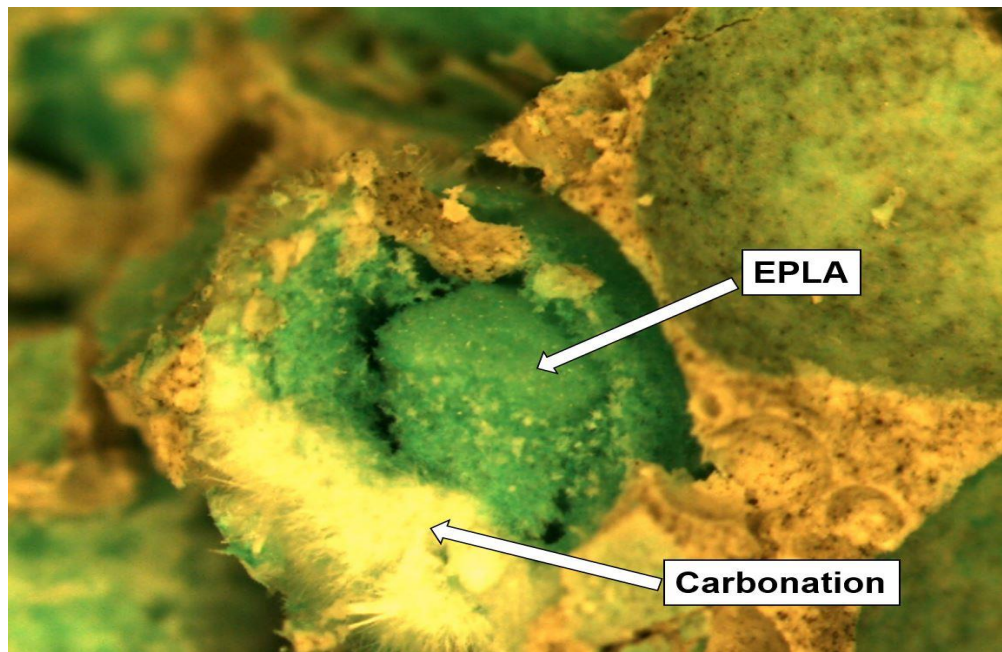


Figure 4. 2 Bond failure at interfacial transition zone (ITZ) of EPLA-vermiculite concrete.

In fact, all EPLA beads shrank and disappeared when water cured and a thick layer of efflorescence occurred on the surface of concrete due to the formation of calcium carbonate (Figure 4. 3). In general, the calcium hydroxide (Ca(OH)_2) formed in the hydration reaction of cement, transported by water to the surface through capillaries in the concrete and combines with carbon dioxide of air to produce calcium carbonate and water. The chemical reactivity of EPLA beads with alkaline components of cement such as Ca, K and Na results in concrete carbonation.



(a)



(b)

Figure 4. 3 Reaction of EPLA particles when subjected to the alkaline environment of cement; (a) dissolution of EPLA particles, b) carbonation of EPLA concrete

Thus, for the same EPLA to vermiculite ratio, it can be concluded that factors such as EPLA degradation in the alkaline environment of cement and a weak interfacial zone of EPLA due to alkaline reactivity were the main source of sudden reduction in compressive strength. In other words, the existence of large voids due to shrinkage of EPLA aggregate and conversion of hydration products to more calcium carbonate results in the concrete crushing at a much lower stress. The rate of reduction in strength development was a factor of the EPLA ratio.

Table 4. 3 Effect of curing conditions on compressive and tensile strength of proposed concrete

Specimen	Compressive strength (MPa)					Tensile Strength (MPa)			
	AC		FC		WC	AC		FC	WC
	28- days	56- days	28- days	56- days	28- days	56- days	28- days	28- days	28- days
V1	0.86	0.92	0.90	1.05	0.92	1.11	0.28	0.29	0.29
V2	0.79	0.83	0.71	0.76	0.66	0.69	0.24	0.17	0.15
V3	0.63	0.66	0.55	0.57	0.53	0.56	0.15	0.13	0.11
V4	0.61	0.63	0.47	0.46	0.42	0.45	0.14	0.11	0.10
V5	0.44	0.45	0.33	0.39	0.28	0.35	0.11	0.09	0.08

*AC: Air Cured, FC: Fog Cured, WC: Water Cured

The compressive strength of lightweight concrete mostly depends on aggregate characteristics and interfacial bond strength between aggregate and paste. Also, the interfacial zone between the aggregate and the paste significantly affects the stress-strain response of concrete under a uniaxial compression load. The micro-cracks are initially starting to propagate at the interfacial zone, which causes an increment in strain rate rather than applied stress. This resulted in a discontinuity of the interconnected network of matrix and aggregate, and thus a failure of the matrix. However, compared with normal concrete, the failure modes of lightweight concrete are considerably different due to the porous structure of lightweight aggregate. In fact, the compressive strength of normal concrete is a factor of aggregate strength, while lightweight aggregate concrete mostly depends on the strength of cement and the interfacial zone of the matrix. In the case of polymer aggregate such as EPLA, the hydrophobic surface of aggregate and higher compressibility of

biopolymer aggregate causes a lower interfacial bond strength and acceleration of bond failure at the interfacial transition zone (ITZ) of concrete.

The fracture process of samples containing EPLA aggregate was completely different to the control specimen (V1). A sudden and brittle behavior was observed in control specimens (Figure 4. 4a). The cracks generate and propagate along the length of concrete cylinders while the inclusion of EPLA changed the failure modes of concrete. The cracks had enlarged and spread on the top of the concrete cylinders due to the absence of resisting components and de-bonding of EPLA (Figure 4. 4b-e). However, the interfacial bond between EPLA and the matrix was zero due to the shrinkage and alkali reactivity of EPLA beads during the hydration process. The debonding of EPLA causes concrete crushing at a much lower stress without visible failure at the other part of the concrete cylinder. The cracks increased and were propagated through the width for samples cured in water (Figure 4. 4d). For instance, a sudden crushing of the top section was observed in the sample with 60% EPLA (V4) and cured in water (Figure 4. 4e).

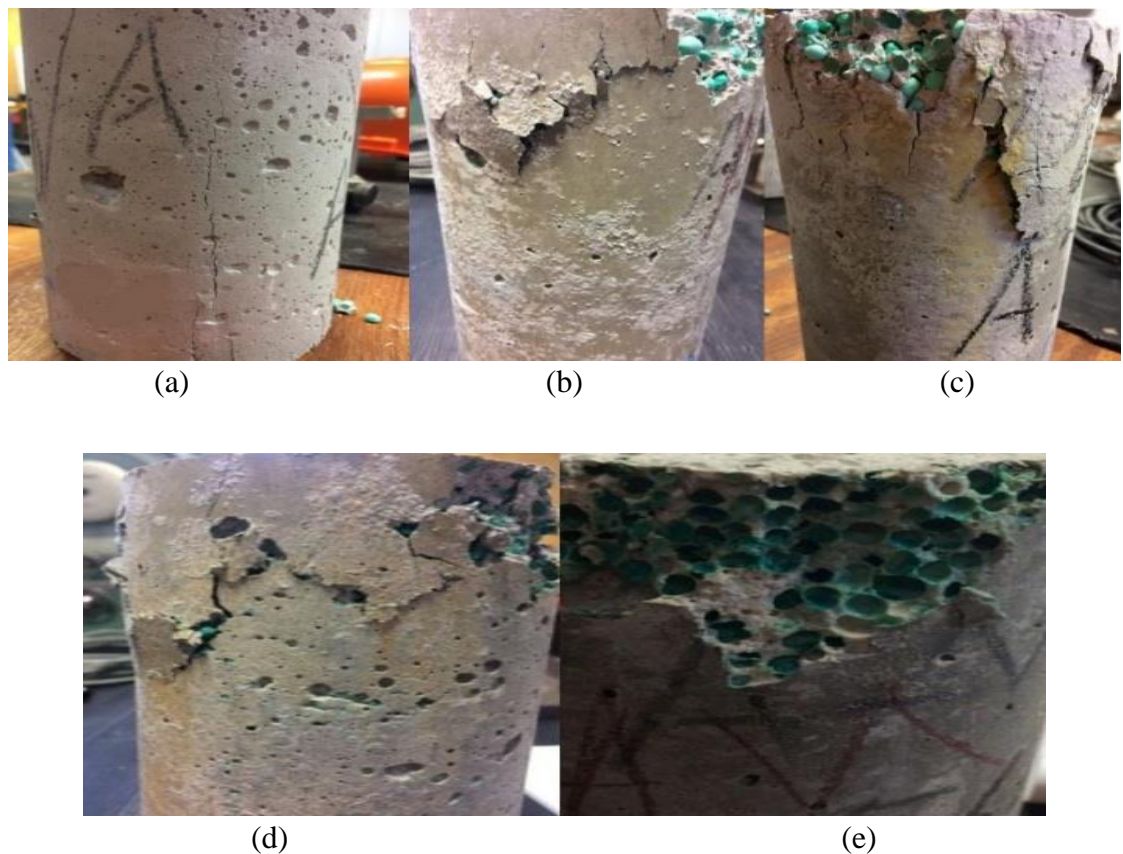


Figure 4. 4 Failure modes of concrete; (a) V1 (ADC), (b) V2 (ADC), (c) V3 (ADC), (d) V4 (ADC), (e) V4 (WC)

4.3.3 Splitting tensile strength

The splitting tensile strength of the proposed concrete mixes is presented in Table 4. 3. The tensile strength is a standard to assess the susceptibility to cracking of concrete. The tensile strength after 28 days of the proposed concrete under different curing conditions of ADC, FC and WC varied from 0.28-0.11 MPa, 0.29-0.09 MPa and 0.29-0.08 MPa, respectively. An improvement in tensile strength of control specimens was observed as the curing method was changed from air curing to moist curing, while this trend shows an inverse effect for concrete containing EPLA aggregate. The highest tensile strength was observed in mix V1 (100% vermiculite) when cured in a moist condition. In the case of the air cured sample, a range of 14-60% reduction in tensile strength was observed for concrete containing EPLA beads compared with mix V1. Also, the tensile strength decreased about 72% in a sample with an EV/EPLA ratio of 0.25 cured in water. This change in strength development can be attributed to the alkaline reactivity of EPLA. In the case of water cured samples and comparison with mix V1, the reduction in tensile strength of mix V2, V3, V4 and V5 was 48%, 62%, 65% and 72%, respectively. It was observed that the tensile strength of the control specimen was increased by about 3% as the sample cured in a moist condition. The splitting tensile strength of the proposed concrete is lower than a structural lightweight concrete grade, which should be greater than 2.0 MPa, based on ASTM [188] . This type of concrete can be categorized as ultra-lightweight concrete for a non-structural component and mostly as filler for an insulating layer. The following equations are showing the relationship between compressive strength and tensile strength of the proposed concretes (Eq. 4.4 – 4.6).

$$f_{ta} = -0.51f_{ca} + 0.87 \quad [4.4]$$

$$f_{tf} = -0.69f_{cf} + 0.868 \quad [4.5]$$

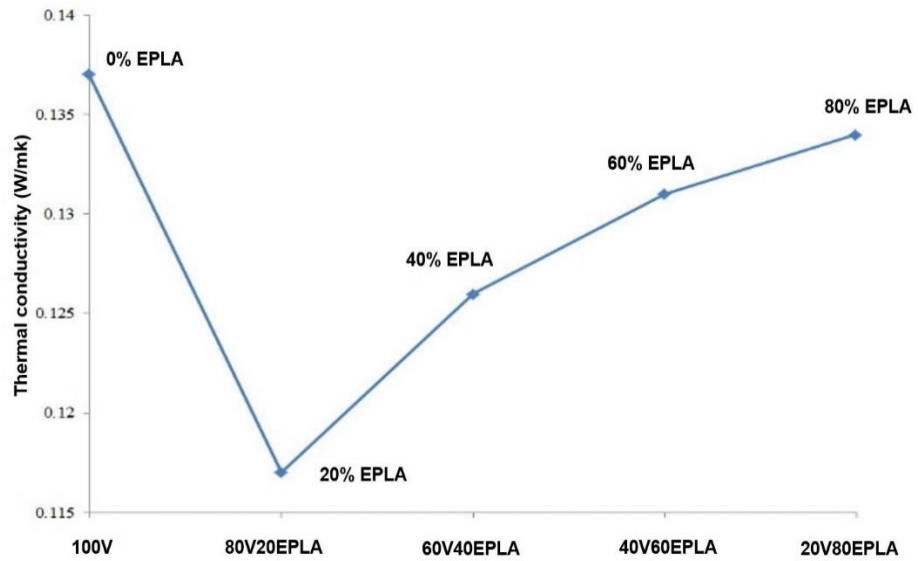
$$f_{tw} = -0.76f_{cw} + 0.866 \quad [4.6]$$

Where, f_{ca} is compressive strength – ADC (MPa), f_{ta} is tensile strength – ADC (MPa), f_{cf} is compressive strength – FC (MPa), f_{tf} is tensile strength – FC (MPa), compressive strength (MPa), f_{cw} is compressive strength - WC (MPa), f_{tw} is tensile strength – WC (MPa).

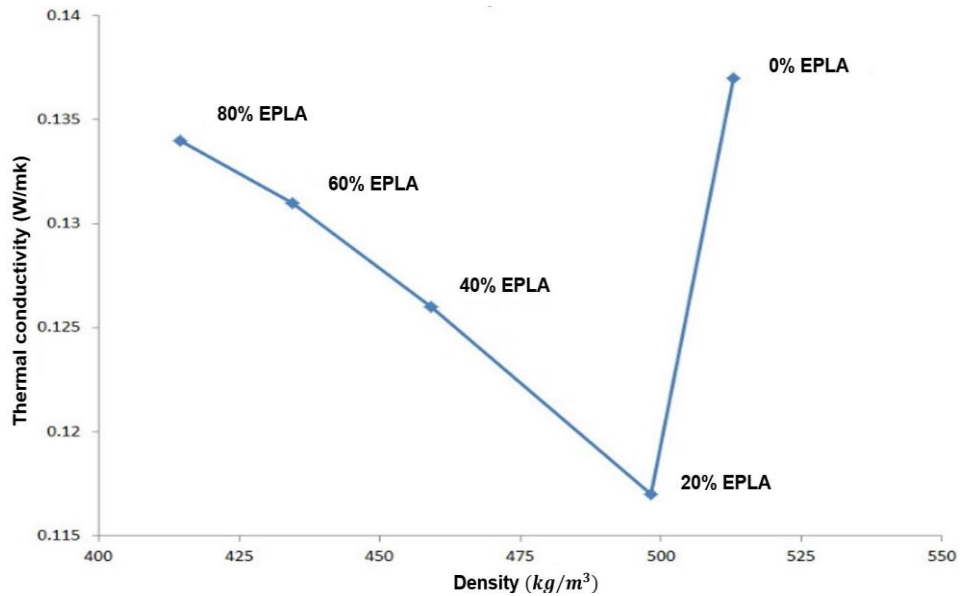
4.3.4 Thermal conductivity

The variation of thermal conductivity (TC) of vermiculite concrete containing a different ratio of EPLA replacement is shown in Table 4. 4 and Figure 4. 5. The parameters such as concrete temperature, moisture content, mineralogical characteristics of aggregate and density are influencing the TC value of concrete [70]. The thermal conductivity of lightweight concrete is about half the one of normal concrete due to the porous structure of lightweight aggregate [189]. However, a further reduction can be obtained with an increase in concrete porosity by using an air-entraining agent [190]. The proposed lightweight concrete with different EPLA to vermiculite ratios showed about 26 to 30 times smaller TC values compared with normal concrete containing quartzite aggregate (about 3.5 W/mK). The highest and lowest value of TC was obtained for samples with 0% (0.1375 W/mK) and 20% (0.1170 W/mK) EPLA, respectively. However, the TC value was increased with an increase in EPLA replacement ratio. For 20%, 40%, 60% and 80% EPLA replacement, the declines in TC value were 14.9%, 8.4%, 4.6% and 2.2%, respectively, compared with the corresponding control sample (V1). The results show that the maximum reduction was observed at the lowest EPLA replacement (V2).

As shown in the Figure 4. 5a, inclusion of EPLA aggregate imposes an inverse effect on thermal conductivity (TC) of concrete as the thermal conductivity was increased with an increase in the ratio of EPLA aggregate. This reduction is relatively high for concrete containing 20% PLA. For a greater EPLA replacement a significant increase in TC was observed due to changes in mineralogical characteristics of the matrix. As the thermal conductivity of vermiculite concrete containing 40% EPLA (V3), 60% EPLA (V4) and 80% EPLA (V5) was 7.7%, 12% and 14% higher than samples containing 20% EPLA (V2). The TC values of the proposed concretes varied from 0.117 to 0.137 W/mK for specimens with 20% EPLA (V2) and 0% EPLA (V1), respectively. In addition, it was found that the TC value of vermiculite-EPLA concrete is proportional to EPLA content rather than concrete density (Figure 4. 5b). These unexpected changes in TC value can be attributed to the alkaline reactivity of EPLA. Concrete carbonation causes a decrease in concrete porosity, pore distribution, deterioration and changes in the microstructure of concrete [191]. In fact, the carbonation products such as calcium carbonate and silica gels occupy a bigger molar volume compared with calcium hydroxide and calcium silicate hydrate [192].



(a)



(b)

Figure 4. 5 Thermal conductivity of EPLA-vermiculite concrete; (a) effect of EPLA ratio, (b) effect of concrete density.

Various researchers indicate that TC of concrete is a factor of its density [193]. However, the thermal conductivity of ultra-lightweight concrete containing polymer products is a factor of lightweight aggregate characteristics and its density along with concrete density. The following equation (Eq. 4.7) is developed with the parameters concrete density, vermiculite

density, vermiculite ratio, the relative density of EPLA and EPLA ratio to predict the thermal conductivity of ultra-lightweight concrete. The results from the experimental investigation and the proposed equation are compared with the ACI equation (Eq. 4.8).

Table 4. 4 Thermal conductivity of vermiculite concrete containing PLA aggregate

Specimen	Density (kg/m^3)	Thermal Conductivity (W/m.K)		
		Experimental results	Proposed Equation	ACI equation
V1	512.85	0.1375	0.1372	0.1632
V2	498.22	0.1170	0.1361	0.1603
V3	459.13	0.1260	0.1299	0.1526
V4	434.50	0.1312	0.1249	0.1480
V5	414.51	0.1345	0.1109	0.1443

$$\lambda = \left(\frac{\sqrt{\gamma_{concrete}}}{(\gamma_{vermiculite} \cdot R_{vermiculite}) + (\gamma_{EPLA} \cdot R_{EPLA})} \right)^{K + \frac{0.5 R_{EPLA}}{R_{vermiculite}^{0.5}}} \quad [4.7]$$

$K = 1.40$ (for vermiculite concrete)

$$\lambda = 0.086e^{0.00125\gamma} \quad [4.8]$$

Where, $\gamma_{concrete}$ is concrete density (kg/m^3), $\gamma_{vermiculite}$ is vermiculite density (kg/m^3), $R_{vermiculite}$ is vermiculite ratio (volume %), γ_{EPLA} is EPLA density (kg/m^3), R_{EPLA} is EPLA ratio (volume %), K is a constant value.

4.3.5 Water absorption

The water absorption test results of all mixes is presented in Table 4. 5 and Figure 4. 6. The quality and durability of concrete is a factor of the water absorption ratio [194]. The water absorption ratio is a parameter for porosity and pore structure characteristics of concrete. The water absorption of lightweight aggregate significantly affects the microstructure of paste and its interfacial zone because of the amount of pore area in the interfacial transition zone

is increasing the absorption of aggregates [195]. It was observed that the absorption characteristic of EPLA samples were much lower than the control sample (V1) due to the presence of hydrophobic aggregate with a zero absorption ratio, i.e. EPLA. The lowest and highest water absorption values were obtained for sample V5 with 80% EPLA and 20% vermiculite and V1 with 100% vermiculite, respectively. Compared with mix V1, a decrease in absorption ratio of EPLA concrete was 60%, 102%, 187% and 306% after 24 hours and 36%, 53%, 118% and 188% after 72 hours for samples V2, V3, V4 and V5, respectively. A set of equations is proposed to estimate the water absorption ratio of vermiculite and EPLA vermiculite concrete (Eq. 4.9). Time (t), relative density (RD_v), absorption ratio (WA_v) of vermiculite, volume of EPLA and volume of vermiculite are considered as key factors for developing the following equations.

Table 4. 5 Water absorption results of proposed concretes.

Specimen	Water absorption ratio (%)						Difference		
	Experimental			Proposed equation			Experimental-Equation		
	1 h	24 h	72 h	1 h	24 h	72 h	1 h	24 h	72 h
V1	58	69	75	58	70	75	1.0	0.9	1.0
V2	36	43	53	39	47	52	0.9	0.9	1.0
V3	26	34	47	25	33	38	1.0	1.0	1.2
V4	17	24	33	17	23	32	1.0	1.0	1.0
V5	8	17	25	8	17	26	1.0	1.0	1.0

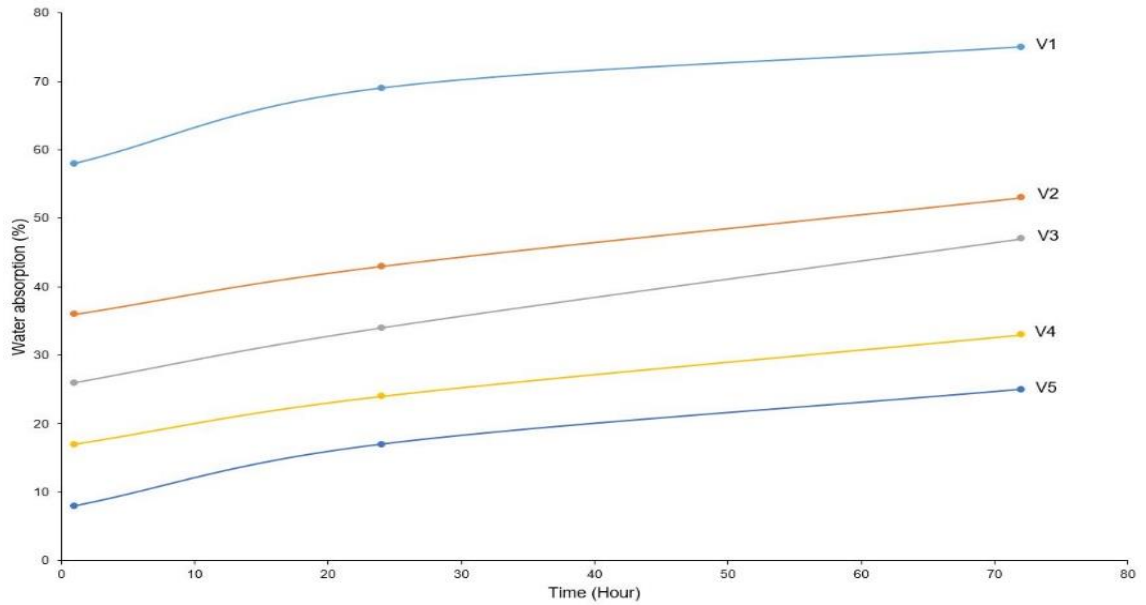


Figure 4. 6 Time vs. water absorption ratio (%) of vermiculite concrete containing EPLA

$$WA_R = \frac{(A)^{0.1}(BC)}{\sqrt{RD_v}} \quad [4.9]$$

Where,

$$A = 60t^{0.6}$$

$$B = RD_v WA_v$$

$$C = R^{R+R^{RD_v} \frac{t}{RD_v}}$$

Where, t is time (hour), RD_v is relative density of vermiculite(kg/m^3), WA_v is water absorption ratio of vermiculite aggregate (%), R is ratio of vermiculite aggregate (Vol. %).

4.3.6 pH evaluation and concrete carbonation

Table 4. 6 shows the changes of pH levels of concrete at the age of 1day, 3 days, 7 days, 14 days and 28 days. The pH of concrete and its levels significantly affect the hydration process of concrete [196]. The experiments show that the application of EPLA aggregate results in

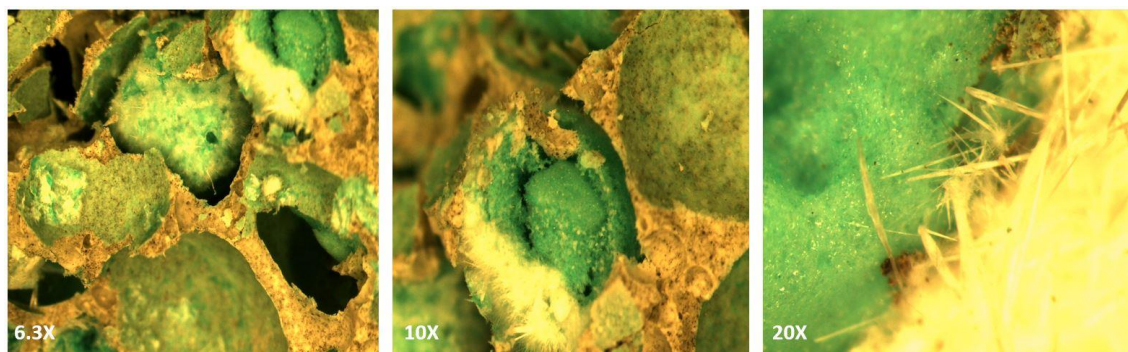
concrete carbonation and significantly changed the microstructure of concrete. In fact, pH lowering below 12.5 causes a decrease of pore liquids acidity and therefore decreases the instability of the hydration product. The decrease of pH also causes to decrease the amount of calcium carbonate and to decrease the reaction rate of the production of C-S-H as a hardening element in concrete [197].

However, the results show that the level of pH was stable and no significant reduction was observed of pH levels in concrete containing EPLA aggregate. In fact, the carbonation process of concrete containing EPLA is significantly different from normal concrete. The changes in pH level and the penetration of carbon dioxide (CO_2) into the hardened concrete and its reaction with portlandite in the existence of moisture form calcium carbonate ($CaCO_3$). Also, the carbonation of concrete can take place by hydroxides and sulfates of either sodium or potassium. These elements are much more soluble in water than calcium and cause efflorescence appear more rapidly than calcium hydroxide. The rate of carbonation in normal concrete is a factor of relative humidity, CO_2 gas concentration, ambient temperature and penetration pressure. In contrast, the rate of carbonation in EPLA concrete depends mostly on the degradation of EPLA and its alkaline reactivity (Figure 4. 7).

Table 4. 6 pH level variation of water and air cured samples with 70% EPLA (V5).

	pH level									
	1 Day		3 Days		7 Days		14 Days		28 Days	
	ADC	WC	ADC	WC	ADC	WC	ADC	WC	ADC	WC
V5	12.9	12.9	13.0	12.9	13.1	13.1	13.0	13.0	13.0	13.1

ADC: Air Cured, WC: Water Cured.



EPLA degradation and concrete carbonation

Figure 4. 7 The degradation of EPLA aggregate and concrete carbonation

The degradation of EPLA takes place because of an attack by the external elements as EPLA itself is unable to break down and be consumed [198]. The factors such as stereochemistry, crystallinity and molecular weight significantly affect the biodegradation behavior of EPLA [199]. This phenomenon can be described by the fact that the surface of EPLA was in contact with alkaline components of cement. The EPLA lost its hydrophobicity and started to take up water. The hydrolysis after the alkaline attack was the main cause of EPLA degradation and breaking loose. The rate of EPLA degradation and concrete carbonation increased in samples cured in a moist condition (Figure 4. 8).

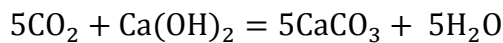
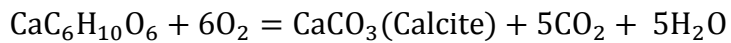
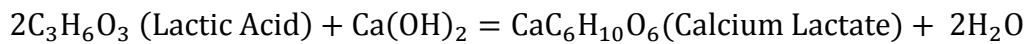
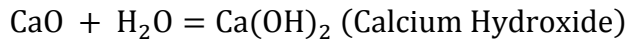


Figure 4. 8 Carbonation of EPLA concrete

EDS and XRD analysis are used to assess the efflorescence of EPLA concrete (Figure 4. 9). The EDS analysis shows that the efflorescence on the surface of concrete and around EPLA beads mostly contains calcium (Ca), silicon (Si), sodium (Na) and magnesium (Mg). It can be found that the chemical reaction of lactic acid with calcium hydroxide and sodium hydroxide was the main cause of EPLA degradation and releasing calcium lactate and sodium lactate. The consumption of oxygen by calcium lactate [200] and the reaction between sodium lactate and calcium sulphate were the main causes of calcite and trona crystal production in the highly alkaline environment of cement [201]. The XRD semi quant (%) analysis shows that the efflorescence contains 54% calcium carbonate (calcite) and 46%

sodium hydrogen carbonate hydrate (trona). The reaction scheme and chemical process of calcium carbonate formation are described as follows.

The chemical reaction between EPLA and calcium hydroxide:



The chemical reaction between EPLA and sodium hydroxide:

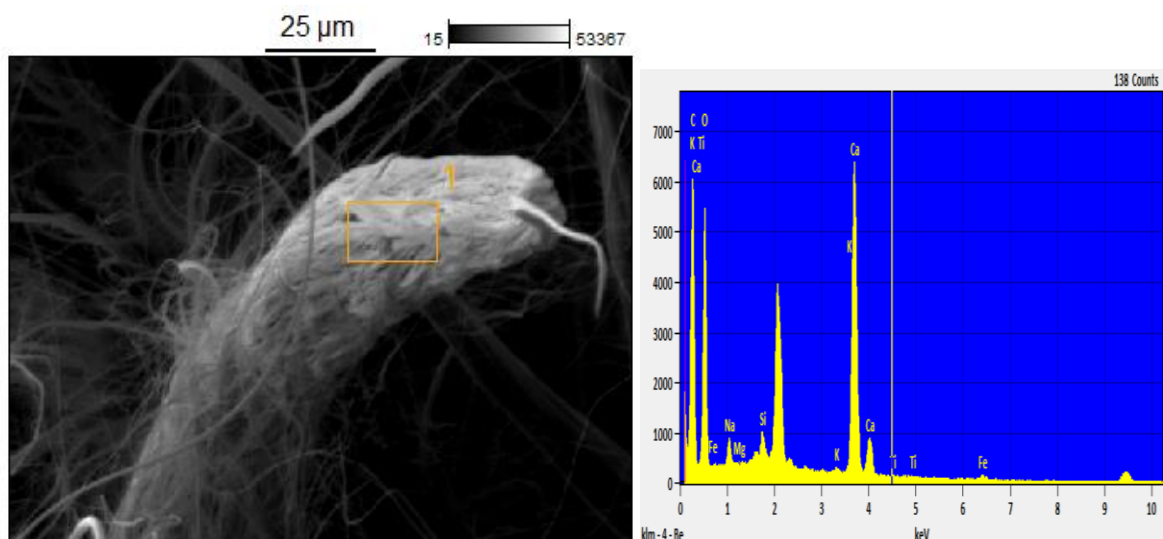
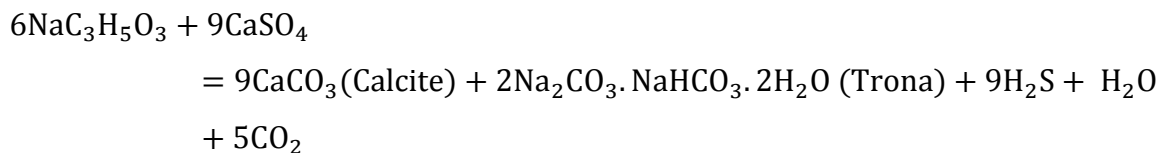


Figure 4. 9 Analysis of concrete efflorescence

4.3.7 Electrical resistivity and setting time

The electrical resistivity response is used to determine the setting time of EPLA concrete with varying EV/EPLA ratios. The parameters such as water-cement ratio, additive, aggregate, the degree of hydration, porosity, pore size distribution and cement paste microstructure significantly affect the electrical resistivity values of concrete. This value is a function of the ion concentration and its mobility in the pore solution [202, 203]. In fact, the electrical conduction takes place because of ion transport through the pore solution and mainly depends on ion concentration and concrete porosity [204]. The experimental results showed a decrease in electrical resistivity with an increase in EPLA ratio. The matrix with a higher EPLA ratio has higher porosity due to the alkaline reactivity of EPLA and insulate aggregate (EPLA) which presents a lower resistivity.

The resistivity of concrete containing EPLA was affected by both hydration age and EPLA ratio. In fact, the alkaline reactivity of EPLA influences the microstructure of the cement matrix concentration and mobility of the ions in the pore solution. The coarser pore size distribution and higher ionic concentration cause a lower electrical resistivity in concrete containing higher EPLA ratio. The electrical resistivity of concrete is primarily associated with the ion transfer through the porous materials and can be used as an indicator of the hydration process. The changes in electrical resistivity of concrete are related to the microstructural changes [205]. Figure 4. 10a, and Figure 4. 10b show the resistivity changes up to 1440 min (1 day) and 10080 min (7 days), respectively. Two critical points namely P_I and P_F are marked and identified to assess the electrical resistivity and setting time of concrete. The minimum point (P_I) is marked at the point where the resistivity is decreased and considered as the initial setting time at the early age of curing. Such a reduction in resistivity can be attributed to the fact that mixing of concrete components with water causes the potassium (K^+), sodium (Na^+), calcium (Ca^{2+}), hydroxyl ions (OH^-) and sulfate (SO_4^{2-}) of cement to dissolve into the water and form electrolyte [205].

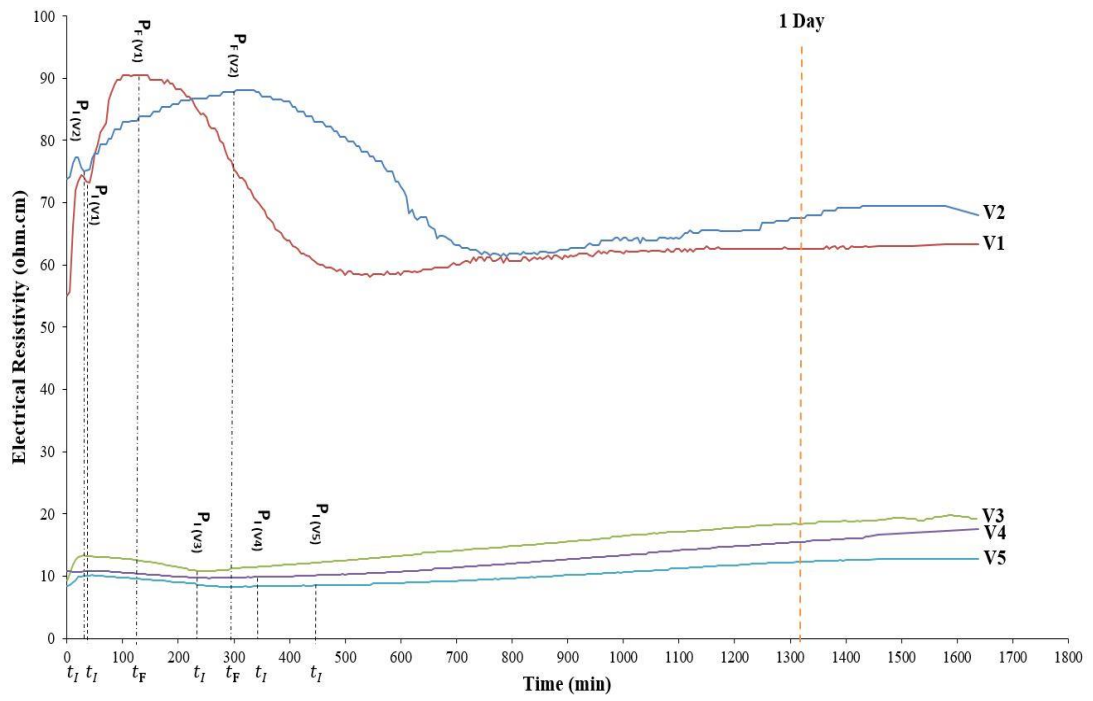
The electrical resistivity response shows that the minimum point for mix V1, V2, V3, V4 and V5 occurred after 40 min (0.67 hours), 20 min (0.34 hours), 265 min (4 hours and 25 min), 400 min (6 hours and 40 min) and 500 min (8 hours and 20 min), respectively (Table 4. 7). As compared with control mix (V1), the addition of EPLA beads leads to a longer time to reach saturation due to the alkaline reactivity of EPLA beads. At the second stage of

hydration, the electrical resistivity of concrete steadily increases with time. The increase in electrical resistivity shows a decrease in porosity and increase in tortuosity. The results show that the changes in electrical resistivity of mixes containing greater amounts of EPLA were much lower than that of the control samples and samples with low percentages of EPLA (Figure 4. 10a,b). A significant delay in setting time, i.e. remaining in a plastic state after 3 days, was observed in the sample V5 containing a higher portion of EPLA. The mixes V1, V2, V3, V4 and V5 transit from the plastic stage to the hardened stage (P_F) after 155 min, 340 min, 1600 min, 3918 min and 4638 min, respectively.

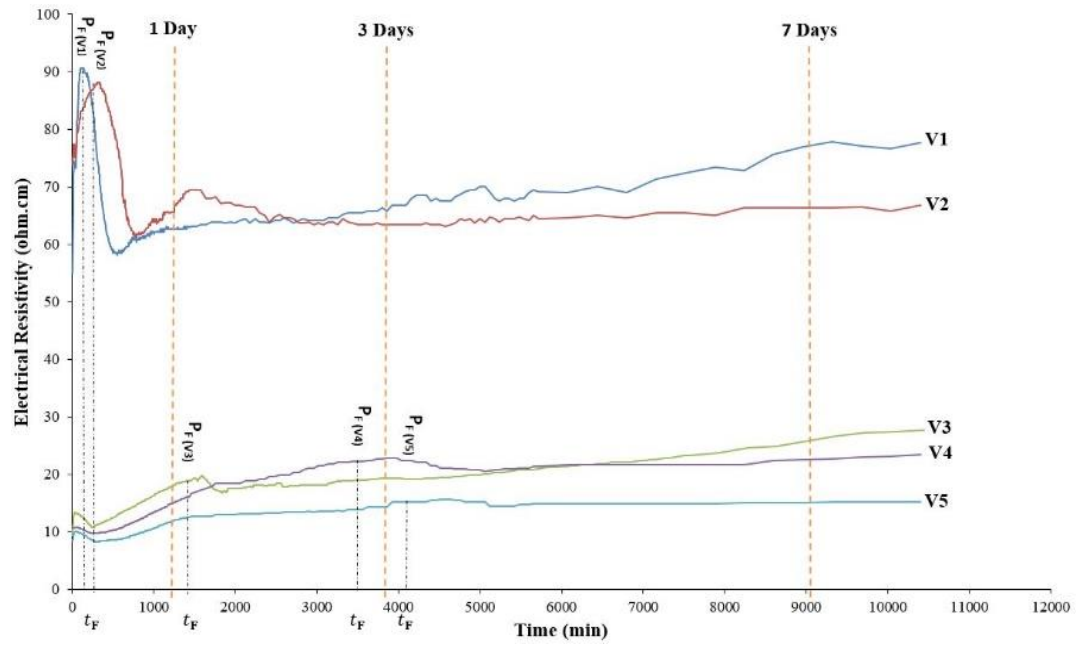
Factors such as alkaline reactivity of EPLA change the microstructure of concrete and the porous structure of the matrix leads to a significant delay in setting time. The calcium sulphate is an important component of cement that controls the setting characteristics and accelerate hydration of calcium silicate. The changes in sulphate content and sulphate consumption by sodium lactate affect the hardening process and cause concrete deterioration and a delay in the setting time of concrete. However, at the later ages (7days) the electrical resistivity of concrete containing EPLA starts to increase (Figure 4. 10b) mainly due to carbonation of concrete and an increase of the amount of calcium carbonate. The incorporation of EPLA causes an increase in $CaCO_3$ amount as a result of chemical conversion of calcium lactate and sodium lactate into calcium carbonate. This process was more pronounced in samples containing larger amounts of EPLA beads.

Table 4. 7 The initial and final setting time of proposed concretes based on electrical resistivity response.

Specimen	Setting time (min)	
	Initial (P_I)	Final (P_F)
V1	40	155
V2	20	340
V3	265	1600
V4	400	3918
V5	500	4638



(a)



(b)

Figure 4. 10 The electrical resistivity response of concrete; (a) up to 1day, (b) up to 7 days

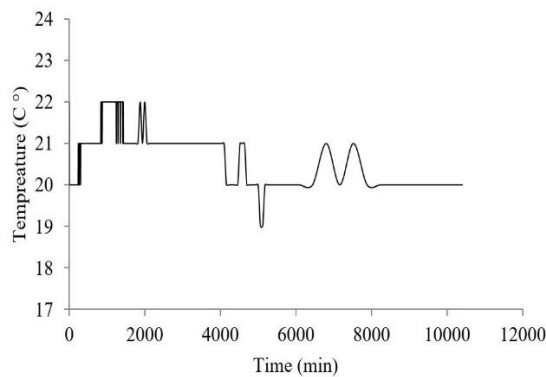
4.3.8 Exothermic reaction

The changes in exothermic reaction of vermiculite concrete with a variation in EV/EPLA ratio is shown in Table 4. 8 and Figure 4. 11. The experimental results reveal that the sample

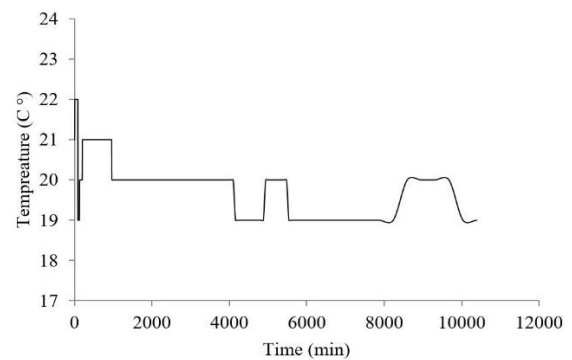
V3 with an EV/EPLA ratio of 1.5 exhibited the highest exothermic reaction intensity, while the sample V5 with the highest EPLA volume of 80% showed the lowest exothermic reaction intensity. It was found that there is a fluctuation in concrete temperature due to the alkaline reactivity of EPLA. In addition, an increase in EPLA content slightly decreases the concrete temperature and causes a delay in setting time. The peak temperature of the control sample was 22 C° which is slightly higher than that of sample V5 with a temperature of 20 C°. It is worth to note that the increase in EPLA volume significantly affects the setting time of concrete, which is mainly related to changes in the hydration process of concrete and alkaline reactivity of EPLA.

Table 4. 8 The peak temperature of curing vermiculite concrete.

	EV/EPLA ratio	Peak temperature, C°	Time at peak temperature, min
V1	-	22	840
V2	4	22	5
V3	1.5	23	25
V4	0.67	22	500
V5	0.25	20	515



(a)



(b)

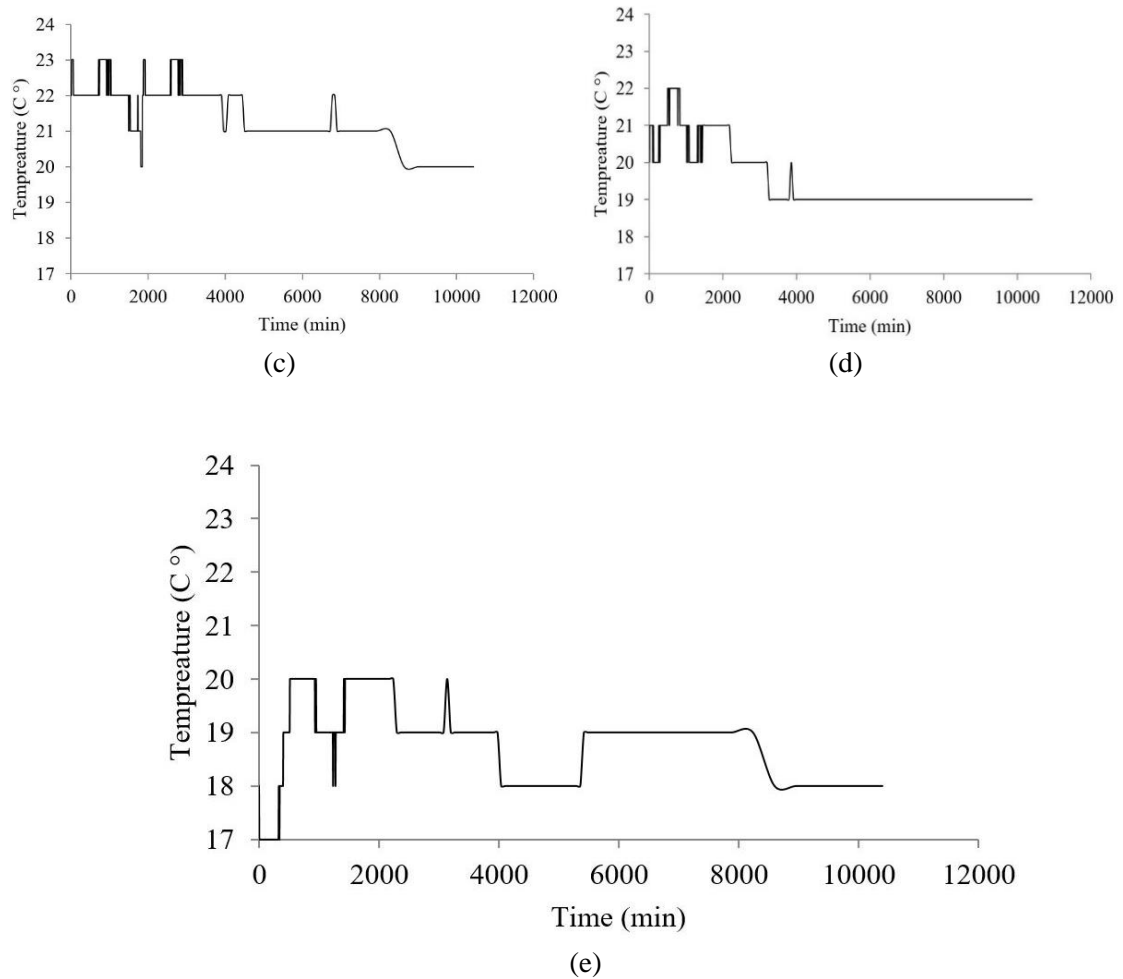


Figure 4. 11 Exothermic reaction of vermiculite and EPLA-vermiculite concrete, (a) V1, (b) V2, (c) V3, (d) V4, (e) V5.

4.3.9 Scanning Electron Microscopy and X-ray Diffraction analysis

A microstructural analysis of a control and mixes containing EPLA was carried out to investigate the effects of using biopolymer materials and reasons for differences in mechanical and thermal properties of concrete. SEM is used to assess and analyses the aggregate phase, paste phase and interfacial transition zone (ITZ) of a concrete matrix. The interfacial zone between aggregate and cement is significantly important as it is the weakest part of the matrix and significantly affects the mechanical properties of concrete [206]. The four main hydration products of the cement-aggregate matrix are calcium silicate hydrate (C-S-H), calcium hydroxide (CH), as well as AFm (Tricalcium aluminate) and AFt (Calcium aluminium sulfate, ettringite) phases [207]. However, parameters such as shape, distribution

of particles, the concentration of particles, the composition of phases and orientation of particles affect the hydration products of the cement-aggregate matrix [206].

The SEM images for the control (V1) and the mix V5 containing 80% EPLA are shown in Figure 4. 12 and Figure 4. 13, respectively. Figure 4. 12 displays the SEM images of the control sample at 2.5K magnification. The microstructure indicated the non-uniform distribution of the hydration products. The phases identified for the control specimen are mostly calcium-silicate-hydrate (C-S-H), calcium hydroxide (portlandite) and calcium sulfoaluminate (ettringite). It was found that C-S-H existed in the form of a fibrous portion (clusters), lapped and joint together by hexagonal plate-like particles (calcium hydroxide) and long whisker-like particles (ettringite). As it is clear from the SEM image, the bond between paste and expanded vermiculite aggregate is lost because of the porous structure of vermiculite and the porous interfacing zone. In addition, the low degree of hydration due to using a high absorbent aggregate (expanded vermiculite) can be another reason for the loose structure and a large number of pores.

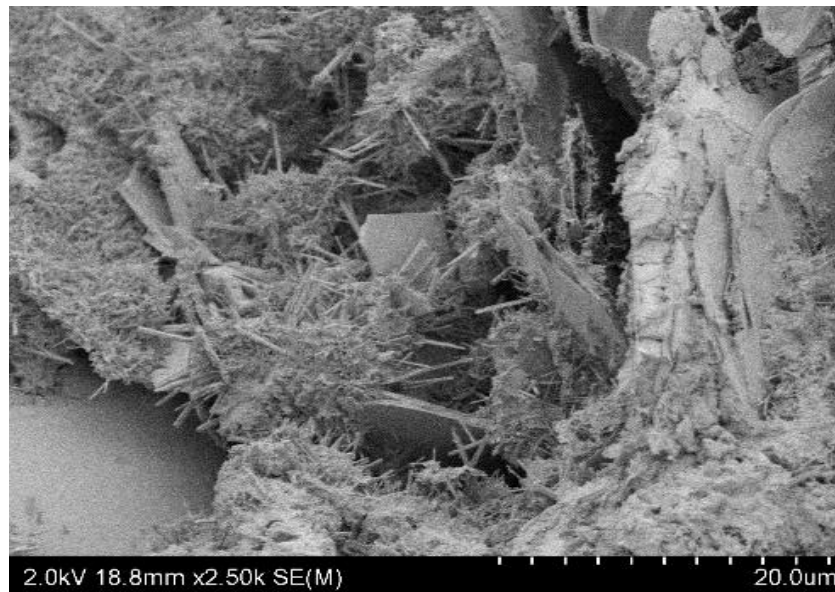


Figure 4. 12 SEM image of mix V1 at 2.5K magnification

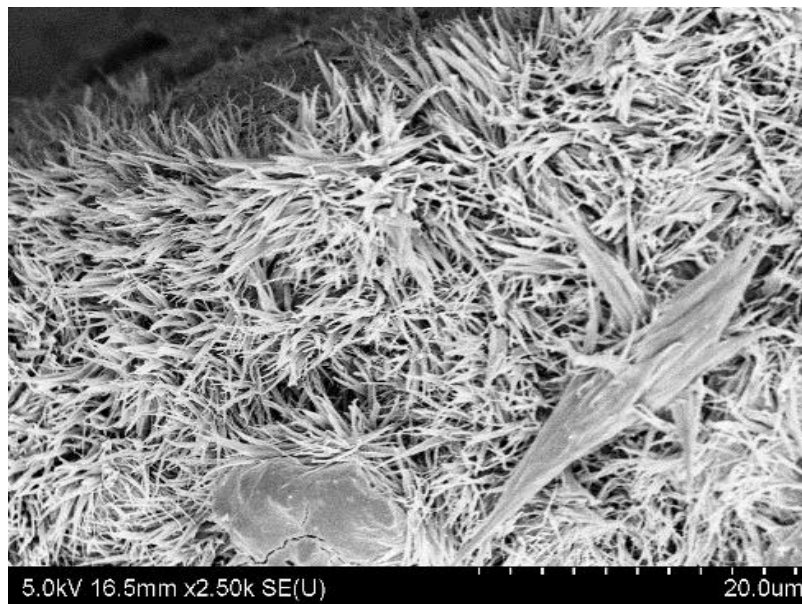
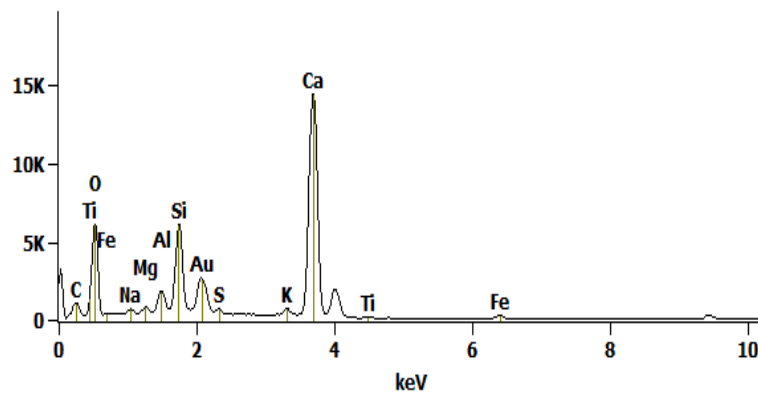
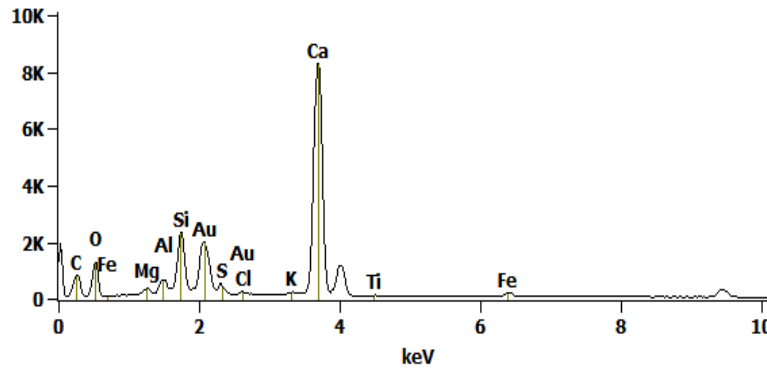


Figure 4. 13 SEM image of mix V5 after 28 days

From the EDS analysis of amorphous substances (Figure 4. 14a), it can be found that the hydration products of vermiculite concrete are mostly comprised of Ca, Si, O as well as Al and C-S-H gel, portlandite and ettringite are present. The semi-quantitative chemical analysis of the control sample shows that the matrix contains 30% calcium hydroxide (portlandite), 28% ettringite and 42% calcium silicate hydrate (Figure 4. 16a).



(a)



(b)

Figure 4. 14 EDS analysis of proposed concrete; (a) sample V1, (b) sample V5.

Figure 4. 13 and Figure 4. 15 show the SEM images of mix V5 after 28 days and one year. The addition of EPLA significantly changed the microstructure and hydration products of concrete due to the degradation of EPLA and its alkaline reactivity. The EDS analysis of mix V5 shows that the hydration products of concrete containing EPLA are composed of Ca, Si, Al, Mg, O and Fe (Figure 4. 14b). As it becomes evident from the SEM image, a large amount of needle crystals appeared in the interfacial zone of paste and aggregate. The semi-quantitative chemical analysis of concrete (Figure 4. 16b) shows that the cement paste is mainly composed of calcite (43%), ettringite (40%) and calcium hydroxide (17%). The presence of a large amount of calcium carbonate may explain the interaction of expanded poly-lactic acid and calcium hydroxide $Ca(OH)_2$. The degradation of EPLA and release of calcium lactate lead to growing calcium carbonate products.

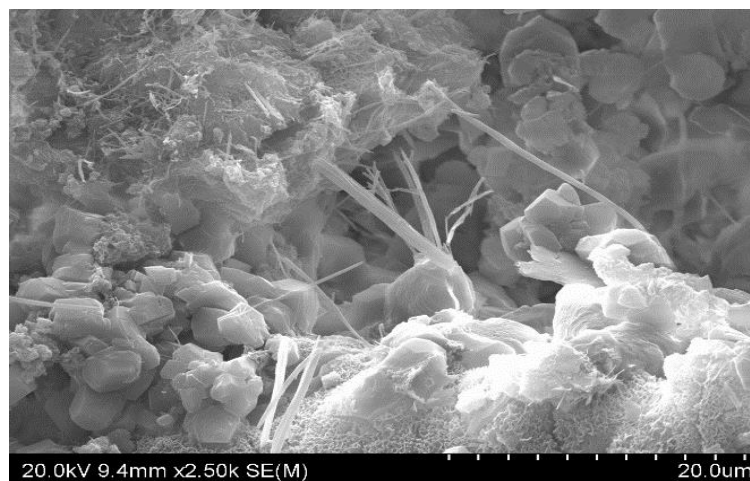
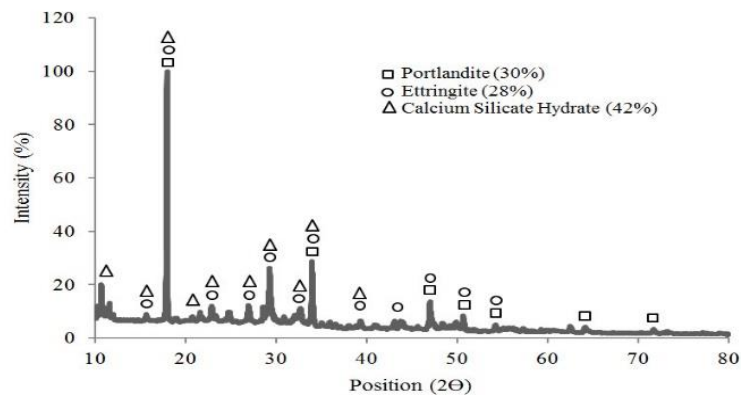
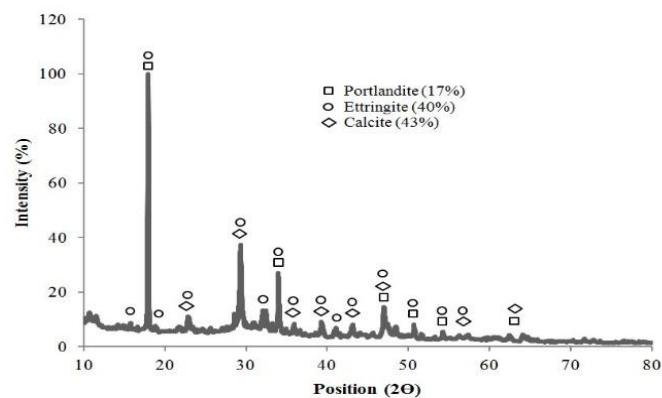


Figure 4. 15 SEM image of mix V5 after one year

These SEM images can provide a visual indication of the microstructural characteristics responsible for the enhancement of the thermal conductivity of the EPLA concrete. The microstructure of the hardened EPLA concrete appeared noticeably denser and compacter with considerably less capillary pores compared to the mix V1. The conversion of calcium silicate hydrate to calcium carbonate was the main microstructural change in concrete containing EPLA. Compared to mix V1, the amount of portlandite decreased from 30% to 17%, while a significant growth in ettringite was observed from 28% to 40% due to the consumption of calcium compound by calcium lactate. However, at the later age of one year the hydration products of EPLA concrete mostly consisted of calcium carbonate (calcite), calcium silicate hydrate (C-S-H), and ettringite (AFt) with significant changes to its microstructure (Figure 4.15 and Figure 4. 17).

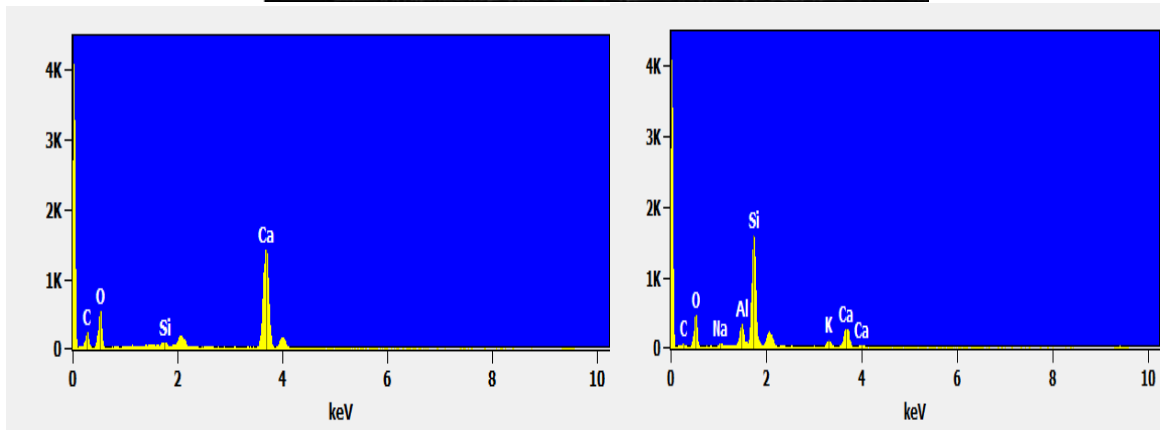
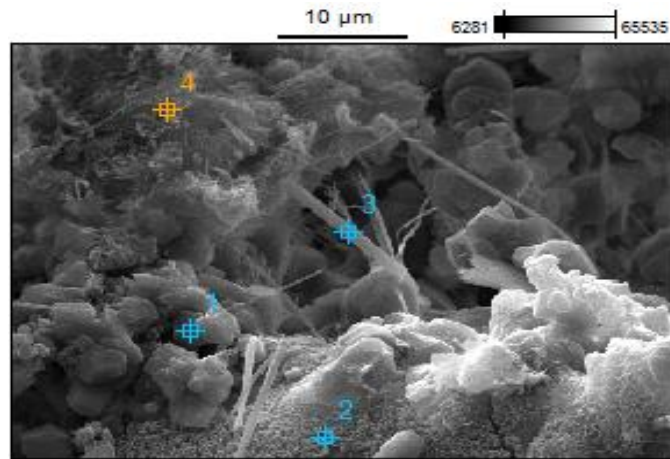


(a)



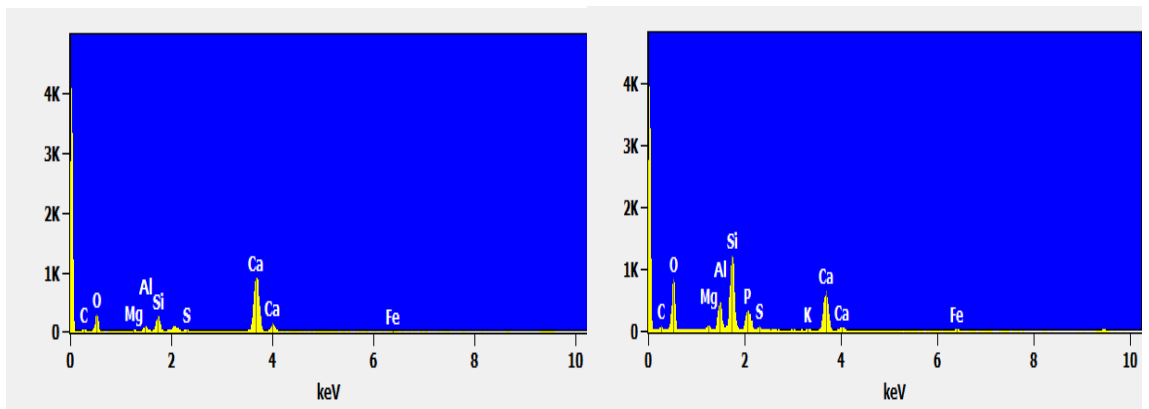
(b)

Figure 4. 16 XRD analysis of proposed concrete; (a) sample V1, (b) sample V5.



(a)

(b)



(c)

(d)

Figure 4. 17 EDS analysis after one year; (a) point 1, (b) point 2, (c) point 3, (d) point 4

4.4 Conclusions

This chapter focused on the development of using expanded poly-lactic acid and expanded vermiculite as aggregates and five different EV to EPLA mix proportions were prepared and assessed to optimize the mix design without visible mix segregation. The parameters studied included density, compressive strength, failure modes, splitting tensile strength, thermal conductivity, water absorption, pH evaluation, evaluation of concrete carbonation, electrical resistivity, setting time, SEM analysis and XRD analysis. Based on the variables assessed, the following conclusions were drawn:

- 1- The replacement of vermiculite aggregate with EPLA aggregate results in a significant reduction in concrete density due to the lower relative density of EPLA compared to EV.
- 2- The compressive strength decreased with an increase in the volume of EPLA mostly due to close to zero strength of EPLA aggregate and bond failure at the interfacial transition zone of aggregate to paste. A further reduction in strength development of EPLA concrete was observed as the sample cured in a moist condition.
- 3- The failure modes of EPLA concrete were significantly different from the control sample. The lack of resisting components, since EPLA beads shrunk and lost their strength in the alkaline environment of cement, and de-bonding of PLA due to alkaline reactivity were the main reasons for changes in the failure mode.
- 4- The inclusion of EPLA beads as lightweight aggregate leads to a lower tensile strength. Compared to the control sample the splitting tensile strength was decreased by 72%.
- 5- The factors such as EPLA ratio and curing condition accelerate the rate of concrete carbonation. Larger amounts of carbonation were observed in samples cured in water.
- 6- The presence of hydrophobic materials leads to a decrease in the water absorption ratio of concrete. However, at the later ages, the degradation of EPLA causes a slight increase in absorption due to water uptake of EPLA beads.
- 7- The influence of EPLA degradation and its chemical reaction with alkaline components of cement on thermal conductivity of concrete was notable. The alkaline reactivity and changes in the microstructure of concrete cause an increase in thermal conductivity values.

- 8- The addition of EPLA aggregate causes a delay in setting time of concrete and its influence on exothermic reaction was almost minimal.
- 9- The hydration products of EPLA concrete were significantly different from the control sample. A larger amount of calcium carbonate (calcite) was observed in the samples containing EPLA aggregate.
- 10- The XRD analysis shows that the amount of calcium carbonate significantly increased in the samples containing EPLA. Calcium silicate hydrate was replaced with calcium carbonate due to the alkaline reactivity of EPLA. However, at the later ages, more calcium silicate hydrate gel was found in the microstructure of concrete.

Furthermore, a set of equations was developed to estimate the required water-cement ratio, required cement content, thermal conductivity, water absorption and the relationship between compressive strength and tensile strength.

CHAPTER 5

PERLITE CONCRETE CONTAINING EPLA

5.1 Introduction

It was found in the previous chapter that the application of vermiculite aggregate with its high absorption ratio causes significant changes to engineering properties and setting time of concrete containing EPLA. The high absorption ratio of vermiculite concrete accelerates the degradation rate of EPLA due to the fact that the EPLA beads experienced a larger period in the moist condition. In this chapter the expanded vermiculite was replaced with expanded perlite which has a lower absorption value and better structural properties compared to vermiculite aggregate. In this regards, seven mixtures were prepared by partially replacing expanded perlite (EP) aggregate with EPLA and EPS to 0%, 30%, 40% and 60% by aggregate volume. The results of EPLA concrete were compared to the EPS concrete with identical mix proportions to evaluate the performance of the proposed concretes. The mechanical properties, thermal conductivity, fire resistance, electrical resistivity, setting time, exothermic reaction, and microstructural properties of the concrete were studied and discussed. The results reveal that the replacement of EP with EPLA causes a considerable reduction in mechanical strength of concrete. It was found that the chemical reaction of EPLA in the highly alkaline environment of cement causes significant changes in the microstructure of concrete. A large amount of calcium carbonate was found as hydration products of EPLA concrete. The carbon dioxide production and heat release rate of EPLA concrete in a fire is much lower than that of concrete containing expanded polystyrene. Contrary, a higher carbon monoxide production was observed in samples containing EPLA. The electrical resistivity and water absorption ratio of concrete increased with an increase in EPLA volume.

5.2 Experimental program

5.2.1 Materials

The specification of materials are explained and provided in Chapter 3.

5.2.2 Mix design and mix proportion

The mix proportions of the proposed lightweight concrete are presented in Table 5. 1. In total nine types of lightweight concrete mixes with variations in EPLA and EPS ratios were prepared with a fixed cement content of 301 kg/m³. The water-cement ratio and cement content are designed based on the proposed equations explained in Chapter 3 (here repeated as Eq. 5.1 and Eq. 5.2). However, some modifications are applied due to the differences in water absorption ratio of perlite and vermiculite aggregate. The EPLA and perlite were mixed with a ratio of 100:100, 40:60, 60:40 and 30:70. The mix design was targeted to attain a density of 488 kg/m³ for samples with 100% perlite (P1). It is worth to note that the cement content is adopted based on the required density.

$$\frac{w}{c} = a = \frac{0.76\gamma^{0.0001\gamma}}{0.0001\gamma \cdot \gamma^{0.5}} \quad [5.1]$$

$$\begin{cases} 1000 = \frac{(\frac{\gamma}{a})^{0.5}}{RD_c \cdot RD_p} C + \frac{215a(\frac{a}{\gamma})^{0.5}}{RD_p} C + 10aV_p \\ \gamma = \gamma^{10a} C + aC + RD_p V_p \end{cases} \quad [5.2]$$

Where, γ is density of concrete (kg/m³), a is water-cement ratio, C is cement content (kg/m³), RD_c is relative density of cement, RD_p is relative density of perlite, V_p is perlite volume (m³).

Table 5. 1 Mix proportion of perlite and perlite-PLA concrete

Mix No.	Mix proportion (kg/m ³)						
	Effective w/c ratio	C	W	EP	PLA	EPS	AEA
P1 (100EP)	0.343	301	289	135	-	-	0.0041
PP2 (60EP40EPLA)	0.343	301	276	81	7.6	-	0.0041
PE2 (60EP40EPS)	0.343	301	276	81	-	4.0	0.0041
PP3 (40EP60EPLA)	0.343	301	265	54	11.4	-	0.0041
PE3 (40EP60EPS)	0.343	301	265	54	-	6.0	0.0041
PP4 (30EP70EPLA)	0.343	301	232	40.5	13.3	-	0.0041
PE4 (30EP70EPS)	0.343	301	232	40.5	-	7.0	0.0041
PP5 (20EP80EPLA)	0.343	301	164	27	15.2	-	0.0041
PE5 (20EP80EPS)	0.343	301	164	27	-	8.0	0.0041

C is Cement, W is water, EP is expanded perlite, EPLA is expanded poly-lactic acid, EPS is expanded polystyrene, AEA: air-entraining admixture.

5.3 Experimental procedure

Two types of curing regimes, namely moist curing (WC) and air dried curing (ADC) were chosen to assess the effect of the curing conditions on mechanical properties of the proposed concretes. In the case of moist curing, the specimens were kept in water at 20 °C for the whole curing period, while air cured samples were kept in a laboratory environment for 28 days after demoulding.

The slump, density, compressive strength, thermal conductivity, water absorption, XRD, EDS, SEM, electrical resistivity, setting time and fire resistance test were carried out. It is worth to note that the average results of three specimens were considered to evaluate the engineering properties of proposed concretes. The descriptions of test methods are provided in Chapter 3.

5.4 Results and discussion

5.4.1 Workability

Table 5. 2 presents the slump values of the proposed concretes. Workability of lightweight concrete is a vital factor and significantly affects the property of concrete. Lightweight concrete is mostly designed to be cast without vibration due to difficulties of compaction and mixture segregation during casting [184]. Although, a slump value of 50-75 mm is suggested for lightweight concrete, but a slump value of 220 mm is adopted for this experiment based on visual observation and trial tests to obtain acceptable compaction and workability. It can be seen that all the mixtures had slump values ranging from 235 to 175mm except sample PP5. The experimental results show that an increase of the fraction replacement of perlite with EPLA initially slightly decreased the slump of the concrete. However, further replacement up to 80% of aggregate volume, causes a significant reduction of slump value and a lower degree of compaction (Figure 5. 1). This phenomenon is mainly attributed to an increase in specific surface area and consequently increase in water demand. Compared to the control sample the workability of concrete was decreased by 2.2%, 4.4%, 20% and 77.7% for samples PP2, PP3, PP4 and PP5, respectively. The same trend of slump reduction was observed in samples containing EPS aggregate.



(a)



(b)

Figure 5. 1 The workability and slump of proposed concrete, (a) sample PP2, (b) sample PP5.

5.4.2 Density

The density of the proposed mixtures is presented in Table 5. 2. The density of lightweight concrete mostly depends on the bulk density of lightweight aggregate and the cement content. As expected, the density of perlite concrete was reduced with an increase in EPLA and EPS ratio. This trend is mainly attributed to the fact that the EPLA and EPS beads are about 92.6% and 88% lighter than the relative density of perlite aggregate (135 kg/m^3). In total two density ranges (fresh and air-dried density) were obtained by replacing perlite aggregate with certain percentages of EPLA aggregate. The fresh and dry densities of EPLA and EPS concrete specimens varied from 765 kg/m^3 to 389.0 kg/m^3 and 493 kg/m^3 to 302.2 kg/m^3 along with from 765 kg/m^3 to 384.0 kg/m^3 and 493 kg/m^3 to 312.6 kg/m^3 , respectively. The application of polymer aggregate leads to an increase in total porosity of concrete and a lower density. The lowest ranges of densities were observed in the sample with larger amounts of polymer aggregates due to the increase in concrete porosity and void spaces in the concrete matrix. However, a further increase in concrete porosity was observed in EPLA concrete due to the chemical interaction of EPLA and alkaline components of cement, which causes an increase in CO_2 gas concentration. The lowest density was observed in the sample with 70% EPLA aggregate.

The density of the control sample P1 was about 79.5% lighter than normal weight concrete (2400 kg/m³). The replacement of perlite aggregate with EPLA and EPS particles in ratios of 40%, 60% and 70% of aggregate volume causes a further reduction in concrete density. The concretes containing 40%, 60% and 70% EPLA were 19%, 27% and 39% lighter than the control sample (P1), respectively. Compared to the EPS concrete, the concrete containing 40% (PP2), 60% (PP3) and 70% (PP4) is about 3.2%, 3.6%, 3.3% heavier than corresponding EPLA concrete due to alkaline reactivity and an increase in total concrete porosity.

Table 5. 2 Effect of EPLA replacement on workability and density of perlite concrete.

Mix No.	Slump (mm)	Density (kg/m ³)	
		Fresh	Air Dried
P1	220	765.0	493.0
PP2	235	568.0	400.2
PE2	220	545.5	415.5
PP3	230	440.8	360.2
PE3	215	447.0	371.5
PP4	180	389.0	302.2
PE4	175	384.0	312.6
PP5	55	Failed	Failed
PP5	50	Failed	Failed

5.4.3 Compressive strength

The compressive strength of perlite concrete containing different ratios of polymer in air and water curing of up to 56 days are presented in Table 5. 3. The curing of concrete plays a significant role in the performance and strength development of concrete. ACI 318 [79] has suggested that concrete should be kept in a moist environment for at least the first seven days. As expected, the compressive strength was found to decrease with an increase in EPLA ratio mainly due to the almost zero strength of EPLA particles. Air-cured samples show a higher compressive strength apart from the control specimen compared to the corresponding water

cured samples after 28 and 56 days. This phenomenon can be attributed to the fact that EPLA particles lost their strength and de-bonded from the surrounding concrete when subjected to an alkaline solution (Figure 5. 2 and Figure 5. 3).

Table 5. 3 Compressive strength of perlite and EPLA-perlite concrete

Mix No.	Compressive Strength (MPa)			
	28 days		56 days	
	Air Cured	Moist Cured	Air Cured	Moist Cured
P1	4.37	4.62	5.29	5.83
PP2	2.88	2.57	3.11	2.85
PE2	3.02	3.17	3.39	3.73
PP3	2.12	1.11	2.21	1.73
PE3	2.57	2.86	2.62	2.97
PP4	1.62	0.64	1.69	1.01
PE4	1.82	2.09	1.90	2.33

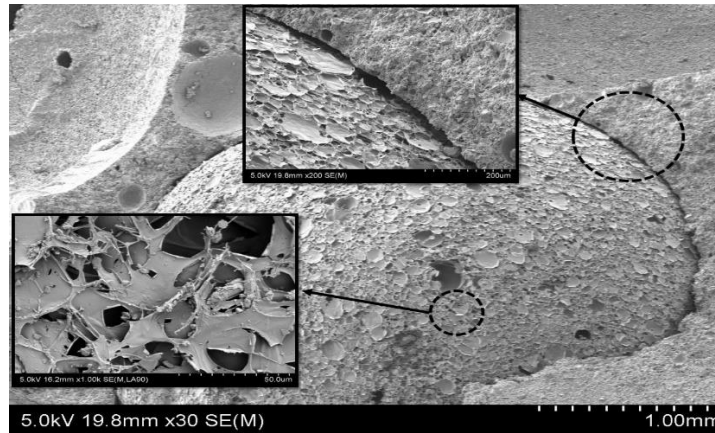


Figure 5. 2 EPLA degradation and bond failure at interfacial transition zone

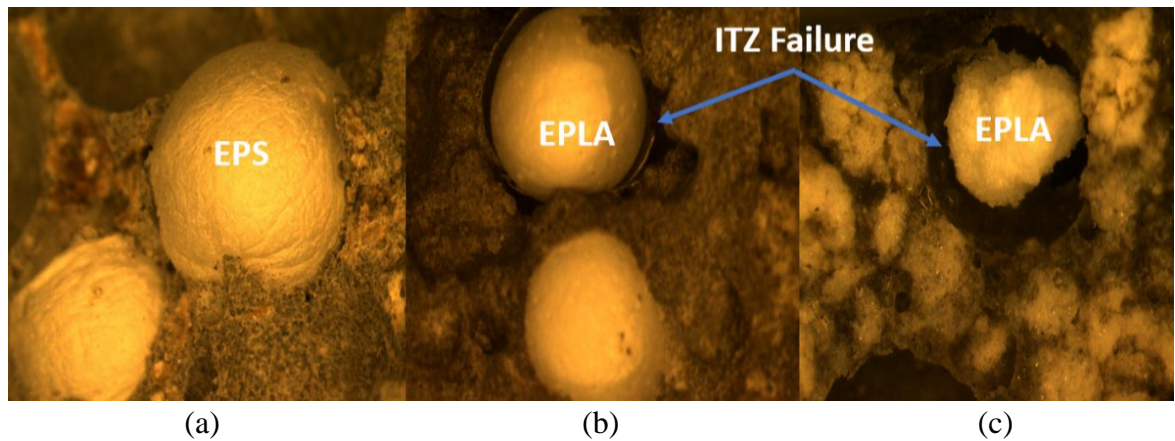


Figure 5. 3 Interfacial transition zone; (a) EPS Concrete, (b) EPLA Concrete - Air Cured, (c) EPLA Concrete – Water Cured

The experimental results show that there is a direct relation between EPLA ratio and compressive strength of concrete. The compressive strength of the sample containing 40% EPLA was 2.88 MPa, which was approximately about 33% lower than the control sample (P1). A further reduction in compressive strength was obtained with an increase in the EPLA ratio. The compressive strengths of 2.12 MPa and 1.62 MPa were obtained as 60%, and 70% of perlite aggregate were replaced with EPLA particles. This trend shows a considerable reduction of 51% and 63% in compressive strength of EPLA concretes. Also, most of the EPLA beads easily de-bonded from the matrix due to close to zero interfacial bonds at the interface area of bead and paste due to the EPLA beads degradation (Figure 5. 4). This trend was much higher for samples cured in water. In the case of water cured samples and compared to air cured samples, the compressive strength was decreased by 11%, 48% and 61% for samples PP2, PP3 and PP4, respectively. This trend can be attributed to the dissolution of EPLA particles and zero interfacial bonds between EPLA beads and the matrix. The existence of large voids due to shrinkage and degradation of EPLA along with the conversion of hydration products due to alkaline reactivity results in the concrete to fail at much lower stresses.

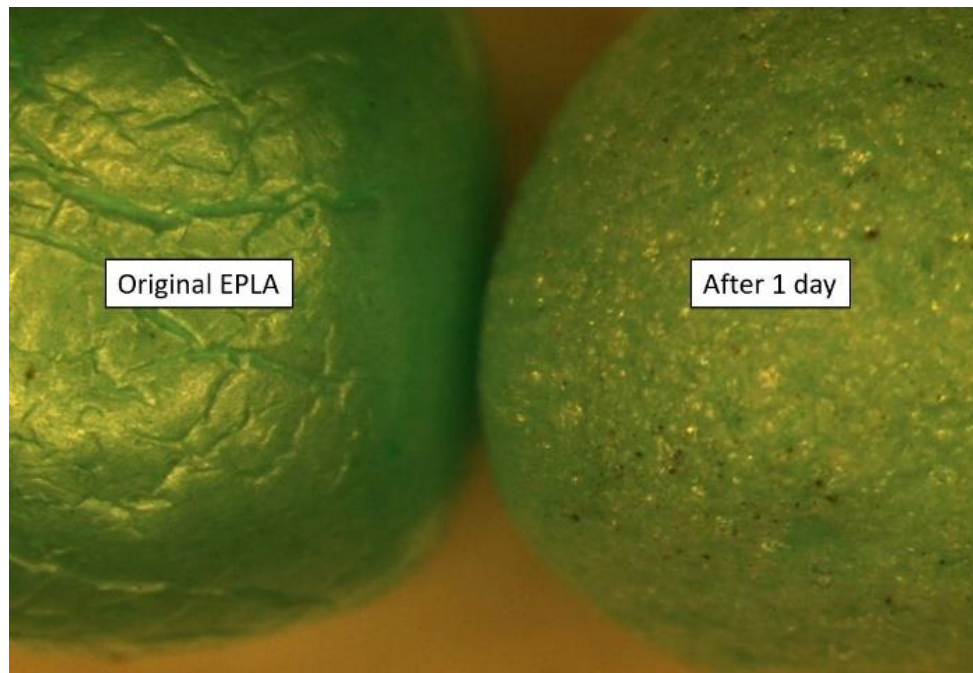


Figure 5. 4 Degradation of EPLA in alkaline environment

The porous structure of perlite aggregate and its high absorption capacity lead to a positive effect on strength development of perlite concrete and concrete containing EPS. The penetration of fresh cement paste into the porous structure of perlite and the release of stored water during the hydration process causes a better strength development [193]. The samples containing EPLA had a lower compressive strength in both the air and moist curing condition compared with EPS concrete. Thus, the EPS and EPLA beads are porous materials and its addition as lightweight aggregate results in a notable reduction in mechanical properties of concrete. Furthermore, the lightweight polymers act as filler without any contribution to stress transfer capabilities.

The fracture process of samples containing EPLA and EPS aggregate was completely different to the control specimen P1. A sudden failure and brittle behavior were observed in control specimens (Figure 5. 5a). The cracks generate and propagate along the length of concrete cylinders while the inclusion of EPLA or EPS changed the failure modes of concrete. The cracks had enlarged and spread on the top or bottom of the concrete cylinders. The EPLA concrete was crushed and failed in a much more brittle way than EPS concrete mainly due to the absence of resisting components, de-bonding and degrading of EPLA (Figure 5. 5b,c). In the case of EPS concrete, the failure mode was more gradual with the ability to retain the load after failure due to the compressible behavior of EPS beads and

better interfacial bond strength. It can be noted EPS beads were sheared off along the failure plane due to proper interfacial bonds between EPS and the matrix (Figure 5. 6a), while all of the EPLA beads were easily de-bonded from the matrix (Figure 5. 6b).

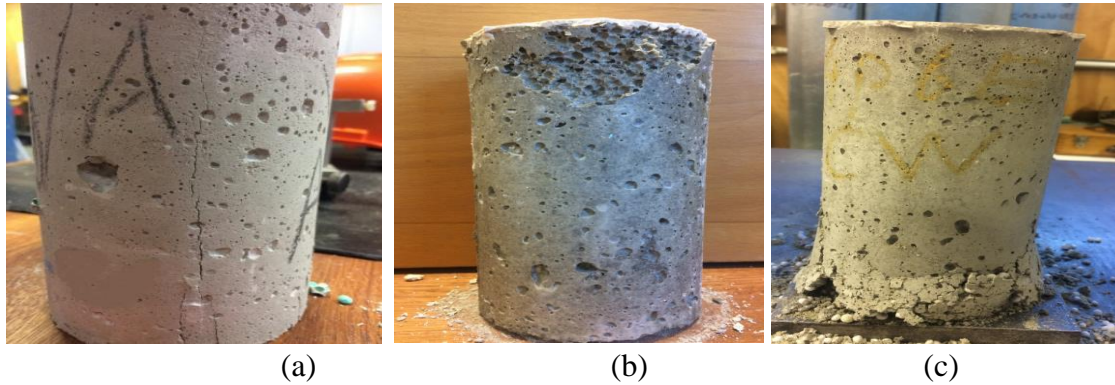


Figure 5. 5 Failure modes of concrete cured in a moist condition; (a) mix P1, (b) mix PP4, (c) mix PE4.



Figure 5. 6 Failure modes of polymer aggregates; (a) EPS concrete, (b) EPLA concrete

5.4.4 Tensile Strength

The splitting tensile strength of perlite-EPLA and perlite-EPS concrete mixes is shown in Table 5. 4. The results demonstrate that the tensile strength of perlite concrete containing polymer aggregate is a factor of polymer fraction and curing method.

Table 5. 4 The tensile strength of proposed concretes

Mix No.	Tensile strength (MPa)	
	Air Cured	Moist Cured
P1	0.97	1.09
PP2	0.62	0.56
PE2	0.66	0.70
PP3	0.43	0.26
PE3	0.55	0.60
PP4	0.32	0.13
PE4	0.38	0.45

The lowest tensile strength was obtained in samples containing 70% EPLA (PP4) aggregate volume with 0.13 MPa. This change in strength development can be attributed to the alkaline reactivity and interfacial bond failure of EPLA beads. Also, moist curing causes an acceleration of EPLA degradation and changes in failure modes. It was observed that tensile strength of the control specimen P1 was increased by 11% as the sample was cured in a moist environment. The same improvement in tensile strength was observed in samples containing EPS aggregates. The tensile strength of concrete was increased by 6%, 9% and 18% for specimens containing 40%, 60% and 70% EPS, respectively. While, the inverse trend was observed in samples containing EPLA. The tensile strength of concrete decreased by 10%, 39% and 59% for samples PP2, PP3 and PP4 as the samples cured in a moist environment. It can be concluded that the factors such as EPLA degradation in the alkaline environment of cement and the weak interfacial zone of EPLA were the main sources of the sudden reduction in splitting tensile strength. In fact, the lack of bond strength of almost zero between EPLA and the surrounding concrete along with changes in the microstructure of the interfacial zone can be considered as a major side effect of using EPLA as lightweight aggregate. The splitting tensile strength of the proposed concrete is lower than that of a structural lightweight concrete grade, which is usually greater than 2.0 MPa as per ASTM C330. The following correlation between compressive strength and tensile strength of the proposed concretes was obtained (Eq. 5.3 – Eq. 5.6).

$$\hat{f}_c = 4.2074 f_t + 0.2862 \text{ (EPLA concrete - ADC)} \quad [5.3]$$

$$\hat{f}_c = 4.2048 f_t + 0.0855 \text{ (EPLA concrete - WC)} \quad [5.4]$$

$$\hat{f}_c = 4.3135 f_t + 0.1844 \text{ (EPS concrete - ADC)} \quad [5.5]$$

$$\hat{f}_c = 4.0981 f_t + 0.2528 \text{ (EPS concrete - WC)} \quad [5.6]$$

Where, \hat{f}_c is compressive strength (MPa) and f_t is tensile strength of concrete.

5.4.5 Stress-strain relationship

Figure 5. 7 presents the stress-strain diagram of the proposed lightweight concretes. The stress-strain diagram represents the strength characteristics and deformations of concrete. The properties such as maximum stress, the modulus of elasticity, the peak strain and the ultimate peak strain are important features of a stress-strain diagram [60].

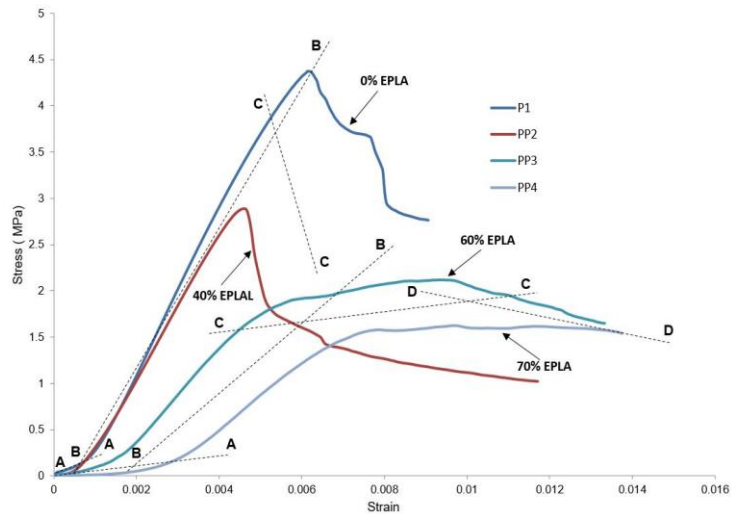


Figure 5. 7 Stress-strain relationship of perlite concrete with different EPLA ratios

Compared with the control specimen (P1), the performance of lightweight concrete with a high EPLA content is quite different. The samples P1 and PP2 show an almost similar behaviour regardless of EPLA content. Contrary for samples PP3 and PP4 the maximum stress was reduced and accompanied by an increase in the strain at the ultimate compressive stress with no clear descending stage. The strain at peak stress of P1, PP2, PP3 and PP4 was found to be 0.00613, 0.00542, 0.00941 and 0.0097, respectively. Normal concrete has strain

ranges of 0.0015-0.002 which is much lower than lightweight concrete. It can be found that concrete containing 70% EPLA (PP4) showed 385% larger strain capacity at peak stress than normal concrete. As shown in Figure 5.7 the stress-strain behaviour of samples P1 and PP2 can be divided into three stages of the elastic platform (A-A), elastic stage (B-B), and descending stage (C-C), while the stress-strain response of sample PP3 and PP4 was quite different. In the case of the samples PP3 and PP4, the deformation of concrete can be divided into four stages of the elastic platform (A-A), elastic stage (B-B), yield and strengthening stage (C-C) and descending stage (D-D). The high rate of increment in strain and corresponding stress normally takes place in the elastic platform due to a breakdown and compaction of the pore structure of the matrix. The steepness of the elastic region was increased with compacting of more collapsed pores. The experimental results show that an increase in EPLA volume causes lower compaction stress due to the higher compressibility of EPLA beads. A higher compaction stress was observed in samples PP4, while this value was much lower in the control specimen (P1).

The elastic stage of stiffness is the linear part of the stress-strain response. The results show that the gradient and yield strength of the elastic segment significantly depends on the EPLA ratio. However, a lower steepness is observed in specimens with a higher EPLA ratio due to the compaction behaviour of EPLA beads. A sudden levelling off in stress values was observed in the control and sample PP2 without shifting to the strengthening stage and followed by a plateau at the descending stage. The samples PP3 and PP4 show an oscillating manner in the strengthening stage due to the compression of EPLA beads and post-crushing of the pore structure. The stress was decreased and levelled off to a plateau at the final stage, the descending stage. At this stage, the stress remains at an almost constant value, while the increment of strain is notable. The fluctuation during the descending stage was due to the compressible behaviour of EPLA beads, crushing and collapsing of remaining pores. The addition of deformable aggregates such as EPLA and EPS reduces the strength of concrete but causes a significant improvement in strain capacity and resistance to cracking due to the length changes. In summary, lightweight concrete with deformable materials can absorb more energy under applied compression loads along with a gradual failure and ability to retain the load after failure without full disintegration.

5.4.6 Elastic Modulus

The elastic modulus of concrete is a vital parameter as this factor is used to evaluate the deflections and cracking of a concrete member. The elastic modulus of concrete mainly depends on the elastic modulus of concrete components such as aggregates and mix proportion of the mixture [60]. The elastic modulus of normal weight concrete and lightweight concrete is between 14 to 41 GPa and 10 to 24 GPa, respectively. The elastic modulus of lightweight aggregate is ranging from 5 to 28 GPa which is much lower than that of normal weight aggregate. The elastic modulus of the proposed concretes was a factor of the EPLA and EPS ratio. The experimental results show that the elastic moduli of concretes containing polymers is quite low due to the very low elastic modulus of the polymer aggregate and an increase in concrete porosity. The moduli of elasticity of P1, PP2, PP3 and PP4 were 1051, 640, 453 and 326 MPa, respectively (Table 5. 5). The results show that the replacement of perlite with 40%, 60%, 70% of EPLA aggregate reduced the elastic modulus of concrete by about 14%, 44% and 60%, respectively. The same trend was observed in samples containing EPS beads. The elastic modulus of EPLA concrete was lower than that of EPS concrete due to the degradation of EPLA beads and an increase in concrete porosity. Thus, the elastic modulus of the proposed concrete was much lower than normal lightweight concrete and can be categorized in the ultra-lightweight concrete range. However, this concrete with a low elastic modulus is mostly used as an infill material. The following equation 5.7 is proposed to estimate the elastic modulus of concrete as a function of concrete density and compressive strength. The results obtained with the equation are compared to the measured results in Table 5.5.

$$E = K\left(\frac{\gamma}{\sqrt{(800-\gamma)}}\right)(\sqrt{f_c}) \quad [5.7]$$

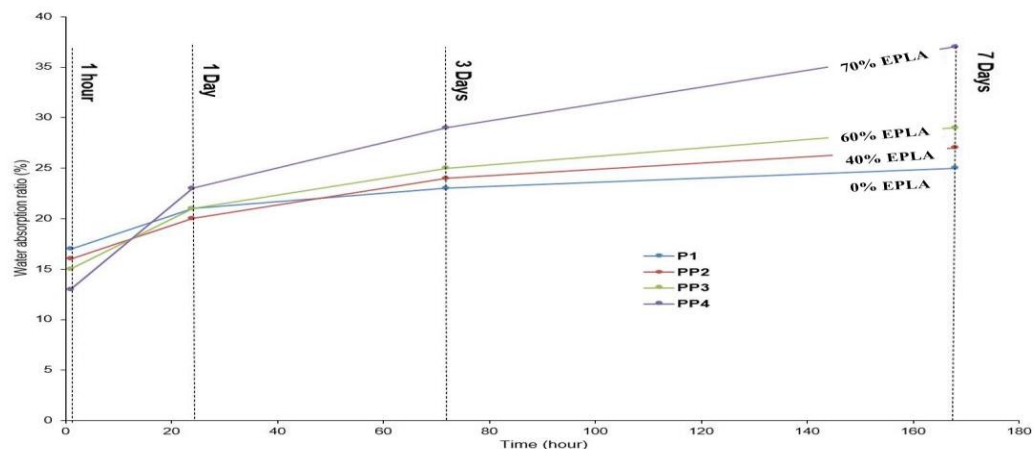
Where K is a constant (18 for this model), γ is density of concrete (kg/m^3), f_c is compressive strength of concrete (MPa).

Table 5. 5 The elastic modulus of proposed concretes.

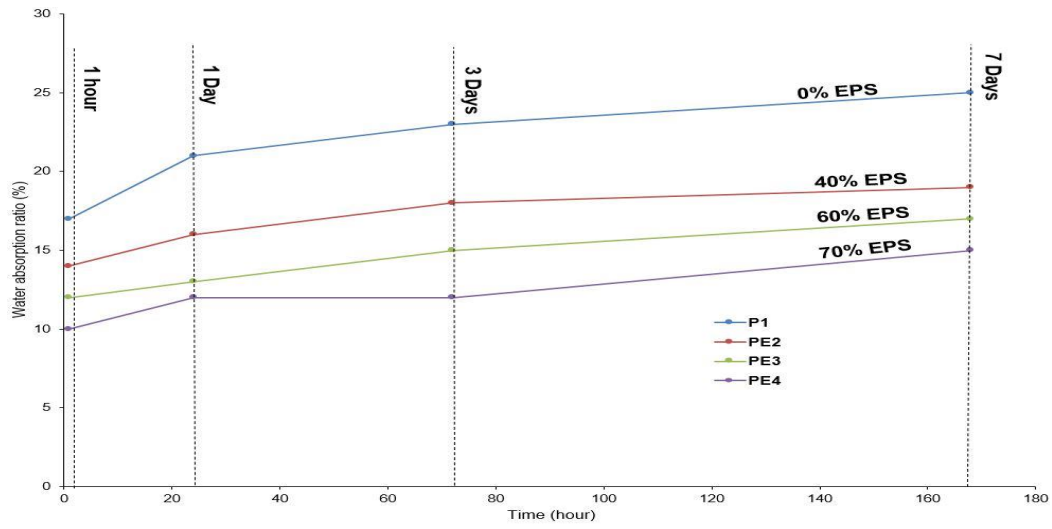
Mix No.	Elastic Modulus (MPa)	
	Experimental results	Proposed equation
P1	1051	1058
PP2	640	611
PE2	670	662
PP3	453	450
PE3	514	518
PP4	326	310
PE4	350	344

5.4.7 Water absorption

The water absorption of all mixes after 1, 24, 72 and 168 hours is shown in Figure 5. 8. The water absorption ratio is a factor in determining the quality and durability of concrete. This factor is an indicator of the porosity and characteristics of the pore structures of concrete. The pore characteristics of concrete directly affect the absorption ratio of concrete and its quality [208]. Also, the absorption ratio of lightweight aggregate significantly affects the microstructure of hardened cement and the interfacial zones of concrete [195]. The higher water absorption ratio of lightweight aggregate is caused by an increase in porosity of the interfacial transition zone of the matrix [209, 210].



(a)



(b)
Figure 5. 8 The water absorption ratio vs time of proposed concretes, (a) EPLA concrete, (b) EPS concrete.

The results show that the water absorption ratio of concrete containing EPLA was lower than that of the control specimens at the early ages (1 hour), while the water absorption of the proposed concretes enhances with an increase in EPLA ratio after 24, 72 and 168 hours. These changes in water absorption can be attributed to the fact that the EPLA lost its hydrophobicity, started to take up water and shrunk when subjected to the alkaline environment of cement (Figure 5. 9). Compared with the control sample, the water absorption was reduced by 6%, 12% and 23% after 1 hour and increased by 8% and 16% and 48% after 168 hours for samples PP2, PP3 and PP4, respectively. The highest and lowest absorption value was observed in samples PP4 and P1. Generally, normal concrete should have an absorption ratio of below 10% by mass to be considered as good concrete [26]. From the experimental results, it can be found that all the samples show a higher absorption ratio mainly due to a high absorption ratio of perlite and changes in the hydrophobicity of EPLA. In contrast, the water absorption of EPS concrete was decreased with an increase in EPS volume. This trend mainly is related to hydrophobicity and zero absorption ratio of EPS and the fact that replacement of high absorbent materials with non absorbent materials causes a significant decrease in absorption ratio.



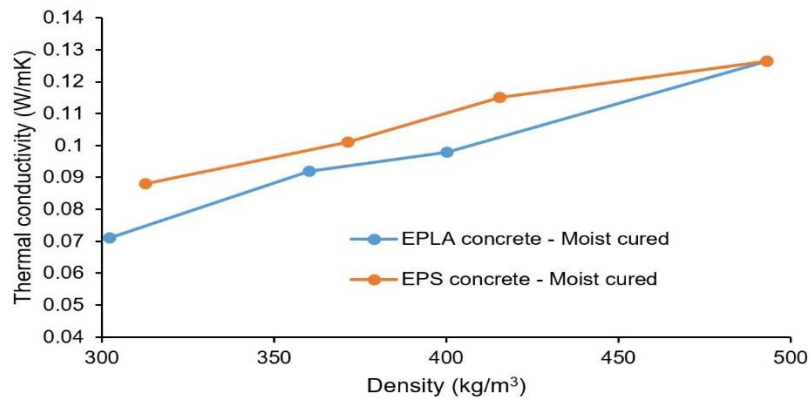
Figure 5. 9 EPLA shirinkages in alkaine enviroment of cement

5.4.8 Thermal conductivity

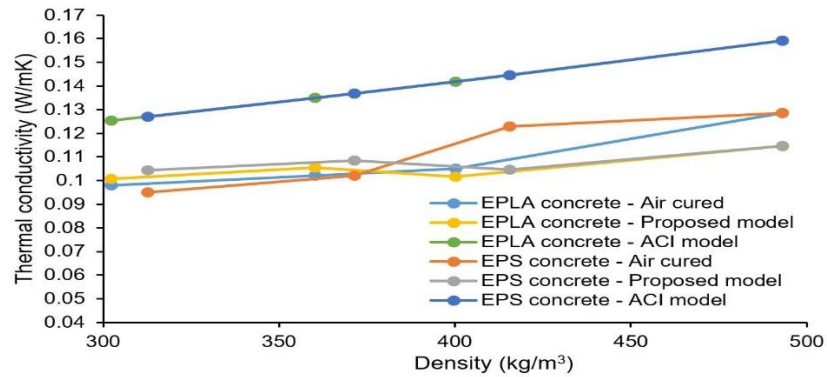
Table 5. 6 and Figure 5. 10 present the variation in thermal conductivity with perlite-EPLA changes. It was found that replacement of normal aggregate with lightweight aggregate causes a considerable reduction in the thermal conductivity value of concrete mainly due to the porous structure of lightweight aggregates [67]. In fact, the thermal conductivity of concrete is a factor of porosity as the thermal capacity of air is much lower than water or solids. Parameters such as density, moisture content, air content, and the temperature of concrete along with mineralogical characteristics of lightweight aggregate substantially affect the thermal conductivity of concrete. There is no information available on thermal conductivity of concrete containing a bio-polymer aggregate like EPLA, but some experiments have studied and assessed the thermal conductivity of lightweight aggregates containing expanded polystyrene aggregate. Referring to previous studies, a thermal conductivity of 0.206 W/mK and 0.06 W/mK were obtained by inclusion of EPS aggregate and the combination of foam and EPS by Bouvard et al. [95] and Chen and Liu [102], respectively.

Table 5. 6 The thermal conductivity of proposed concretes

Mix No.	Density (kg/m^3)	Thermal Conductivity (W/m.K)			
		Experimental Results		Proposed Equation	ACI 213R-03
		Air Cured	Water Cured	Air Cured	Air Cured
P1	493.0	0.1285	0.1265	0.1146	0.1592
PP2	400.2	0.1050	0.0980	0.1017	0.1418
PE2	415.5	0.1230	0.1150	0.1047	0.1445
PP3	360.2	0.1020	0.0920	0.1056	0.1349
PE3	371.5	0.1020	0.1010	0.1086	0.1368
PP4	302.2	0.0980	0.0710	0.1008	0.1254
PE4	312.6	0.0950	0.0880	0.1043	0.1271



(a)



(b)

Figure 5. 10 The correlation between thermal conductivity and concrete density

With a similar strength, the thermal conductivity of EPLA concrete is 44% lower and 47% higher than EPS concrete and foamed EPS concrete, respectively. A thermal conductivity of 0.11 W/mK with a density of 400 kg/m³ was obtained by [102]. In this study, the sample containing 60% EPLA had a density of 389.0 kg/m³ with a thermal conductivity value of 0.1073 W/mK which is 2.5% lower than EPS concrete. The experimental results show that the thermal conductivity decreased with an increase in EPLA ratio. This trend was different for samples cured in water. The water curing imposes an inverse effect on thermal conductivity of concrete containing EPLA. The thermal conductivity values of mixes PP2, PP3 and PP4 were 11%, 16% and 25% lower and 13%, 3% and 1% higher than the control specimen (P1) for specimens cured in air and water, respectively. An increase in thermal conductivity of the moist samples are mainly attributed to the more densified matrix and changes in the microstructure of concrete. The microstructure of concrete becomes denser because of sufficient water is supplied during the hydration process. Thus, the addition of polymer aggregate increases the total porosity of concrete and lowers thermal conductivity values. However, the alkaline reactivity of EPLA beads in the highly alkaline environment of cement also contributed to increasing the porosity of concrete as a result of an increase in CO₂ gas concentration. Compared with EPS concrete, the EPLA concrete shows slightly lower thermal conductivity values.

The thermal conductivity of the proposed concretes is affected by factors such as concrete density, EPLA ratio, EPS ratio, perlite ratio and curing method. The ACI Committee [78] has proposed an equation to estimate the thermal conductivity of lightweight concrete (Eq. 5.8). However, the proposed equation relies on the density of concrete without concerning other relevant factors. To estimate the thermal conductivity of the proposed concretes, equation 5.9 with five variables of concrete density, perlite density, EPLA density, perlite ratio and EPLA ratio was developed and its results compared with the proposed equation by ACI and experimental results in Table 5. 6 and Figure 5. 10b.

$$\lambda = 0.086e^{0.00125\gamma} \quad [5.8]$$

$$\lambda = \left(\frac{\sqrt{\gamma_{\text{concrete}}}}{(\gamma_{\text{Perlite}} \cdot R_{\text{Perlite}}) + (\gamma_{\text{EPLA/EPS}} \cdot R_{\text{EPLA/EPS}})} \right)^{K + \frac{0.65R_{\text{EPLA/EPS}}}{R_{\text{Perlite}}^{0.5}}} \quad [5.9]$$

K = 1.2 (for perlite concrete)

Where, γ_{Concrete} is the concrete density (kg/m^3), R_{perlite} is the ratio of perlite, $R_{\text{EPLA/EPS}}$ is the ratio of EPLA and EPS, K is a constant (1.20 for perlite aggregate).

5.4.9 Setting time and degradation mechanisms of EPLA

The electrical resistivity response is used to analyse the initial and final setting time of concrete. The electrical resistivity is the measure of the resistance offered to the movement of ions through the concrete matrix. The water-cement ratio, additives, aggregates, the degree of hydration, porosity, pore size distribution and cement paste microstructure significantly influence the electrical resistivity value [203]. As shown in Figure 5. 1, the electrical resistivity of samples are marked at the initial (P_I) and final (P_F) setting time [204]. The initial and final parts are the periods of slow reaction and acceleration period [204]. The experimental results show a significant delay in setting time of the control sample due to the absorption of water from the perlite aggregate during the hydration process [84].

However, at the later stages, the difference in the pressure of water between the voids of expanded perlite and cement paste leads to the release of stored water to contribute to the hydration process. As presented in Table 5. 7, the initial setting time of concrete decreased from 1080 min to 190 and 195 min for samples PP3 and PP4 in comparison to the control sample (P1). These changes in setting times are attributed to the alkaline reactivity of EPLA. The alkalis present are sulfates, in the form of K_2SO_4 , Na_2SO_4 , $\text{Na}_2\text{SO}_4 \cdot 3\text{K}_2\text{O}$ (aphthitalite) and $2\text{CaSO}_4 \cdot \text{K}_2\text{SO}_4$ (calcium langbeinite). Immediately after mixing cement with water, the liquid phase is saturated with calcium and SO_4^{2-} ions, which leads to an increase in pH level of close to 12.5 [207, 211]. The alkaline components sodium (Na) and potassium (K) ions are released to produce an alkaline sulphate-rich solution [207]. The alkalis released during the initial cement hydration, which are small amounts of Na^+ and K^+ ions, start the surface deterioration of EPLA through a base-catalysed hydrolysis that then continues in the highly alkaline environment of cement. The degradation of EPLA in the alkaline environment of cement causes a slow release of lactic acid into a hydrating cementitious system.

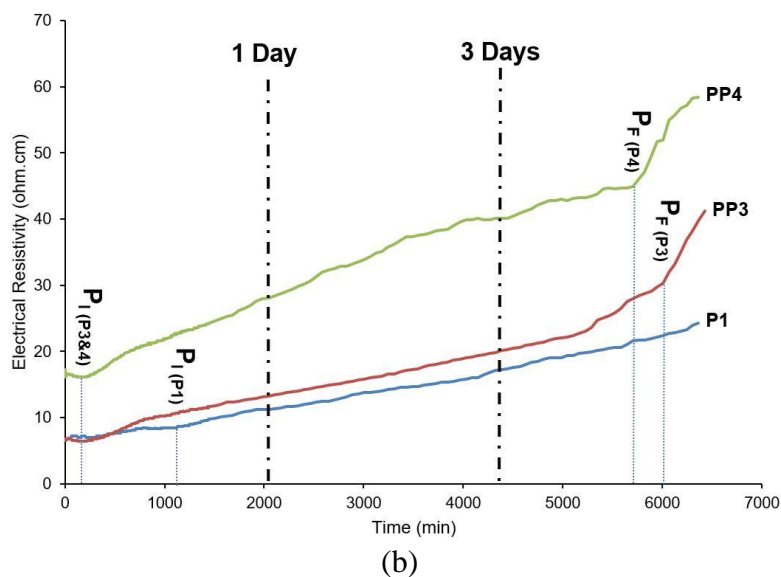
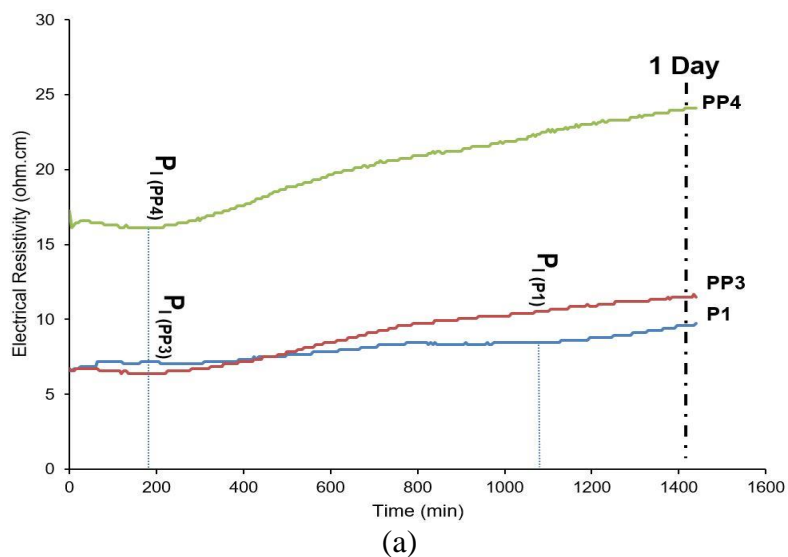


Figure 5. 11 The electrical resistivity response of concrete; (a) up to 1 day, (b) up to 5 days

In order to have a better understanding of the degradation mechanisms of EPLA and its degradation rate, sodium hydroxide and calcium hydroxide solutions were prepared. The EPLA beads were placed in a 1.3M, 1.0M, 0.5M, 0.25M and 0.1M NaOH solution and its degradation rate was recorded. In addition to this, the 0.25M NaOH solution with an approximate pH of 13 was used as a reference having the same alkalinity level as cement. A rapid chemical reaction was observed in 1.3M NaOH solution with a pH of 14.1. The EPLA beads were completely dissolved after 14 hours. While no reaction was observed in 0.1M solution with a pH level of 13. In the case of the reference solution (0.25M NaOH) the EPLA beads start to degrade after 24 hours and a complete degradation was observed after 10 days (Figure 5. 12). The same trend at a lower rate was observed in a saturated calcium hydroxide

solution with a pH value of 11.8 (dissolved after 21 days). Thus, it can be concluded that the chemical reaction of sodium and calcium was the main cause of EPLA degradation at the early age of hydration.

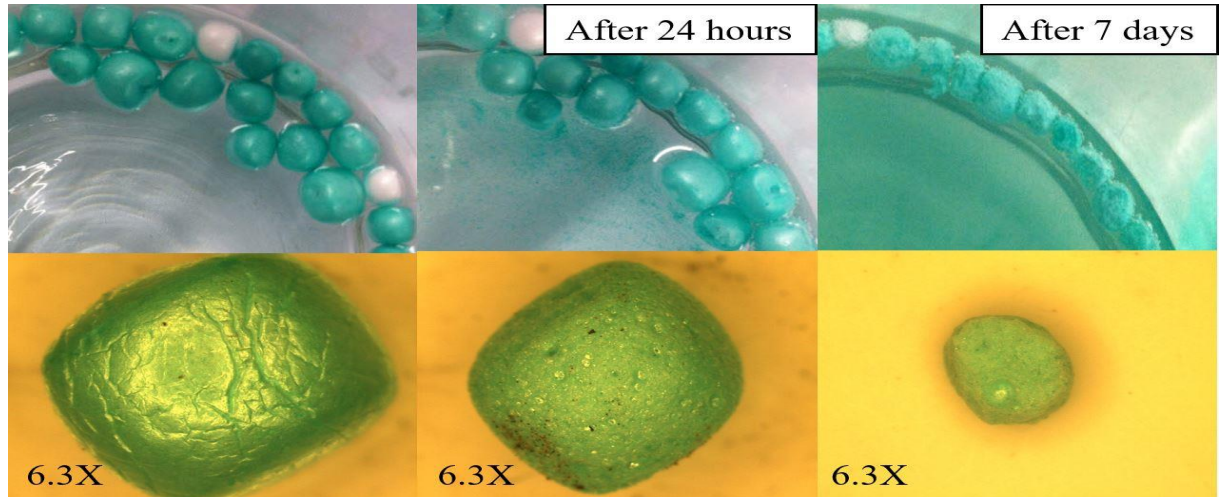
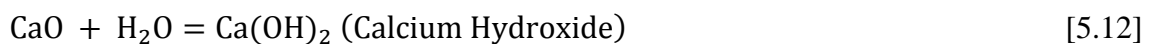
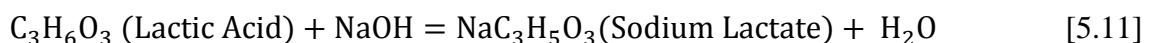


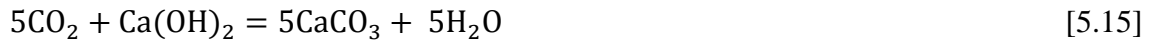
Figure 5.12 EPLA degradation in sodium hydroxide solution (NaOH)

The initial setting time of concrete mainly depends on alkalis present as impurities in the cement phases with sodium especially in the aluminates ($3\text{CaO} \cdot \text{Al}_2\text{O}_3$) phase and potassium in calcium and aluminates phases. In fact, the changes in the liquid phase composition and changes in Ca^{2+} , SO_4^{2-} and $\text{Al}(\text{OH})_4^-$ concentrations significantly influence the hydration process and setting time of concrete. The sodium (Na) and calcium Ca^{2+} ions react with the released lactic acid to form sodium lactate and calcium lactate. Thus, the alkaline reactivity and degradation of the EPLA along with a decrease in the amount of perlite aggregate causes significant changes in the liquid phase composition and setting time of concrete. The reaction scheme and chemical process of EPLA degradation are described as follows (Eq. 5.10 - 5.13).

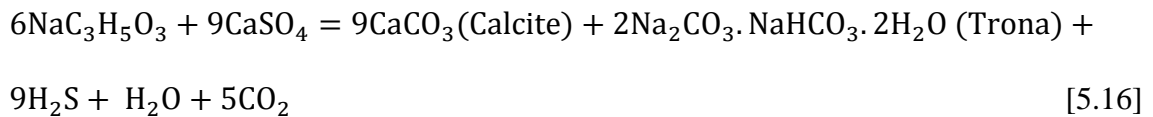


The experimental results showed an improvement in final setting time with the inclusion of EPLA. Compared with the control sample (P1), the final setting time was decreased from 6553 min to 6005 and 5645 min for samples PP3 and PP4, respectively (Table 5. 7 and Figure 5. 11). The changes in electrical resistivity of concrete are related to microstructural changes [204, 205]. At the second stage of hydration, the alite and belite of cement start to react to form calcium silicate hydrate and calcium hydroxide. The calcium hydroxide (Ca(OH)₂) and sodium hydroxide (NaOH) of cement reacts with lactic acid to form calcium lactate (CaC₆H₁₀O₆) and sodium lactate (NaC₆H₁₀O₆). After the chemical attack of alkaline components, the sodium lactate and calcium lactate reacts with calcium sulfate and oxygen to form calcium carbonate (calcite) and trisodium hydrogendicarbonate dihydrate (trona), respectively. The reaction scheme of sodium lactate and calcium lactate are described as follows (Eq. 5.14 - 5.16).

The chemical reaction of poly-lactic acid and calcium hydroxide:



The chemical reaction of polylactic acid and sodium hydroxide:



The chemical reaction of lactate products and the transformation of calcium hydroxide (Ca(OH)₂) and calcium silicate hydrate (C-S-H) to calcium carbonate (CaCO₃) were the main causes for changes of the final setting time. This process causes a significant conversion of hydration products. The maximum resistivity was observed in sample P4 (60% EPLA) due to the lower porosity compared with the control sample. Thus, the propagation and growth of calcium carbonate decreased the porosity of concrete and caused a higher electrical resistivity in the samples containing EPLA.

Table 5. 7 The initial and final setting time of the control sample and samples containing higher amounts of EPLA based on electrical resistivity response.

Specimen	Setting time (min)	
	Initial (P_I)	Final (P_F)
P1	1080	6553
PP3	190	6005
PP4	193	5645

5.4.10 Fire resistance test

The heat release rate of materials is a significant factor in a fire hazard evaluation [212]. Cone calorimeter tests were done to evaluate the fire reaction of concretes containing bio-polymers as a substitution for petrochemical polymers. The heat release rate (HRR), total heat released (THR), carbon monoxide production (COP), and carbon dioxide production (CO₂P) of EPLA concrete are evaluated and compared with perlite and EPS concrete. The failure modes of samples subjected to high temperature are shown in Figure 5. 13. All the samples failed with some minor thermal cracks without losing integrity. In addition a slight change in surface coloring of sample PP4 and PP5 were observed due to the physical and chemical changes of the samples along with burning of EPLA and EPS aggregate.

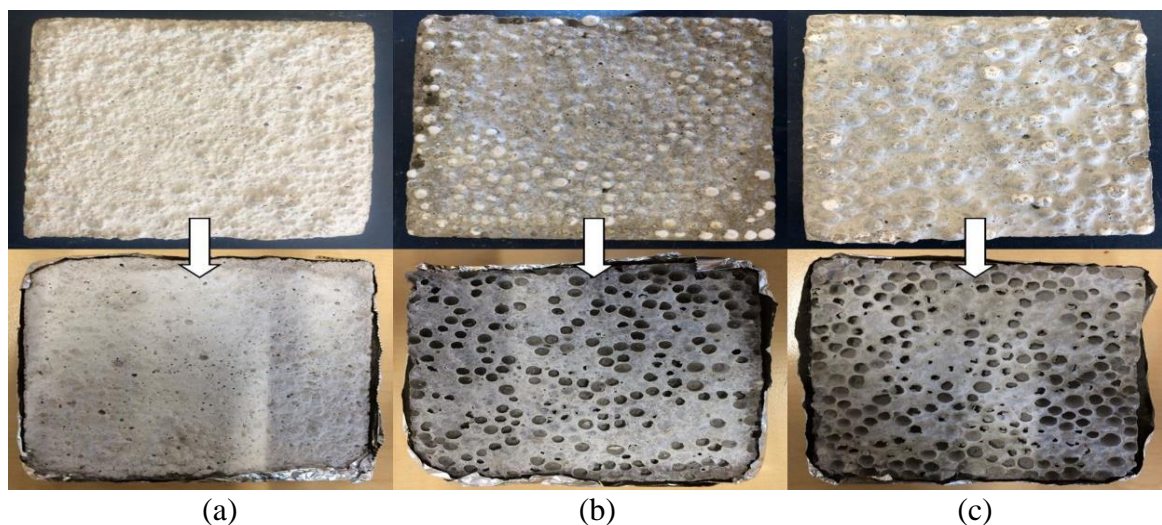


Figure 5. 13 Fire resistance of concrete and its failure modes; (a) Perlite concrete (P1), (b) EPLA concrete (PP4), (c) EPS concrete (PE4).

The heat release rate (HRR) and total heat released (THR) curves of the proposed concretes under 50 kW/m^2 heat flux are presented in Figure 5. 14 and Figure 5. 15, respectively. The experimental results reveal that the sample P1 can be graded as noncombustable material as the maximum HRR and THR was below 200 kW/m^2 and 8 MJ/m^2 . Although, the maximum HRR of sample PP4 and PE4 was below 200 kW/m^2 but both samples exceeded the maximum THR and can be graded as quasi-noncombustable with a relative maximum THR of 15.70 and 16.52 MJ/m^2 , respectively. The ignition and flameout points of proposed concretes are presented in Table 5. 8. The mix P1 did not contribute to fire growth and no ignition point was observed. The EPS concrete burned and reached a peak of 36.40 kW/m^2 after 810 seconds. The heat release rate of concrete was decreased to the amount of 15.54 kW/m^2 (about 57%) as the EPS was replaced with EPLA mainly due to the application of a non petroleum product. The EPLA and EPS concrete start to ignite after 555 s and 711 s with a heat release rate of 13.04 kW/m^2 and 10.54 kW/m^2 , respectively. It is worth to note that the addition of EPLA caused a delay in the ignition point but extended the flameout point due to the higher rate of carbon monoxide production of EPLA compared to EPS.

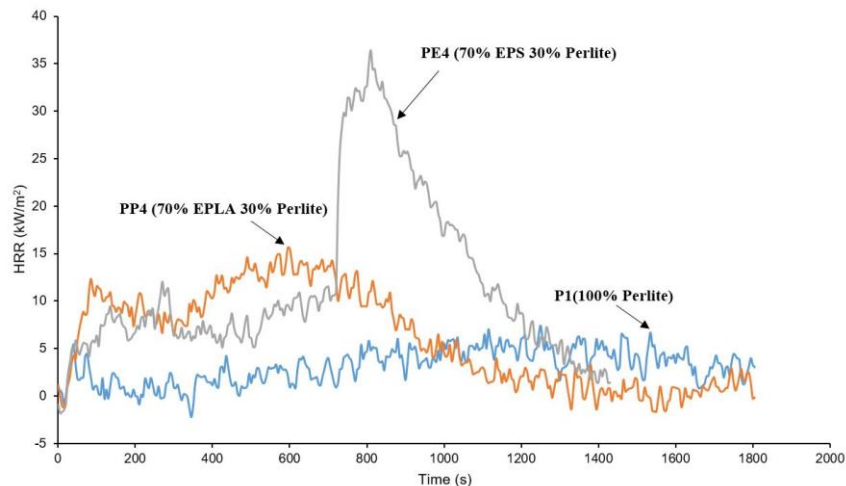


Figure 5. 14 Heat release rate (HRR) response of proposed concretes under 50 kW/m^2 external heat flux.

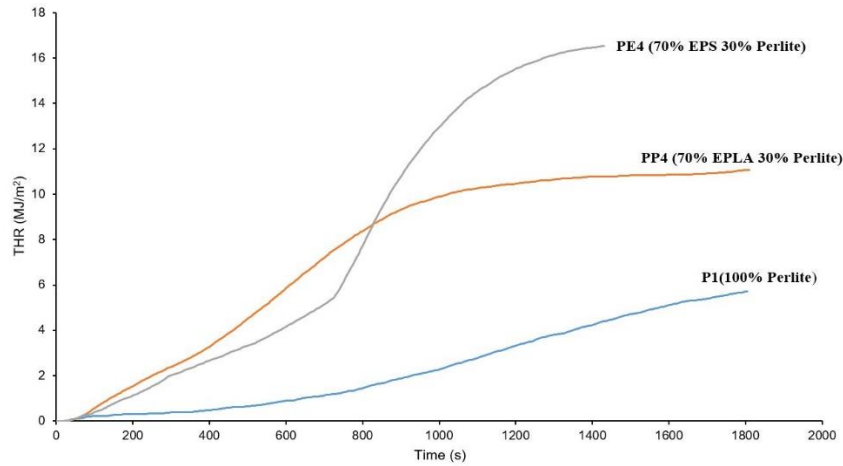


Figure 5. 15 Total heat released (HTR) of proposed concretes.

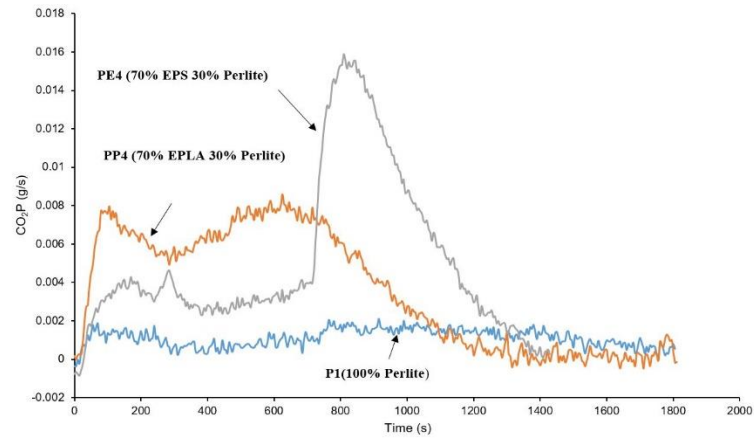
Table 5. 8 The time to ignition and flameout of proposed concretes.

Mix No.	Time to ignition (s)	Time to flameout (s)
P1	0	0
PP4	555	1162
PE4	711	1311

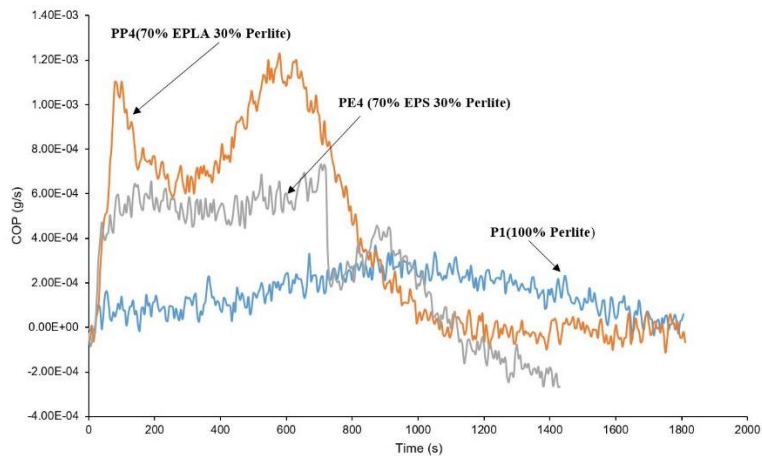
The carbon dioxide (CO₂) production of the proposed concretes is presented in Figure 5. 16a. A sharp growth in the concentration of CO₂ was observed after ignition in the sample containing EPS. The increase in the amount of released CO₂ gas is associated with the combustion of petroleum polymer. The released CO₂ gas reached its maximum value of 0.002 g/s, 0.008 g/s and 0.0156 g/s after 915 s, 625 s and 810 s for mix P1, PP4 and PE4, respectively. In the case of the sample PP4, the amount of CO₂ gas decreased by 48% compared to PE4. The level of CO₂ gas remains low and almost constant throughout the test for mix P1.

The concentration levels of carbon monoxide (CO) are presented in Figure 5. 16b. The CO gas production of sample P1 was lower than that of sample PP4 and PE4. The highest and fastest growth in CO gas production were observed in EPLA concrete. In fact, the CO is a volatile and flammable gas which is associated with retaining the flame over the surface of the samples. Compared to the PP4 and PE4 samples, there was a delay in time (870 s) where the CO gas production reached its highest amount in sample P1. In addition, there was a

certain fluctuation in CO production which causes an increase and decrease in CO₂ gas production mainly due to the incomplete combustion.



(a)



(b)

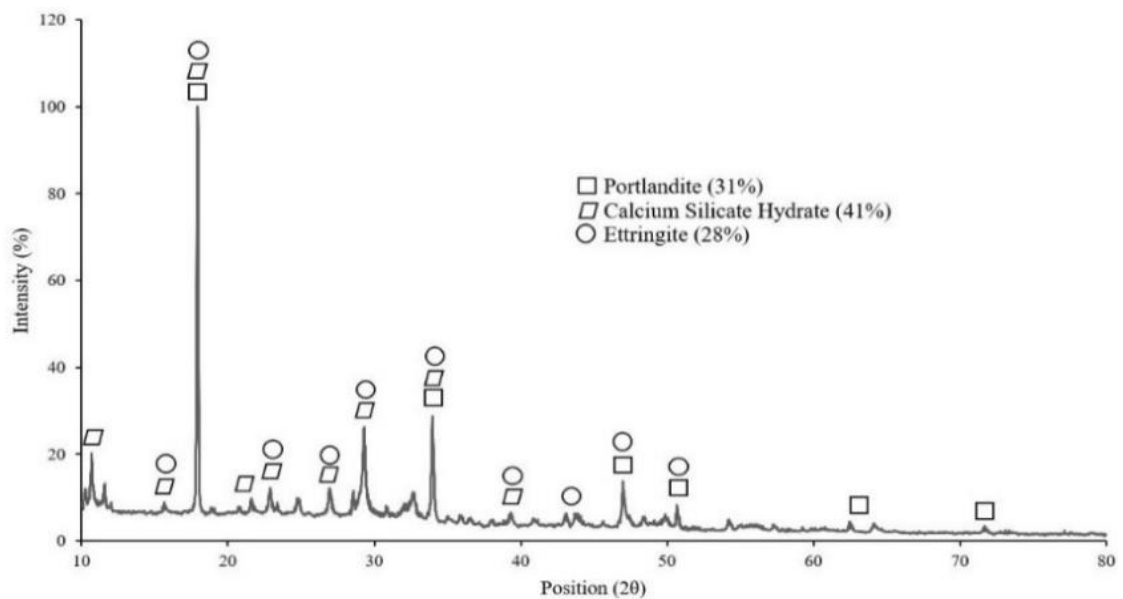
Figure 5. 16 (a) Carbon dioxide and (b) carbone monoxide production curves of proposed concretes during combustion.

5.4.11 XRD analysis

X-ray diffraction analysis was used to identify and compare the mineralogical compositions of concrete mixtures using PANalytical's HighScore Plus software by fitting each powder diffraction profile [181]. The hydration products of the EPS and EPLA concrete are presented in Figure 5. 17. Based on the XRD results, portlandite, CH [Ca(OH)₂], calcium silicate hydrate [C-S-H], ettringite, AFt [Ca₆Al₂(SO₄)₃(OH)₁₂·26H₂O], calcite [CaCO₃], and magnesium silicate hydrate [M-S-H] were identified in the EPS and EPLA concrete, respectively. As expected, the major hydration phase of the PE4 was portlandite, calcium

silicate hydrate and ettringite. The presence of EPLA caused significant changes to the hydration products of concrete.

The quantitative Rietveld analysis reveals that the matrix mostly contains portlandite (17.2%), calcite (43.4%), ettringite (33.3%) and magnesium silicate hydrate (6.1%). The presence of a large amount of calcite (CaCO_3) shows the interaction between the EPLA and portlandite ($\text{Ca}(\text{OH})_2$). The degradation of poly-lactic acid and the release of calcium lactate ($\text{CaC}_6\text{H}_{10}\text{O}_6$) due to alkali reactivity led to the growth of calcite products. Compared with PE4, the amount of portlandite and C-S-H content decreased from 31% to 17.2% and 41% to 0%, respectively. The absence of C-S-H gel in sample PP4 was possibly due to the consumption of portlandite by lactic acid ($\text{C}_3\text{H}_6\text{O}_3$) to form calcium lactate and consequently calcite during hydration. In addition to this, the decrease of the amount of portlandite indicates more calcite was formed during hydration and its reaction with carbon dioxide (CO_2). The chemical reaction of calcium lactate and oxygen (O_2) led to an increase in the amount of carbon dioxide in the matrix and a transformation of more portlandite to calcite. This process leads to a significant reduction in concrete porosity and results in a more compact matrix.



(a)

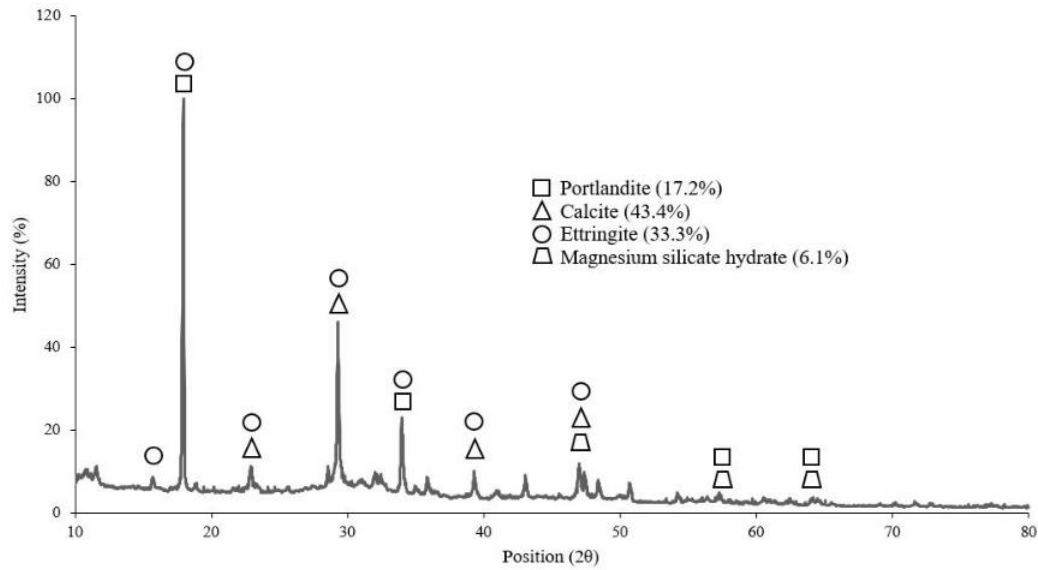


Figure 5. 17 XRD Profiles (a) PE4, (b) PP4

5.4.12 SEM-EDS analysis

Figure 5. 18 and Figure 5. 19 show the elemental composition of the sample PE4 and PP4, respectively. The elements Ca, Si, Al, Na, Mg, S, K and Fe along with Ca, Si, Al, Mg, S, Cl, K and Fe were detected in the matrix of sample PE4 and sample PP4, respectively. The EDS analysis shows that the addition of EPLA significantly changed the elemental composition of concrete. A considerable change in the atomic concentration of the Ca, Na, S, Cl, K, Fe was observed. For instance, the atomic concentration of Ca, Cl, Na and S changed from 29.33%, 0%, 0.53% and 0.33% to 42.76%, 0.62%, 0% and 1.03% for samples PE4 and PP4, respectively. These changes can mainly be attributed to the concrete carbonation and EPLA degradation in the alkaline environment of cement. The EDS analysis of the selected zone shows that the ratios CaO/SiO_2 , $\text{CaO}/(\text{SiO}_2 + \text{Al}_2\text{O}_3)$ and $\text{SiO}_2/(\text{CaO} + \text{Al}_2\text{O}_3)$ were changed from 0.734, 0.303 and 0.463 to 1.105, 0.467 and 0.405 for PE4 and PP4, respectively. Based on the EDS analysis of the selected zone and the detected elements, the presence of calcium silicate hydrate (C-S-H), calcium hydroxide (CH) and calcium aluminium sulphate (AFt) for the sample PE4 and calcium hydroxide (CH), calcium carbonate (CaCO_3), calcium aluminium sulfate (AFt) and magnesium silicate hydrate (M-S-H) for sample PP4 can be seen as hydration products of concrete. The hydration products were observed during the microstructure analysis of the concretes. The SEM images show the formation of fibrous type products (C-S-H), elongated and needle-like shapes (AFt) and

CH plates in the microstructure of the PE4 (Figure 5. 20). Contrary a large amount of needle crystals appeared in the interfacial zone of the paste and aggregate of the sample containing EPLA (Figure 5. 21). The formation of large amounts of calcium carbonate (CaCO_3) and calcium aluminium sulfate (AFt) shows that the degradation of EPLA leads to a chemical conversion of hydration products as no calcium silicate hydrate was found in the microstructure of sample PP4. Regarding strength, the conversion of C-S-H gel to calcium carbonate causes a reduction in engineering properties of concrete.

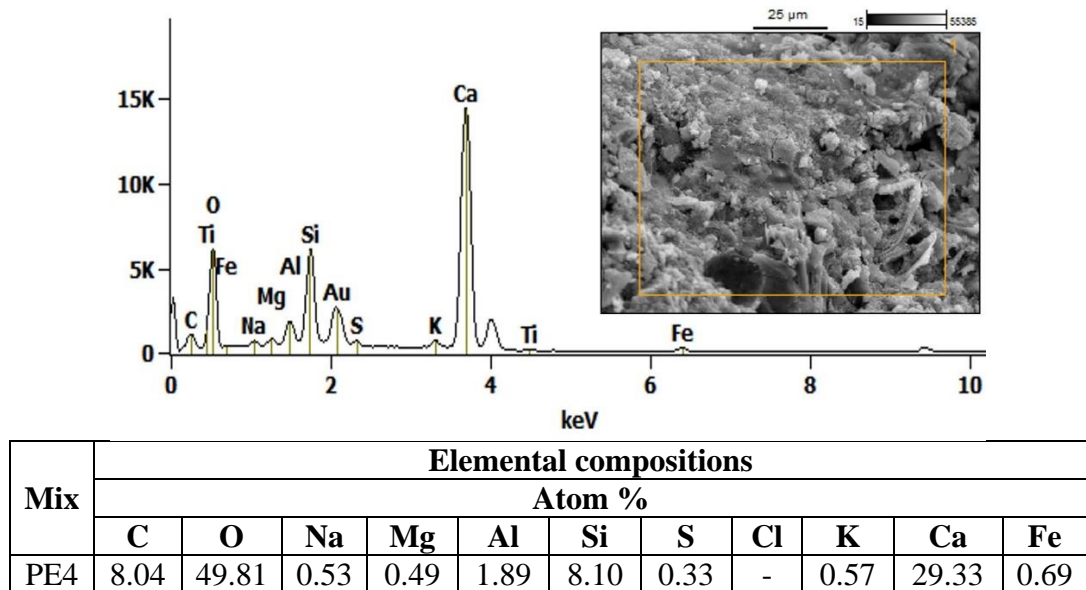


Figure 5. 18 EDS analysis of sample containing 60% EPS (PE4)

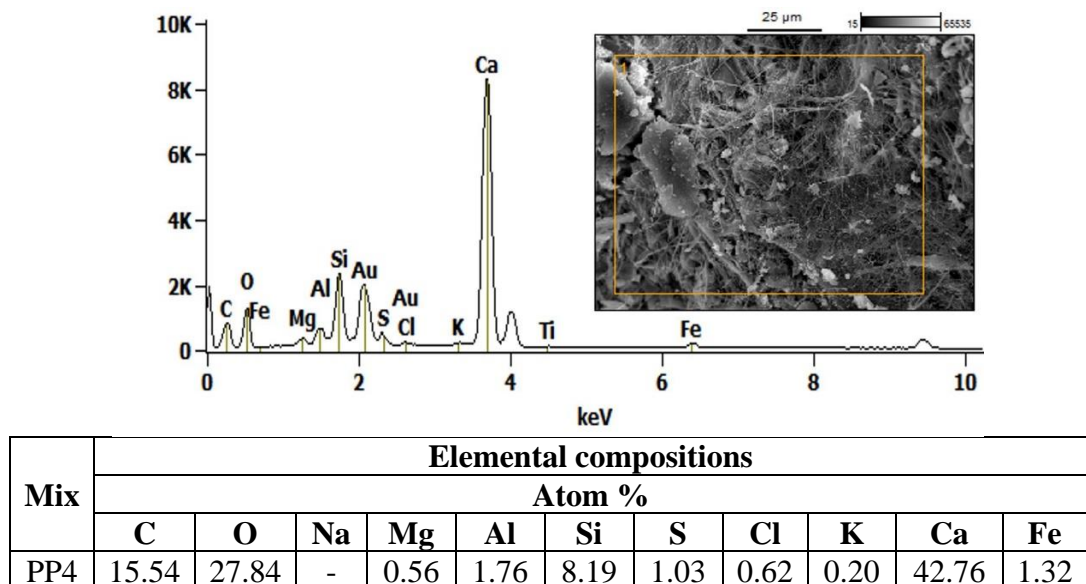
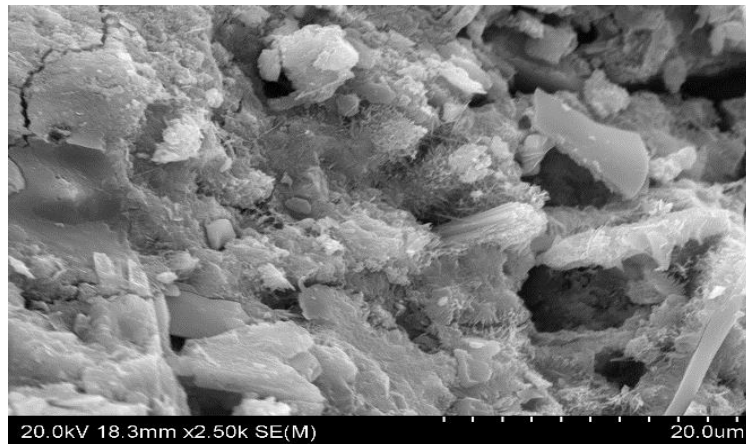
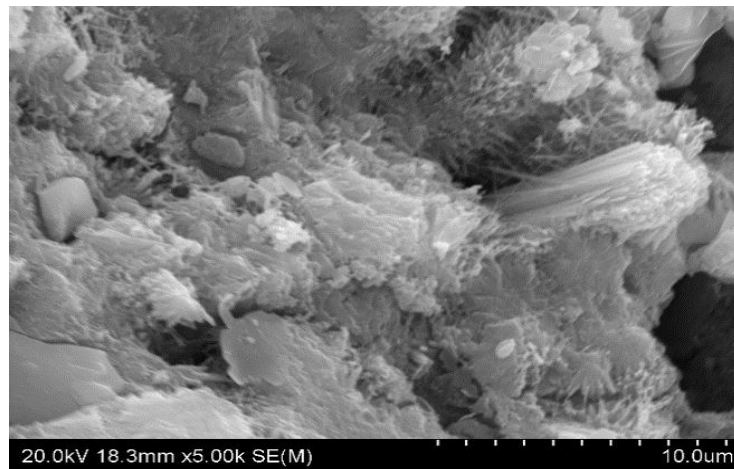


Figure 5. 19 EDS analysis of sample containing 60% EPLA (PP4)

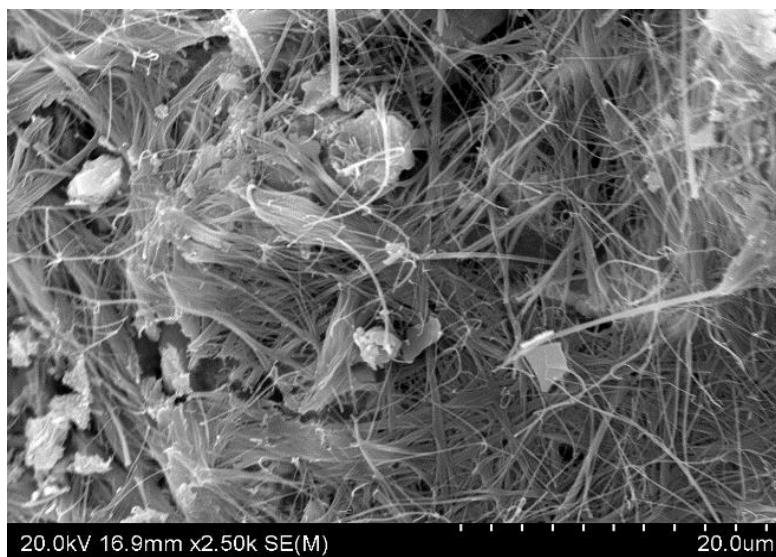


(a)

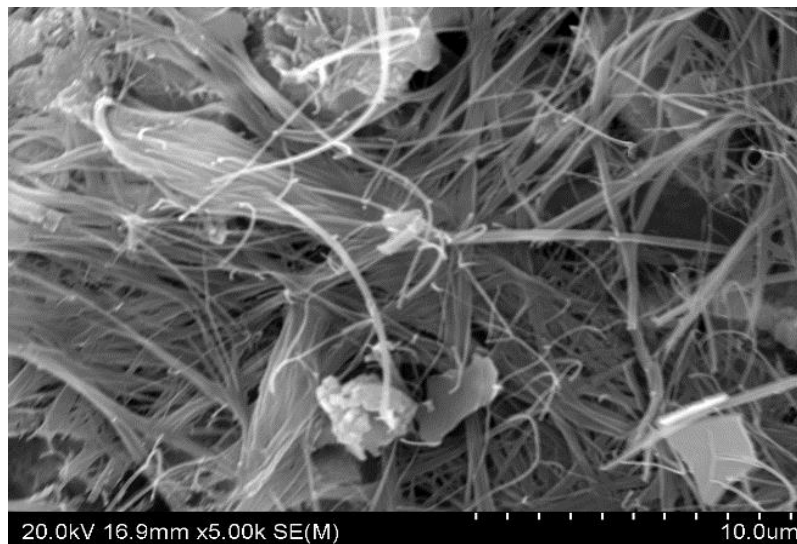


(b)

Figure 5. 20 SEM image of mix PE4; (a) at 2.5k magnification, (b) at 5.0k magnification



(a)



(b)

Figure 5. 21 SEM image of mix PP4; (a) at 2.5k magnification, (b) at 5.0k magnification.

5.5 Conclusions

Based on the experimental study carried out of utilising EPLA as a bio-plastic aggregate the following conclusions can be drawn:

- 1- The replacement of expanded perlite with expanded poly-lactic acid shows an inverse effect on the workability of concrete due to an increase in specific surface area. The reduction in the workability with the replacement of 20%, 40% and 60% aggregate volume in EP by EPLA shows 7%, 17% and 74% lower values than the control sample. The same trend of slump reduction was observed with an increase in EPS proportion.
- 2- The density ranges of EPLA and EPS concrete was found to be between 493.0 and 302.2 kg/m³ and 493.0 and 312.2 kg/m³, respectively. An increase in polymer volume significantly decreased the density of concrete. The EPLA concrete shows a slightly lower density mainly due to the alkaline reactivity of EPLA and an increase in CO₂ concentration and consequent increase in concrete porosity.
- 3- An increase in EPLA and EPS content led to a significant reduction in compressive strength and elastic modulus of concrete. The highest and lowest compressive strengths of 4.62 MPa and 0.62 MPa were observed in a sample containing 0% and

60% EPLA, respectively. Also, the curing condition directly affects the strength development of concrete. In the case of the high EPLA content sample, the compressive strength was decreased by 60% as the curing condition was changed from air cured to moist cured. With the identical polymer content, the compressive strength of EPS concrete was higher than that of EPLA concrete. The degradation of EPLA aggregate, interfacial bond failure due to the EPLA shrinkages and changes in hydration products of EPLA concrete are the main causes of strength reduction.

- 4- The addition of EPLA shows an inverse effect on water absorption ratio of concrete. The highest and lowest water absorption ratio was found in a sample containing 60% and 0% EPLA because EPLA lost its hydrophobicity and shrunk in the alkaline environment of cement. Contrary, an increase in EPS content results in a lower absorption ratio.
- 5- The inclusion of EPLA was found to be beneficial in terms of lowering thermal conductivity. This trend was reversed in samples cured in a moist condition. The degradation of EPLA in the alkaline environment of cement and concrete carbonation caused a decrease in concrete porosity and a higher thermal conductivity value. Compared to a control sample, the thermal conductivity decreased by 10%, 16% and 25% and increased by 14%, 4% and 2% for samples containing 20%, 40% and 60% EPLA which were cured in air and moist conditions, respectively. The thermal conductivity of EPS concrete was slightly higher than that of EPS concrete.
- 6- The alkaline reactivity of EPLA decreased the initial and final setting time of concrete mainly due to changes in the liquid phase composition. Sodium and calcium were found to be the main causes of EPLA degradation at the initial cement hydration stage.
- 7- The inclusion of EPLA led to a lower heat release rate (HRR) and carbon dioxide production (CO_2P). Compared to EPS concrete, the HRR and CO_2P were decreased by 57% and 48% as EPLA replaced EPS. The inclusion of EPLA aggregate causes an increase in carbon monoxide production and extended the flameout point.
- 8- The addition of EPLA significantly changed the microstructure and hydration products of concrete due to the degradation of EPLA and its alkaline reactivity. The phases identified in the EPS concrete are mostly calcium-silicate-hydrate (C-S-H), calcium hydroxide (portlandite) and calcium sulfoaluminate (ettringite). The hydration products of EPLA concrete were mainly composed of calcite, ettringite and

calcium hydroxide. The presence of a large amount of calcium carbonate (calcite) explains the interaction of EPLA with calcium and sodium.

Furthermore, a set of equations was developed to estimate the required water-cement ratio, required cement content, elastic modulus and thermal conductivity of the proposed concretes.

6.1 Introduction

It was found in chapter 4 and chapter 5 that the alkaine components of cement cause EPLA degrading which causes significant changes in engineering properties of concrete. This chapter presents the experimental results of GGBS concrete containing EPLA and perlite aggregate which has a lower alkalinity level compared to cement. The main idea of investigating GGBS was to reduce the alkalinity of the matrix as a solution to keep the EPLA beads alive. However, after a primary test, the same trend of degradation at a lower rate was observed. Therefore, only a limited number of parameters such as density, compressive strength, thermal conductivity, fire resistance and exothermic reaction were studied. In total, ten mixtures with a variation of activator content and polymer types are prepared. Calcium oxide (CaO) and magnesium oxide (MgO) are used as activators of GGBS concrete and replaced with 30% of GGBS weight at a CaO/MgO ratio of 30/60, 60/30, 45/45, 90/0 and 0/90. The results of GGBS concrete containing EPLA were compared to the EPS samples as a reference. The experimental results show that calcium carbonate even in small amounts causes EPLA degradation. The alkaine reactivity of EPLA leads to a considerable reduction of strength of GGBS concrete. Moreover, the influence of calcium oxide on thermal conductivity and exothermic reaction of concrete was notable.

6.2 Experimental procedure

6.2.1 Materials

The specification of materials are explained and provided in Chapter 3.

6.2.2 Specimen preparation and test methods

The content of magnesium oxide (MgO) and calcium oxide (CaO) as an activator of GGBS concrete was kept constant at 30% of binder weight. As shown in Table 6. 1, ten samples with a variation in MgO, CaO and aggregate types EPLA and EPS were prepared at a constant

water-binder ratio of 0.5. The materials are fully mixed in a dry condition. The EPLA aggregate, MgO, CaO and GGBS were mixed in a rotary mixer for about 1 min. Before adding the pre-determined amount of water, an appropriate amount of air entraining agent was mixed with the required amount of water, and then 70% of the mixed water (water + air entraining agent) were added to the mixture and mixed for 3 min. Expanded perlite aggregate was slowly added to the mixture followed by the remaining water for 2 min, to avoid the compaction of expanded perlite during the mixing process. To have a better understanding on the influence of curing conditions on properties of GGBS concrete containing EPLA aggregate, the samples were exposed to two different curing conditions of air curing (AC) and water curing (WC). In the case of air curing, the samples were kept in the laboratory at the relative temperature of 20 ± 2 °C, whereas the water cured samples were immersed in a water curing tank at a temperature of 16 ± 2 °C. It worth to note that the average results of three specimens were considered to evaluate the engineering properties of proposed concretes.

Table 6. 1 Mix proportion of magnesium phosphate concrete containing EP and EPLA.

Specimen	Effective w/b	CaO / MgO	Mix proportion (kg/m ³)							
			G	M	C	w	EP	EPLA	EPS	AE
PGMC 1	0.5	30/60	210	60	30	239.5	40.5	13.3	-	0.0041
PGMC 2	0.5	60/30	210	30	60	239.5	40.5	13.3	-	0.0041
PGMC 3	0.5	45/45	210	45	45	239.5	40.5	13.3	-	0.0041
PGMC 4	0.5	0/90	210	90	0	239.5	40.5	13.3	-	0.0041
PGMC 5	0.5	90/0	210	0	90	239.5	40.5	13.3	-	0.0041
EGMC 1	0.5	30/60	210	60	30	239.5	40.5	-	7.0	0.0041
EGMC 2	0.5	60/30	210	30	60	239.5	40.5	-	7.0	0.0041
EGMC 3	0.5	45/45	210	45	45	239.5	40.5	-	7.0	0.0041
EGMC 4	0.5	0/90	210	90	0	239.5	40.5	-	7.0	0.0041
EGMC 5	0.5	90/0	210	0	90	239.5	40.5	-	7.0	0.0041

w/b: water / binder ratio, G: Ground granulated blast-furnace slag (GGBS); M: Magnesium oxide (MgO); C: Calcium oxide (CaO); w: water; EP: expanded perlite, EPLA: Expanded poly-lactic acid; EPS: Expanded polystyrene; AE: Air entraining agent.

6.3 Results and discussion

6.3.1 Density and compressive strength

Table 6. 2 presents the density and strength development of GGBS concrete after 7 and 28 days with a variation of magnesium oxide (MgO) content, calcium oxide content (CaO) and curing conditions. The experimental results show that regardless of the MgO/CaO ratio, the dry density of samples containing EPLA was much lower than that of EPS concrete. The decline of unit weight in the dried density of GGBS concrete containing EPLA is an indication of a higher amount of open pores in the matrix structure due to the chemical reactivity of EPLA and its degradation.

Table 6. 2 Density and compressive strength of GGBS concrete containing EPLA and EPS aggregate.

Specimen	Density (kg/m ³)		Compressive strength (kg/m ³)			
			Air Cured		Moist Cured	
	Fresh	Air dried	7 days	28 days	7 days	28 days
PGMC 1	546.5	220.2	0.214	0.434	0.259	0.382
PGMC 2	569.7	217.6	0.312	0.421	0.286	0.360
PGMC 3	533.6	214.4	0.163	0.302	0.070	0.252
PGMC 4	540.0	218.0	0.208	0.308	0.161	0.341
PGMC 5	590.1	203.2	0.294	0.444	0.168	0.196
EGMC 1	600.0	259.6	0.482	0.681	0.803	1.255
EGMC 2	623.0	242.2	0.531	0.881	0.721	1.792
EGMC 3	577.5	230.4	0.430	0.663	0.834	1.381
EGMC 4	570.0	216.8	0.327	0.396	0.558	1.027
EGMC 5	628.3	212.4	0.819	0.868	0.763	1.310
PP4	389.0	302.2	-	1.620	-	0.640
PE4	384.0	312.6	-	1.820	-	2.090

As shown in Figure 6. 1, the addition of calcium oxide accelerates the degradation of EPLA, while the application of magnesium oxide as GGBS activator reduced the rate of degradation. The sample PGMC5 shows a lower density compared to the other samples containing EPLA. In fact, an increase in CaO content accelerates the degradation of EPLA beads as a result of chemical reactivity of lactic acid and calcium hydroxide. Also, an increase in CO₂ concentration as a result of chemical reactivity of lactic acid and calcium hydroxide causes an increase in porosity and consequently lower density.

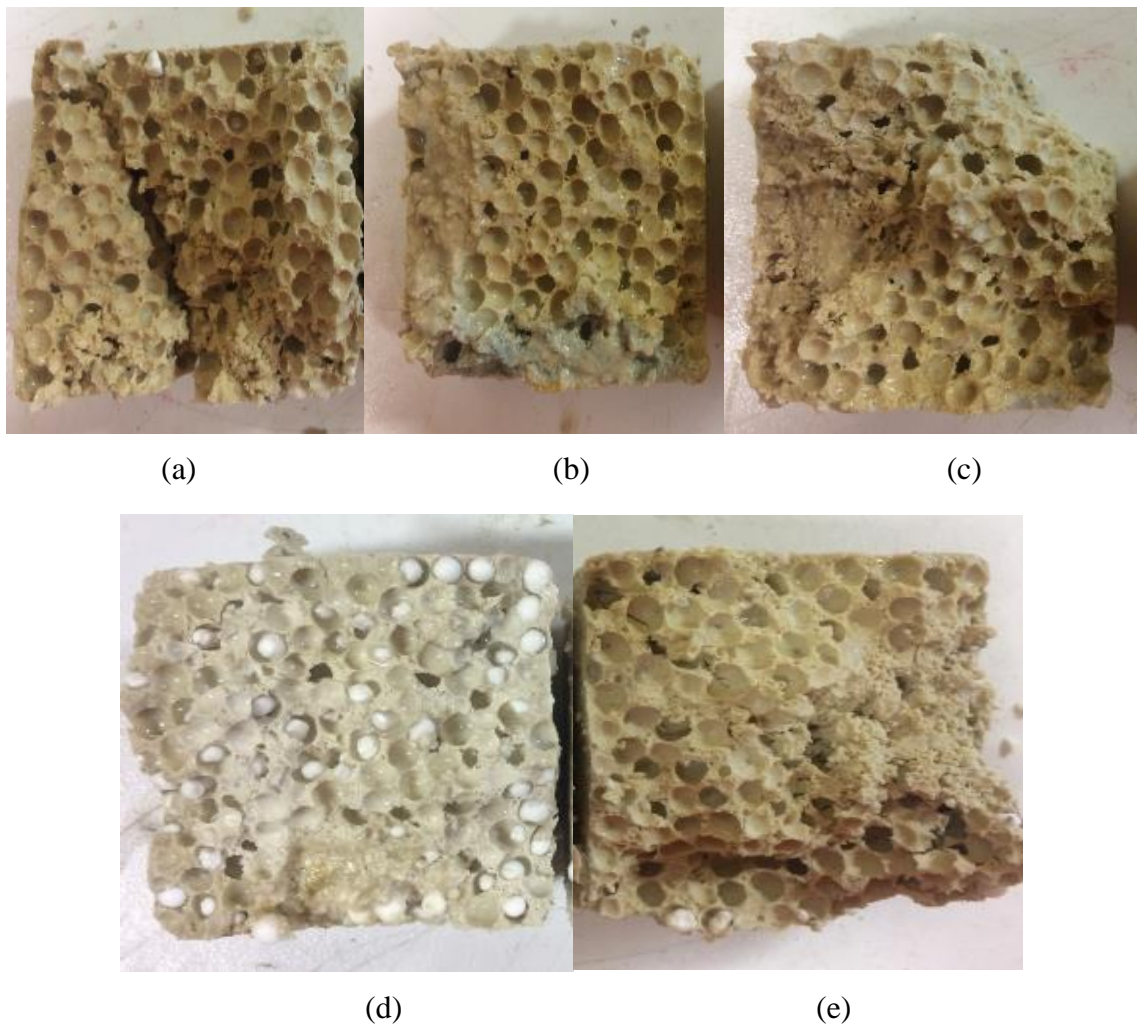


Figure 6. 1 The influence of GGBS activator on rate of EPLA degradation; (a) PGMC1, (b) PGMC2, (c) PGMC3, (d) PGMC4, (e) PGMC5

According to the experimental results in Table 6. 2, it was found that the strength development of samples containing EPLA aggregate, which cured in water was smaller than those cured in the ambient environment. This trend was inverse in GGBS concrete containing EPS aggregate. Regardless of the MgO/CaO ratio, the average compressive strength obtained for samples cured in water at the age of 7 days and 28 days were about 29% and 22% lower than the samples cured in air, respectively. The rate of strength reduction was much higher in a sample containing a larger amount of calcium oxide (PGMC5) due to the alkaline reactivity of EPLA, which results in significant changes in hydration products of concrete and conversion of hydration products to more calcium carbonate. The highest compressive strength was observed in sample PGMC1 with a relative MgO/CaO content of 60/30. It was found that the amount of calcium oxide significantly affects the strength development of GGBS concrete containing EPLA. The average 28 days compressive strength of GGBS concrete containing EPS aggregate was about 65.5% and 314.77% higher than that of the EPLA sample when cured in air and water, respectively.

6.3.2 Thermal conductivity

The variation of thermal conductivity (TC) of GGBS concrete containing EPLA and EPS is presented in Table 6. 3. The thermal conductivity of the proposed concretes was found to be 26 to 30 times smaller compared with normal concrete containing quartzite aggregate (about 3.5 W/mK). The experimental results show that the factors such as aggregate types (EPLA and EPS), calcium oxide content and magnesium oxide content significantly affect the TC value of GGBS concrete. In the case of EPLA samples, the thermal conductivity decreased with an increase in calcium oxide content. This trend was mainly attributed to the increase in concrete porosity due to the EPLA degradation in the alkaline environment of the matrix and an increase in CO₂ gas concentration. The lowest and highest TC value were observed in samples PGMC5 and PGMC4 with relative TC values of 0.0923 W/mK and 0.1251 W/mK. A thermal conductivity of 0.1046, 0.0976 and 0.1146 W/mK was obtained for samples PGMC1, PGMC2 and PGMC3, respectively. It was established that any changes in calcium oxide content affect the TC values, which is directly related to the alkaline reactivity of EPLA. In contrast, the influence of the activator content on thermal conductivity of EPS samples was minimal.

Table 6. 3 Thermal conductivity of proposed concrete

Specimen	Density (kg/m³)	Thermal conductivity (W/m.K)
PGMC 1	220.2	0.1046
PGMC 2	217.6	0.0976
PGMC 3	214.4	0.1146
PGMC 4	218.0	0.1251
PGMC 5	203.2	0.0923
EGMC 1	259.6	0.1013
EGMC 2	242.2	0.1051
EGMC 3	230.4	0.0993
EGMC 4	216.8	0.1016
EGMC 5	212.4	0.0979
PP4	302.2	0.0710
PE4	312.6	0.0880

6.3.3 Exothermic reaction

The influence of activators on the exothermic reaction of GGBS concrete is shown in Figure 6. 2. A higher exothermic reaction intensity was found in samples containing larger amounts of calcium oxide. This trend mostly related to the highly reactive properties of calcium oxide when mixed with water to form calcium hydroxide. The addition of magnesium oxide causes an extension of the peak time temperature and consequently lower concrete temperature. The peak temperature of samples PGMC5 and PGMC3 was 45 °C and 22 °C, which occurred after 5 and 15min of mixing time, respectively. Compared with normal concrete containing EPLA (PP4), both samples PGMC5 and PGMC3 showed an immediate increase in concrete temperature, which was followed by a sudden drop in exothermic reaction, while the temperature changes of sample PP4 was minimal.

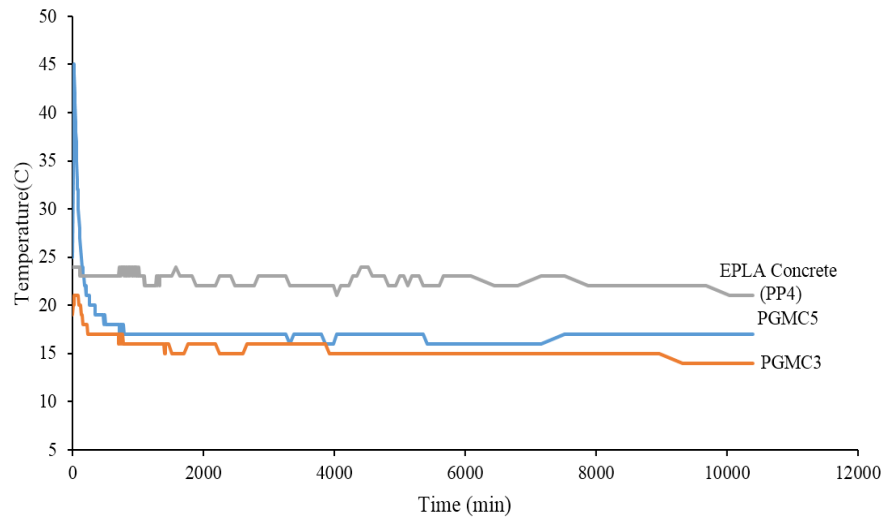


Figure 6. 2 The exothermic reaction of GGBS concrete.

6.3.4 Fire resistance

The fire properties of GGBS concrete were evaluated through a cone calorimeter test according to ASTM E1354. In order to have a better understating of the performance of GGBS concrete, its results are compared with samples of EPLA concrete (PP4) and EPS concrete (PE4). The parameters such as heat release rate (HRR), total heat released (THR), carbon monoxide production (COP), carbon dioxide production (CO2P), mass reduction and failure modes during fire test were evaluated and assessed.

As shown in Figure 6. 3, no visible thermal cracks and matrix degradation was observed in samples PGMC3 and EGMC3, while some minor thermal cracks were observed in samples PP4 and PE4. The slight changes in surface colouring were visible in all samples except GGBS concrete containing EPLA aggregate. The surface changes of GGBS concrete containing EPLA could be related to the burning of polymer aggregate for a much longer time as a result of producing larger amounts of CO gas which is associated with retaining the flame over the surface of samples.

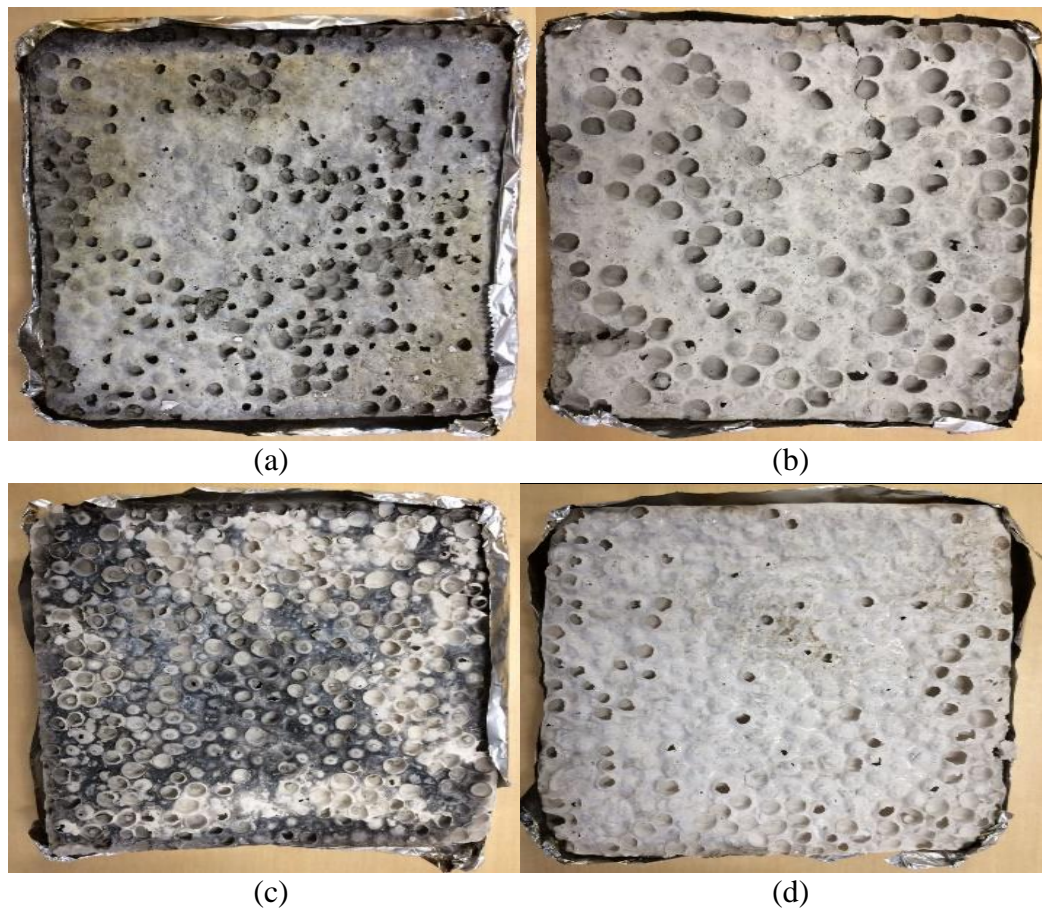
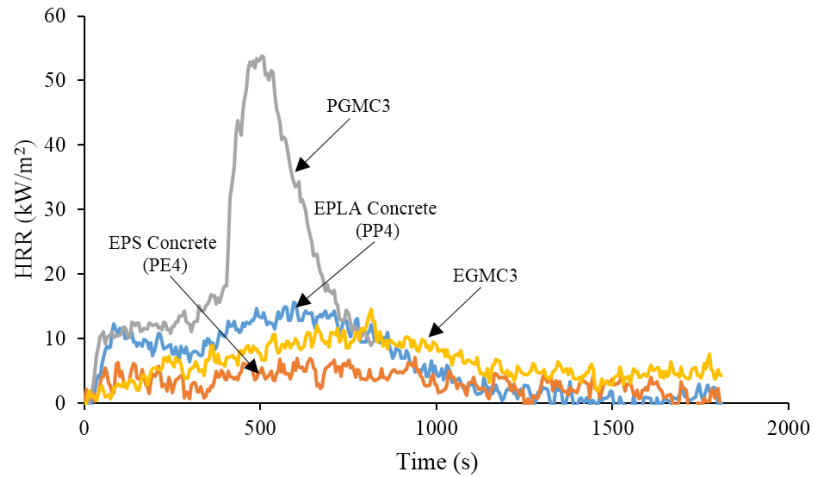


Figure 6. 3 Fire test results; (a) EPLA concrete, (b) EPS concrete, (c) PGMC 3, (d) EGMC3 3.

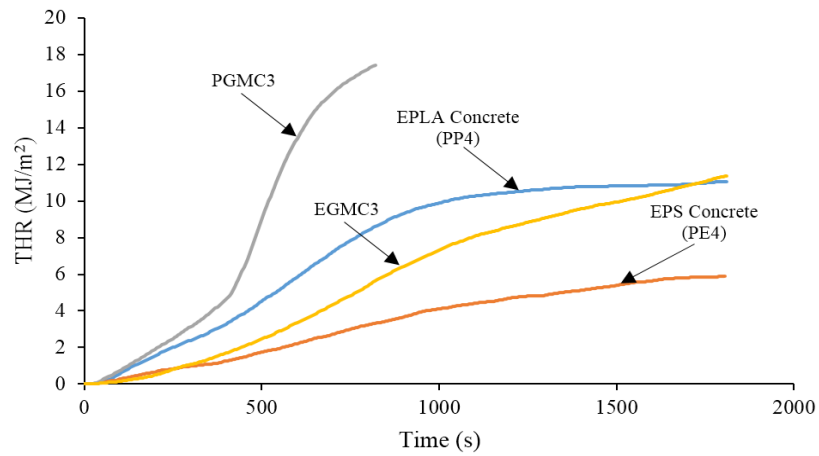
Based on the experimental results of the fire tests, the PGMC3 and EGMC3 samples are categorized as quasi non-combustible with a relative HRR and THR of 14.566 kW/m^2 and 11.379 MJ/m^2 along with 53.83 kW/m^2 and 17.401 MJ/m^2 , respectively. The heat release rate of the proposed concretes was much higher than the standard limit of 200 kW/m^2 and the total heat released of the samples exceeded the limit of the standard of 8 MJ/m^2 . It was found that the heat release rate of GGBS concrete containing EPLA was much higher than that of the sample containing EPS aggregate. Compared to cement-based samples PP4 and PE4, the HRR and THR of GGBS concrete containing EPLA were much higher (Figure 6. 4). The GGBS concretes containing EPLA and EPS ignited after 394s and 763s and flame out took place after 698s and 1012s (Table 6. 4). It was found the addition of EPLA causes an increase in ignition time of GGBS concrete, while a considerable delay was observed in the sample containing EPS aggregate. In the case of EPS concrete, the application of GGBS causes also a slight delay in ignition time compared to sample PP4 and PE4.

Table 6. 4 The time to ignition and flameout of proposed concretes.

Mix No.	Time to ignition (s)	Time to flameout (s)
PGMC3	394	698
EGMC3	763	1012
PP4	555	1162
PE4	711	1311



(a)



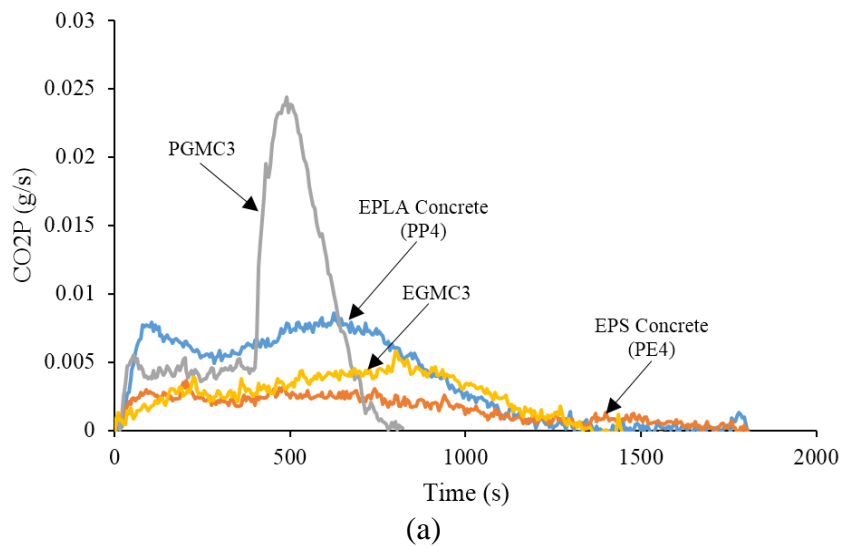
(b)

Figure 6. 4 Cone calorimeter test results; (a) Heat release rate (HRR), (b) Total heat released (THR).

As it is shown in Figure 6. 5a, a sharp increase in CO₂ gas production was observed after ignition which mainly related to the combustion process of EPS aggregate generating a considerable amount of CO₂ gas. Although a significant delay in CO₂ gas production was

observed, the rate of gas production was much higher than that of a sample containing EPS. In contrast, the level of CO₂ gas production has remained low and almost constant throughout the test with no considerable sharp point. Compared to sample PGMC3, the amount of gas production was about 65% higher than that of sample PP4. It was found that the combination of GGBS and EPLA causes an increase in CO₂ gas production, which can be counted as the negative impact of using EPLA in GGBS concrete.

The concentration levels of carbon monoxide (CO) are presented in Figure 6. 5b. The CO gas production of sample PGMC3 was significantly higher than that of EPLA and EPS concrete. The highest and fastest growth in CO gas production was observed in sample PGMC3. It was found that the difference between the ignition and flash point of EPLA concrete was greater than that of EPS concrete due to the production of larger amounts of CO gas. The same trend of a lower amount of gas was observed in sample PP4. It can be found that the addition of EPLA leads to an increase in CO gas production, which retains the flame over the surface of samples and increases HRR and THR.



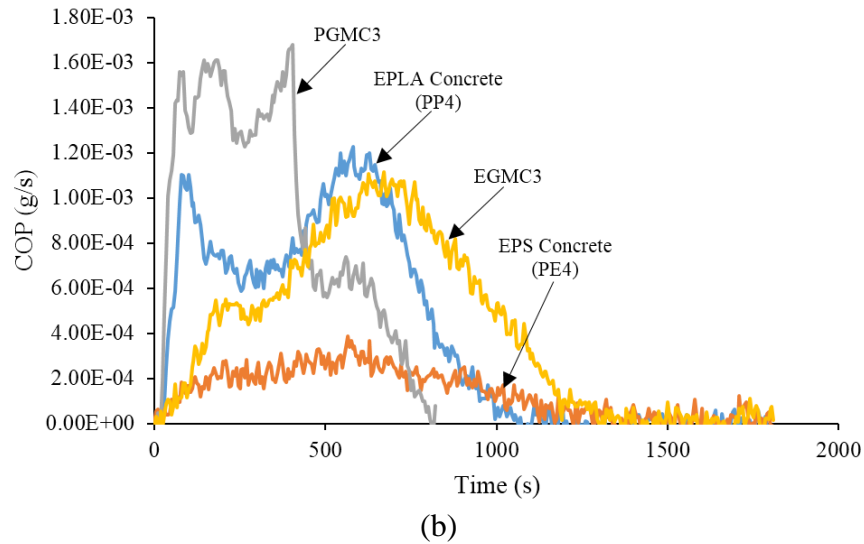


Figure 6. 5 Cone Calorimeter test results; (a) Carbon dioxide production (CO₂P), (b) Carbon monoxide production (COP).

6.4 Conclusions

Based on the assessment and evaluation of mechanical and thermal properties of GGBS concrete the following conclusions are drawn:

- 1- The addition of calcium oxide accelerates the rate of EPLA degradation, while the degradation was lower when magnesium oxide is used as an activator of GGBS.
- 2- The density of GGBS concrete ranged from 203.2 kg/m³ to 220.2 kg/m³ and from 212.4 kg/m³ to 259.6 kg/m³ for samples containing EPLA and EPS, respectively. A significant decrease in density of concrete was observed with samples containing larger amounts of calcium oxide mainly due to the alkaline reactivity of EPLA and calcium hydroxide. This causes an increase in CO₂ gas concentration and concrete porosity.
- 3- The strength development of GGBS concrete is influenced by curing regimes and activator content. The compressive strength of GGBS concrete containing EPLA decreased with an increase in calcium oxide content. However, the moist curing condition accelerates the rate of strength reduction in samples containing EPLA, while this trend was inverse in EPS samples. The strength reduction is mainly attributed to the changes in hydration products of concrete as the alkaline reactivity of EPLA with alkaline components of GGBS leads to the formation of calcium carbonate as a hydration product.

- 4- The alkaline reactivity of EPLA significantly affects the thermal conductivity value of GGBS concrete. A lower TC value was observed in samples containing larger amounts of calcium oxide. The chemical reactivity of lactic acid and calcium hydroxide causes an increase in concrete porosity. The influence of the activator on thermal conductivity of EPS concrete was minimal.
- 5- The exothermic reaction of GGBS concrete was a factor of activator content. A rapid increase in concrete temperature occurred in samples containing larger amounts of calcium oxide due to the rapid reaction of calcium oxide and water to form calcium hydroxide.
- 6- No visible cracks were found in samples containing EPLA and EPS and they were categorized as a quasi-non-combustible. The heat release rate of samples containing EPLA was much higher than that of EPS samples. The same trend was observed in terms of carbon monoxide production and carbon dioxide production. Compared to EPS samples, the addition of EPLA causes an increase in COP, which leads to the flame being retained over the surface of samples for a longer period.

7.1 Introduction

The degradation of expanded poly-lactic acid (EPLA) in the high alkaline environment of cement basically eliminates the use of a bio-polymer aggregate as a substitution for lightweight petroleum derived aggregate such as EPS. The chemical reaction of EPLA beads and alkaline components of cement causes a significant change in properties of concrete. It was found in previous chapters that the replacement of cement with GGBS as a lower alkaline binder slightly decreased the degradation rate of EPLA. In addition, it was concluded that the rate of degradation depends on the volume percentages of calcium oxide.

This chapter aims to evaluate the performance of EPLA beads in the acid-based environment of magnesium phosphate cement. The magnesium phosphate concrete is prepared by mixing magnesium oxide (MgO), ammonium dihydrogen phosphate ($\text{NH}_4\text{H}_2\text{PO}_4$), expanded perlite (EP), expanded poly-lactic acid and Borax as a retarder at a certain ratio and proportions. The mechanical properties of the proposed concrete were assessed at the period of 1 hour to 90 days. Also, the thermal conductivity, electrical resistivity, setting time, fire resistance, pH, exothermic reaction and microstructure of the concrete were investigated. The phosphate to magnesium ratio (P/M), water to cement ratio (w/c) and retarder content were the variables of this study. The experimental results show that the EPLA beads are stable in the acid-based reaction of magnesium phosphate cement and no degradation was observed. Moreover, the P/M ratio and retarder content affect the setting time and exothermic reaction of concrete. The electrical resistivity decreased with an increase in phosphate content. The magnesium phosphate concrete lost its strength when subjected to higher temperatures. The XRD analysis reveals that the reduction in concrete strength after 7 days is mainly attributed to the formation of calcium chloride.

7.2 Experimental procedure

7.2.1 Materials

The specification of materials are explained and provided in Chapter 3.

7.2.2 Specimen preparation and test methods

As presented in Table 7. 1, a total of 18 magnesium phosphate concrete samples were prepared. The phosphate-magnesium ratio was varied at the mix ratio of 1/6, 1/5 and 1/3. At each P/M ratio, the water-cement ratio ranged from 0.9 to 1.1 in increments of 0.1. In addition, the retarder content was considered as another variable in this study. Borax was added to the matrix at a ratio of 5 and 10% of the cementitious weight. For instance, the sample PM15-1.0-05 is prepared with a P/M ratio of 1:5, water-cement ratio of 1.0 and borax content of 5%. The ratio of expanded perlite to expanded poly-lactic acid was kept fixed at 0.428 by aggregate volume. All the materials are fully mixed in a dry condition and blended in a small rotary mixer for about 1 min. Before adding water, an appropriate amount of air entraining agent was mixed with the required water. The required water was added to dry materials and mixed only for 1 min due to the immediate hardening of magnesium phosphate cement.

The samples were cast into standard steel moulds of 50x50x50 mm cube size and demoulded after 1 hour. The compressive strength tests were done by an Instron 100 kN tester at a rate of 50 mm/min after 1 hour, 3 hours, 1 day, 3 days, 7 days, 28 days, 56 days and 90days. Prisms of 70x20x20 mm sizes were used for studying the thermal conductivity. The thermal conductivity, XRD analysis, EDS analysis, SEM imaging, electrical resistivity and fire resistance tests were carried out to investigate the various properties. The descriptions of the test methods are contained in more detail in Chapter 3. It is worth to note the hydration process of samples was stopped by immersion of the samples in acetone for 3 days followed by a vacuum oven for 3 days and oven drying for 1 day at 35°C [182]. The average results of three specimens were considered to evaluate the engineering properties of proposed concrete.

Table 7. 1 Mix proportions of magnesium phosphate concrete containing EP and EPLA.

Specimen	P:M	*w/b	Mix proportion (kg/m ³)							
			w	C	P	M	EP	B	EPLA	EPS
EPLA Concrete (PP4)	-	0.624	193.5	310	-	-	40.5	-	13.3	-
EPS Concrete (PE4, reference)	-	0.624	193.5	310	-	-	40.5	-	-	7.0
PM16-0.9-10	1:6	0.9	360.5	-	43	257	40.5	30	13.3	-
PM16-0.9-05	1:6	0.9	360.5	-	43	257	40.5	15	13.3	-
PM16-1.0-10	1:6	1.0	390.5	-	43	257	40.5	30	13.3	-
PM16-1.0-05	1:6	1.0	390.5	-	43	257	40.5	15	13.3	-
PM16-1.1-10	1:6	1.1	420.5	-	43	257	40.5	30	13.3	-
PM16-1.1-05	1:6	1.1	420.5	-	43	257	40.5	15	13.3	-
PM15-0.9-10	1:5	0.9	360.5	-	50	250	40.5	30	13.3	-
PM15-0.9-05	1:5	0.9	360.5	-	50	250	40.5	15	13.3	-
PM15-1.0-10	1:5	1.0	390.5	-	50	250	40.5	30	13.3	-
PM15-1.0-05	1:5	1.0	390.5	-	50	250	40.5	15	13.3	-
PM15-1.1-10	1:5	1.1	420.5	-	50	250	40.5	30	13.3	-
PM15-1.1-05	1:5	1.1	420.5	-	50	250	40.5	15	13.3	-
PM13-0.9-10	1:3	0.9	360.5	-	75	225	40.5	30	13.3	-
PM13-0.9-05	1:3	0.9	360.5	-	75	225	40.5	15	13.3	-
PM13-1.0-10	1:3	1.0	390.5	-	75	225	40.5	30	13.3	-
PM13-1.0-05	1:3	1.0	390.5	-	75	225	40.5	15	13.3	-
PM13-1.1-10	1:3	1.1	420.5	-	75	225	40.5	30	13.3	-
PM13-1.1-05	1:3	1.1	420.5	-	75	225	40.5	15	13.3	-

*w/b: (effective w/b ratio + required water for saturating of expanded perlite), C: Cement content, P: Ammonium dihydrogen phosphate; M: Magnesium oxide; EP: Expanded perlite; B: Borax; EPLA: Expanded poly-lactic acid; AE: air entraining agent; w: water.

7.3 Results and discussion

7.3.1 Density

Table 7. 2 presents the dry density of magnesium phosphate concrete (MP) with a variation in phosphate content, magnesium content, borax content and water-cement ratio. The density of concrete decreased slightly with an increase in water-binder ratio. In the case of identical phosphate-magnesium ratios ($P/M = 1/6$), the density decreased from 462.2 kg/m^3 to 383.2 kg/m^3 as the water-cement ratio increased from 0.9 to 1.1. This trend is mainly related to the increase in concrete flowability and sufficient water being available for the activation of the air mix agent, which causes an increase in concrete porosity. The influence of the P/M ratio on the dry density of concrete was minimal. Compared with $P/M = 1/5$ the average density of all samples of each group was about 8.21% and 4.18% lower than that of $P/M = 1/6$ and $P/M = 1/3$, respectively.

The highest and lowest dry density were observed in the samples PM16-0.9-10 and PM15-1.1-05 with relative densities of 467.7 and 367.0 kg/m^3 . Compared with the reference sample prepared with cement, the lowest density obtained by magnesium phosphate concrete was about 18% of that of EPLA concrete. The changes in density can be attributed to the relative density of magnesium phosphate and alkaline reactivity of EPLA. In fact, the chemical reactivity of EPLA in the alkaline environment of cement leads to an increase in CO_2 gas concentration and consequently decreases in concrete porosity. No alkaline reactivity was observed in magnesium phosphate cement containing EPLA aggregate due to the acid-based environment of magnesium phosphate cement.

7.3.2 Compressive strength

As shown in Table 7. 2, the compressive strength of the proposed concrete improved with an increase in MgO content. The chemical reaction of magnesium phosphate cement occurs with the dissolution of MgO and $\text{NH}_4\text{H}_2\text{PO}_4$ in an acid-based environment. The strength development of magnesium phosphate cement mainly depends on the hydration of MgO as the strength of hydrated MgO is much higher than that of phosphate hydrates [P1]. It was

found that the optimum ratio of phosphate and magnesium is the ratio with which the phosphate hydrates can surround the grains of MgO thoroughly.

The experimental results show that the strength development of concrete at different curing ages increased rapidly up to 7 days and decreased slightly at later ages (up to 90days). For instance, the compressive strengths of sample PM15-1.1-10 at 3 days, 7 days, 28 days, 56 days and 90 days were 0.47, 0.49, 0.37, 0.31 and 0.28MPa, which shows the strength reduction during the curing time. It is worth to note that the 1 hour and 3 hours and 1-day compressive strength of sample PM15-1.1-10 were 46% increased, 10% decreased and 13.52% decreased from the 28day compressive strength. It is very likely, that the addition of perlite aggregate with its relatively high absorption ratio initially hinders the hydration process and later hydration of unreacted magnesium oxide and phosphate causes a significant reduction in strength development of concrete. The same trend of strength reduction was observed in other samples with different P/M ratios. In comparison with a reference sample, the compressive strength of magnesium phosphate concrete was about 78% higher than that of EPLA concrete. The main causes of strength reduction can be attributed to the alkaline reactivity of EPLA aggregate and changes in hydration products, which causes more calcium carbonate to appear as hydration products of concrete containing EPLA particles. In addition, the interfacial bond between EPLA and the matrix breaks down due to shrinkages and degradation of EPLA particles. In fact, the degradation process, changes in hydration products, the existence of large void sizes due to shrinkages of EPLA and increases in concrete porosity lead to a considerable reduction in concrete strength compared with magnesium phosphate concrete.

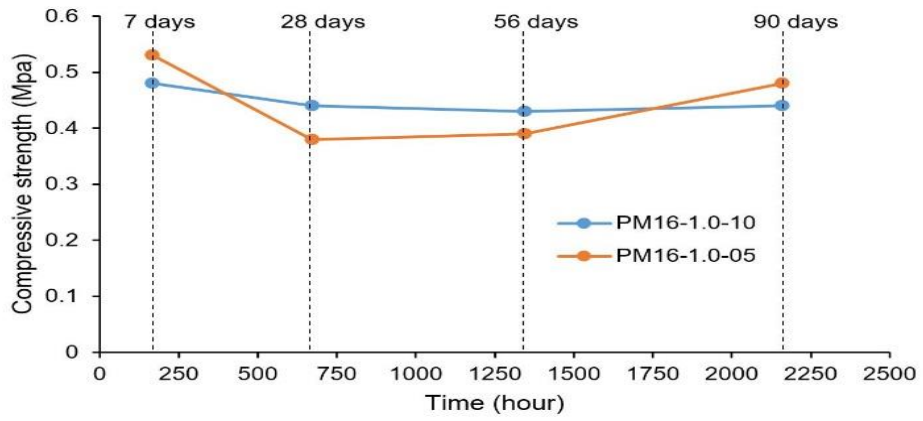
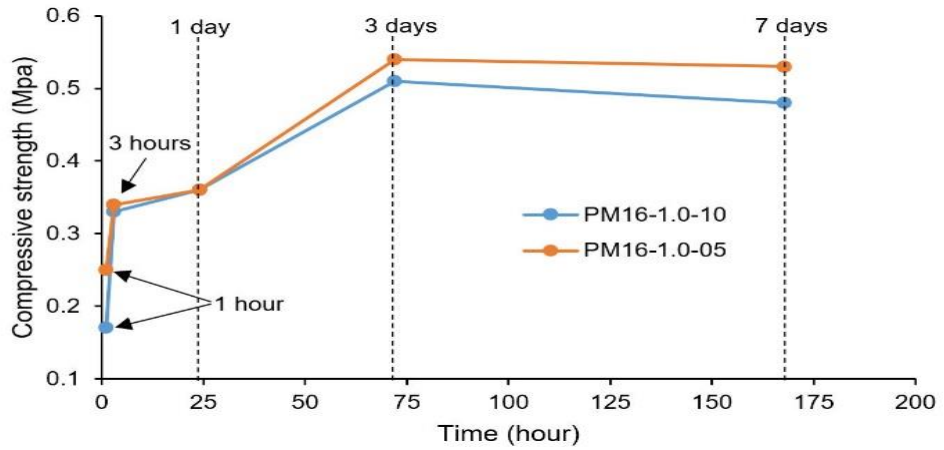
As shown in Figure 7. 1, all the samples reveal a parabolic strength development up to 7 days with a relatively high strength development at early stages. However, this trend starts to decrease after that. The effectiveness of retarder content increases with its amount. The increase in borax content causes a decrease in compressive strength while this trend was inversed in the sample with a P/M ratio of 1/3. It was found there is a direct relationship between phosphate content and borax content as the retarder materials show a better performance in a sample containing a larger amount of phosphate. However, the addition of retarder caused an increase in 28-days compressive strength of samples with a P/M ratio of 1/5 and 1/6 but decreased at the later ages.

The experimental results show that the 28-day and 56-day compressive strengths of sample PM13-1.0 were increased from 0.37 MPa to 0.48 MPa and 0.42 MPa to 0.49 MPa as the

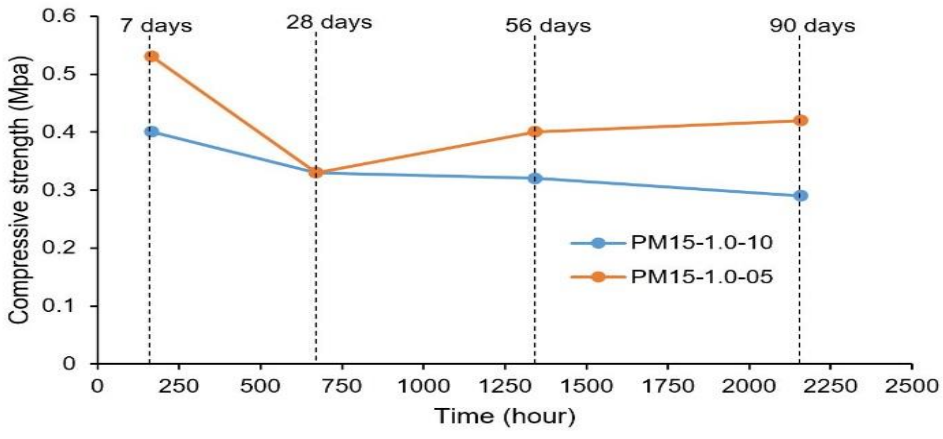
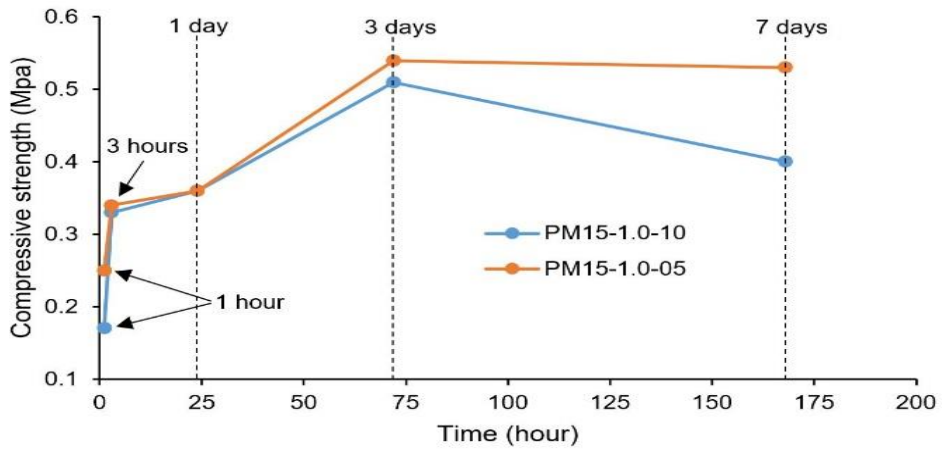
borax content increased from 5% to 10%, respectively. Compared to the strength development of magnesium phosphate concrete at 90-day strength, the ranges were 48-61% lower after 1 hour, 25-30% lower after 3 hours, 18-25% lower after 1 day, 12-15% higher after 3 days and 8-10% higher after 7 days, while the rate of strength development was varied at the time of 28-day and 56-day. The application of perlite as a lightweight aggregate causes a significant reduction in long-term strength development of magnesium phosphate concrete and this trend was much higher at the sample containing a larger amount of phosphate. Also, it can be concluded that the high absorbent characteristics of perlite aggregate and high concrete temperatures at the initial stage of mixing causes a significant reduction in concrete flow-ability and consequently lower concrete strength.

Table 7. 2 The density and compressive strength of magnesium phosphate concrete.

Specimen	P/M	Density (kg/m ³)	Compressive strength (MPa)							
			1 Hour	3 Hours	1 Day	3 Days	7 Days	28 Days	56 Days	90 Days
EPLA Concrete (PP4)	-	302.2	-	-	-	-	-	0.11	0.13	0.15
PM16-0.9-10	1/6	467.7	0.26	0.41	0.55	0.57	0.59	0.54	0.49	0.51
PM16-0.9-05	1/6	462.2	0.32	0.36	0.40	0.54	0.55	0.44	0.38	0.42
PM16-1.0-10	1/6	443.7	0.17	0.33	0.36	0.51	0.48	0.44	0.43	0.44
PM16-1.0-05	1/6	417.9	0.25	0.34	0.36	0.54	0.53	0.38	0.39	0.48
PM16-1.1-10	1/6	426.1	0.20	0.41	0.42	0.47	0.49	0.53	0.41	0.45
PM16-1.1-05	1/6	383.2	0.24	0.30	0.31	0.41	0.44	0.39	0.33	0.36
PM15-0.9-10	1/5	429.8	0.26	0.41	0.55	0.57	0.59	0.55	0.35	0.32
PM15-0.9-05	1/5	406.3	0.32	0.36	0.40	0.54	0.55	0.45	0.41	0.49
PM15-1.0-10	1/5	412.2	0.17	0.33	0.36	0.51	0.40	0.33	0.32	0.29
PM15-1.0-05	1/5	397.3	0.25	0.34	0.36	0.54	0.53	0.38	0.40	0.42
PM15-1.1-10	1/5	390.9	0.20	0.41	0.42	0.47	0.49	0.37	0.31	0.28
PM15-1.1-05	1/5	367.0	0.24	0.30	0.31	0.40	0.43	0.38	0.33	0.30
PM13-0.9-10	1/3	448.8	0.27	0.30	0.53	0.61	0.67	0.63	0.65	0.58
PM13-0.9-05	1/3	406.4	0.31	0.32	0.34	0.41	0.42	0.40	0.38	0.37
PM13-1.0-10	1/3	417.6	0.25	0.40	0.44	0.47	0.51	0.49	0.47	0.48
PM13-1.0-05	1/3	412.0	0.30	0.35	0.37	0.38	0.44	0.42	0.40	0.37
PM13-1.1-10	1/3	415.2	0.15	0.31	0.35	0.36	0.43	0.51	0.48	0.49
PM13-1.1-05	1/3	404.0	0.24	0.31	0.34	0.39	0.41	0.35	0.37	0.35



(a)



(b)

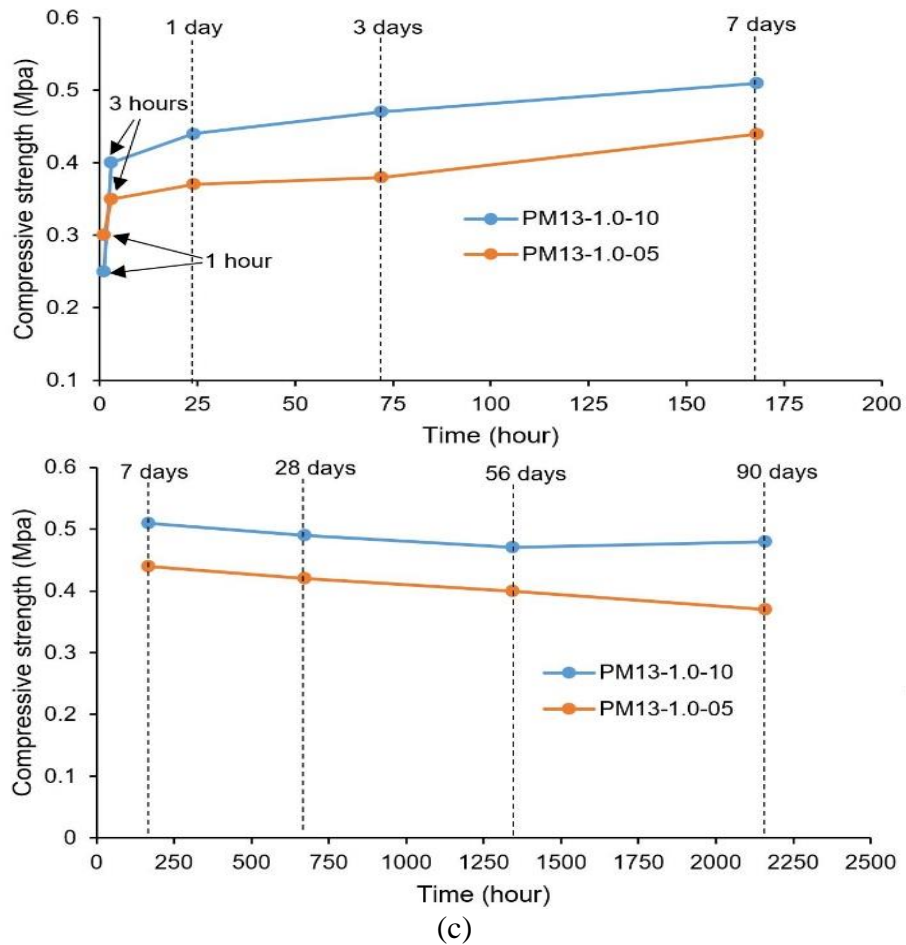


Figure 7. 1 The strength development of magnesium phosphate concrete; (a) PM16-1.0, (b) PM15-1.0, (c) PM13-1.0.

7.3.3 pH assessment

Figure 7. 2 shows the pH variation of magnesium phosphate concrete at different curing ages. A slight increase in pH values of concrete was observed at the early stages of curing of up to 7 days and remained almost stable at the later stages of up to 90 days. The increase in pH level at the early stage of curing is mainly related to the gradual dissolution of MgO [213, 214]. In fact, the hydration process and hardening of magnesium phosphate concrete in the acid-based environment depends on the dissolution of magnesium oxide in ammonium dihydrogen phosphate [213]. The dissolution of ammonium dihydrogen phosphate and the released hydrogen ions form an acid-based solution, which accelerates the dissolution of magnesium and the release of hydroxide ions. As the pH of the solution climbs above 7, the struvite analogue ($\text{MgKPO}_4 \cdot 6\text{H}_2\text{O}$) started to form, accompanied with its amorphous counterpart [215]. The matrix starts to set and hardens with an increase in the amount of struvite of potassium and amorphous substances.

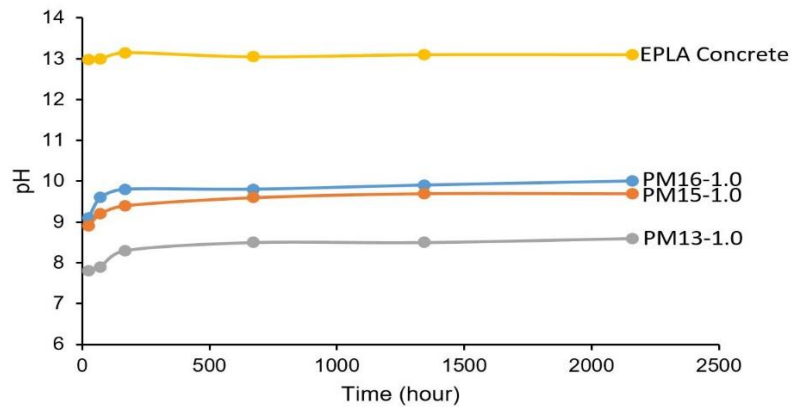
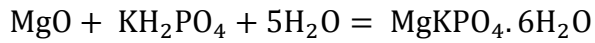
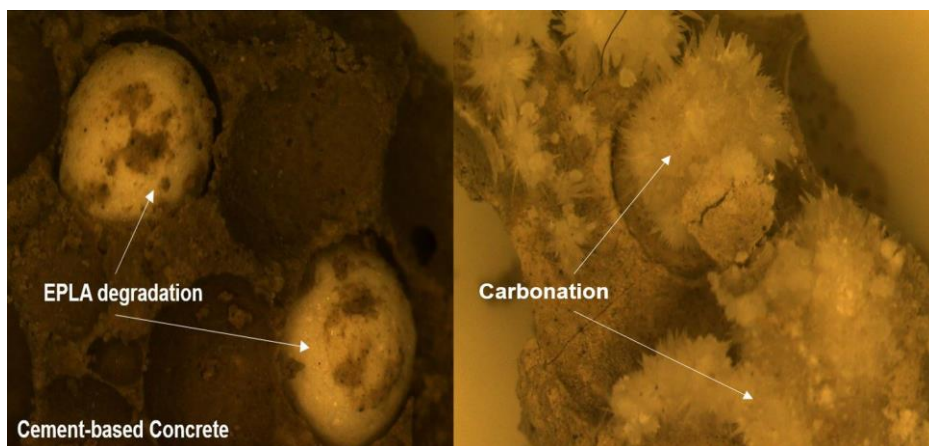


Figure 7. 2 The comparison between pH variation of magnesium phosphate concrete and cement-based concrete.

The pH values of concrete increased with an increase in magnesium content (M). The sample PM13-1.0 with a P/M ratio of 1/3 shows a lower pH value throughout curing compared to PM15-1.0 and PM16-1.0 with a relative P/M ratio of 1/5 and 1/6, respectively. The pH level of samples with a P/M ratio of 1/6 and 1/5 was about 14-19% after 1 day, 16-21% after 3 days, 13-18% after 7 days, 13-15% after 28 days, 14-16% after 56 days and 13-16% after 90 days higher than that of sample PM15-1.0. Compared with the cement-based concrete the pH level of magnesium phosphate concrete was much lower due to its acid-based environment. The most likely reason is that the cement-based concrete has a higher alkalinity due to the chemical reactivity of alkaline components and the formation of calcium hydroxide. The highest and lowest pH levels of 9.9 and 8.6 were observed in samples PM16-1.0 and PM13-1.0. The EPLA beads were stable in the acid-based environment of magnesium phosphate concrete with no degradation (Figure 7. 3).



(a)



(b)
 Figure 7. 3 Effect of alkaline-based and acid based environment on degradation of EPLA beads, (a) cement based concrete, (b) magnesium phosphate concrete

7.3.4 Thermal conductivity

Table 7. 3 reveals the variation in thermal conductivity of magnesium phosphate cement with a variation in P/M ratio, w/c ratio and borax content. The increase in concrete porosity using lightweight aggregate and an air entraining agent is the common method to decrease the thermal conductivity value of concrete [5]. The researchers found that the thermal conductivity of concrete is influenced by concrete density, moisture content, air content, concrete temperature and mineralogical characteristics of lightweight aggregate. The thermal conductivity of magnesium phosphate concrete ranged from 0.096 to 0.116 W/mK.

Referring to previous studies, a thermal conductivity of 0.206 W/mK and 0.06 W/mK were obtained by inclusion of EPS aggregate and the combination of foam and EPS by Bouvard [95] and Chen [102], respectively. Also, the thermal conductivity of magnesium phosphate concrete is about 32 times lower than that of normal concrete with a relative thermal conductivity of 3.5 W/mK for normal concrete containing quartzite aggregate. It can be found that an increase in Borax content results in a slightly higher thermal conductivity in the sample with a P/M ratio of 1/5 and 1/6 and lower thermal values in sample PM13-1.0. The thermal conductivity values of PM16-1.0, PM15-1.0 and PM13-1.0 were 0.110, 0.105 and 0.105 W/m.K, In addition, the thermal conductivity of magnesium phosphate concrete was about 35% higher than that of the EPLA concrete

(PP4). The reason is the alkaline reactivity of EPLA and the increase in concrete porosity as a result of an increase in CO₂ concentration.

Table 7. 3 The comparison between thermal conductivity of magnesium phosphate concrete and EPLA concrete.

Specimen	Density (kg/m ³)	Thermal conductivity (W/m. K)		
		Experimental results	Proposed model	ACI model
EPLA Concrete (PP4)	302.2	0.071	0.070	0.125
PM16-1.0-05	417.9	0.105	0.105	0.145
PM16-1.0-10	443.7	0.116	0.114	0.149
PM15-1.0-05	397.3	0.096	0.098	0.141
PM15-1.0-10	412.2	0.114	0.103	0.144
PM13-1.0-05	412.0	0.110	0.103	0.144
PM13-1.0-10	417.6	0.101	0.105	0.145

Several researchers concluded that there is a direct relationship between concrete density and thermal conductivity values [38]. In the case of ultra-lightweight concrete, the factors such as aggregate volume and lightweight aggregate density significantly affect the thermal properties of concrete. The ACI Committee [78] has proposed an equation to estimate the thermal conductivity of lightweight concrete (Eq. 7.1). However, the proposed equation relies on the density of concrete without concerning the other effective factors. To estimate the thermal conductivity of the proposed concrete, equation Eq. 7.2 with five variables of concrete density, perlite density, EPLA density, perlite ratio and EPLA ratio was developed and its results compared with the proposed equation by ACI and experimental results. The newly developed equation provides a better fit with experimental data than the ACI equation as can be seen from Table 7.3.

$$\lambda = 0.086e^{0.00125\gamma} \quad [7.1]$$

$$\lambda = \left(\frac{\sqrt{\gamma_{\text{concrete}}}}{(\gamma_{\text{Perlite}} \cdot R_{\text{Perlite}}) + (\gamma_{\text{EPLA}} \cdot R_{\text{EPLA}})} \right)^{K + \frac{0.5 R_{\text{EPLA}}}{R_{\text{Perlite}}}} \quad [7.2]$$

$K = 1.9$ (for Perlite concrete)

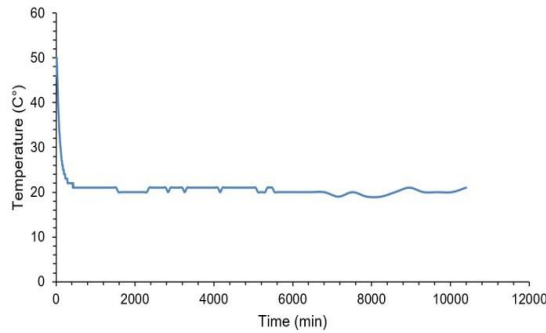
Where, γ_{Concrete} is the concrete density (kg/m^3); R_{perlite} is the ratio of perlite; R_{EPLA} is the ratio of EPLA. K is a constant value of 1.9.

7.3.5 Exothermic reaction

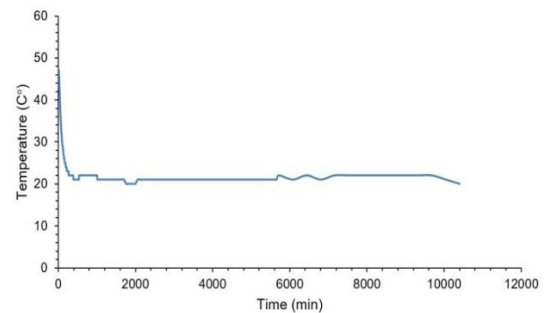
The effect of P/M ratio and retarder content on the exothermic reaction of magnesium phosphate concrete containing EPLA are displayed in Table 7. 4 and Figure 7. 4. The experimental results show that the sample PM13-1.0-05 with a P/M ratio and retarder content of 1/3 and 5% (binder weight) exhibited the highest exothermic reaction intensity, while the sample PM15-1.0-10 showed the lowest exothermic reaction intensity. It was found that an increase in phosphate content leads to a significant increase in the peak temperature and setting time. The application of retarder materials causes an extension of the peak time temperature and consequently lower concrete temperature. The peak temperature of sample PM13-1.0-05 and PM13-1.0-10 was 50 °C and 47 °C, which occurred after 10 and 15min of mixing time, respectively. The effectiveness of retarder materials on controlling the fast hardening of magnesium phosphate concrete was more significant in a sample containing higher magnesium content (1/5). In consideration of all samples, the retarder content and P/M ratio plays a significant role in the exothermic reaction intensity and setting time of concrete. The decrease in P/M ratio slowed down the heat development of magnesium phosphate concrete, and its exothermic peak decreased with the addition of more retarder materials. The reaction and hardening process of magnesium phosphate concrete can be summarized as (1) dissolution of magnesium oxide and phosphate, (2) exothermic reaction between magnesium oxide and phosphate ion leading to an increase in matrix temperature, and (3) formation of gel and condensation into MPC [214].

Table 7. 4 The peak temperature of magnesium phosphate concrete.

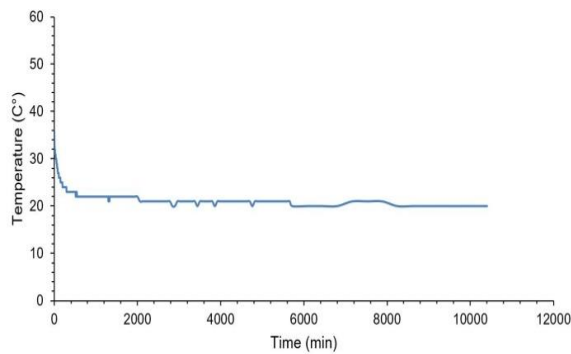
	Peak temperature (C°)	Time at peak temperature (min)
PM 13-1.0-05	50	10
PM13-1.0-10	47	15
PM15-1.0-05	33	5
PM15-1.0-10	29	20



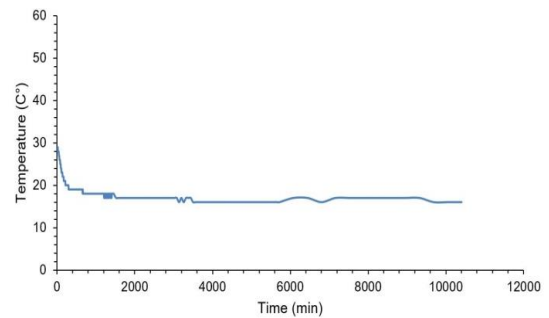
(a)



(b)



(c)



(d)

Figure 7. 4 Exothermic reaction of magnesium phosphate concrete, (a) PM13-1.0-05, (b) PM13-1.0-10, (c) PM15-1.0-05, (d) PM15-1.0-10.

7.3.6 Electrical resistivity

The setting time of magnesium phosphate concrete is measured by the electrical resistivity response. Several researchers concluded that factors such as connectivity of pores, porosity and conductivity of pore solution, moisture content and temperature affect the electrical resistivity of a matrix. The electrical resistivity is a function of ion

concentration and the mobility of the ions in the pore solution. The changes in electrical resistivity of concrete are also related to microstructural changes [205].

The electrical resistivity response of magnesium phosphate concrete was completely different from normal concrete. As shown in Figure 7. 5, a sudden increment in electrical resistivity at the initial stage of curing reflects the immediate changes in the microstructure of magnesium phosphate concrete. It was found that an increase in concrete temperature leads to a decrease in electrical resistivity of concrete due to the increase in ionic movements. In fact, the more ionic movement the higher the electrical conductivity and the lower the resistivity values will be. However, in the case of magnesium phosphate concrete the immediate exothermic reaction and fast changes in the microstructure of concrete result in a sudden increase in electrical resistivity. There is a direct relationship between exothermic reaction and electrical resistivity as a higher electrical resistivity was observed in the sample with higher internal matrix temperature. The highest electrical resistivity occurred in the samples PM13-1.0-10 and PM13-1.0-05 with resistivity of 418.40 and 406.74 ohm.cm, respectively. It was found that the addition of a larger amount of Borax as retarder results in a slight decrease in matrix temperature but increases the resistivity of concrete.

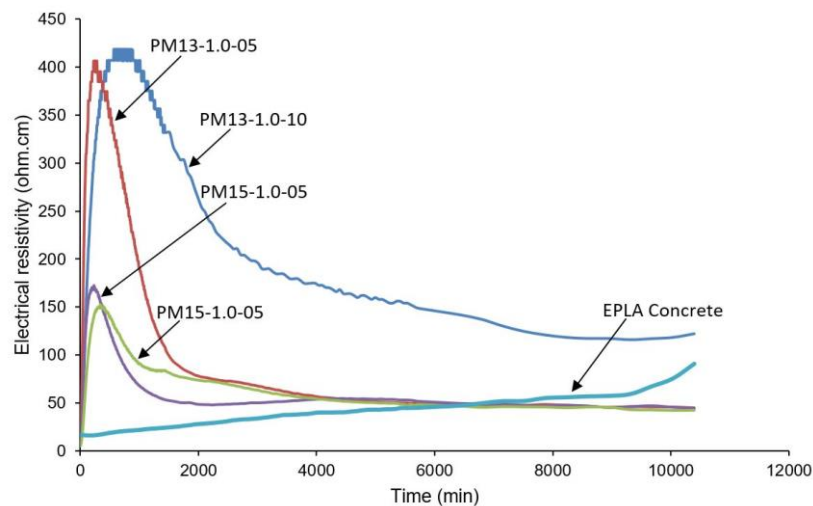


Figure 7. 5 The electrical resistivity response of magnesium phosphate concrete and EPLA concrete.

The electrical resistivity response shows that the maximum resistivity of 152.19 and 172.15 ohm.cm for samples PM15-1.0-10 and PM15-1.0-05 after 345 min (5 hours and 45 min) and 235 min (3 hours and 55 min), respectively. The results demonstrate that the influence of P/M ratio on setting time of magnesium phosphate concrete was minimal and

the setting time mostly depends on the retarder content. All the samples experienced a sudden decrease in electrical resistivity due to the shifting to the hardening stage and formation of hydration products such as magnesium phosphate hydrate. An increase in Borax content from 5% to 10% causes a significant delay of six and two hours in setting time of the samples PM13-1.0 and PM15-1.0. It was found that the effectiveness of the retarder was more significant in samples containing larger amounts of phosphate.

Compared with EPLA concrete as a cement-based concrete, the electrical resistivity of magnesium phosphate concrete at the initial stage of curing of up to 12 hours was much higher. The changes in electrical resistivity are mainly related to the fast hydration reaction of magnesium phosphate concrete. However, a larger electrical resistivity was observed in EPLA concrete after 6438 min (107 hours and 18 min) which reveals the changes in the microstructure of EPLA concrete, the formation of hydration products and the increase in concrete porosity. In the case of EPLA concrete, the alkaline reactivity of EPLA changes the microstructure of concrete and the porous structure of the matrix leading to a significant delay in setting time. Calcium sulphate is an important component of cement that controls the setting characteristics and accelerates hydration of calcium silicate. The changes in sulphate content and sulphate consumption by sodium lactate affect the hardening process and cause concrete deterioration and a delay in the setting time of EPLA concrete. The summary of the electrical resistivity response of magnesium phosphate concrete is presented in Table 7. 5.

Table 7. 5 The initial and final setting time of proposed concretes based on electrical resistivity response.

	Peak electrical resistivity (ohm.cm)	Setting time (min)
PM13-1.0-10	418.40	570
PM13-1.0-05	406.74	230
PM15-1.0-10	152.19	345
PM15-1.0-05	172.15	235

7.3.7 Fire resistance

Cone calorimeter tests were performed to assess the fire reaction of magnesium phosphate cement as per ASTM E1354 [183]. The results of magnesium phosphate concrete containing EPLA are compared with cement-based concrete containing EPLA and EPS aggregate. The concrete containing EPS aggregate is used as a reference for EPLA samples. The parameters such as heat release rate (HRR), total heat released (THR), carbon monoxide production (COP), carbon dioxide production (CO₂P), mass reduction and failure modes during fire test were evaluated and assessed.

Figure 7. 6 shows the samples before and after fire tests. The magnesium phosphate concrete prepared with expanded perlite and EPLA aggregate lost its strength with an explosive spalling and visible cracks. The reason for the severe matrix degradation is the high water absorption of perlite sucking up the free water in the magnesium phosphate paste and chemically bonding water of hydrated products. This causes a significant reduction in strength development of concrete and eliminates the formation of hydration products at the initial stage of hardening. In fact, the heat can be dissipated with the bonded free water and can significantly improve the fire resisting capacity. In the case of EPLA and EPS concrete, some minor thermal cracks were observed, and the sample integrity maintained after tests in both samples. In addition, slight changes in surface colouring occurred in all samples. The reasons are physical and chemical changes in matrix microstructure and the burning of polymer aggregates.

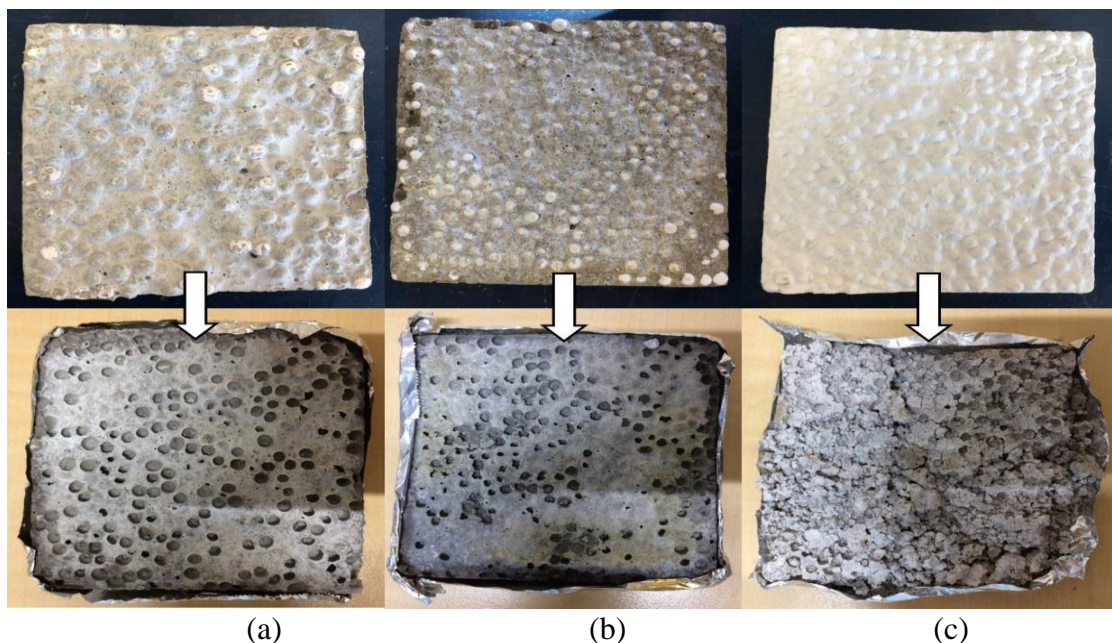
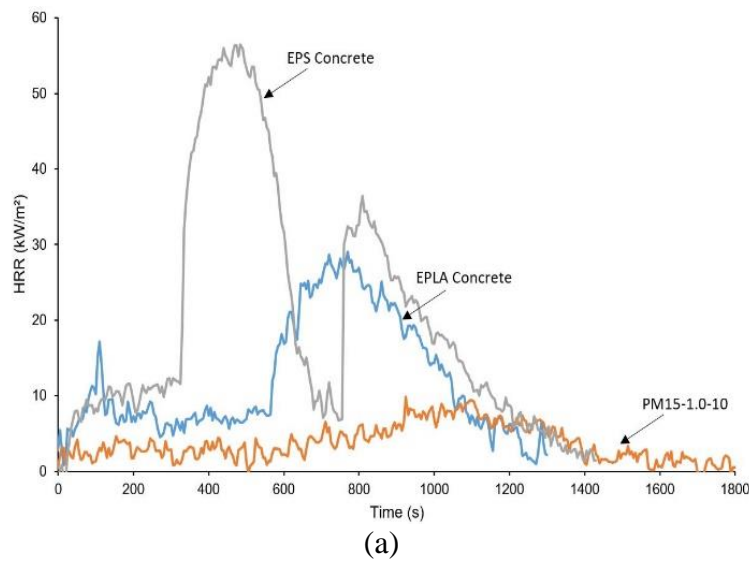
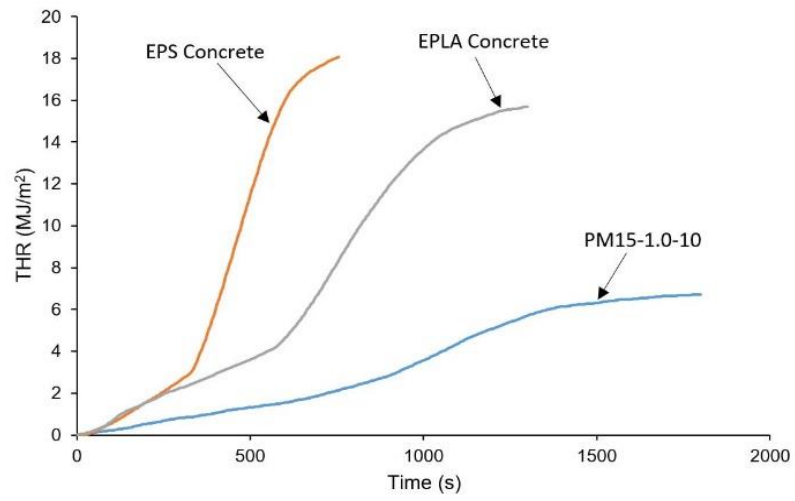


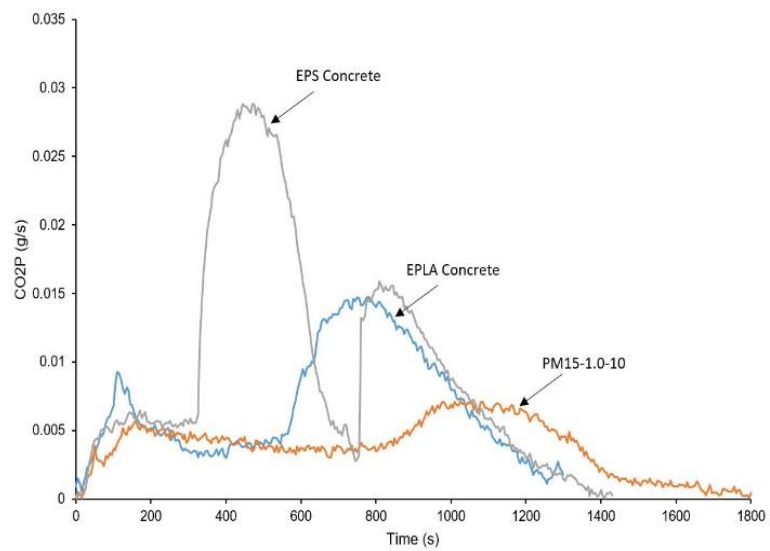
Figure 7. 6 Fire tests of concrete; (a) EPS concrete, (b) EPLA concrete, (c) Magnesium phosphate concrete

The experimental results show that the magnesium phosphate concrete can be graded as non-combustible (below 200 kW/m² and 8 MJ/m²) with a HRR and THR of 9.87 kW/m² and 6.73 MJ/m² which is much lower than that of EPS and EPLA concrete (Figure 7. 7a and Figure 7. 7b). The heat release rate of EPLA and EPS concrete was lower than 200 kW/m² but the total heat released of both samples exceeded the limit of 8MJ/m² and they are therefore graded as quasi-non-combustible. The total heat released of EPS and EPLA concrete were 15.70 and 18.10 MJ/m², which is twice the standard limit. With identical polymer aggregate and compared with EPLA concrete, an increase in HRR and THR was observed as cement-based concrete was replaced with magnesium-based cement concrete. In addition, no ignition point was recorded for samples containing magnesium phosphate concrete and it did not contribute to the fire development due to excellent fire resistance properties of magnesium-based cement. By contrast, the EPLA and EPS concrete ignite after 555 and 322s after the start of the fire test and flame out after 1162 and 645s. As shown in Figure 7. 7a and Figure 7. 7b, the addition of EPLA caused a delay in the ignition point but extended the flameout point.

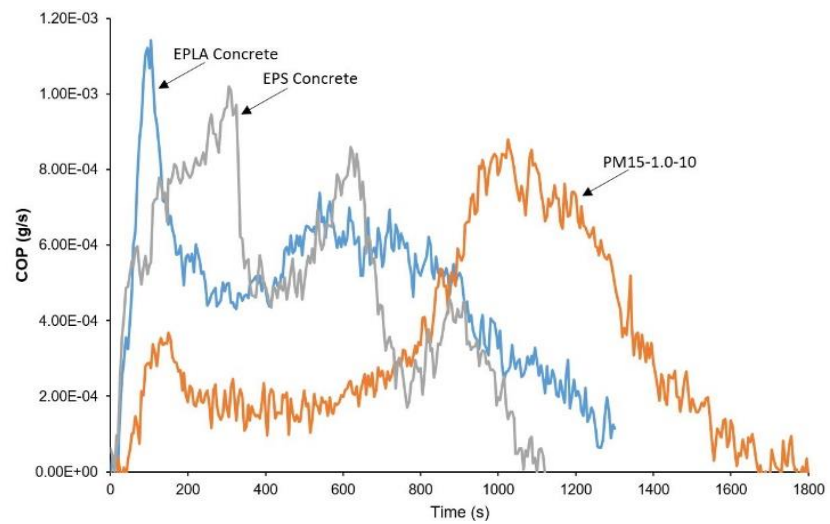




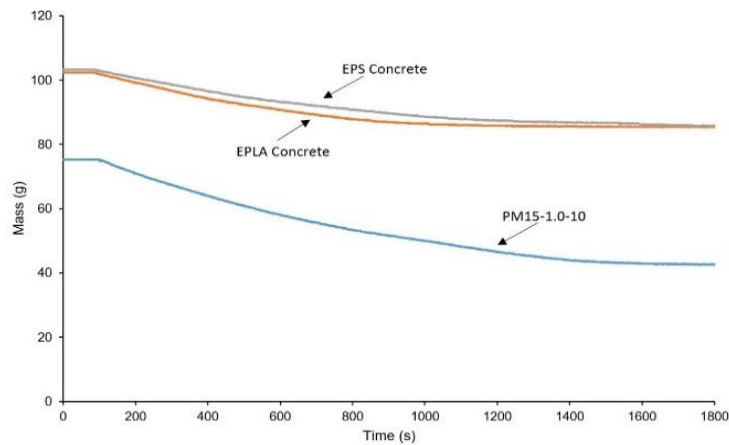
(b)



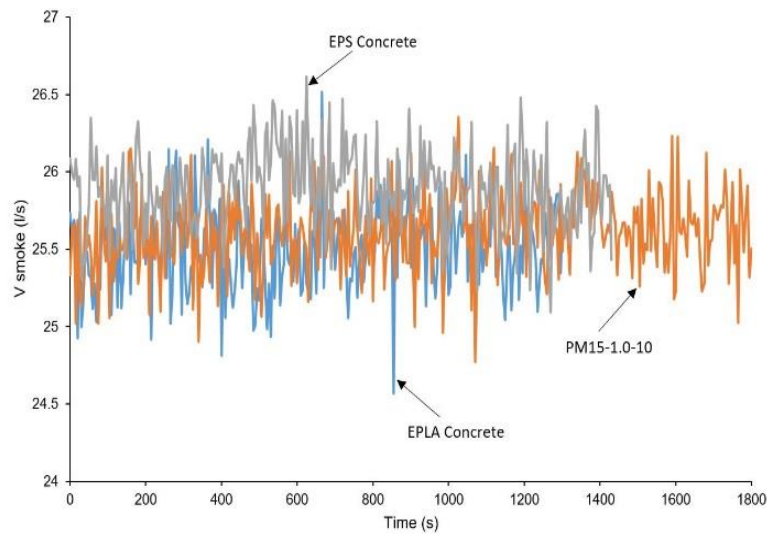
(c)



(d)



(e)



(f)

Figure 7. 7 The cone calorimeter test results, (a) heat release rate (HRR), (b) total heat released (HTR), (c) carbone monoxide production (COP), (d) carbone dioxide production (CO2P), (e) mass reduction, (f) smoke volume.

Figure 7. 7c shows the carbon dioxide production (CO2P) of the proposed concrete during the fire test. No sharp point is visible in the sample containing magnesium phosphate, and the level of CO₂ gas production has remained low and almost constant throughout the test. A sharp increase in CO₂ gas production was observed in the sample containing EPS aggregate after the ignition. The sudden increase in CO₂ gas production is mainly related to the combustion process of EPS aggregate, which generates a considerable amount of CO₂ gas. In the case of EPLA concrete, the amount of CO₂ gas production was about 49% lower than that of EPS concrete and 41% higher than that of magnesium phosphate concrete. It was found the sample containing EPLA aggregate generates less CO₂ gas and significantly delays the ignition point.

The concentration levels of carbon monoxide (CO) are presented in Figure 7. 7d. The CO gas production of magnesium phosphate concrete was slightly lower than that of EPLA and EPS concrete. The highest and fastest growth in CO gas production were observed in EPLA concrete. In fact, the CO is a volatile and flammable gas, which is associated with retaining the flame over the surface of samples. It was found that the difference between the ignition and flash point of EPLA concrete was greater than that of EPS concrete due to the production of larger amounts of CO gas. Compared with EPLA and EPS concrete, there was a delay of 1025s until the CO gas production reached its highest amount for magnesium phosphate concrete. In addition, there was a certain fluctuation in CO production, which causes a decrease in CO₂ gas production mainly due to the incomplete combustion.

Figure 7. 7e displays the mass reduction of the proposed concretes during the test. The rate of mass reduction was higher in magnesium phosphate concrete compared with EPLA and EPS concrete. The rate of mass reduction during the fire test was about 44%, 16% and 17% for magnesium phosphate concrete, EPLA concrete and EPS concrete, respectively. In the case of the smoke volume production (Figure 7. 7f), the EPS concrete produced slightly more smoke compared to other samples due to the combustion of the petroleum polymer. The summary of the cone calorimeter test results are presented in Table 7. 6.

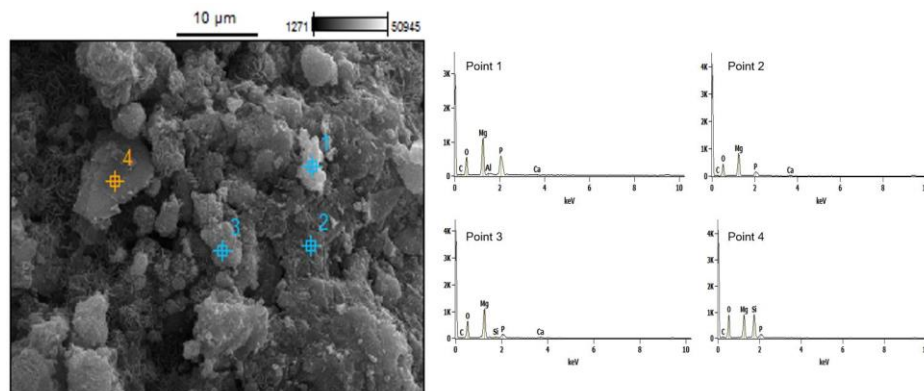
Table 7. 6 The summary of cone calorimeter test results of magnesium phosphate, EPLA and EPS concrete.

Specimen	HRR		THR		COP		CO ₂ P	
	Peak HRR (KW/m ²)	Time (s)	THR (MJ/m ²)	Time (s)	Peak COP (g/s)	Time (s)	Peak CO ₂ P (g/s)	Time (s)
PM15-1.0-10	9.87	925	6.73	1800	0.000878	1025	0.00715	1025
EPLA Concrete (PP4)	29.04	770	15.70	1300	0.001140	105	0.01478	780
EPS Concrete (PE4)	56.48	485	18.10	755	0.001020	305	0.02880	445

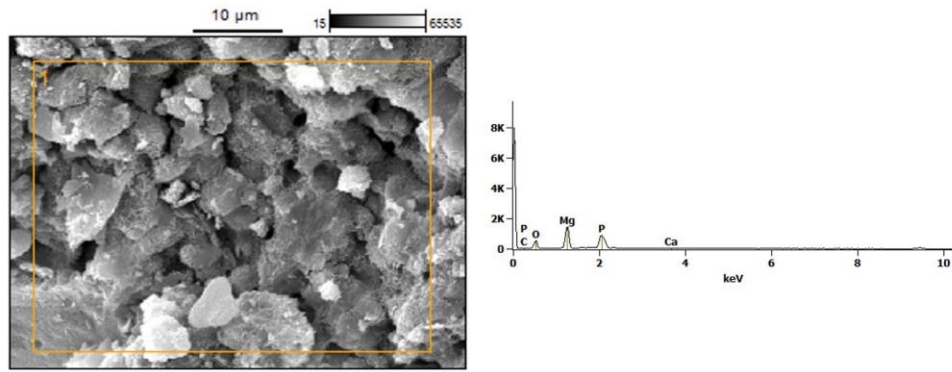
7.3.8 Phase analysis

The strength development and microstructural changes of magnesium phosphate concrete cured in air were assessed by X-ray diffraction (XRD), scanning electron microscopy (SEM) and energy-dispersive X-ray spectroscopy (EDS) at the ages of 1 day, 3 days, 28 days and 90 days. The samples PM15-1.0-5 and PM15-1.0-10 are used to investigate the influence of a retarder on strength development and hydration products.

Figure 7. 8 presents the EDS analysis of samples PM15-1.0-05 and PM15-1.0-10 after 1 day. The atomic concentration at selected zones is presented in Table 7. 7. It can be found that the major detected elements of sample PM15-1.0-5 were O, Mg, P, Al, Si, Ca, P and C which indicated the formation and existence of magnesium phosphate hydrate ($Mg_2(P_2O_7) \cdot (H_2O)_6$), silica (SiO_2) and magnesia (MgO). The remaining elements Al and Ca indicate the presence of aluminate phosphate ($AlPO_4$) [37, 38] and unhydrated calcium oxide. Wang et al. [39] found that the dissolution of alumina in phosphate solution forms $AlPO_4 \cdot H_2O$ which reacts with the remaining alumina to form $AlPO_4$. In the sample PM15-1.0-10 with a higher retarder percentage of 10% the major elements are Mg, P, C and O in the presence of magnesium phosphate hydrate ($Mg_2(P_2O_7) \cdot (H_2O)_6$) and magnesia (MgO). The XRD results of the samples PM15-1.0-05 and PM15-1.0-10 show significant changes in magnesium phosphate hydrate content with an increase in retarder content. The magnesium phosphate hydrate contents of the sample with 5% Borax was higher than that of sample containing 10% Borax. This trend causes a reduction in the amount of un-hydrated magnesia. It can be found that the addition of Borax influences the production of less magnesium phosphate hydrate.



(a)



(b)

Figure 7. 8 The EDS analysis of magnesium phosphate concrete after 1 day, (a) PM15-1.0-5, (b) PM15-1.0-10.

Table 7. 7 The summary of EDS analysis of magnesium phosphate concrete after 1 day.

	Atom %						
	C	O	Mg	Si	Al	P	Ca
Point 1	6.70	41.43	32.75	-	0.49	18.05	0.58
Point 2	6.84	51.06	35.17	-	-	6.46	0.48
Point 3	4.38	54.19	35.02	0.94	-	4.16	1.31
Point 4	3.61	55.31	19.13	19.34	-	2.61	-
Zone 1	5.47	35.01	36.31	-	-	22.68	0.53

Figure 7. 9 presents the XRD results of PM15-1.0-05 and PM15-1.0-10 after 1 day. As shown in the figure, the sharp peak intensity mostly represents the magnesium phosphate hydrate as the main hydration product of magnesium phosphate concrete. It also can be found that some silica and magnesia remains in the magnesium phosphate concrete matrix [182]. The rapid reaction of magnesia causes the hydration products to cover the surface of magnesia and restrict its further reaction. The diffraction peak intensity of magnesium phosphate hydrate and magnesia decreased with the addition of a larger amount of Borax.

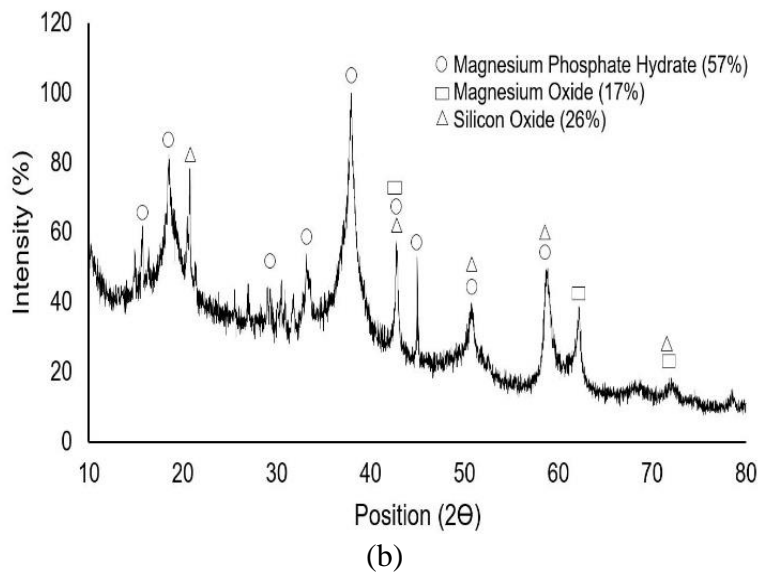
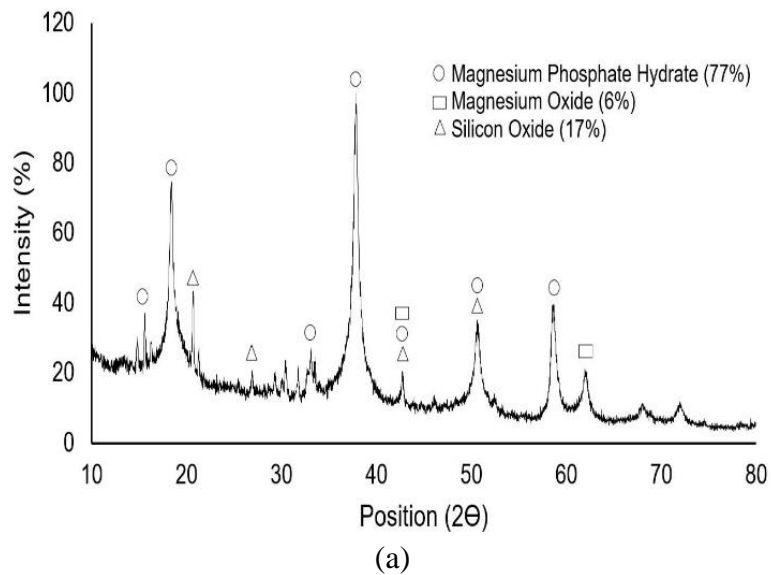
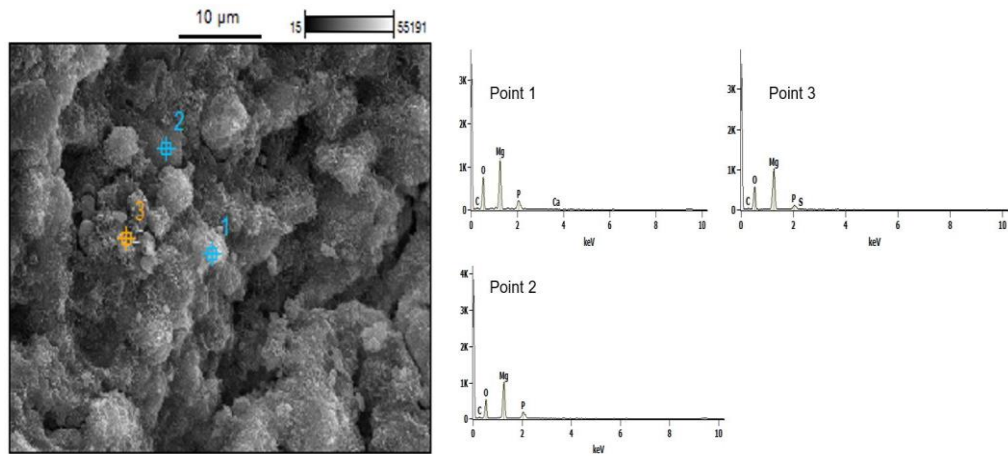
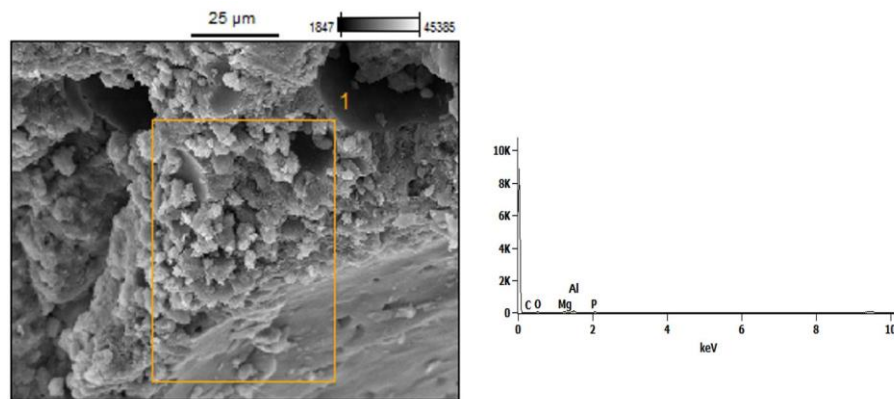


Figure 7. 9 The XRD spectra of magnesium phosphate concrete after 1 day of curing, (a) PM15-1.0-5, (b) PM15-1.0-10.

Figure 7. 10 presents the EDS analysis of samples PM15-1.0-05 and PM15-1.0-10 after 3 days of curing. The elemental statistics of the selected zones are presented in Table 7. 8. The elements detected in different zones of the paste are mostly O, Mg, P, Al and Ca which form magnesium phosphate hydrate ($Mg_2(P_2O_7) \cdot (H_2O)_6$) and unreacted magnesia (MgO). The semi-quantitative chemical analysis of samples PM15-1.0-05 and PM15-1.0-10 indicates the changes of hydrated products with a variation in retarder amount. The contents of magnesium phosphate hydrate were higher in the sample PM15-1.0-05 (90%) compared to PM15-1.0-10 (83%).



(a)



(b)

Figure 7. 10 EDS results of magnesium phosphate concrete after 3 days of curing (a) PM15-1.0-05, (b) PM15-1.0-10.

Table 7. 8 The summary of EDS analysis of magnesium phosphate concrete after 3 days.

	Atom (%)					
	C	O	Mg	P	Ca	Al
Point 1	6.51	56.07	31.25	5.80	0.37	-
Point 2	5.65	51.27	36.45	6.63	-	-
Point 3	3.89	55.31	36.99	3.81	-	-
Zone 1	23.63	29.61	12.09	9.45	-	25.22

The XRD patterns of magnesium phosphate concrete with a variation in Borax content after 3 days are presented in Figure 7. 11. The dominant crystalline hydration product of magnesium phosphate concrete was magnesium phosphate hydrate

($\text{Mg}_2(\text{P}_2\text{O}_7) \cdot (\text{H}_2\text{O})_6$). Unreacted magnesia was also detected as a second main element of the magnesium phosphate paste.

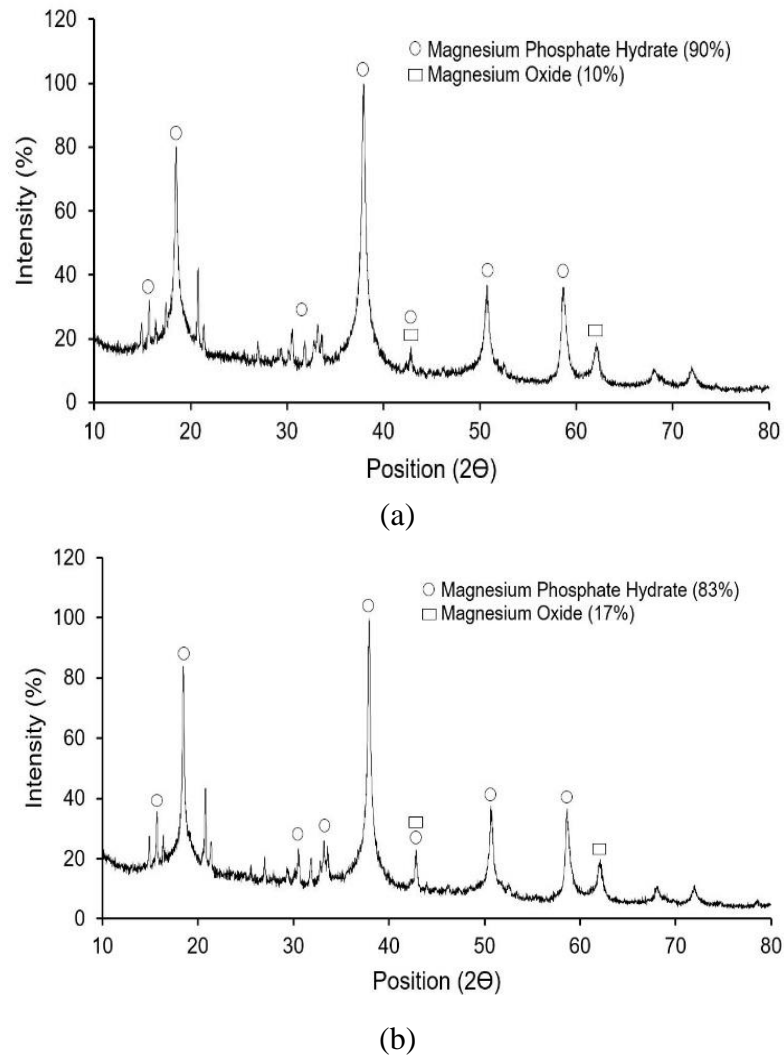
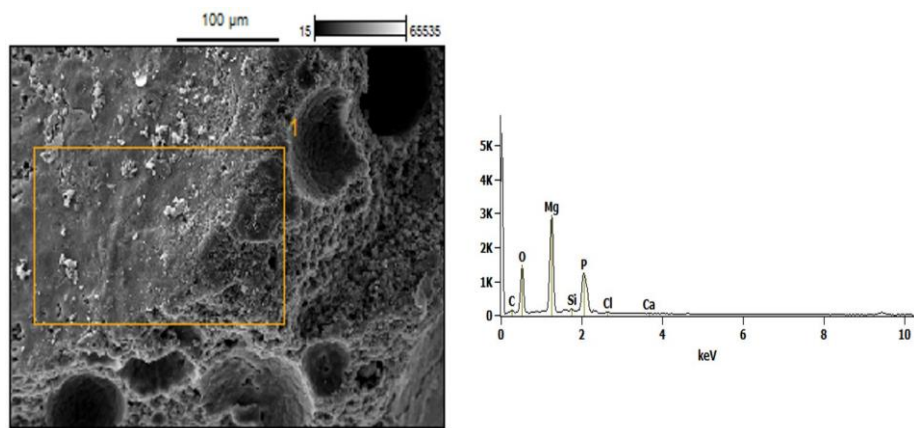


Figure 7. 11 The XRD spectra of magnesium phosphate concrete after 3 days of curing, (a) PM15-1.0-5, (b) PM15-1.0-10.

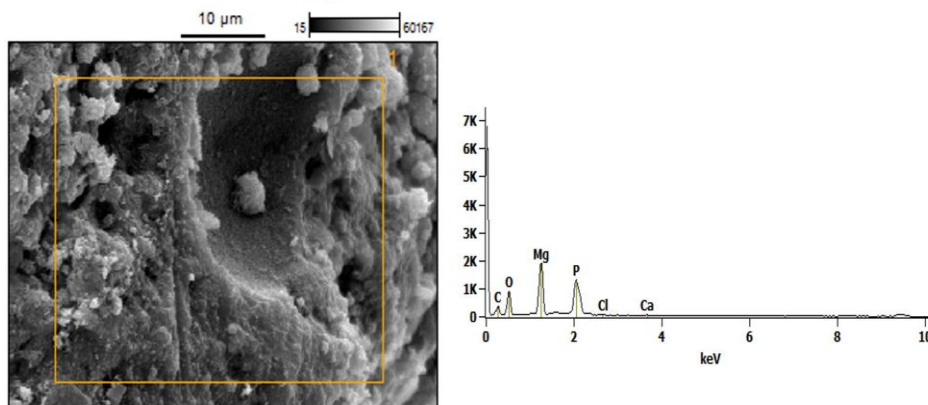
Figure 7. 12 shows the EDS analysis of sample PM15-1.0-05 after 28 days and 90 days. The elemental statistics of the selected zones are presented in

Table 7. 9. The predominantly detected elements were C, O, Mg, Si, P, Cl and Ca, which indicates that the main hydration products of the sample were magnesium phosphate hydrate and silicon oxide and unreacted magnesium oxide. In addition, calcium hydroxide is unable to exist in the low alkaline environment of magnesium phosphate concrete. However, the diffraction peak of crystalline calcium chloride was detected as a

possible neutralization product of calcium hydroxide. The existence of calcium chloride causes a volume expansion of the magnesium phosphate paste, which affects the strength development of the concrete. The experimental results show that the compressive strength of magnesium phosphate concrete decreased after 28 days, which can be directly related to the formation of calcium chloride. Figure 7. 13 shows the XRD spectra of sample PM15-1.0-05 at the age of 28 days and 90 days. The magnesium phosphate hydrate and calcium chloride hydrate were the main hydration products of magnesium phosphate concrete along with some unreacted magnesium and silicon oxide [182].



(a)

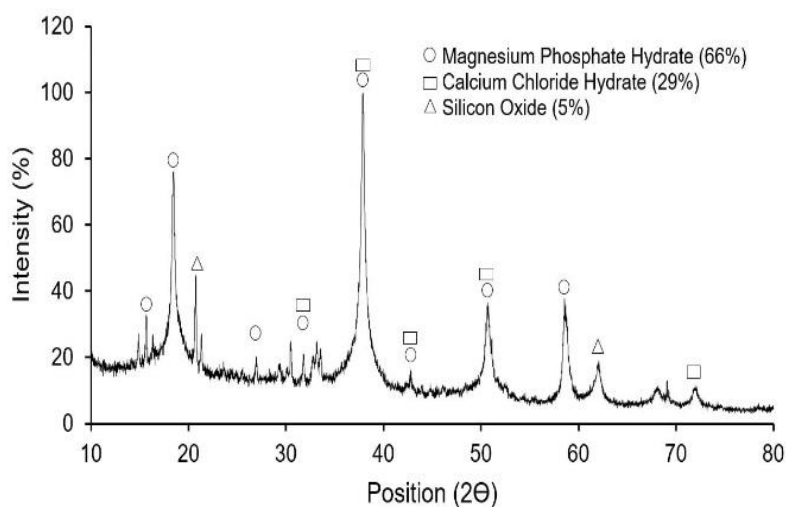


(b)

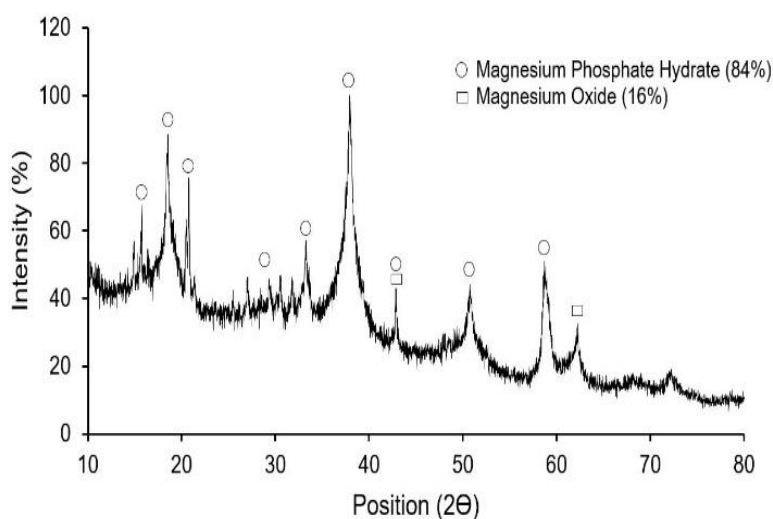
Figure 7. 12 The EDS results of PM15-1.0-05 at the age of, (a) 28 days, (b) 90 days.

Table 7. 9 The summary of EDS analysis of samples PM-1.0-05 and PM15-1.0-10 after 28 days and 90 days.

	Curing age (day)		Atom (%)						
			C	O	Mg	Si	P	Cl	Ca
PM15-1.0-05	28	Zone 1	8.51	40.88	33.32	1.03	15.01	0.95	0.29
	90	Zone 1	27.52	30.77	24.50	-	16.54	0.36	0.32



(a)



(b)

Figure 7. 13 The XRD spectra of sample PM15-1.0-05 after, (a) 28 days, (b) 90 days.

7.4 Conclusions

Novel ultra-lightweight concretes are prepared with expanded poly-lactic acid (EPLA), expanded perlite (EP) and magnesium phosphate cement. The mechanical properties of the proposed concretes are assessed after 1 hour, 3 hours, 1 day, 3 days, 7 days, 28 days, 56 days and 90 days. In addition, the thermal conductivity, fire resistance, pH level, exothermic reaction, electrical resistivity, setting time and phase analysis are evaluated at certain stages of curing. The influence of the phosphate-magnesium (P/M) ratio, water-cement (w/c) ratio and retarder content are also investigated. Based on these evaluations, observations and obtained results, the following conclusions are drawn:

1- The magnesium phosphate cement with its acid-based reaction is a proper binder for EPLA aggregate as no alkaline reactivity and degradation were observed during the curing stages.

2- A density range of 367.0 kg/m^3 to 467.7 kg/m^3 was obtained with a fixed EP and EPLA ratio. The w/c and P/M ratio influence the density of concrete as the increase in w/c ratio causes a decrease in density while an increase in Borax content and P/M ratio shows an inverse effect on density.

3- A rapid hardening and high early strength were observed in magnesium phosphate concrete, but this trend starts to decrease after 7 days. The 28 days, 56 days and 90 days compressive strength of magnesium phosphate concrete was about 88%, 77% and 70% of the 7 days compressive strength. The compressive strength of the proposed concrete depends mostly on the w/c ratio and retarder content. The strength of magnesium phosphate concrete increased with a decreasing water-cement ratio while increasing the amount of retarder and magnesium oxide causes an improvement in strength development.

4- The thermal conductivity of magnesium phosphate concrete is a factor of the Borax content and P/M ratio as an increase in Borax content causes an increase in thermal conductivity value in a sample containing a higher amount of magnesia. This trend was inverse in a sample containing a lower amount of magnesia.

5- The exothermic reaction of magnesium phosphate concrete mainly depends on the phosphate content as a higher internal temperature was observed in the sample with a P/M

ratio of 1/3. The influence of the Borax content on the exothermic reaction was almost minimal.

6- A higher electrical resistivity was observed in samples containing a higher amount of phosphate. Moreover, the addition of a larger amount of Borax causes a slight decrease in electrical resistivity and setting time.

7- The magnesium phosphate concrete lost its strength with explosive spalling and visible thermal cracks when subjected to a high temperature. The heat release rate, total heat released, carbon monoxide production and carbon dioxide production were much lower than that of EPS and EPLA concrete. In addition, magnesium phosphate concrete does not contribute to a fire.

8- Magnesium phosphate hydrate was found as the main hydration product of magnesium phosphate concrete. The existence of Cl and Ca elements causes the formation of calcium chloride after 7 days, which leads to a significant reduction in concrete strength due to its expansion.

CHAPTER 8

PERLITE CONCRETE CONTAINING CEPLA

8.1 Introduction

This chapter presents the experimental results of coated EPLA (CEPLA) as a solution for using EPLA aggregate in the high alkaline environment of cement. Coating is a common technique to improve the characteristics of a specific material. It was found in previous chapter that the EPLA beads are sensitive to the alkaline environment of cement and GGBS, which cause significant changes to the mineralogical characteristics of concrete. The degradation of EPLA causes concrete carbonation and significant changes in hydration products of concrete. This approach deals with the composition and method for the production of a lightweight concrete whereby EPLA beads are coated with lime lock paint and a layer of ultrafine expanded perlite along with a layer of anti-carbonate paint to eliminate the reaction of EPLA with alkaline components of cement and to limit the formation of calcium carbonate at the coating layer. The strength of the coating layer leads to greater stiffness of the aggregate and to a better overall matrix-aggregate bond characteristic compared with hydrophobic materials such as EPS and EPLA.

8.2 Experimental procedure

8.2.1 Materials

The specifications of the materials are explained and provided in Chapter 3.

8.2.2 CEPLA preparation

The EPLA beads are coated with an anti-carbonate paint, ultrafine expanded perlite and lime lock paint. The coating process starts with lime lock paint to eliminate the chemical reactivity of EPLA with calcium hydroxide followed by a layer of ultrafine perlite as a finishing layer of the first stage. The beads are dried and kept in ambient environment for two days. For the second stage of coating, the beads are covered by an anti-carbonate

paint to eliminate the carbonation process of concrete due to the alkaline reactivity of EPLA followed by a layer of ultrafine perlite as finishing layer of the second stage. In order to compact the layers, the beads are placed in a rotary mixer and mixed for 30 min. The second layer of coating is dried for 7 days before using the coated beads as aggregate in concrete (Figure 8. 1).



Figure 8. 1 The preparation of CEPLA aggregate, a) non-coated EPLA, b) coated EPLA

8.2.3 Mix proportions

The mix proportions of the CEPLA concrete are presented in Table 8. 1. In total four types of lightweight concrete mixes with a variation of CEPLA ratios were prepared with a fixed effective water-cement ratio and cement content of 0.343 and 301 kg/m³. The cement content and water-cement ratio were obtained based on Eq. 3.4 and Eq. 3.6. The expanded perlite and CEPLA aggregate were mixed at the ratio of 100:0, 60:40, 40:60 and 30:70 of aggregate volume percentages. The mix design was targeted for a density of 488 kg/m³ for samples with 100% perlite (P1).

Table 8. 1 The mix proportions of CEPLA concrete.

Mix No.	Mix proportion					
	Effective w/c ratio	Cement (kg/m ³)	Water (kg/m ³)	EP (kg/m ³)	CEPLA (kg/m ³)	AEA (kg/m ³)
P1 (100P)	0.343	301	289	135.0	0	0.0041
PC2 (60P40CEPLA)	0.343	301	276	81.0	85.2	0.0041
PC3 (40P60CEPLA)	0.343	301	265	54.0	127.8	0.0041
PC4 (30P70CEPLA)	0.343	301	232	40.5	149.1	0.0041

8.2.4 Experimental procedure

Two types of curing regimes, namely moist curing and air curing were chosen to assess the effect of the curing conditions on mechanical properties of the CEPLA concrete. In the case of moist curing, the specimens were kept in water of 20 °C for the whole curing period, while air cured samples were kept in a laboratory environment for 28 days after demoulding. The properties density, compressive strength, thermal conductivity, electrical resistivity, setting time and fire resistance have been tested. It worth to note that the average results of three specimens were considered to evaluate the engineering properties of proposed concrete. The descriptions of the test methods are provided in Chapter 3.

8.3 Experimental results

8.3.1 Density and compressive strength

The air-dried densities of perlite concrete containing CEPLA, EPLA and EPS are given in Table 8. 2. The dry density of CEPLA concrete varied from 431.62 to 512.23 kg/m³. From the previous chapters, it was found that the density of EPLA and EPS concrete was decreased as the volume of EPLA and EPS increased. This trend of reduction was expected due to the lower specific gravity of EPLA and EPS compared to expanded perlite aggregate. However, in the case of CEPLA concrete, the same trend of reduction was observed in the sample containing 40% CEPLA but a further increase in CEPLA

volume results in a higher density due to the higher specific gravity of CEPLA (213kg/m^3) than that of perlite aggregate (135kg/m^3).

Table 8. 2 Density of perlite concrete and perlite concrete containing EPLA, EPS and CEPLA.

Mix No.	Density (kg/m^3)			
	Sample 1	Sample 2	Sample 3	Average Density
P1 (100P)	500.74	492.89	485.37	493.00
PC2 (60P40CEPLA)	430.44	427.57	436.86	431.62
PP2 (60P40 EPLA)	384.00	401.88	414.73	400.20
PE2 (60P40EPS)	397.17	425.10	424.23	415.50
PC3 (40P60CEPLA)	464.15	488.07	464.10	472.10
PP3 (40P60 EPLA)	353.15	360.55	366.92	360.20
PE3 (40P60EPS)	358.26	387.95	368.32	371.51
PC4 (30P70CEPLA)	492.19	520.19	524.33	512.23
PP4 (30P70EPLA)	305.83	304.94	295.9	302.22
PE4 (30P70EPS)	311.37	312.53	314.12	312.67

The compressive strengths of the proposed concretes cured in a moist and dry condition are presented in

Table 8. 3. The 28-day compressive strength of air cured CEPLA concrete varied from 3.45 MPa to 2.23 MPa, which is much higher than that of EPLA and EPS concrete with the same mix proportion. A comparison between the strength development of EPLA as non-coated aggregate and CEPLA as coated aggregate shows that the compressive strength of concrete increased by 20%, 53% and 37% for the air cured samples and 50%, 239% and 349% for the moist cured samples as 40%, 60% and 70% of EPLA was replaced with CEPLA aggregate.

Table 8. 3 The compressive strength of proposed concretes with variation of aggregate types

Mix No.	Compressive Strength (MPa)	
	28 days	
	Air Cured	Moist Cured
P1 (100P)	4.37	4.62
PC2 (60P40CEPLA)	3.45	3.86
PP2 (60P40 EPLA)	2.88	2.57
PE2 (60P40EPS)	3.02	3.17
PC3 (40 P 60 CEPLA)	3.23	3.76
PP3 (40P60 EPLA)	2.12	1.11
PE3 (40P60EPS)	2.57	2.86
PC4 (30 P 70 CEPLA)	2.23	2.87
PP4 (30P70 EPLA)	1.62	0.64
PE4 (30P70EPS)	1.82	2.09

In the case of EPLA concrete, the moist cure condition causes a significant reduction in strength development of concrete as a result of changes in hydration products of concrete, while a coating of EPLA improved the compressive strength of concrete. This trend is mainly related to the fact that the coating layers with a high absorption ratio absorb the lactic acid, which is released due to the alkaline reactivity of EPLA. This eliminates the distribution of lactic acid into the matrix. In fact, immediately after mixing cement with water, the liquid phase is saturated with calcium and SO_4^{-2} ions causing an increase in pH level of the matrix [207, 211]. The alkaline components sodium (Na) and potassium (K) ions are released to produce an alkaline sulphate-rich solution [207]. The alkali released at the initial stage of cement hydration, which are small amounts of Na^+ and K^+ ions, start the surface deterioration of EPLA through base-catalysed hydrolysis that then continues in the highly alkaline environment of cement (Figure 8. 2).

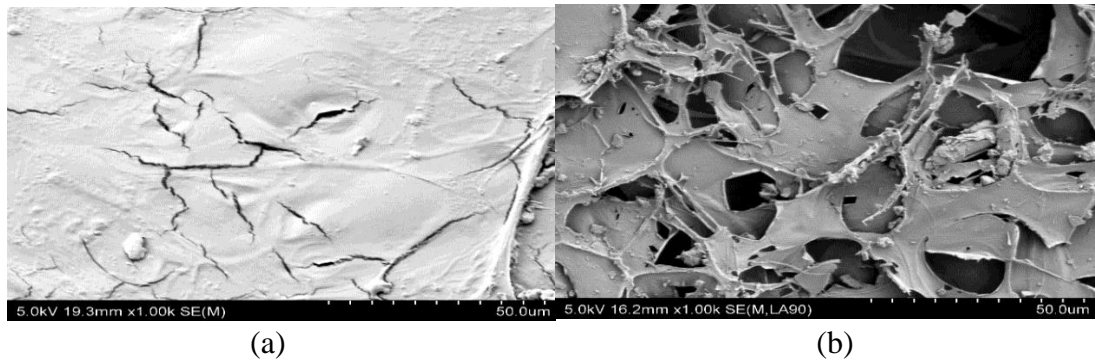


Figure 8. 2 EPLA degradation, a) Before subjecting to alkaline environment, b) after subjecting to alkaline environment.

The degradation of EPLA in the alkaline environment of cement causes a slow release of lactic acid into a hydrating cementitious system. The released lactic acid can be absorbed by the coating layers to form calcium carbonate at the layers of the coating materials (Figure 8. 3). This causes an increase in strength of the coating layer.

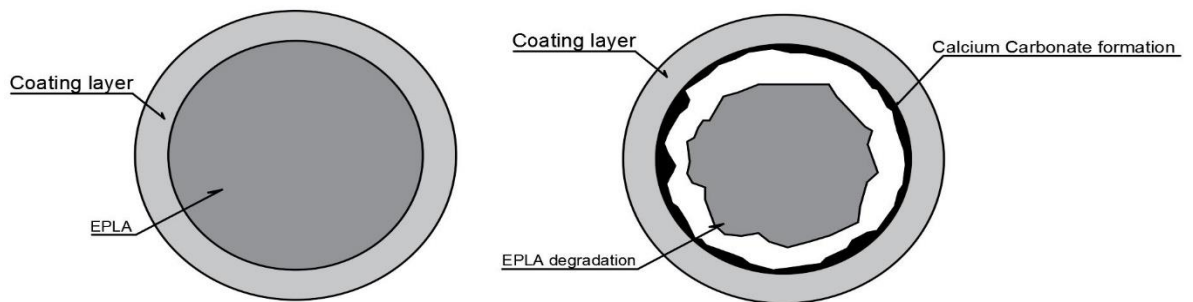


Figure 8. 3 The mechanism of calcium carbonate formation at CEPLA aggregate

It was also found that the elimination of lactic acid distribution at the initial stage of hardening decreased the changes of the generation of hydration products of concrete compared with non-coated EPLA. Apart from the alkaline reactivity of EPLA, the better interfacial bond between CEPLA and matrix can be counted as another parameter of the strength development of CEPLA concrete (Figure 8. 4). The degradation of EPLA aggregate and its shrinkages cause bond failure at the interfacial transition zone of the matrix. In the case of CEPLA aggregate, the cement can easily penetrate to the layers of coating materials and provides an excellent bond between CEPLA and matrix.

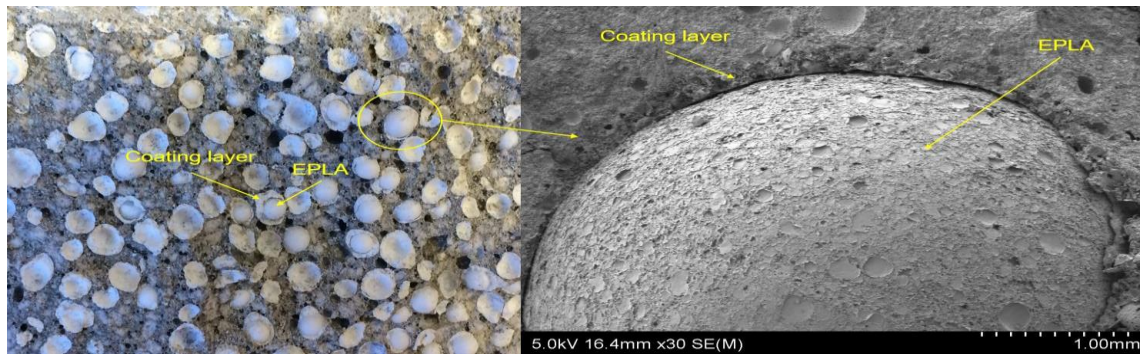


Figure 8. 4 Coated EPLA aggregate and its interfacial bonding

8.3.2 Thermal conductivity

The thermal conductivity of perlite concrete containing CEPLA is presented in Table 8. 4. The thermal conductivity of CEPLA concrete was in the range of 0.1078 to 0.1173 W/m.K and 0.1014 to 0.1168 W/m.K for samples cured in moist and air conditions, respectively. The lowest thermal conductivity of 0.1078 W/m.K was observed in the sample PC4, which was prepared with 70% CEPLA aggregate volume. The comparison between the thermal conductivity of EPLA, EPS and CEPLA concrete reveals that the thermal conductivity of CEPLA concrete was slightly higher than that of EPS and EPLA concrete which is mainly related to the thermal properties of the coating layers. The differences between thermal conductivity of coated and non-coated EPLA was much higher in the samples containing 70% polymer aggregate.

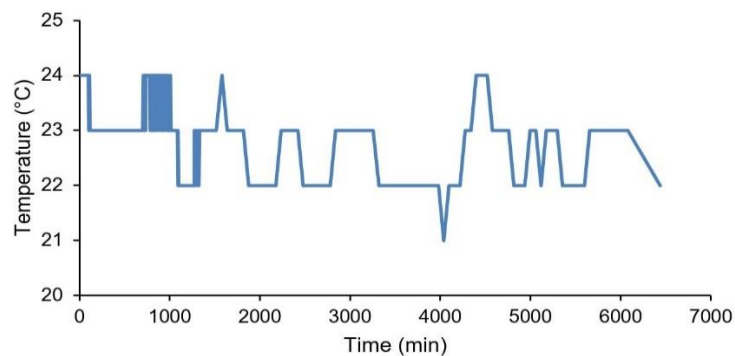
Table 8. 4 The results of thermal conductivity of proposed concretes.

Specimen No.	Density (kg/m ³)	Thermal Conductivity (W/m.K)	
		Moist Cured	Air Cured
P1 (100P)	493.00	0.1265	0.1285
PC2 (60P40CEPLA)	431.62	0.1173	0.1168
PP2 (60P40 EPLA)	400.20	0.0980	0.1050
PE2 (60P40EPS)	415.50	0.1150	0.1230
PC3 (40 P 60 CEPLA)	472.10	0.1126	0.1047
PP3 (40P60 EPLA)	360.20	0.0920	0.1020
PE3 (40P60EPS)	371.51	0.1010	0.1020
PC4 (30 P 70 CEPLA)	512.23	0.1078	0.1014
PP4 (30P70 EPLA)	302.22	0.0710	0.0980
PE4 (30P70EPS)	312.67	0.0880	0.0950

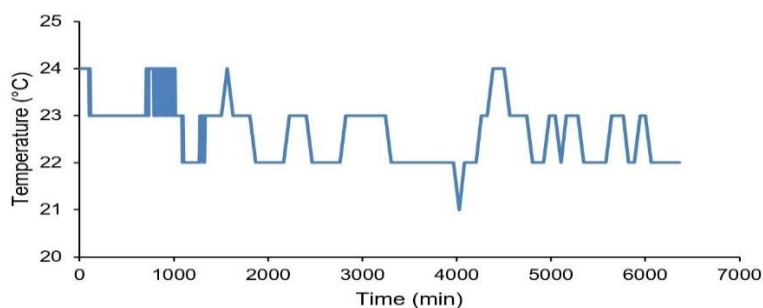
The differences in thermal conductivity of concrete are mainly attributed to the alkaline reactivity of EPLA and the increase in concrete porosity as a result of an increase in the CO₂ concentration of the matrix. The increase in CO₂ concentration is related to the chemical reactivity of lactic acid with calcium hydroxide and sodium hydroxide during the hydration process. Another effect is the coating layers eliminate the distribution of lactic acid into the matrix, which leads to a decrease in concrete porosity and higher thermal conductivity. The proposed concrete with its relatively lower thermal properties can be used as an insulating material.

8.3.3 Exothermic reaction and electrical resistivity

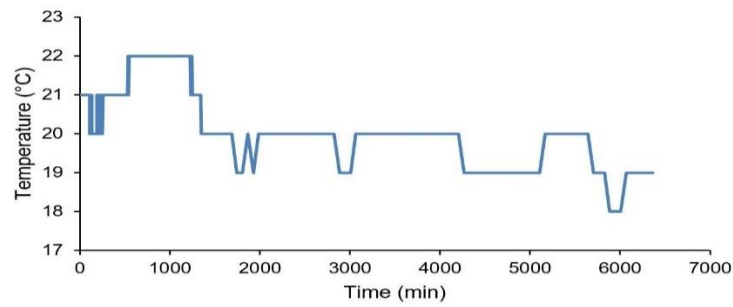
The variations in the exothermic reactions of CEPLA, EPLA and EPS concrete are presented in Figure 8. 5. The results reveal that the coated and non-coated EPLA show almost the same exothermic reaction intensity patterns during the hydration process. The sample P1 with 100% perlite demonstrates the lowest exothermic reaction due to the retarder properties of perlite aggregate.



(a)



(b)



(c)

Figure 8. 5 Exothermic reaction of concrete, a) CEPLA, b) EPLA, c) Perlite.

The electrical resistivity response is used to measure the setting time of concrete containing CEPLA aggregate. It can be found that there is an apparent difference between electrical resistivity response of coated EPLA and non-coated EPLA which is mainly related to changes in and formation of hydration products [205]. The rate of the resistivity increment of CEPLA concrete was much higher than that of EPLA and perlite concrete which is caused by the lower percentage of porosity and indicates a more permeable concrete (Figure 8. 6). Also, the degree of hydration which causes a significant reduction of concrete porosity and the interconnection between the pores affects the electrical resistivity. The coating of EPLA and eliminating the distribution of lactic acid into the matrix leads to a decrease in CO_2 concentration and consequently higher electrical resistivity. The alkaline reactivity of EPLA causes changes in the liquid phase composition and changes in Ca^{2+} , SO_4^{2-} and $\text{Al}(\text{OH})_4^-$ concentration which directly affects the hydration process and setting time of concrete.

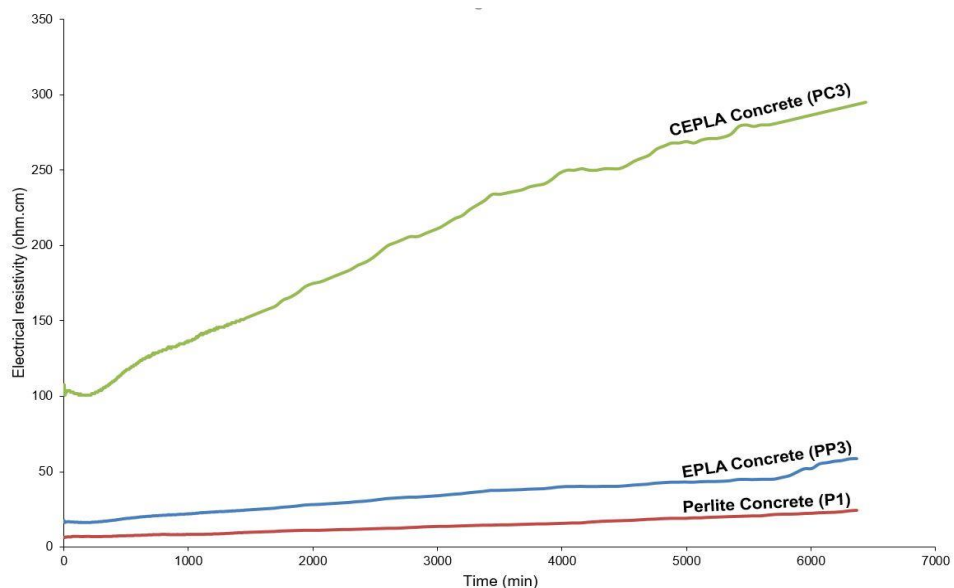


Figure 8. 6 Electrical resistivity response of CEPLA, EPLA and perlite concrete.

8.3.4 Fire resistance

Cone calorimeter tests were performed to assess the fire reaction of CEPLA concrete as per ASTM E1354 [183]. In order to have a better understanding of the performance of CEPLA aggregate concrete, the results were compared with EPS, EPLA and perlite concrete. The parameters such as heat release rate, total heat released, carbon monoxide production, and carbon dioxide production are assessed and investigated.

The failure modes of the proposed samples before and after the fire test are presented in Figure 8. 7. All the samples experienced minor thermal cracks and sample integrity was maintained after the test due to the fire resistance properties of perlite aggregate. A visible change in surface colouring was observed in all samples containing polymer aggregate due to the burning of polymers along with changes in the microstructure of concrete. This effect was a bit stronger in the sample containing CEPLA due to the burning of the coating layer.

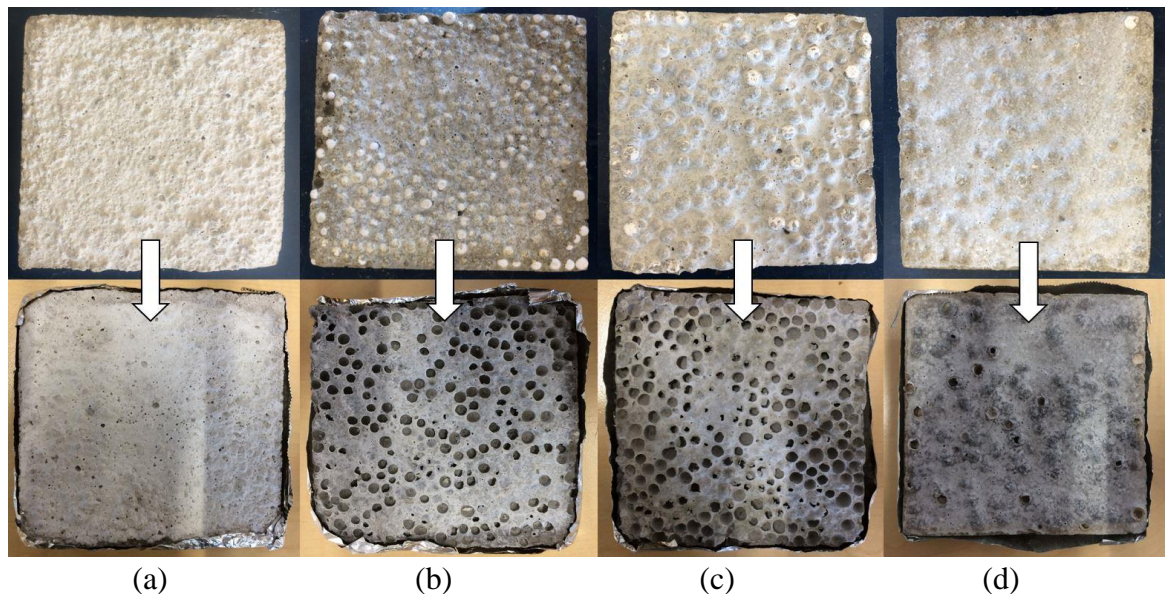
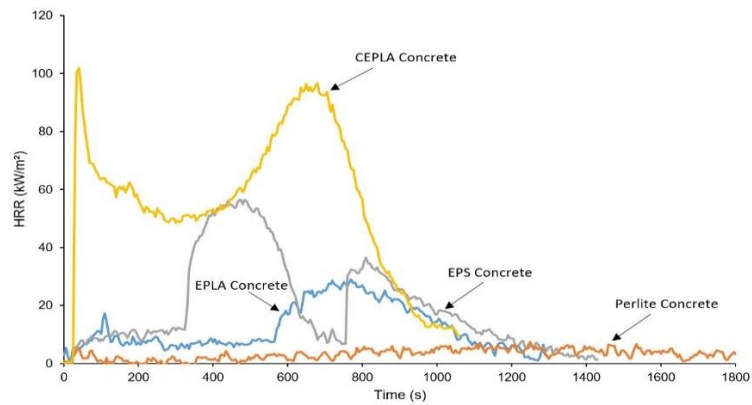


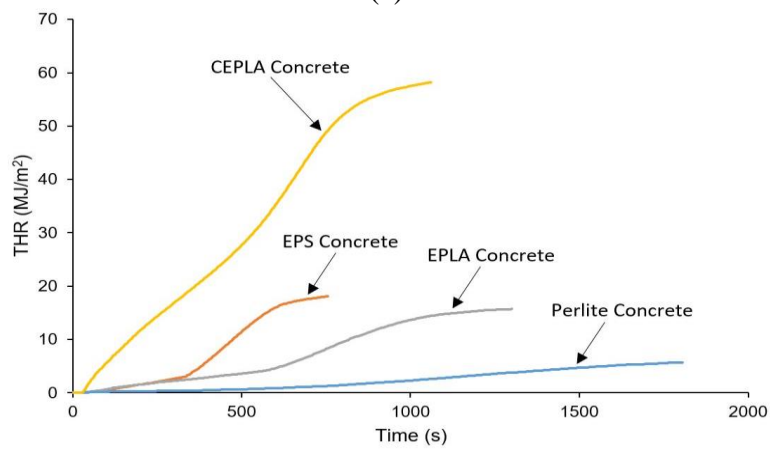
Figure 8. 7 Fire resistance of concretes, (a) Perlite concrete, (b) EPLA concrete, (c) EPS concrete, (d) CEPLA concrete.

The total heat released and heat release rate of the proposed concretes are presented in Figure 8. 8a and Figure 8. 8b, respectively. The THR and HRR of CEPLA concrete was 101.89 kW/m^2 and 58.21 MJ/m^2 . The CEPLA concrete is graded as a quasi-non-combustible material based on the standard limits. The THR of CEPLA concrete was lower than that of the standard limits of 200 kW/m^2 , while the total heat released rate of

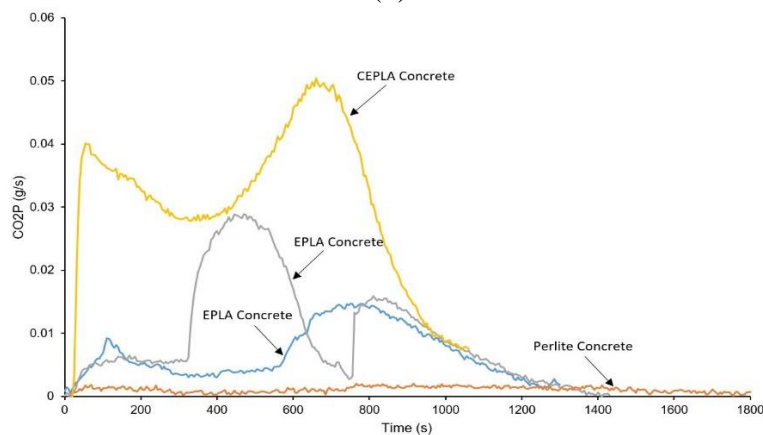
CEPLA concrete exceeded the limit of 8 MJ/m^2 . The EPLA and EPS concrete are also categorized as quasi non-combustible materials with a THR of 15.70 and 18.10 MJ/m^2 . It can be found that the THR of CEPLA concrete was about 4 times greater than that of EPLA concrete mainly due to the burning of coating layers, which contain two layers of paint products. This caused an ignition of the sample containing CEPLA after 12 seconds, while the time to ignition was much longer in samples with EPS and EPLA. It is worth to note that no ignition was observed in the sample made with 100% perlite (P1) (Table 8.5).



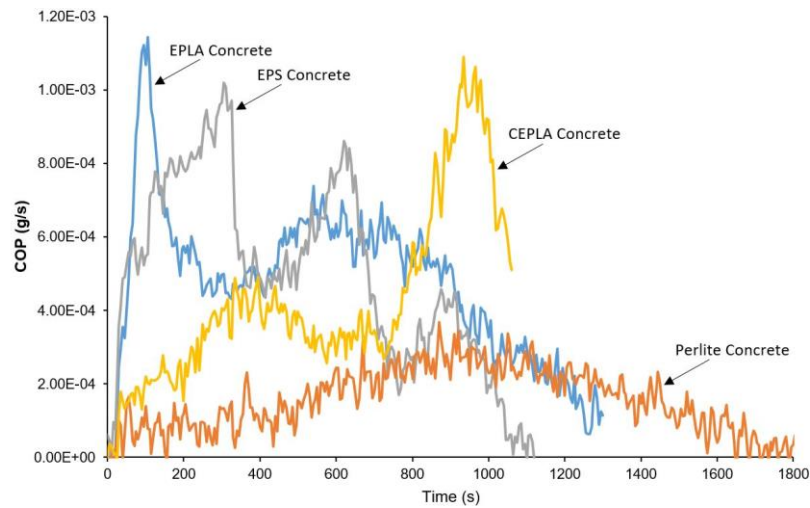
(a)



(b)



(c)



(d)

Figure 8. 8 Cone calorimeter tests of proposed concretes, a) HRR, b) THR, c) CO₂P, d) COP

Table 8. 5 The ignition and flameout point of proposed concretes

Mix No.	Time to ignition (s)	Time to flameout (s)
Perlite Concrete (P1)	0	0
EPLA Concrete (PP4)	555	1162
EPS Concrete (PE4)	711	1311
CEPLA Concrete (PC4)	12	949

The carbon dioxide production and the carbon monoxide production of CEPLA concrete are presented in Figure 8. 8c and Figure 8. 8d, respectively. As shown in Figure 8. 8c, the carbon dioxide production of CEPLA concrete was much higher than that of the EPS, EPLA and perlite concrete. The sharp increase in CO₂ gas production observed in the CEPLA sample is mainly related to the combustion process of the coating layers and EPLA aggregate with a considerable amount of CO₂ gas. The maximum value was reached after 685 seconds. In the case of EPLA concrete, the amount of CO₂ gas production was about 241% lower than that of CEPLA concrete. The concentration levels of carbon monoxide are presented in Figure 8. 8d. The CO gas production of CEPLA concrete was slightly lower than that of EPLA concrete. The highest and fastest growth in CO gas production were observed in EPLA and EPS concrete after 105s and 305s, respectively, while the CEPLA concrete reached its maximum value after 935s. A certain fluctuation in CO production occurred, which corresponds to a decrease in CO₂ gas production mainly due to incomplete combustion.

8.4 Conclusions

Based on the experimental study of CEPLA aggregate as a solution for expanded polylactic acid in the high alkaline environment of cement the following conclusions can be drawn:

1- The lowest density was observed in a sample containing 40% CEPLA aggregate as a further increase in CEPLA volume causes an increase in concrete density mainly due to the higher specific gravity of CEPLA compared to perlite aggregate. With the identical mix proportion, the density of CEPLA concrete was about 70% and 64% higher than that of EPLA and EPS concrete, respectively.

2- An increase in CEPLA content results in a decrease in compressive strength, however, the rate of strength reduction was much lower than that of EPS and EPLA concrete. The compressive strength of CEPLA concrete was about 349% and 37% higher than that of the EPLA and EPS concrete. The higher differences in strength development were observed in samples cured in moist conditions. The EPLA concrete shows the lowest compressive strength among the other samples mainly due to the degradation of EPLA and changes in hydration products of concrete. The better interfacial bond strength was observed in CEPLA concrete due to the porous structure of the coating layer and the penetration of the cement paste into the layers of the coating material.

3- The thermal conductivity of CEPLA concrete was slightly higher than that of the EPS and EPLA concrete. Larger differences were observed in a sample containing 70% polymers, because the sample containing 70% EPLA shows the lowest thermal conductivity compared to the CEPLA concrete due to an increase in concrete porosity caused by the alkaline reactivity of EPLA.

4- The electrical resistivity of CEPLA concrete was much higher than that of the EPLA concrete due to the lower percentages of porosity in the concrete matrix. It can be found that the coating of EPLA aggregate is a proper method to eliminate the chemical reactivity of EPLA at the initial stage of the hydration process which leads to a significant reduction in the alkaline reactivity of EPLA and limits the carbonation process. The differences between the exothermic reaction of EPLA and CEPLA was minimal, and both samples show the same exothermic reaction patterns.

5- The CEPLA concrete was graded as a quasi-noncombustible material like EPS and EPLA concrete. However, the total heat released and heat release rate of CEPLA concrete was much higher than that of the EPS and EPLA concrete due to the combustion of coating layers. A higher rate of carbon dioxide production was observed in CEPLA

concrete. The CO₂ gas production of CEPLA concrete was about 241% higher than that of EPLA concrete. The carbon monoxide production of CEPLA was slightly lower than that of EPLA concrete with a significant delay in its maximum peak value.

CHAPTER 9

BOND-SLIP BEHAVIOR OF EPLA CONCRETE

9.1 Introduction

The performance of composites structural assemblies (CSAs) depends on the bond strength of the embedded components of composite panels and infill materials. A new type of eco-friendly ultra-lightweight concrete with expanded poly-lactic acid (EPLA) was prepared to assess the possibility of using biopolymer concrete as a replacement for expanded polystyrene (EPS) lightweight concrete. The bond properties of EPLA and EPS concrete for the parameters compressive strength, strip locking patterns, as well as elastic and inelastic interlocking areas were assessed. However, the magnesium phosphate cement and CEPLA concrete are found as solution for EPLA degradation but due to limitations in the availability of samples the bond slip behaviour of CEPLA and magnesium phosphate have not been studied and further study is encouraged to have a better understanding on engineering properties of suggested concrete.

The results indicate that the application of biopolymers significantly changed the mechanical and bond properties of concrete. The chemical reactivity of EPLA and its degradation in the alkaline environment of cement causes bond failure at the interfacial transition zone of the aggregate-paste. Two different failure modes of splitting cracks and pullout failure were observed. A bond stress-slip model for EPS and EPLA concrete was found to give a reasonable estimation of experimental results of the bond-slip behaviour. Also, a new method is proposed to estimate the elastic and inelastic length of embedded components in ultra-lightweight concrete.

9.2 Experimental program

9.2.1 Materials

The specification of materials are explained and provided in Chapter 3.

9.2.2 Mix proportions

The variables chosen were the types of polymers (bio-plastic and petrochemical plastic) and galvanised strip patterns (Table 9. 1). Two mix proportions were used to produce EPLA and EPS concrete. A fixed water-cement ratio (w/c) and cement content of 0.343 and 301 kg/m³ were adopted for all mixes. The water-cement ratio and cement content are obtained as per Eq. 3.4 and Eq. 3.6.

Table 9. 1 Mix proportions of EPLA and EPS concrete.

Mix No.	Effctvie w/c ratio	Content (kg/m ³)					
		Cement	Water	Perlite	EPLA	EPS	SP
CPL (PP4)	0.343	301	193.5	40.5	13.3	-	0.0041
CEP (PE4)	0.343	301	193.5	40.5	-	7.0	0.0041

CPL is EPLA concrete, CEP is EPS concrete.

It has been found that propagating of locking holes instead of single holes is a proper technique to enhance tensile capacity mainly due to the fact that propagation of locking components results in a larger contact area engaging to resist the applied load [139, 140]. In total, seven different interlocking patterns were prepared (Figure 9. 1). The strip patterns were altered in the cut shape and cut area in the elastic, A_e and inelastic, A_{in} region of their embedded length. All the strips have a cut area of 678.9 mm², as per previous studies [139, 140]. The strips with a thickness of 2mm were placed at the centre of the sample with an equal concrete cover size of 50mm on all sides (Figure 9. 2). The strips were labelled by cutting patterns. The sample 9R4.9 from a previous study is used as a reference for the other patterns [139, 140]. This sample shows the highest tensile capacity and due to this success, different locking patterns with a similar cut area are prepared to investigate the effect of a variation in locking patterns, locking angle and locking length on bond stress behaviour.

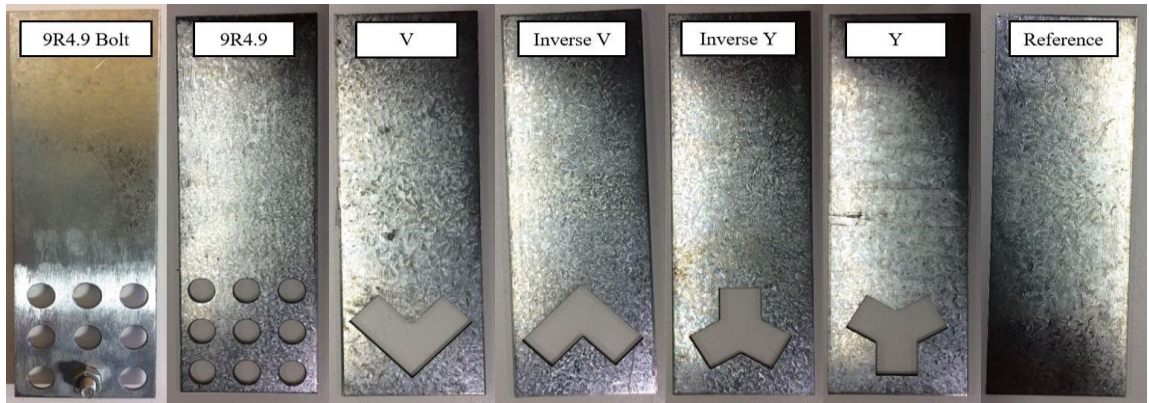


Figure 9. 1 Patterns of embedded galvanized strips

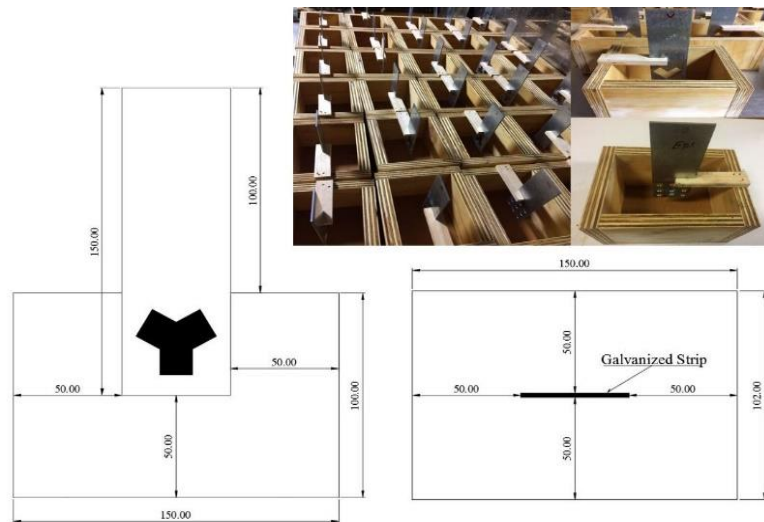


Figure 9. 2 Pull out test configuration

9.2.3 Test methods

Standard cylinders with dimensions of 100×200 mm (diameter x height) were used for density, compressive strength and tensile strength as per ASTM C567 [176] , ASTM C495 [177] and ASTM C496 [178]. All the tests were done after 28 days of curing. The bond strength test was carried out on concrete samples using a pull-out test method. The galvanized strips were placed at the centre of prisms of sizes $100 \times 102 \times 150$ mm [139, 140]. Seven different cut patterns are proposed to explore the significance of locking patterns on bond strength of embedded strips. The samples were categorised into two groups of EPS concrete and EPLA concrete and tested on forty-two samples and compared with two control samples from a pervious study. The samples were gripped and

subjected to a pulling force at a rate of 1 mm/min by an INSTRON 33R4469 tester. It worth to note that the average results of three specimens were considered to evaluate the bond properties of proposed concrete with variation on locking patterns.

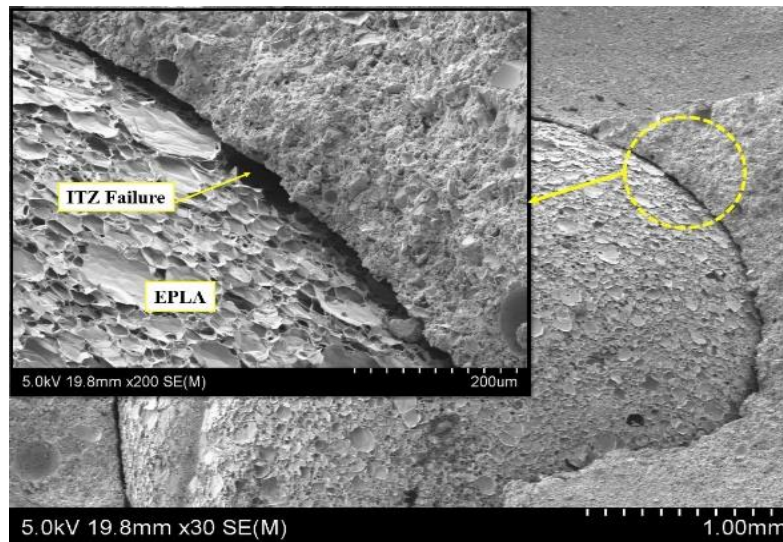
9.3 Results and discussion

9.3.1 Mechanical properties

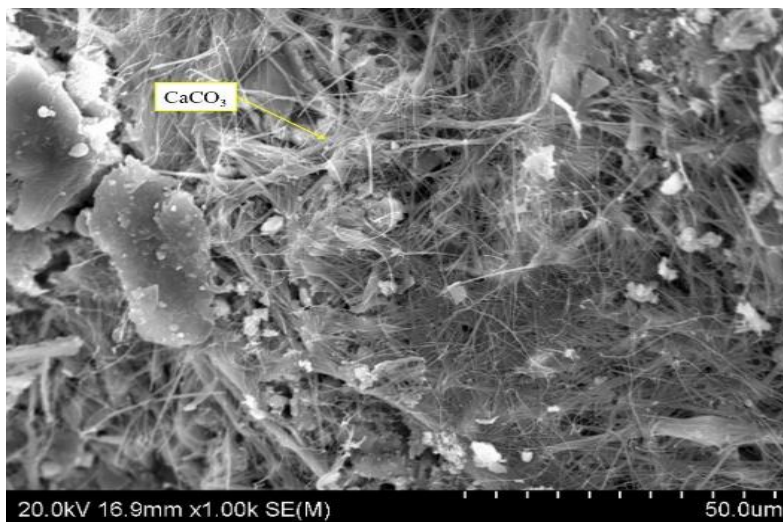
Two different average concrete densities of 294.0 and 348.0 kg/m³ were obtained with the inclusion of EPLA and EPS aggregate (Table 9. 2). The test results show again that the density of EPLA concrete is lower than that of EPS concrete, while the relative density of EPS beads (10 kg/m³) is about half the one of EPLA beads (19 kg/m³). The compressive strength of concrete decreased by 37.5% as the EPS beads were replaced with EPLA beads. The compressive strengths of EPS and EPLA concrete were found to be in the range of 0.7-0.79 MPa and 0.9-1.50 MPa, respectively. The same trend of strength reduction was observed on the tensile strengths of the concretes as the tensile strength of EPS concrete was about twice the one of EPLA concrete. The significant reduction in the compressive and tensile strength of EPLA concrete mostly related to the alkaline reactivity of EPLA, bond failure at the interfacial transition zone (ITZ) (Figure 9. 3a) and changes in the microstructure of concrete (Figure 9. 3b).

Table 9. 2 Mechanical properties of EPLA and EPS concrete

Mix No.	Average Density (kg/m ³)	Compressive strength (MPa), f_c			Average Compressive Strength (MPa), f_c	Average Tensile Strength (MPa), f_t
		Sample 1	Sample 2	Sample 3		
CPL (PP4)	294.0	0.79	0.70	0.76	0.75	0.025
CEP (PE4)	348.0	1.20	0.90	1.50	1.20	0.051



(a)



(b)

Figure 9. 3 EPLA degradation in alkaline environment of cement; (a) bond failure at ITZ zone, (b) changes in hydration product (more calcium carbonate)

9.3.2 Bond stress

Table 9. 3 shows the slip behaviour related to the ultimate bond stress for the proposed concretes with a variation in strip configuration. The experimental results show that the interlocking patterns and compressive strength of concrete play a significant role in the tensile capacity of the proposed concretes. The ultimate bond stress of EPS and EPLA concrete with a variation in locking patterns of embedded strips were of a range of 0.131-0.518 MPa and 0.045 - 0.277 MPa, respectively. Moreover, the bond stress at a slip of 0.25mm was considered as the critical stress which is associated with the chemical

adhesion forces between strips and concrete [216] . The critical bond stress of normal concrete is mostly in the range of 0.67-0.71 [216] which is about 80% and 64% higher than that of EPLA and EPS concrete.

Table 9. 3 The ultimate and critical bond stress of proposed concretes

		Ref.	9R4R	9R4.9 Bolt	Y	Inv. Y	V	Inv. V
CPL (PP4)	Critical bond stress (MPa)	0.098	0.112	0.114	0.277	0.077	0.101	0.045
	Ultimate bond stress (MPa)	0.124	0.130	0.152	0.277	0.102	0.221	0.045
	Slip at ultimate bond stress (mm)	0.417	0.416	0.424	0.216	0.911	0.463	0.213
CEP (PE4)	Critical bond stress (MPa)	0.243	0.130	0.309	0.302	0.168	0.243	0.073
	Ultimate bond stress (MPa)	0.280	0.131	0.512	0.518	0.291	0.479	0.142
	Slip at ultimate bond stress (mm)	0.616	2.811	2.820	3.410	1.614	2.806	2.208

The experimental results show that the addition of EPLA aggregate causes a significant reduction in initial stiffness and ultimate tensile capacity of embedded strips. For the EPS concrete, the highest ultimate bond stress was around 0.518 MPa in the sample with the locking pattern "Y". Interestingly, the bond stress of the Y pattern is comparable to the sample with the external locking key (9R4.9 bolt). The lowest bond stress with a rapid failure was observed in the sample with the locking pattern "Inverse V" due to a bond failure at the interface of the embedded strip and concrete and also insufficient confinement pressure at the locking zone of the proposed pattern. In the case of EPLA concrete and regardless of locking patterns, the average bond stress was significantly lower than that of EPS concrete. This occurrence can be attributed to: a) bond failure at the ITZ of the aggregate-paste zone as results of EPLA degradation, and b) changes in

the microstructure of concrete due to the chemical reactivity of EPLA. These changes lead to EPLA concrete having a more brittle behaviour compared to EPS concrete. The highest and lowest bond stress was observed in the samples "Y" and "Inverse V" with the relative bond stress of 0.277 and 0.045 MPa, respectively. The bond stress of the sample 9R4.9 Bolt was about 45% lower than that of the "Y" sample due to the splitting of concrete and the low tensile strength of EPLA concrete.

The influence of locking patterns on the tensile capacity of embedded strips was almost the same for both proposed concretes. The better performance in both EPS and EPLA concrete was observed in the "Y" sample due to its better confinement effects and an interlocking mechanism. The chemical reactivity of EPLA leads to a decline in adhesion between embedded strips and concrete and a decrease in concrete crushing strength. On the other hand, the adhesion failure at the interface of embedded strips and EPLA concrete occurs mostly due to the brittleness of EPLA concrete which causes cracks to propagate more rapidly and which results in a significant reduction in bearing forces.

In the case of the sample 9R4.9 and compared with test results of foamed concrete reported by Sayadi et al. [139, 140], the tensile capacity of foamed concrete with a relative density of 800 kg/m³ and 1200 kg/m³, was about fourteen and two times greater than that of EPLA concrete, respectively. While, the tensile capacity of EPS concrete was 7% higher and 83% lower for samples FC8 and FC12, respectively. Also, it was found that the slip at the ultimate bond stress of EPLA concrete was much higher than that of EPS concrete due to the sudden splitting failure of concrete containing EPLA beads. Conversely, the low tensile strength of EPLA concrete leads to a rapid bond failure at the interface area between embedded strips and concrete as a result of an increase in internal splitting cracks. Thus, the results from foamed concrete, EPS concrete and EPLA concrete confirmed that a larger bond stress is transferred by the embedded strips in the samples with higher compressive strength. In fact, the compressive strength of concrete is the most influential parameter that significantly affects the bond behaviour and failure modes of embedded strips.

9.3.3 Effects of elastic and inelastic zone on bond stress

Table 9. 4 presents the effects of the interlocking position on tensile capacity. The elastic and inelastic region of the embedded strip is determined as per the proposed method for an integrated steel bar in normal concrete [142, 143, 217]. However, in the case of lightweight concrete with its low compressive strength of 0.5 to 1.2 MPa some

modifications are required. The proposed method by Sayadi et al. [139, 140] was used to calculate the elastic and inelastic length of a galvanised steel strip with modifications on elastic bond stress (u_e), inelastic bond stress (u_{in}), inelastic length (l_{in}) and elastic length (l_e). Based on the experimental results the uniform bond stress at the elastic and inelastic range was approximated as $0.26\sqrt{f_c}$ and $0.13\sqrt{f_c}$ along with $0.14\sqrt{f_c}$ and $0.07\sqrt{f_c}$ for EPS and EPLA concrete, respectively. The inelastic length of the embedded component of lightweight concrete is a function of strip thickness and compressive strength. A correction factor of $l_{ec}/t.l_{inc}$ is developed and used to modify the inelastic length of the embedded components in the lightweight concrete. The following equation Eq. 9.1 is proposed to determine the effect of the interlocking system on the elastic and inelastic region of the embedded strip in lightweight concrete (Table 9. 4).

$$l_{In.LWC} = \frac{l_{e.NC}}{(f_u - f_y)^{t.l_{in.NC}} (bt)} \frac{2(b+t)u_{in}}{2(b+t)u_{in}} \quad [9.1]$$

$$\text{Where } l_{in.NC} = \frac{(f_u - f_y)bt}{2(b+t)u_{in}}$$

$$l_{e.NC} = \frac{f_u bt}{2(b+t)u_e}$$

$$u_{e \text{ EPS}} = 0.26\sqrt{f_c}$$

$$u_{in \text{ EPS}} = 0.13\sqrt{f_c}$$

$$u_{in \text{ EPLA}} = 0.07\sqrt{f_c}$$

$$u_{e \text{ EPLA}} = 0.14\sqrt{f_c}$$

Where f_u is the ultimate tensile strength, f_y is the yield tensile strength, b is the width of strip, t is thickness of strip, l_e is elastic length, l_{in} is inelastic length and u_{in} is uniform bond stress in the inelastic zone.

Table 9. 4 Pull-out test results of embedded strips in EPS and EPLA concrete

		f_c (MPa)	l_e (mm)	l_{in} (mm)	A_{CT} (mm ²)	A_{Ce} (mm ²)	A_{Cin} (mm ²)	f_t (kN)	u_b (MPa)
CPL (PP4)	Ref.	0.75	32.9	17.10	0	0.0	0.0	0.64	0.12
	9R4.9	0.75	32.9	17.10	678.9	452.6	226.3	0.68	0.13
	9R4.9 Bolt	0.75	32.9	17.10	678.9	377.1	226.3	0.79	0.15
	Y	0.75	32.9	17.10	678.9	501.8	177.1	1.44	0.27
	Inv. Y	0.75	32.9	17.10	678.9	539.8	139.1	0.52	0.10
	V	0.75	32.9	17.10	678.9	561.9	117.0	1.15	0.22
	Inv. V	0.75	32.9	17.10	678.9	620.4	58.5	0.25	0.05
CEP (PE4)	Ref.	1.20	32.9	17.10	0	0.0	0.0	1.46	0.28
	9R4.9	1.20	32.9	17.10	678.9	452.6	226.3	1.62	0.31
	9R4.9 Bolt	1.20	32.9	17.10	678.9	377.1	226.3	2.71	0.51
	Y	1.20	32.9	17.10	678.9	501.8	177.1	2.70	0.52
	Inv. Y	1.20	32.9	17.10	678.9	539.8	139.1	1.44	0.27
	V	1.20	32.9	17.10	678.9	561.9	117.0	2.49	0.48
	Inv. V	1.20	32.9	17.10	678.9	620.4	58.5	0.74	0.14
FC8 [140]	Ref.	0.95	32.9	17.10	0	0.0	0.0	2.64	0.50
	9R4.9	0.95	32.9	17.10	678.9	452.6	226.3	1.55	0.29
FC12 [139]	Ref.	8.8	32.9	17.10	0	0.0	0.0	7.8	1.50
	9R4.9	8.8	32.9	17.10	678.9	452.6	226.3	9.73	1.87

f_c : compressive strength, A_{CT} : Total cutting area, A_{Ce} : Cutting area in elastic zone, A_{Cin} : Cutting area in inelastic zone, f_t : tensile strength, u_b : average bond stress.

Researchers found that the bond strength of a steel bar is a factor of the locking components in the elastic and inelastic length of the embedded components [142, 143]. They have confirmed that an increase in locking components in the inelastic zone leads to a higher tensile capacity (Figure 9. 4). The same trend was observed in this study.

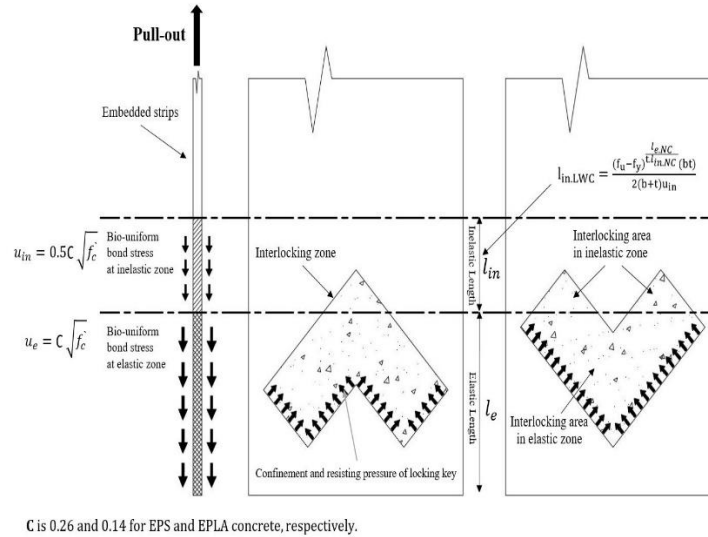


Figure 9. 4 Confinement effect and elastic and inelastic length of embedded strips

The results show that the area of the locking key significantly affects the tensile capacity of the embedded strip. In the case of the “Y” and “Inverse Y” patterns, the tensile capacity in the EPLA concrete was increased from 0.52 MPa to 1.44 MPa as the cut area in the inelastic zone decreased from 177.1 mm² to 139.1mm². The same trend was observed in EPS concrete. An increase in the cut area in the elastic zone leads to a significant reduction of 73% in the tensile capacity of the embedded strip. A significant reduction in tensile strength of the strip was observed in the sample “Inverse V” with an elastic cut area of 620.4 mm². Compared to sample “V” with an elastic cut area of 561.9 mm², the tensile capacity decreased by 78% and 39% for EPLA and EPS concrete, respectively. However, referring to the control sample (9R4.9) from the previous study and compared with sample “Y”, it can be seen that the sample 9R4.9 with the larger cut area in the inelastic zone shows the lower tensile capacity. This can be attributed to the pattern configuration and lack of proper cement paste penetration in the cut section of the embedded strips.

Regardless of the cut area at the elastic zone, the application of a bolt as an additional locking key (9R4.9 Bolt) slightly increased the bond stress compared to sample 9R4.9. Nevertheless it was found that an external locking key such as a rib is an inappropriate

method for ultra-lightweight concrete with less than 1.0 MPa due to its low mechanical properties. Compared with the control sample with no cut area in both the elastic and inelastic zone, the tensile capacity of the embedded strips increased by 6%, 19%, 125% and 80% along with 11%, 85%, 85% and 75% for samples 9R4.9, 9R4.9 Bolt, “Y” and “V” when embedded in EPLA and EPS concrete, respectively. The inverse form of the cut patterns imposes an opposite effect on the tensile capacity of embedded strips. It can be found that the locking area in the elastic and inelastic zone is the dominant factor for increasing the bond strength of ultra-lightweight concrete. Thus, it can be concluded that when adequate concrete strength is provided, the splitting failure of concrete could be eliminated and embedded strips could achieve a larger bond capacity.

9.3.4 Effect of locking components angle on bond strength

Figure 9. 5 shows the angle and direction of resisting components of the proposed interlocking patterns. The locking configuration is another major factor that directly affects the bond strength. The experimental results show that the interlocking mechanism of embedded strips and surrounding concrete also depends on the angle of the bottom cutting edge to the direction of the applied load and length of the locking area along the applied tensile stress. A decrease in the tensile capacity was seen with an increase in the angle of the bottom cut part. As observed from sample “V” and “Inverse V”, the tensile capacity decreased by 78%, when the angle of the bottom edge of the resisting components increased from 45° to 135° . The same trend is displayed in the “Y” and “Inverse Y” section. The tensile strength of concrete was decreased from 1.44 MPa to 0.52MPa and 2.70 MPa to 0.74 MPa for EPLA and EPS concrete as the angle of the resisting components increased from 90° to 120° , respectively.

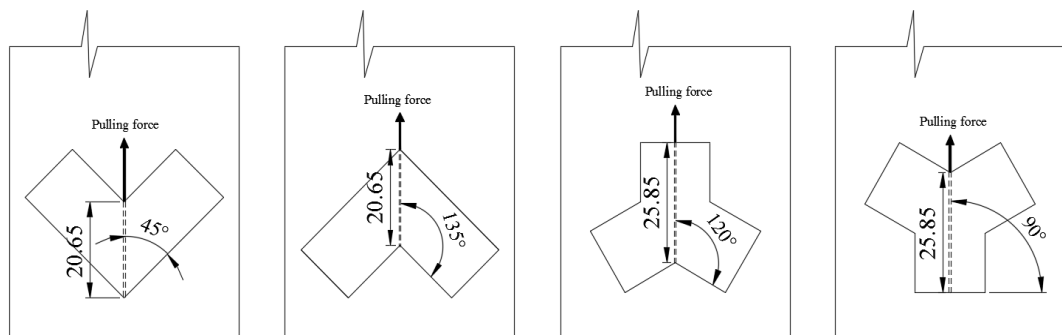


Figure 9. 5 Effects of interlocking patterns on bond strength

There is a direct relation between the angle of resisting elements and tensile capacity. This phenomenon can be related to an increase in confinement pressure as a more substantial confinement pressure was applied to the penetrated concrete at the locking area with a decrease in the bottom angle of the resisting components. The sample “V” and “Y” with a relative angle of 45° and 90° show the highest tensile capacity among the other locking patterns. However, the sample “Y” obtained the highest tensile capacity of 1.44 MPa and 2.70 MPa compared with sample “V” with a relative strengths of 1.15 MPa and 2.48 MPa when embedded in EPLA and EPS concrete, respectively. These changes in tensile capacity can be attributed to the length of locking components along the applied tensile stress. An increase in the length of locking elements leads to a larger area between concrete and embedded strips to resist the applied pressure and causes a more significant shear stress transfer to the matrix. Also, a higher compressive strength leads to an increase in resistance to concrete crushing and shearing between embedded strips and surrounding concrete.

9.3.5 Effect of compressive strength on bond stress

Table 9. 4 and Figure 9. 6 show the response in tensile capacity and bond strength with respect to the compressive strength of concrete. Researchers found that there is a direct relationship between the compressive strength of concrete and bond strength. The experimental results show that the compressive strength of EPS concrete is about twice that of EPLA concrete. The changes in strength development of the proposed concretes can be related to the chemical reactivity of EPLA which leads to debonding of EPLA beads and significant changes in the microstructure of concrete. In addition to this, the conversion of hydration products to more calcium carbonate as a result of EPLA’s chemical reactivity and makes the matrix more brittle compared with EPS concrete.

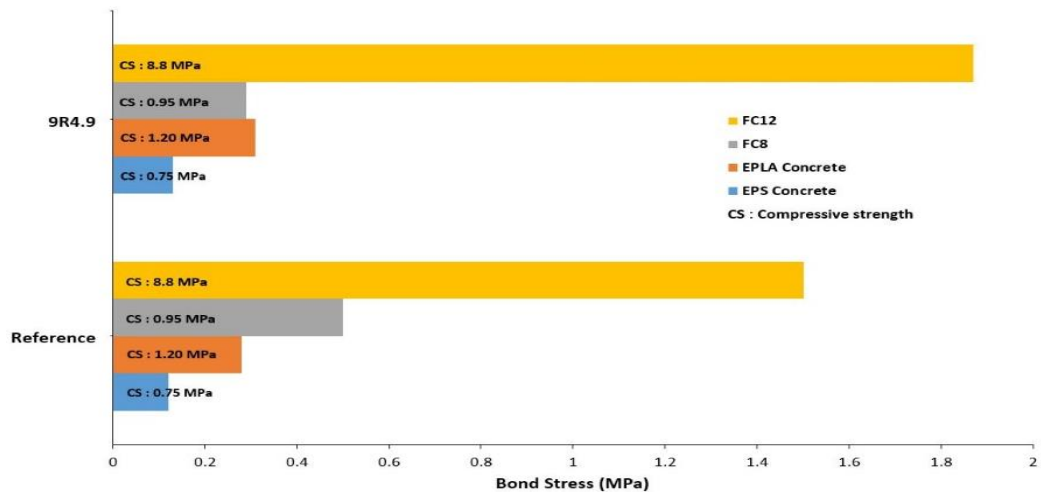


Figure 9. 6 The correlation between bond stress and compressive strength of concrete EPLA, EPS and foamed concrete (FC12 and FC8) [139, 140]

The compressive strength of the proposed concrete ranged between 0.7 to 0.79 MPa and 0.9 to 1.50 MPa for EPLA concrete and EPS concrete, respectively. As expected, the EPS samples exhibited a higher tensile strength compared to EPLA concrete due to the better interfacial bond strength at the ITZ zone. The bond strength of EPS concrete was about 42 to 476% higher than that of EPLA concrete. The average bond stress of 0.13, 0.15, 0.27, 0.10, 0.22 and 0.05 MPa along with 0.31, 0.52, 0.51, 0.14, 0.48 and 0.27 MPa was observed for the samples 9R4.9, 9R4.9 Bolt, “Y”, “Inverse Y”, “V” and “Inverse V” when embedded in EPLA and EPS concrete, respectively. Besides the variation in locking patterns, the concrete with higher compressive strength shows the better chemical adhesion to the embedded strips which leads to an improvement in bond characteristics of concrete. In comparison with a previous study on the bond performance of foamed concrete with relative density and compressive strength of 1200 kg/m³ and 8.8 MPa (FC12), the tensile strength of sample 9R4.9 was about six times and fourteen times greater than that of the EPS and EPLA concrete.

9.3.6 Failure modes

Table 9. 5 presents the failure modes of the proposed concretes. Two failure modes of pullout and splitting crack were observed for concretes containing EPS and EPLA (Figure 9. 7). The experimental results show that the variations in interlocking patterns and mechanical properties of concrete affect the failure modes and crack propagation. A sudden splitting failure and visible cracks were formed on both sides of the embedded strips in EPLA concrete due to the bond strength between EPLA concrete and embedded

strips being much higher than that of the tensile strength of about 0.025 MPa [140]. While the failure mode of all EPS concrete samples was pullout failure without any noticeable cracks except sample “9R4.9 Bolt” due to its external locking key. In fact, as the tensile stress applies to the embedded strips, the inclined cracks form at the interface of the embedded strips and surrounding concrete. This leads to inclined forces to radiate outwards and causes a tensile ring stress and consequently an appearance of splitting cracks [216].

Table 9. 5 Failure modes of proposed concretes

Specimen	Failure Modes						
	Ref.	9R4.9	9R4.9 Bolt	Y	Inv. Y	V	Inv. V
CPL (PP4)	SP	SP	SP	SP	SP	SP	SP
CEP (PE4)	PO	PO	PO	PO	PO	PO	PO

SP: splitting failure, PO: Pull-out failure.

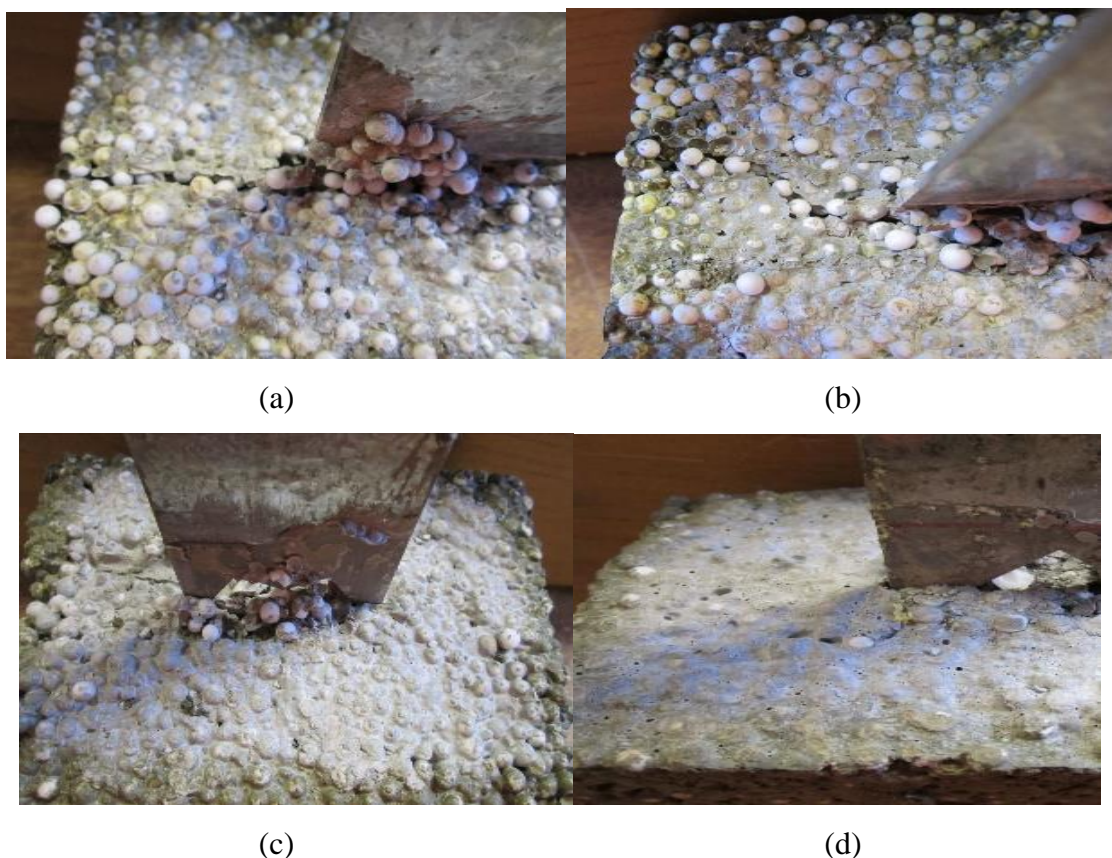


Figure 9. 7 Failure modes of proposed concretes; (a) CPL-Y, (b) CPL-Inverse V, (c) CPE-Y, (d) CPE-Inverse V

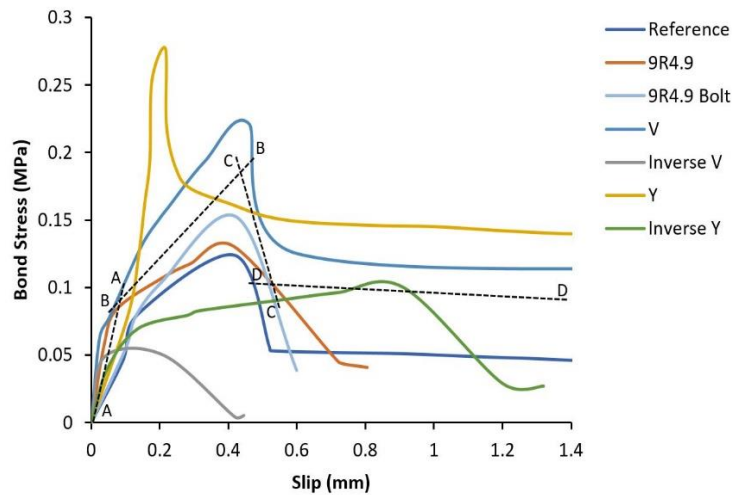
In the case of EPLA concrete, the sample “Inverse V” and “Inverse Y” failed immediately after the tensile stress was applied due to an insufficient confinement effect of the interlocking elements and low tensile strength of concrete to resist against the internal tensile load. A higher tensile capacity and a delay in splitting cracks were observed in samples “V” and “Y” due to a better locking engagement and confinement effect of the proposed locking key. Thus, a greater intensity of cracks was observed in concrete containing EPLA in comparison to EPS concrete as a result of the brittle behaviour of EPLA concrete.

Surprisingly, no splitting cracks were detected in samples containing EPS aggregate. However, the compressive strength and tensile strength of EPS concrete are about twice the one of EPLA concrete, but the main causes of splitting failure of EPLA concrete was its brittle behaviour and weaker adherence compared to EPS concrete. A possible cause of the pull out failure of concrete containing EPS is the weak mechanical interlocking between EPS concrete and embedded strips. Also, the bond stress at the interface of strips to concrete is much lower than the applied stress. The highest and lowest bond stress was observed in the sample “9R4.6 Bolt” and “Inverse V”, respectively. In comparison with the previous study and with identical locking patterns, the failure mode of foamed concrete was changed from vertical splitting failure to horizontal splitting failure and pullout failure as the EPLA and EPS concrete are used as infill materials. From both experimental studies it can be found that the adhesion of foamed concrete to the embedded strips is much higher than the one of EPS and EPLA concrete.

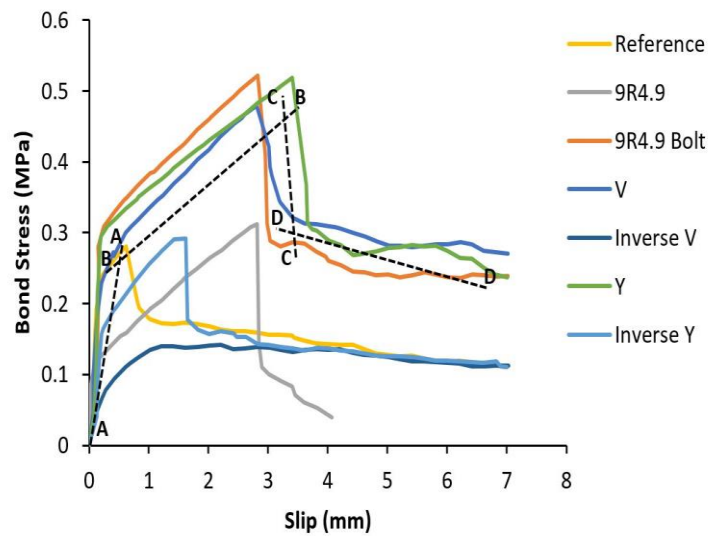
9.3.7 Bond stress-slip behaviour

Figure 9. 8 displays the bond stress-slip behaviour of EPS concrete and EPLA concrete. The experimental results show that the stiffness and tensile capacity of concrete directly depend on the strength of concrete and locking patterns of the embedded galvanised strips. Compared with EPS concrete, the application of EPLA considerably reduced the tensile capacity of concrete because of the chemical reactivity of EPLA beads and its degradation in the alkaline environment of cement. The results demonstrate that the shape and position of the locking system have a significant effect on the bond performance of concrete. Regardless of the concrete’s compressive strength, a higher bond stress and tensile capacity were observed in samples which provide a more efficient confinement pressure at the locking zone. In addition to this, the sample with the smaller cut area and

locking angles in the elastic region present the better interlocking performance. As shown in Figure 9. 8a, the tensile strength of EPLA concrete mostly relies on chemical bonding rather than mechanical interlocking bond as the majority of the samples failed soon after the tensile stress was applied, i.e. through concrete splitting failure. This can be attributed to the low compressive strength of the base matrix and inadequate bearing mechanisms at the interface area of concrete to strips to prevent the slippages of embedded strips.



(a)



(b)

Figure 9. 8 The bond stress-slip behaviour; (a) EPLA concrete, (b) EPS concrete

The bond stress-slip behaviour of EPLA and EPS concrete breaks down into four stages of: a) chemical adhesion or chemical bond (line A-A), b) mechanical interlocking bond (line B-B), c) shear off (line C-C), and d) pull-out (line D-D). The line A-A presents the linear behaviour which contributed to the chemical bond between strips and concrete.

Compared with EPLA concrete the greater bonding stress and higher stress corresponding to the lower slippage is transferred along the length of embedded strips as a result of the higher compressive strength of EPS concrete and better adhesional bond strength at the interface area. As far as locking key patterns are concerned, a higher bond stress was observed in the samples with smaller locking areas in the elastic zone because of the existence of larger bond stress in this zone. In addition to this, an increase in the interface area between concrete and strips results in greater regional adhesion stress. As the load increased, the slope of the bond stress-slip diagram started to decrease due to chemical bond failure at the interface area of strip to concrete (line B-B). At this stage, the majority of the EPLA samples failed due to the existence and propagation of internal splitting cracks, which cause strip slippage and concrete splitting failure.

In the case of EPS concrete, the second segment of the bond stress-slip diagram significantly relies on the interlocking mechanism of embedded strips and concrete. The samples with the better confinement mechanism and smaller locking key at the elastic zone transferred the higher tensile stress. For instance, the tensile strength of sample “Y” with an elastic locking key area of 501.8 mm^2 is about four times greater than that of the “Inverse V” sample with a locking area of 620.4 mm^2 . At the unloading stage (line C-C), the partial bond failure of mechanical interlocking and splitting cracks along the embedded strips lead to a sudden decrease in tensile capacity due to a breakdown and compaction of concrete at the locking area of the embedded strips. A larger rate of increment in strip displacement with a relatively low bond stress was observed at the last stage of stiffness due to failures of all resisting components and breaking of concrete at the interlocking zone of the embedded strips.

9.3.8 Analytical model of bond stress-slip behaviour

An analytical model is developed to predict the bond stress-slip relationship of embedded galvanised steel strips. This model is formulated based on modification of the bond-slip equations (Eq. 9.2) proposed by Sayadi et al. [139, 140]. The bond stress development of the proposed model was divided into four stages of stiffness, namely chemical adhesion, mechanical interlocking stage, shear off stage and softening phase at the slip range of $0 \leq \delta \leq \mu\delta_u$, $\mu\delta_u < \delta \leq \delta_u$, $\delta_u < \delta \leq \beta\delta_u$ and $\delta > \beta\delta_u$, respectively. As shown in Figure 9. 9, the first linear part refers to the adhesional bond stress at the interface of embedded strips and matrix. The maximum slippage of this ascending part is $\mu\delta_u$. The

second ascending part is mostly related to interlocking mechanisms of locking patterns with maximum slippages at δ_u . At this stage, the stiffness and the angle in the bond stress-slip diagram decreased as a result of adhesional bond failure at the interfacial zone. The stress of this segment depends on the confinement effect of locking components and their engagement with the surrounding concrete. The decreasing segment refers to mechanical interlocking bond failure due to the splitting cracks along the embedded strips where the maximum slippage is $\beta\delta_u$. The last segment represents the residual bond strength and is almost horizontal.

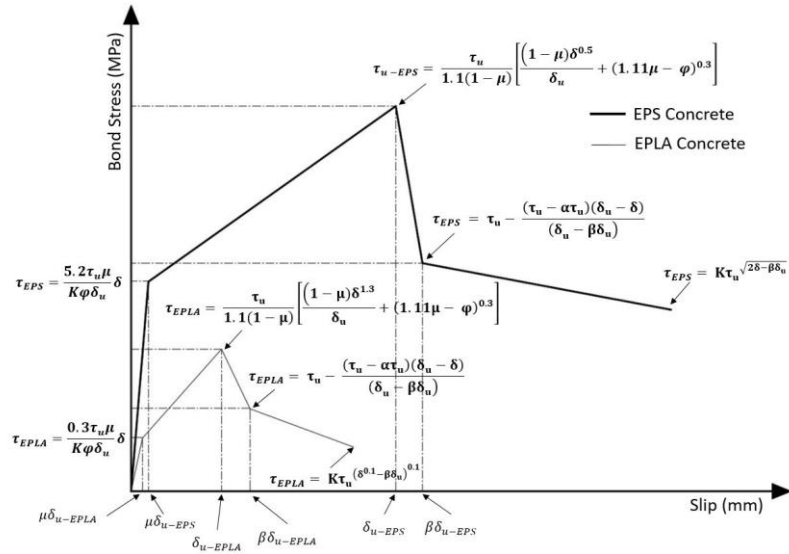


Figure 9. 9 The bond stress-slip model for EPS and EPLA concrete.

The presented model is developed based on the critical parameters compressive strength, f_c , strip thickness, t_s , embedded length of strip, l_e , embedded area, A_e and locking area, A_c .

$$\tau = \begin{cases} \frac{\tau_u \mu}{0.7\phi\delta_u} \delta, & 0 \leq \delta \leq \mu\delta_u \\ \frac{\tau_u}{1.1(1-\mu)} \left[\frac{(1-\mu)\delta}{\delta_u} + (1.4\mu - \phi) \right], & \mu\delta_u < \delta \leq \delta_u \\ \tau_u - \frac{(\tau_u - \alpha\tau_u)(\delta_u - \delta)}{(\delta_u - \beta\delta_u)}, & \delta_u < \delta \leq \beta\delta_u \\ K\tau_u \sqrt{2\delta - \beta\delta_u}, & \delta > \beta\delta_u \end{cases} \quad [9.2]$$

Where

$$\mu = \frac{\sqrt{L_e t_s^{0.2 + \frac{1}{t_s}}}}{2.2 \sqrt{(A_e - A_c)}}$$

$$\varphi = \frac{2.5 \ln(L_e)}{\sqrt{(A_e - A_c)}}$$

Where, τ_u is ultimate tensile stress (MPa), δ_u is ultimate displacement (mm), L_e is embedded length of strips (mm), t_s is strip thickness (mm), A_e is strip embedded area (mm^2), A_c is locking area of embedded strips (mm^2), $K = 0.55$, $\alpha = 0.05$, $\beta = 1.20$.

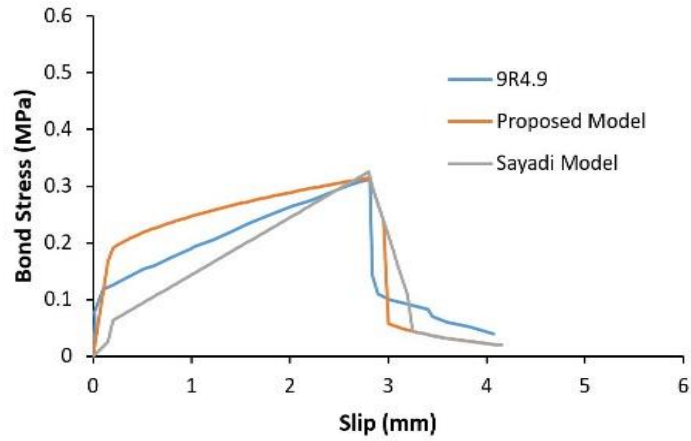
In the case of EPS and EPLA concrete, some modifications are suggested of the defining parameters of the recommended bond model for EPS (Eq. 9.3) and EPLA (Eq. 9.4).

$$\tau_u = \begin{cases} \frac{5.2 \tau_u \mu}{K \varphi \delta_u} \delta, & 0 \leq \delta \leq \mu \delta_u \\ \frac{\tau_u}{1.1(1-\mu)} \left[\frac{(1-\mu) \delta^{0.5}}{\delta_u} + (1.11\mu - \varphi)^{0.3} \right], & \mu \delta_u < \delta \leq \delta_u \\ \tau_u - \frac{(\tau_u - \alpha \tau_u)(\delta_u - \delta)}{(\delta_u - \beta \delta_u)}, & \delta_u < \delta \leq \beta \delta_u \\ K \tau_u \sqrt{2\delta - \beta \delta_u}, & \delta > \beta \delta_u \end{cases} \quad [9.3]$$

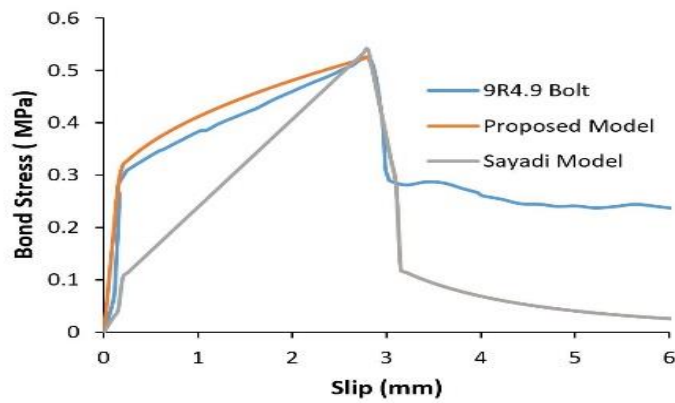
$$\tau_u = \begin{cases} \frac{0.3 \tau_u \mu}{K \varphi \delta_u} \delta, & 0 \leq \delta \leq \mu \delta_u \\ \frac{\tau_u}{1.1(1-\mu)} \left[\frac{(1-\mu) \delta^{1.3}}{\delta_u} + (1.11\mu - \varphi)^{0.3} \right], & \mu \delta_u < \delta \leq \delta_u \\ \tau_u - \frac{(\tau_u - \alpha \tau_u)(\delta_u - \delta)}{(\delta_u - \beta \delta_u)}, & \delta_u < \delta \leq \beta \delta_u \\ K \tau_u (\delta^{0.1} - \beta \delta_u)^{0.1}, & \delta > \beta \delta_u \end{cases} \quad [9.4]$$

Sayadi et al. have studied the bond behaviour of galvanised strips in foamed concrete with different locking areas, locking patterns and foamed concrete densities. Based on their experimental results, the influence of compressive strength and locking key were significant. The proposed model of bond stress-slip of their work was used as a comparison for the modified model. A correlation between the proposed model and experimental results was made to validate the suggested modified bond model. The

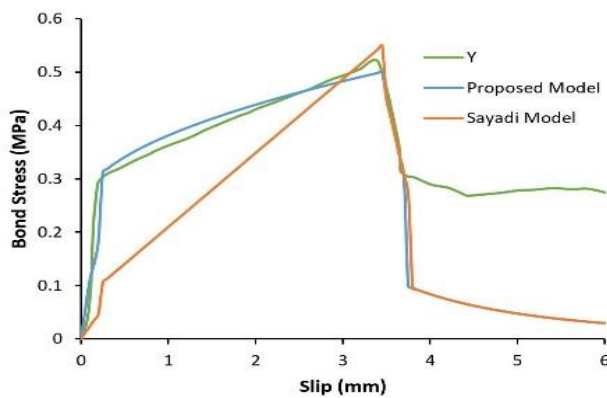
revised model presents a good correlation with experimental results of pull-out tests especially for concrete containing EPLA beads compared to the proposed model by Sayadi et al. [139, 140] (Figure 9. 10 and Figure 9. 11).



(a)

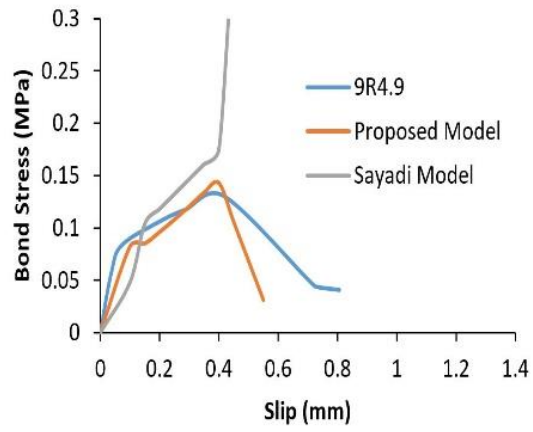


(b)

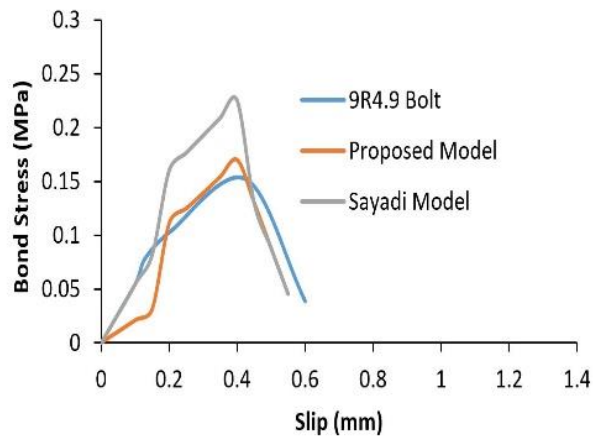


(c)

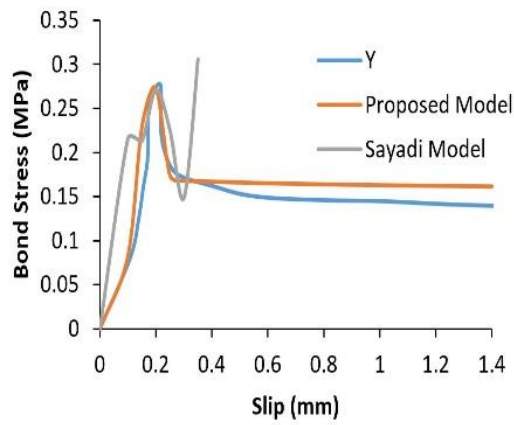
Figure 9. 10 The comparison between the experimental results, new proposed model and proposed model by Sayadi et al. [140] for EPLA concrete; (a) sample 9R4.9, (b) sample 9R4.9 Bolt, (c) sample Y.



(a)



(b)



(c)

Figure 9. 11 The comparison between the experimental results, new proposed model and proposed model by Sayadi et al. [140] for EPS concrete (a) sample 9R4.9, (b) sample 9R4.9 Bolt, (c) sample Y.

9.4 Conclusions

This study focused on the bond properties of concrete containing EPLA as an eco-friendly replacement for EPS aggregate. Based on the assessment of bond properties of EPLA and EPS concrete carried out in this study, the following conclusions were drawn:

- 1- EPLA concrete samples with a compressive strength of 0.75 MPa exhibited splitting bond failure where the EPS concrete samples failed by pull-out failure as a result of higher compressive strength and better interfacial bond strength at the transition zone of aggregate to paste.
- 2- The parameters such as concrete compressive strength, locking area at the elastic and inelastic zone, and locking patterns significantly affect the bond performance and its failure modes.
- 3- A greater effect of locking keys was found in the samples with smaller bottom locking angle and larger locking length.
- 4- The tensile bond stress of concrete containing EPS during pull-out failure was about 57% higher compared to the corresponding EPLA concrete which experienced concrete splitting failure.
- 5- The use of a larger locking area at the elastic zone of embedded strips gave lower bond strength due to the decrease in interaction area between concrete and strips.
- 6- Regardless of concrete compressive strength, a more significant bond strength was observed in the samples with a larger locking area in the inelastic zone, longer locking key length and smaller locking angle.
- 7- The failure modes of concrete changed from pull-out failure to concrete splitting failure as the EPS aggregate was replaced with EPLA aggregate due to the chemical reactivity of EPLA.
- 8- The EPS concrete with a compressive strength of 1.2MPa had a higher bond strength than EPLA concrete without any visible splitting cracks.
- 9- A modified bond-slip model gave a good approximation of the experimental bond stress-slip curves of EPS and EPLA concrete.
- 10- A new method is developed to estimate the elastic and inelastic length of embedded components.

10.1 Introduction

This chapter presents results of an experimental study of flexural strength of cold-formed channel and box section beams encasing bio- and petro-chemical polymer lightweight concretes. Three different concrete types of perlite concrete (PC), perlite-EPS concrete (PEC) and perlite-EPLA concrete (PPC) were used to establish the influence of mechanical properties of braced materials on the load-bearing capacity of beams. In total, sixteen beam specimens with variations in encased concrete and beam cross-sectional area were prepared and tested through four-point bending. A significant improvement in load carrying capacity of the channel beams was observed as the steel core was filled with lightweight concrete. This trend was much lower in the box section beams. The bracing of beams with lightweight concrete restrained the global and distortional buckling modes of beams. However, the influence of bracing properties on the load carrying capacity of the beams was minimal, its effect on lateral torsional buckling was significant. The PPC sample shows the lowest load carrying capacity in both channel and box section beams due to the alkaline reactivity and shrinkages of EPLA particles in the alkaline environment of cement. A set of equations are proposed to predict the load-displacement behaviour of the proposed composite beams.

10.2 Experimental program

10.2.1 Sample preparation and test set-up

Three different concrete mixtures were prepared as filler and bracing components for cold-formed profiles with a variation in aggregate types (Table 10. 1). The mix design was targeted to attain a density of 500 kg/m³ for the sample containing 100% perlite aggregate concrete (PC) according to a proposed method by Sayadi et al. [22, 186]. In other mixtures, EPLA-perlite concrete (PPC) and EPS-perlite concrete (PEC), the perlite aggregate was replaced with EPLA and EPS aggregate at 70% by aggregate volume. The water-cement ratio was kept at 0.343 as in [22, 186]. The density, compressive strength

and tensile strength of the proposed concretes were evaluated with a standard cylinder of 100x200 mm as per ASTM [176-178]. The flexural strength of concrete was measured on prisms 500x100x100 mm as per ASTM [218]. The entire experimental tests were done after 28 days of curing.

Table 10. 1 Mix proportions of perlite and perlite-EPLA concrete.

Mix No.	Mix proportion (kg/m ³)						
	Effective w/c* ratio	C	W	EP	EPLA	EPS	AE
Perlite Concrete (PC)	0.343	310	350	135	-	-	0.0041
EPS-Perlite Concrete (PEC)	0.343	310	193.5	40.5	-	7.0	0.0041
EPLA-Perlite Concrete (PPC)	0.343	310	193.5	40.5	13.3	-	0.0041

w/c: water-cement ratio, C: Cement, W: Water, EP: Expanded perlite, EPLA: Expanded poly-lactic acid, EPS: Expanded polystyrene, AE: Air entraining agent.

The experimental study comprises of 16 quasi-static bending tests with various cross-sections and filler types to evaluate the stability behaviour of the proposed beams. The samples were subjected to two point loads at a rate of 1 mm/min by an INSTRON 33R4469 tester. An additional experiment was done on a control sample without filler as a reference. The experiments were split into two groups according to the cross-sections of the profile. Two types of cross-sections namely channel and box with height (h), width (b) and thickness (t) of 85 mm, 40 mm and 0.75 mm were tested. The box section was built up by two lipped channel sections, which were connected at the flanges with no joining component. The thickness of the box flange (t^ˆ) was 1.5 mm due to the overlapping of channel flanges to make a box section (Figure 10. 1a). The main reason for no joining screws was to assess the effectiveness of the filler as a holding component. The total length of the beams was 1000 mm for all samples with a constant moment region length of 300 mm.

The schematic test setup of the quasi-static bending is shown in Figure 10. 1b. The two load transferring points were placed at a distance of 300 mm and 600 mm from the support to provide a constant moment region between the applied point loads. The side surface of the beams at the middle span was equipped with two strain gauges. The strain gauges were bonded longitudinally (S.G.x) and tangentially (S.G.y). A linear variable differential transformer (LVDT) was used to assess the beam deflection at mid-span as shown in Figure 10. 1b. The load was applied at a displacement rate of 0.1 mm/s until it reached the maximum load carrying capacity and experienced the unloading stage where excessive deformation took place. No restriction was applied at both supports for the beams to easily follow the local and global deformations, which leads to having a better understanding of the effectiveness of the infill concrete on controlling the lateral buckling and rotation of the beams and their failure modes. It worth to note that the average results of three specimens were considered to evaluate the flexural performance of proposed cold formed beams.

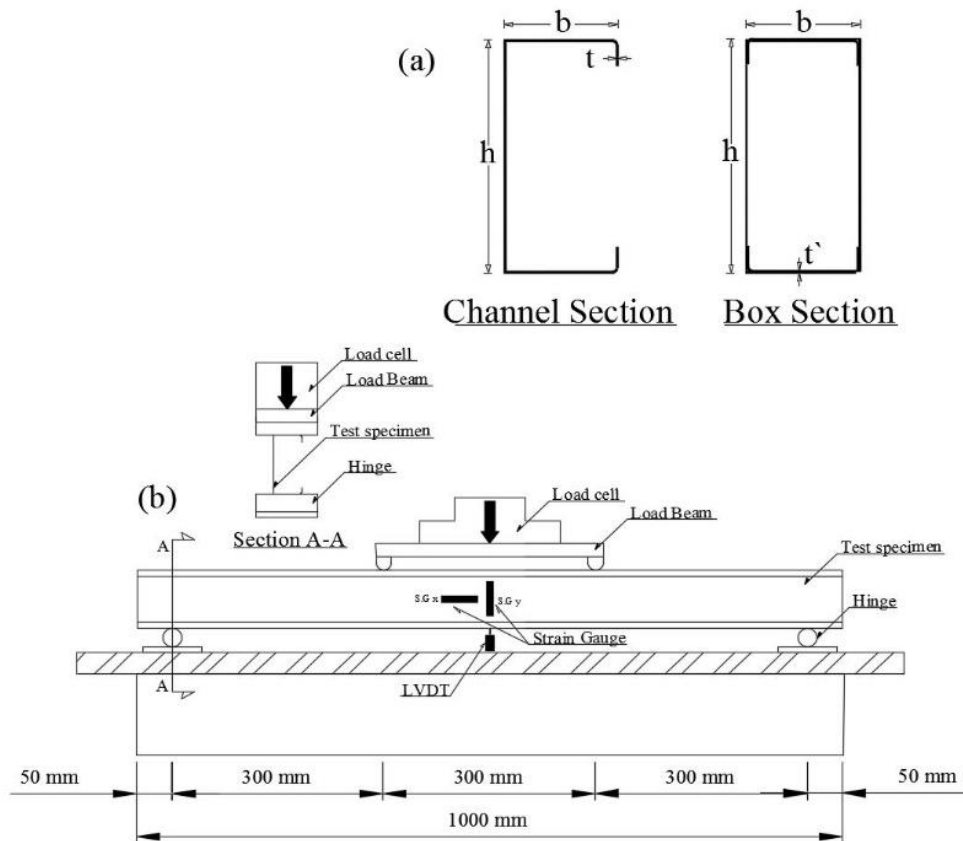


Figure 10. 1 Test setup; (a) cross-section, (b) bending test.

10.3 Experimental results and discussion

10.3.1 Mechanical properties of infill concrete

The mechanical properties of the proposed concretes with a variation in aggregate types and polymer volume are presented in Table 10. 2. The density of lightweight concrete mostly depends on the bulk density of lightweight aggregate and the cement content. In total three different ranges of concrete density were obtained in perlite concrete (PC), perlite concrete containing EPLA (PPC) and EPS (PEC) aggregate. The average dry densities of the concretes were 521.0 kg/m³, 384.0 kg/m³ and 360.0 kg/m³ for PC, PEC and PPC concrete, respectively. The replacement of perlite aggregate with EPLA and EPS particles results in a reduction of 26% and 31% in unit weight of concrete, respectively. The test results show that the density of EPLA concrete is lower than that of EPS concrete, while the relative density of EPS beads (10 kg/m³) is about half the one of EPLA beads (19 kg/m³). The changes in concrete density can be attributed to the chemical reactivity of EPLA and its chemical reaction with the alkaline components of cement. The PPC concrete reveals the lowest density as a result of an increase in concrete porosity due to EPLA degradation and an increase in CO₂ concentration.

As expected, the compressive strength was found to decrease with an increase in the polymer particles ratio mainly due to the almost zero strength of the particles and an increase in concrete porosity. The compressive strength of concrete decreased by 64% and 89% as the EPS and EPLA particles replaced perlite aggregate. The compressive strengths of PC, PEC, and PPC concrete were found to be in the range of 3.1-3.7 MPa, 0.95-1.50 MPa and 0.33-0.42 MPa, respectively. The same trend of strength reduction was observed in the tensile strength and flexural strength of concrete. It is worth noting that the significant reduction of mechanical properties of PPC concrete is directly related to the alkaline reactivity of EPLA, bond failure at the interfacial transition zone (ITZ) and changes of the microstructure of concrete. In addition to this, the existence of large voids due to shrinkage and degradation of EPLA along with the conversion of hydration products due to alkaline reactivity results in the concrete to fail at much lower stresses. In general the degradation of EPLA takes place because of an attack by the external elements [198]. Factors such as stereochemistry, crystallinity and molecular weight significantly affect the biodegradation behaviour of EPLA [199]. In this investigation the

surface of EPLA was in contact with an alkaline component of cement. The EPLA lost its hydrophobicity and started to take up water.

Table 10. 2 Mechanical properties of infill materials

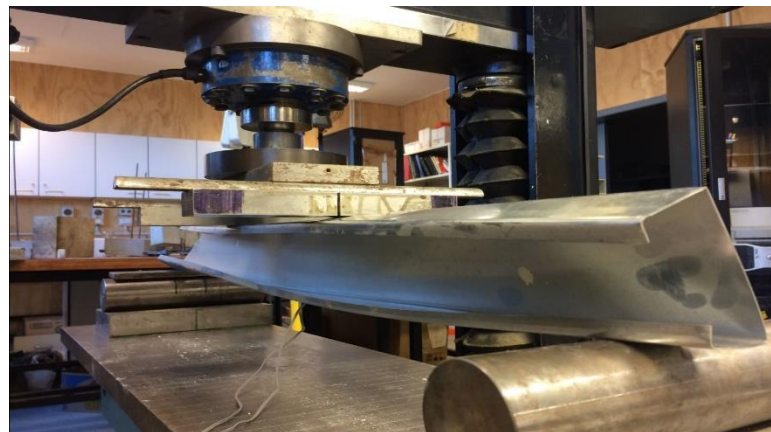
	Bulk density (kg/m³)	Compressive Strength (MPa)	Tensile Strength (MPa)	Flexural Strength (MPa)
PC	521.0	3.35	0.88	1.12
PEC	384.0	1.20	0.05	0.51
PPC	360.0	0.37	0.03	0.25

10.3.2 Bending tests

10.3.2.1 Channel section

10.3.2.1.1 Failure modes

The failure modes of filled and unfilled channel sections subjected to bending forces are shown in Figure 10. 2. The flexural behaviour of a channel section and its failure modes largely depend on the infill materials. The failure modes of a reference sample with no filling materials were completely different to the composite beams. Deformations of the compressed flange and web at the mid-span along with a significant lateral torsional deformation were observed as primary failure modes of the control sample.



(a)



(b)



(c)



(d)

Figure 10. 2 Failure modes of channel sections under bending force, (a) control sample, (b) filled with perlite concrete, (c) filled with EPLA concrete, (d) filled with EPS concrete.

The composite samples are showing a different failure mode along with lower deformation due to the bracing action of the lightweight infill concrete. The infill materials caused a significant reduction in shear buckling of the web and transferred the buckling failure from the middle of the sample to the load transferring points. The excessive deformation of the composite samples caused crack propagation at the shear span region. The largest amount of shear cracks was observed in samples filled with PPC concrete due to its low mechanical properties and brittle behaviour. In addition, the alkaline reactivity of EPLA and cement paste causes EPLA shrinkage and bond failure at the interfacial transition zone of the aggregate-paste and crushing of concrete at a much lower stress level. In addition to this, the cracks also appeared in the load transmitting zone as results of larger localized deformations of the beam. Other samples filled with EPS concrete and perlite concrete showed similar failure modes with lower shear cracks at the shear span zone. The experimental results demonstrate that the differences between the flexural stiffness of filled and unfilled channel sections are significant. The load carrying capacity of a channel section increased by 3 to 4 times as the channel section was filled with concrete. It is also evident that a greater resistance exists along with a smaller area experiencing local buckling of the web due to a bracing action of lightweight concrete and an increase in the effective cross-section of the beam. In addition, greater lateral torsional bulking was observed in the control sample due to the absence of resisting components against channel deformation (Figure 10. 3). In fact, the great influence of the filler concrete was observed at the post-ultimate strength behaviour of the sample, which decreased the steel core deformation.

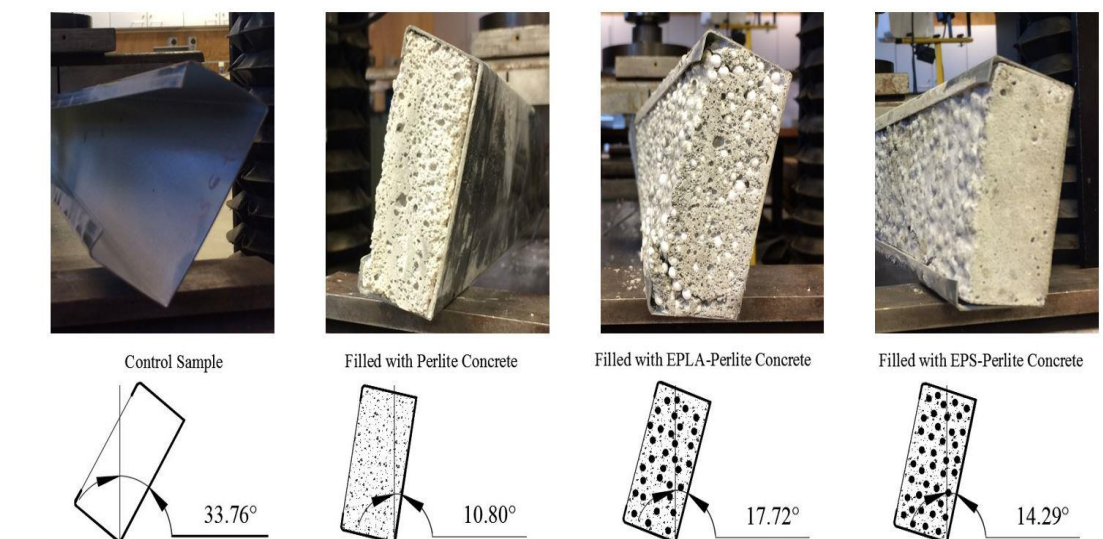


Figure 10. 3 The effect of infill materials on lateral torsional bulking of channel sections

10.3.2.1.2 Load-displacement response

Figure 10. 4 presents the load-displacement curves of the control and composite cold-formed steel beams. The results reveal that the samples filled with lightweight concrete exhibited a much higher ultimate load capacity than the control sample due to a reinforcing action of the infill concrete. In fact, the lightweight concrete controls the excessive deformations of cold-formed beams. The control sample showed an ultimate tensile capacity of 1.25 kN, which is much lower than that of the composite beams. The maximum load carrying capacity of cold-formed beams filled with PEC, PPC and PC concrete was over 5, 4 and 4.5 times higher than that of the control sample. As detected from the reference sample and PEC sample, the load carrying capacity of beams enhanced from 1.25 kN to 5.94 kN when the PEC concrete was used as bracing filler for channel beams. The same trend was observed in the samples PPC and PC.

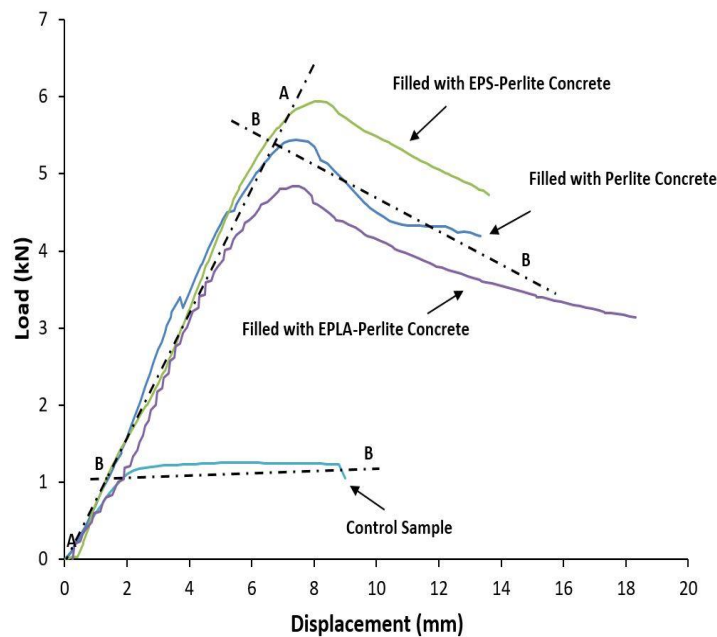


Figure 10. 4 Load-deflection curves of channel sections subjected to bending

It can be found that the increase in cross-sectional area using lightweight concrete can significantly decrease the distortional buckling of a beam and counts as a proper method of increasing the flexural stiffness of cold-formed channel beams. In addition, the results show that the mechanical properties of lightweight concrete as bracing components have minor effects on the ultimate load carrying capacity. The load carrying capacity of cold-formed beams containing perlite concrete with a relative density and compressive

strength of 521.0 kg/m³ and 3.35 MPa was about 9% lower than that of EPS concrete with a relative density and compressive strength of 384.0 kg/m³ and 1.20 MPa, respectively. The highest load carrying capacity and lowest shear cracks were observed on PEC samples due to the compressible behaviour of EPS aggregate and greater deformability. The PPC composite beams showed the lowest strength among the other samples due to the detachment and shrinkages of EPLA aggregate as a result of its chemical reactivity in the alkaline environment of cement.

The ductility of the filler concrete significantly effects the stability of the composite beams. The PC and PPC concrete failed in a more brittle way compared to EPS concrete. Compared to PEC concrete the load carrying capacity of beams decreased by 10% and 23% with the inclusion of perlite and PPC concrete as bracing components of channel beams. Although, the application of lightweight concrete as filler causes an increase in load carrying capacity, its influence on the overall weight of a section is significant. The inclusion of PEC, PC, and PPC concrete causes an increase of 158%, 116% and 109% of total weight of a channel section, respectively. However, the improvement in flexural strength of composite beams was much higher than the increase in section weight. The highest strength to weight increment of 3.23 was observed in channel beams filled with PEC concrete. This improvement was 2.12 and 2.62 times for a channel filled with PC and PPC concrete, respectively (Table 10. 3). Thus, the application of lightweight filler as a bracing material for composite members under a bending force is an effective method to increase member stiffness due to the decrease in torsional buckling.

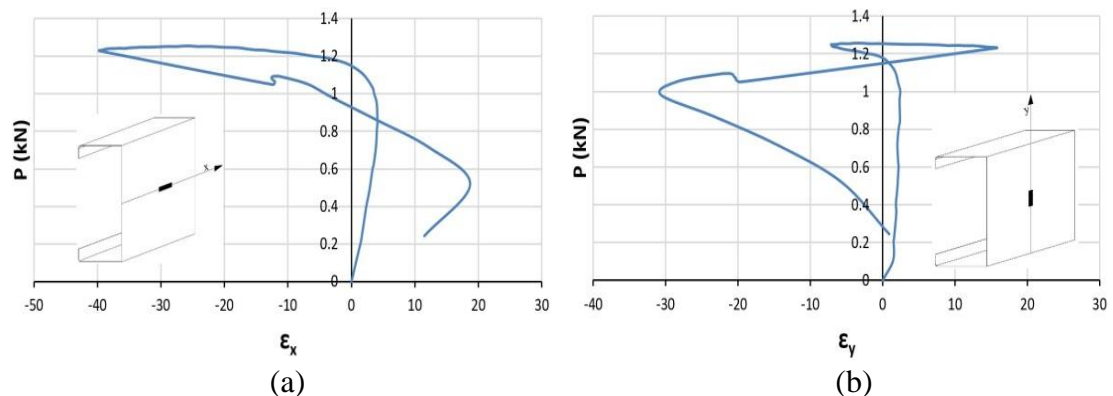
Table 10. 3 The section weight and maximum load capacity of channel sections

		Section Weight (kg)	Ultimate Load (kN)	Increment (%)		Ultimate Load Increment (%) / Section Weight Increment (%)
				Section weight	Ultimate Load	
Channel Section	Ref.	1.120	1.25	0	0	0
	PC	2.905	5.43	158	335	2.12
	PEC	2.440	5.94	116	375	3.23
	PPC	2.360	4.83	109	286	2.62

10.3.2.1.3 Load-strain response

Figure 10. 5 shows the strain evolution in longitudinal and tangential directions of beams as a function of applied load. The strain gauges SGx and SGy are placed at the constant moment region of the profile to record the strain in longitudinal and tangential directions. All the readings of strain gauges positioned in the longitudinal direction of the beams showed similar trends during the loading stage except for the sample filled with EPS concrete due to the more compressible behaviour of EPS concrete with its gradual failure. Also, a non-uniform tangential strain was observed in samples filled with EPLA-perlite and perlite concrete due to the brittle behaviour of the infill concrete which causes significant changes in the strain development of the sample.

A strain of -40, 22, 78, and 6.5 was measured as the maximum tensile strain of the control sample, PC, PEC and PPC at the maximum load level, respectively. The tensile strain converted to compressive strain soon after it reached the maximum capacity due to the buckling and deformation of the web. However, this trend was different in the control sample. The maximum compressive strain of -6.5, -0.17, 6 and -0.055 was observed for the control sample, PC, PEC and PPC at the ultimate load level, respectively. From these results, it can be found that the maximum strain is significantly varied at the proposed samples. The deformation of cold formed steel and crushing of concrete leads to changes in strain development. Based on experimental results, the cold formed steel channel filled with PEC concrete causes a delay in section deformation and distortion buckling and remains in the elastic stage at much higher strain values compared with other samples. Although the mechanical properties of infill concrete are small compared with steel, it significantly affects the strain development and deformability of composite beams.



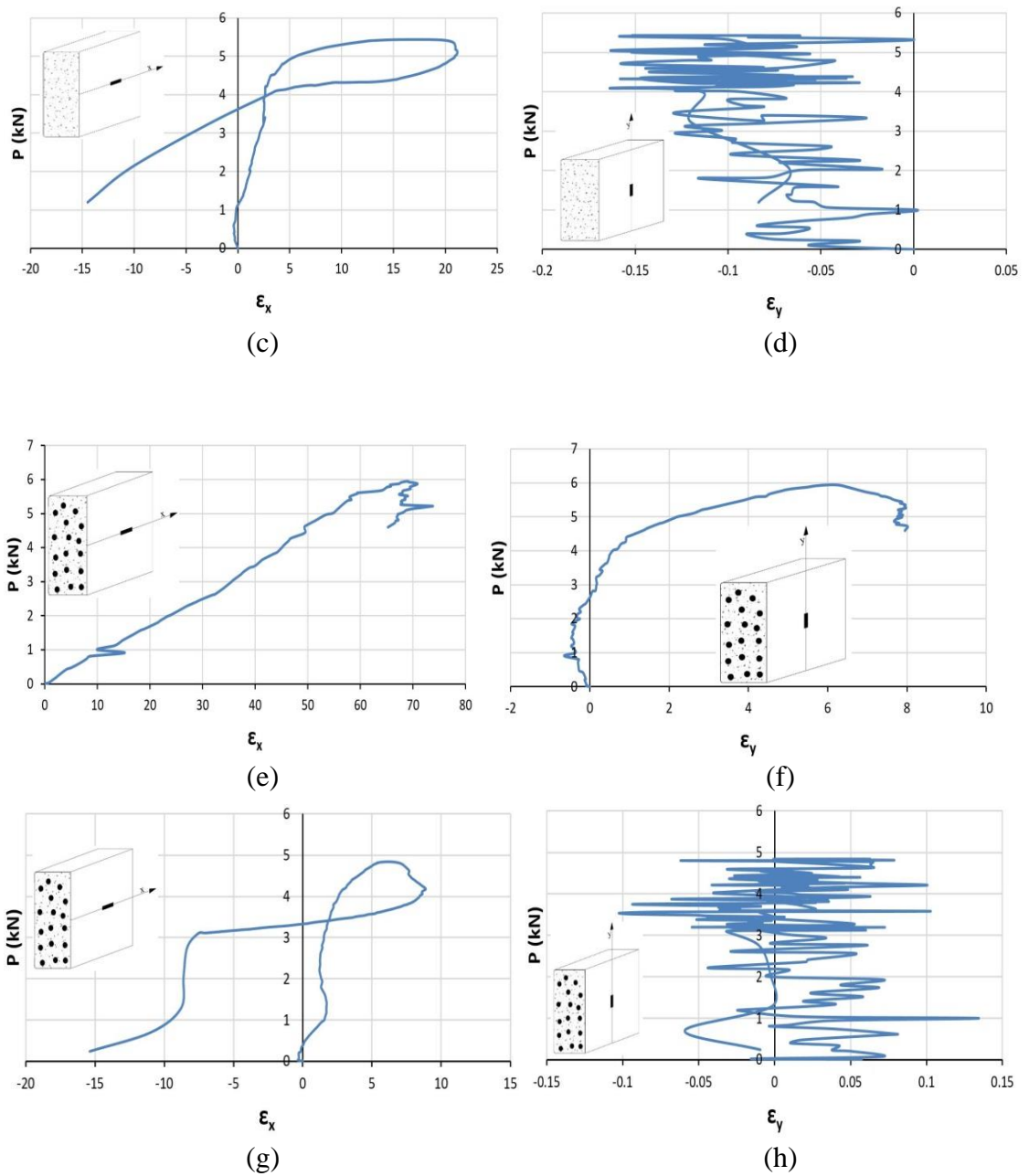


Figure 10. 5 Load-strain curves obtained from the strain gauges placed at the middle of channel beams; (a) Ref. in X direction, (b) Ref. in Y direction, (c) PC in X direction, (d) PC in Y direction, (e) EPS in X direction, (f) EPS in Y direction, (g) PLA in X direction, (h) PLA in Y direction.

10.3.2.2 Box section

10.3.2.2.1 Failure modes

Figure 10. 6 shows the failure modes of the tested control and composite box section beams. The experimental results show that the composite beams follow the same path of failure when subjected to bending stress. The simply supported composite box section beams mostly failed due to compressed flange distortion and buckling of the web at the constant moment region and bearing failure under the two load transferring points. While no significant plastic deformation was observed in the control sample due to channel profile segregation where no joining screw was used to control the deformation of the connected channels. In the case of composite beams, the application of filler concrete prevents the segregation of box profiles due to the bracing and holding action of the lightweight concrete.

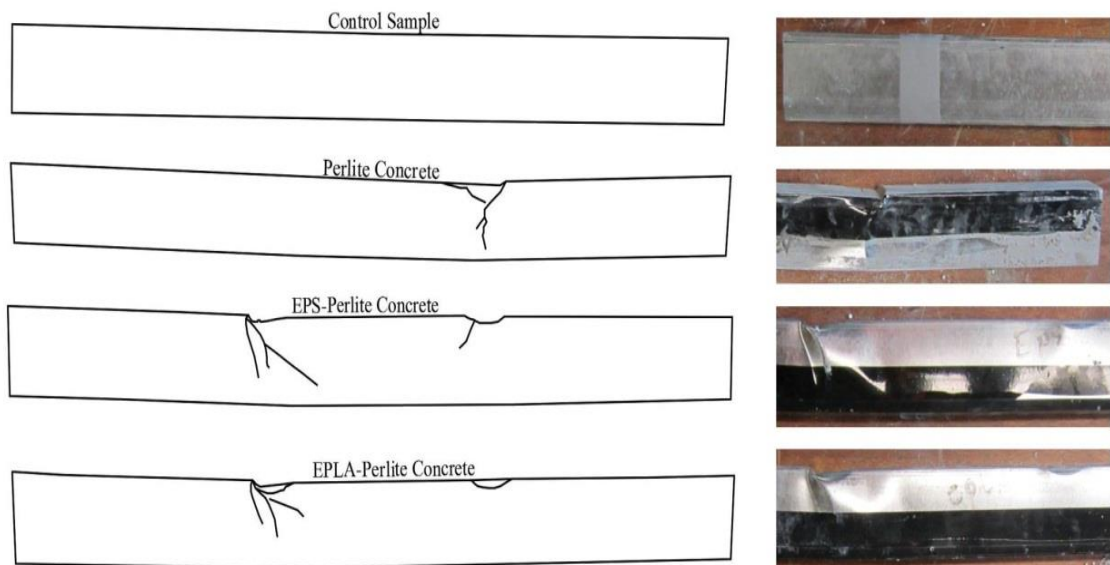


Figure 10. 6 Failure modes of box section beams under bending force.

The PEC composite components failed due to the crumbling of the web and flange under bearing stress with a larger failure zone compared to the other samples (Figure 10. 7a). In fact, the brittle behaviour of PC and PPC concrete leads to sudden changes in beam stiffness, which causes failure occurring at one loading point (Figure 10. 7b). This causes all the plastic deformation and bearing stress to concentrate at the weak point where the sudden concrete crushing happened. However, the failure modes of PC and PPC concrete

samples were almost the same, but the contours of the buckled shape were different. Larger and sharper buckling shape contours were observed on PC samples compared to the PPC ones due to the better bracing action of perlite concrete, which leads to an increase in ultimate load capacity and buckling of the more compressed flange and web. Although the load carrying capacity of composite beams was about 80-100% higher than that of the control sample, the influence of mechanical properties of infill materials on the load carrying capacity of the beam was minimal.



(a)



(b)

Figure 10. 7 Failure modes; (a) profile segregation of control sample, (b) bearing failure of composite beam

10.3.2.2.2 Load-displacement behaviour

The load-displacement curves of the control and composite beams are shown in Figure 10. 8. The strength and flexural stiffness of the beams increased, which was caused by the lightweight filler concrete as a bracing component. The behaviour of the composite beams was more ductile with a lower displacement at the initial stage of loading compared with the control sample. A large initial displacement of the control sample is primarily related to the absence of joining components. The experimental results show that the application of lightweight concrete causes a significant improvement in the load capacity of the box section beams. In fact, the filler materials control and reduce the excessive deformation of the assembled profiles and cause an increase in load carrying capacity of the beams.

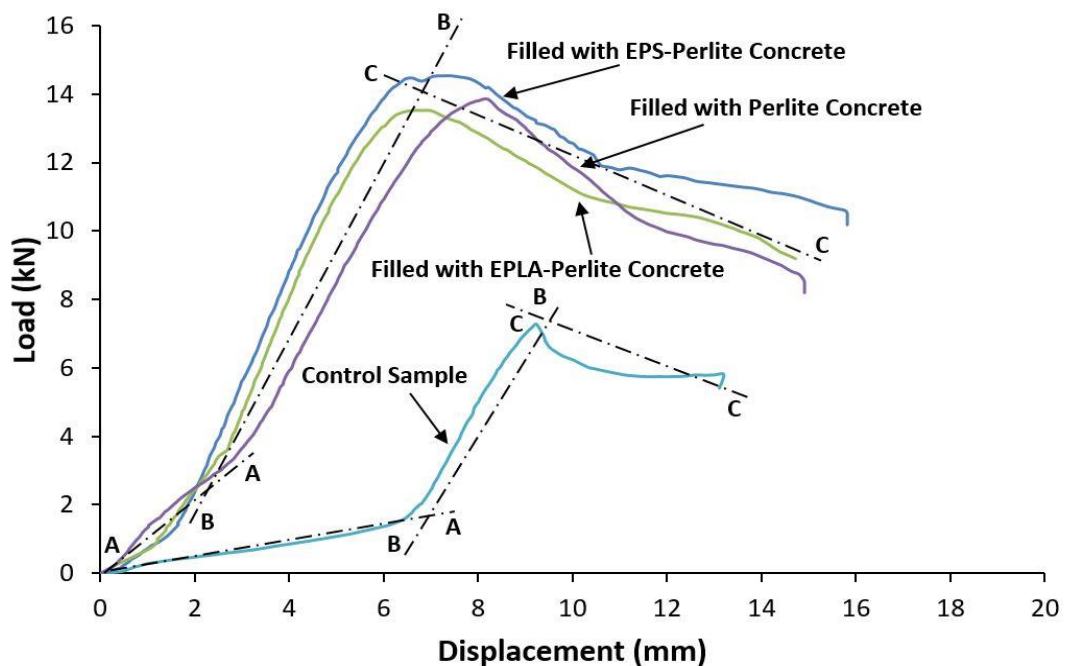


Figure 10. 8 Load-deflection curves of box sections subjected to bending

The highest and lowest load carrying capacity was observed in the PEC and the control sample with a relative maximum amount of 14.52 kN and 7.26 kN, respectively. The same trend of improvement was observed in beams filled with PPC and PC concrete as the load carrying capacity increased by 87% and 91% compared with the control sample. In the case of composite beams, all the samples show an almost identical flexural behaviour and stiffness with a minimal difference in ultimate load capacity. The load

carrying capacity of PC and PPC was about 4 and 6% lower than that of the PEC sample. The primary role of filler materials is to provide a full support against the global and local distortion movements despite their lack of mechanical strength. Thus, the load-bearing capacity of composite beams mainly depends on the cross-section area of the steel section along with its configuration and the contribution by filler materials through bracing and holding the sections together. The strength to unit weight increment of PC, PEC and PPC specimens was 0.91, 1.26 and 1.11, respectively (Table 10. 4). Thus, the influence of filler materials as bracing components of composite beams was more significant in the channel section as the rate of strength development was much higher than that of the box section as a comparison of Table 10. 3 and Table 10. 4 demonstrates.

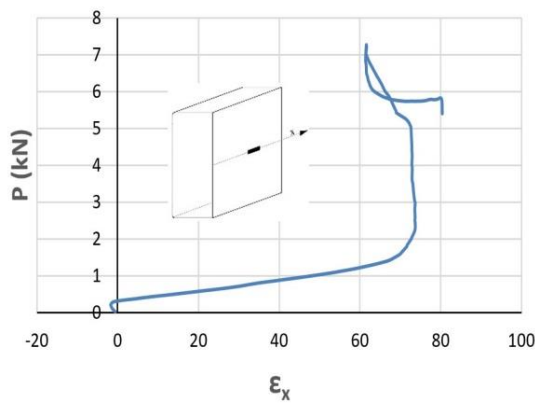
Table 10. 4 The section weight and maximum load capacity of box sections

		Section Weight (kg)	Ultimate Load (kN)	Increment (%)		Ultimate Load Increment (%) / Section Weight Increment (%)
				Section weight	Ultimate Load	
Box section	Ref.	2.265	7.26	0	0	0
	PC	4.530	13.85	100	91	0.91
	PEC	4.050	14.52	79	100	1.26
	PPC	4.045	13.55	78	87	1.11

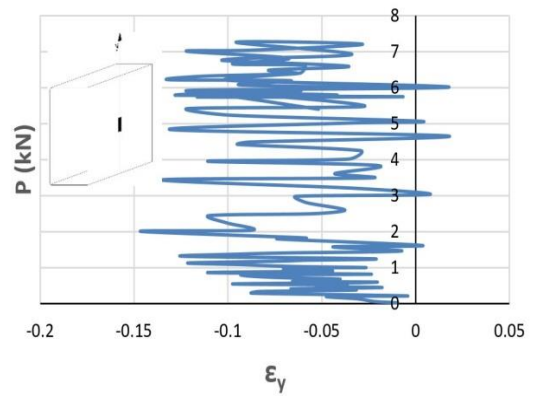
10.3.2.2.3 Load-strain response

The strain behaviour at the web region of the box sections was measured by two strain gauges in longitudinal, S.G.x and tangential, S.G.y direction which were located at the mid-span of the beams. The load-strain curves of the box sections are presented in Figure 10. 9. A non-uniform compression strain was obtained for all samples due to the web buckling and sudden changes in the developed strain during the loading. Two forms of tension strain distributions were recorded. The tension strain distribution of the control and PC sample was the same without any shifting to the compression strain, while the sample PEC and PPC showed a compression strain up to the ultimate load and shifted to tension strain at the de-loading stage due to the lateral deformation of beams. This can be

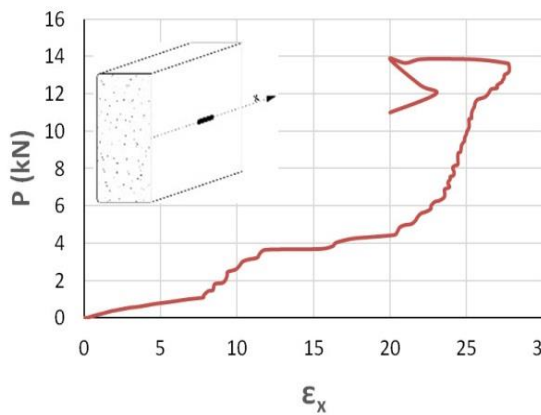
attributed to the failure modes of the beams as a larger area experienced web buckling in composite beams with PEC and PPC. The maximum strain of 62, 26.5, -1.8 and -4.8 along with -0.08, -0.04, -0.06 and -0.07 was measured by the longitudinal and tangential strain gauges at maximum load for the control, PC, PEC and PPC samples, respectively. The bracing of the cold-formed sections with lightweight concrete causes a significant reduction in beam deformation as the measured tension strain of the control sample was about twice the one of the PC sample.



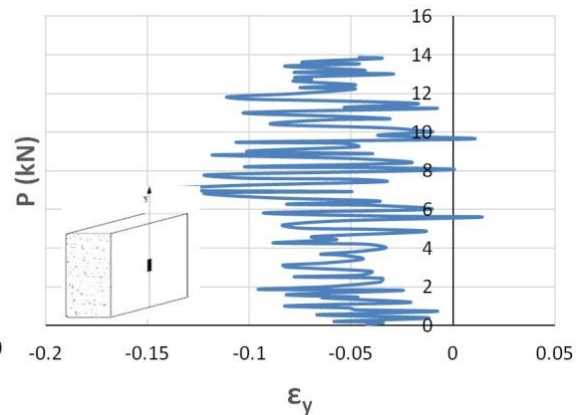
(a)



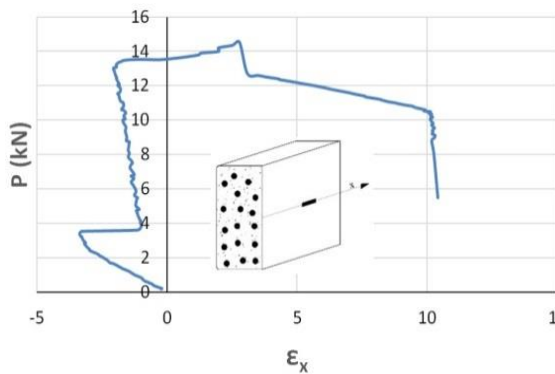
(b)



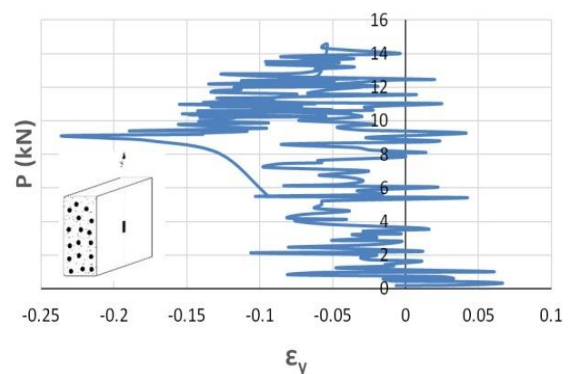
(c)



(d)



(e)



(f)

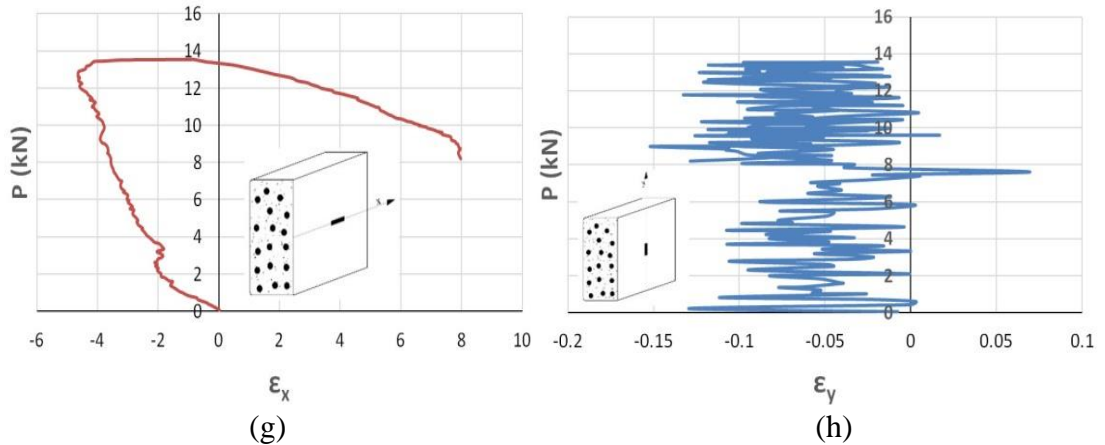
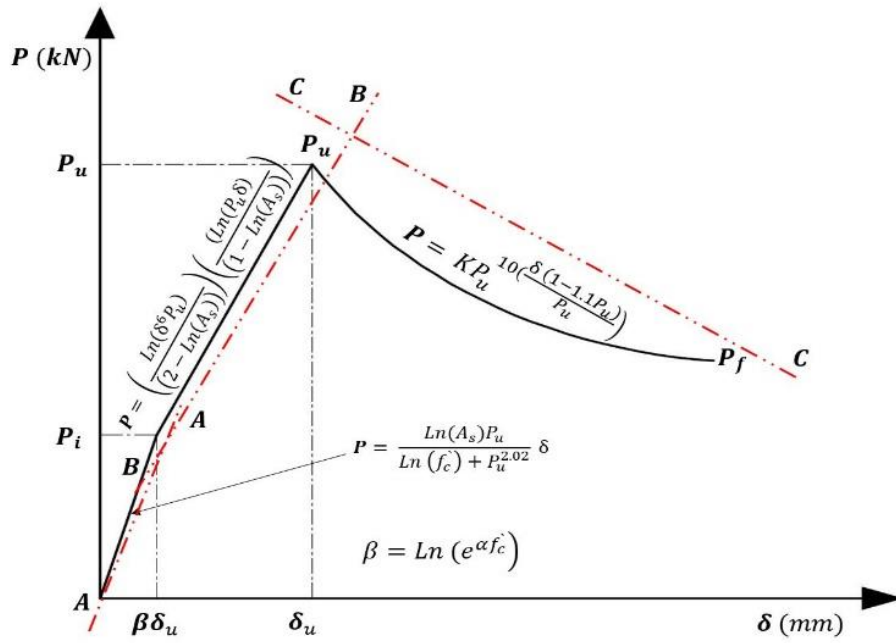


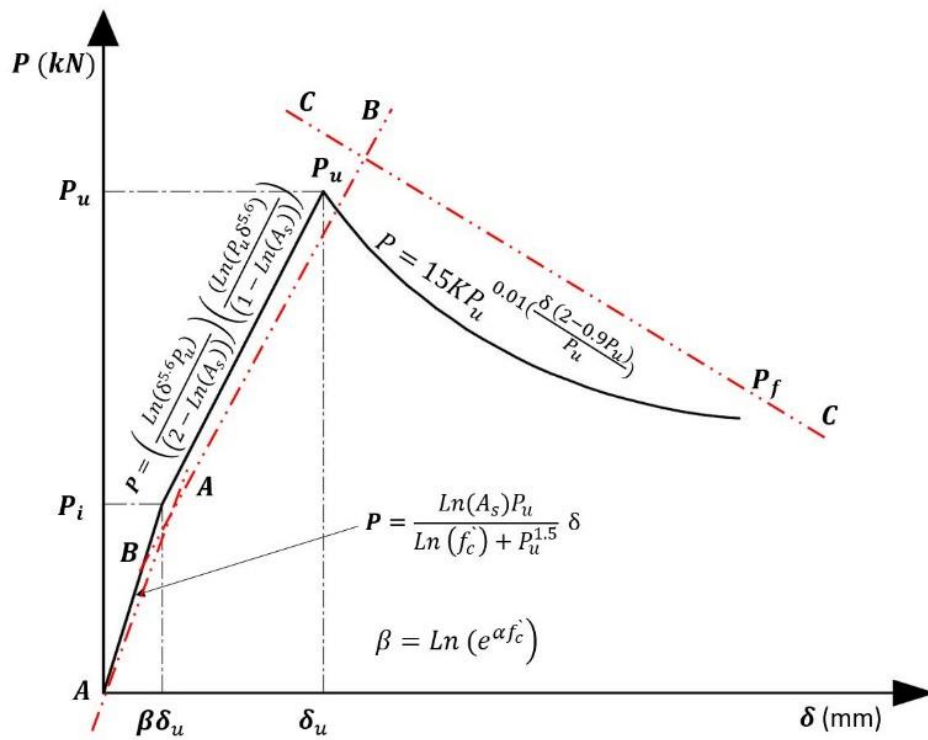
Figure 10.9 Load-strain curves obtained from the strain gauges placed at the middle of box beam; (a) Ref. in X direction, (b) Ref. in Y direction, (c) PC in X direction, (d) PC in Y direction, (e) EPS in X direction, (f) EPS in Y direction, (g) PLA in X direction, (h) PLA in Y direction.

10.3.3 Analytical model

An analytical model has been developed to predict the flexural behaviour of the proposed composite beams for the steel grade G550. The flexural stiffness of channel and box sections is divided into three stages of deformation namely; A-A, B-B, and C-C as shown in Figure 10.10. Two models are built by considering the critical parameters of the flexural performance of composite beams such as the cross-section area of the cold-formed section (A_s) and compressive strength (f_c') of the infill materials. As shown in Figure 10.10, the load-displacement curves are divided into three segments, which exhibit the beam stiffness during loading. The first part (A-A) is related to the concrete cracking and propagation of cracks which shows a linear beam stiffness. The first stage was considered as the distance between the displacement values from zero to $\beta\delta_u$, where β is a factor of concrete strength, f_c' [Eq. 10.1]. The following equations are proposed to predict the load carrying capacity and flexural behaviour of a channel [Eq. 10.2] and a box [Eq. 10.3] section composite beam at this stage.



(a)



(b)

Figure 10. 10 Load-displacement model; (a) channel section, (b) box section.

$$\beta = \text{Ln}(e^{\alpha f_c}) \quad [10.1]$$

Where,

		PC	PEC	PPC
α	Channel section	1.40	4.0	11.6
	Box section	0.89	1.36	7.25

$$P = \frac{\text{Ln}(A_s)P_u}{\text{Ln}(f_c) + P_u^{2.02}} \delta, \quad (0 \leq \delta \leq \beta\delta_u) \quad [10.2]$$

$$P = \frac{\text{Ln}(A_s)P_u}{\text{Ln}(f_c) + P_u^{1.5}} \delta, \quad (0 \leq \delta \leq \beta\delta_u) \quad [10.3]$$

Where, f_c is compressive strength of concrete (MPa), A_s is cross-section area of cold-formed steel beam (mm^2), P_u is ultimate load capacity (kN), δ is relative displacement (mm).

As the load increases, the slope of the load-displacement diagram decreases in the second part (B–B) as a result of (a) concrete failure and (b) beam deformation. At this stage, the beam behaves linearly up to the ultimate load. The displacement ranges of $\beta\delta_u < \delta \leq \delta_u$ is assumed as a second elastic segment. The following equations are proposed to predict the ultimate load capacity, and load-displacement behaviour of the channel [Eq. 10.4] and the box [Eq. 10.5] section beam at the second stage of loading.

$$P = \left(\frac{\text{Ln}(\delta^6 P_u)}{(2 - \text{Ln}(A_s))} \right) \left(\frac{\text{Ln}(P_u \delta)}{(1 - \text{Ln}(A_s))} \right), \quad (\beta\delta_u < \delta \leq \delta_u) \quad [10.4]$$

$$P = \left(\frac{\text{Ln}(\delta^{5.6} P_u)}{(2 - \text{Ln}(A_s))} \right) \left(\frac{\text{Ln}(P_u \delta^{5.6})}{(1 - \text{Ln}(A_s))} \right), \quad (\beta\delta_u < \delta \leq \delta_u) \quad [10.5]$$

Where, A_s is cross-section area of cold-formed steel beam (mm^2), P_u is ultimate load capacity (kN), δ is relative displacement (mm).

The linear behaviour changed to a nonlinear one with relatively large displacements and lower load increments as a result of plastic deformation and post-buckling of the beam. The region of displacements of $\delta > \delta_u$ is considered as the third stage of stiffness (C-C). The Eq. 10.6 and Eq. 10.7 are proposed to predict the plastic behaviour of the beam at the last stage of stiffness for channel and box sections.

$$P = KP_u^{10\left(\frac{\delta(1-1.1P_u)}{P_u}\right)}, \quad (\delta > \delta_u) \quad [10.6]$$

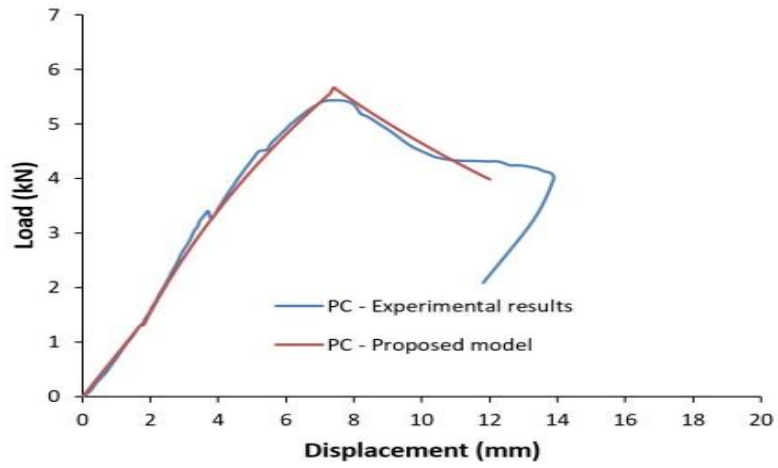
$$P = 15KP_u^{0.01\left(\frac{\delta(2-0.9P_u)}{P_u}\right)}, \quad (\delta > \delta_u) \quad [10.7]$$

Where,

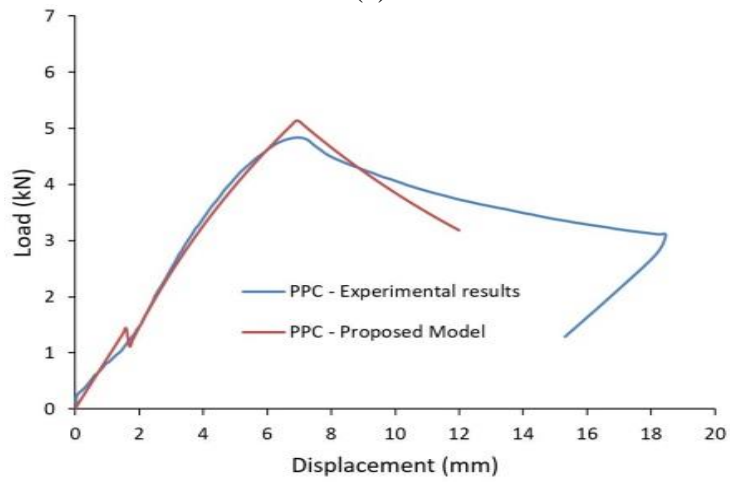
		Perlite Concrete	EPS-Perlite Concrete	EPLA- Perlite Concrete
K	Channel section	0.20	0.18	0.23
	Box section	21.5	19.5	17.5

Where, P_u is ultimate load capacity (kN), δ is relative displacement (mm).

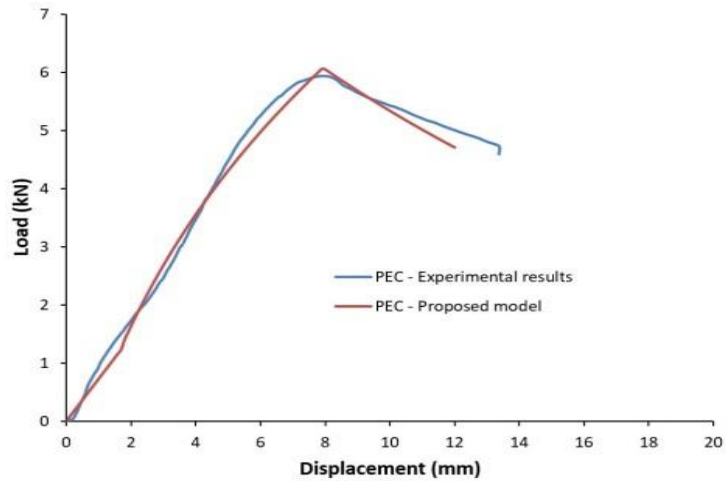
The proposed equations showed a good agreement with experimental test results, which demonstrates the accuracy of the proposed model as can be seen from Figure 10. 11 and Figure 10. 12.



(a)

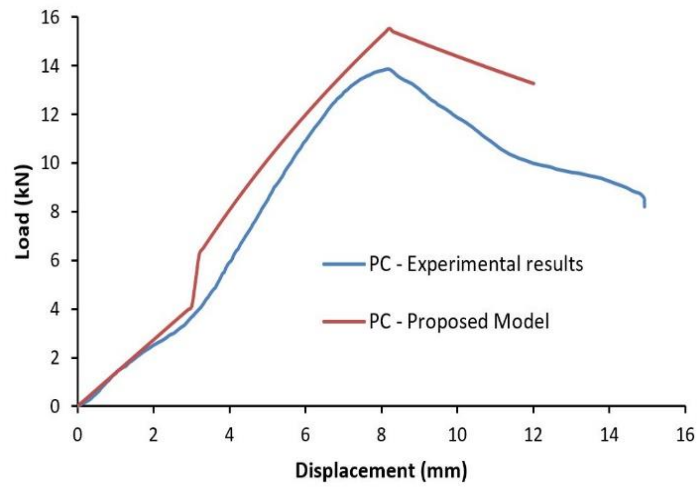


(b)

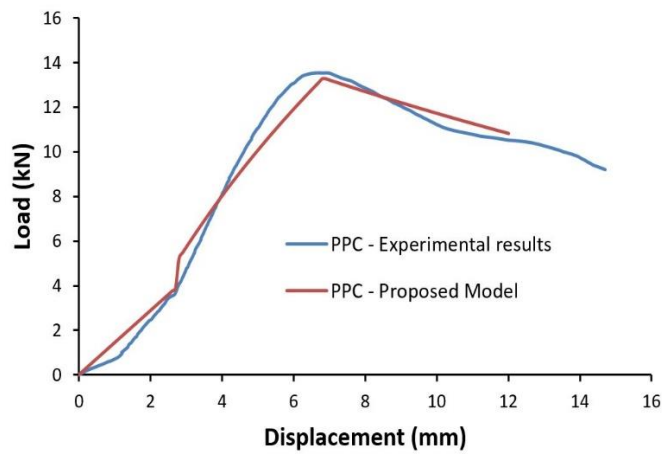


(c)

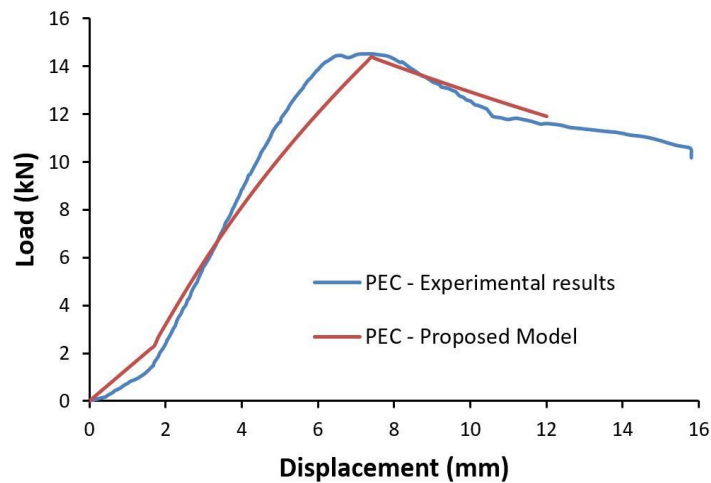
Figure 10. 11 The comparison between load-displacement response of proposed model and experimental results of composite channel section beam; (a) PC concrete, (b) PPC concrete, (c) PEC concrete.



(a)



(b)



(c)

Figure 10. 12 The comparison between load-displacement response of proposed model and experimental results of composite box section beam; (a) PC concrete, (b) PPC concrete, (c) PEC concrete.

10.4 Conclusions

Based on the experimental test results and observed behaviour modes the following can be concluded:

- 1- The distortion, local and global buckling were observed as primary failure modes of unbraced cold-formed steel beams. The samples filled with lightweight concrete were capable of restraining the global deformation and local buckling. The failure modes of channel section beams were changed from lateral torsional buckling to local buckling of the web due to the increase in cross-section area and bracing action of the filler concrete. However, a compressed flange distortion and web buckling under the two load transferring points were the failure modes of the composite box section beams.
- 2- The load carrying capacity of braced channel beams (filled with lightweight concrete) increased up to 5 times compared to unbraced samples, which is mainly attributed to the existence of resisting components against the channel deformation. In fact, the significant influence of bracing materials was found to be in the post-ultimate load behaviour, which is controlled by excessive distortion buckling.
- 3- The effect of mechanical properties of infill concrete on the load carrying capacity of the beams was minimal, and no significant differences were observed based on the full composite action due to the low strength and elastic modulus of lightweight concrete. However, the mechanical properties of concrete mostly affect the degree of lateral torsional buckling as lower torsional buckling was observed in samples filled with PC concrete with a relative compressive strength of 3.35 MPa.
- 4- Larger cracks appear on the shear span of channel beams filled with PPC concrete due to the inelastic behaviour of concrete containing EPLA as a result of its chemical reactivity and changes in microstructure and hydration products. The samples filled with EPS concrete (PEC) showed the better performance and higher ultimate load capacity due to its ductile behaviour compared to PPC and PC concrete.
- 5- The strength increment to unit weight increment ratio of channel and box sections was three and two times greater than that of an unbraced beam. The lower

increment ratio of a box section is mainly related to the increase in the steel cross-section area.

6- The application of lightweight concrete as a bracing component causes a significant delay in section deformation and distortional buckling. This trend leads to the beams remaining in the elastic stage at much higher strain values compared to unbraced samples.

In addition, a set of equations were developed to predict the load-displacement behaviour of infilled beams.

CHAPTER 11

CONCLUSIONS AND RECOMMENDATIONS

11.1 Introduction

The main findings of this study are summarized in this chapter. Recommendations for the design with and for further investigations of the application of expanded poly-lactic acid as a construction material are also given.

11.2 Conclusions

The degradation of poly-lactic acid in the alkaline environment of cement is the main problem facing EPLA aggregate. After a comprehensive study of different types of binders, magnesium phosphate cement was found as a proper binder for EPLA aggregate. Another solution to this problem is coating of EPLA (CEPLA) aggregate with special coating materials. The experimental results of coated EPLA show that the proposed coating is an effective method for using EPLA aggregate in a high alkaline environment. The mechanical properties, thermal properties, electrical properties, fire resistance and phase analysis of expanded poly-lactic acid concrete made with ordinary Portland cement (OPC), ground granulated blast-furnace slag (GGBS) and magnesium phosphate cement (MPC) as binder along with expanded vermiculite (EV) and expanded perlite (EP), and coated expanded poly-lactic acid as aggregate have been studied and presented throughout this thesis. Concrete with expanded polystyrene (EPS) as a lightweight aggregate was used for comparison reasons. The main findings derived from this experimental study are summarised and presented as follows.

11.2.1 Fresh properties of proposed concretes

The workability of lightweight concrete is a vital factor and significantly affects the properties of concrete. Ultra-lightweight concrete is mostly designed to be cast without vibration due to difficulties of compaction and mixture segregation during casting [184]. A slump value of 50-75 mm is suggested for lightweight concrete, but due to the

compaction and segregation problems of ultra-lightweight concrete, a slump value of 220 - 250 mm is adopted for this project. The replacement of perlite or vermiculite aggregate with EPLA or EPS aggregate reduces the workability of concrete due to an increase in specific surface area. It was suggested that the polymer ratio of 70% aggregate volume (30 % perlite or vermiculite – 70% EPLA or EPS) should be taken as the maximum replacement ratio to guarantee a good compaction ratio. A further increase in the polymer ratio results in mix segregation.

As expected the unit weight of concrete decreased with an increase in polymer volume as a result of lower relative density of the polymer aggregate (EPLA and EPS) compared to expanded vermiculite and expanded perlite. The density ranges of perlite and vermiculite concrete containing EPLA and EPS aggregate was varied between 512.85 and 203.2kg/m³. In the case of CEPLA concrete, the lowest density was observed in a sample containing 40% CEPLA aggregate. A further increase in CEPLA volume leads to an increase in concrete density mainly due to the higher specific gravity of CEPLA compared to perlite aggregate. With the identical mix proportion, the density of CEPLA concrete was about 70% and 64% higher than that of EPLA and EPS concrete, respectively.

In the case of magnesium phosphate cement concrete and GGBS concrete the density ranges of 467.7 kg/m³ to 367.0 kg/m³ and 259.6 kg/m³ to 203.2 kg/m³ were obtained at the polymer ratio (EPLA or EPS) of 70%, respectively. It was found that the factors such as w/c and P/M ratio influence the density of magnesium concrete containing EPLA as the increase in w/c ratio causes a decrease in density. An increase in borax content and P/M ratio shows an inverse effect on density.

An increase in calcium oxide content of GGBS concrete as an activator causes a significant reduction on concrete density, due to alkaline reactivity of EPLA with calcium hydroxide and an increase in concrete porosity and CO₂ gas concentration in the matrix.

The density of magnesium phosphate concrete with the same polymer ratio of 70% was about 21% and 18% higher than that of EPLA and EPS concrete containing perlite aggregate, while this trend was inverse in concrete containing CEPLA. The density of CEPLA concrete with an identical polymer ratio was about 40% higher than that of magnesium phosphate concrete. The lowest concrete density was observed in GGBS concrete containing EPLA (30% perlite – 70% EPLA) with relative density of 203.2kg/m³, while the density ranges were higher in cement and magnesium phosphate concrete. With identical mix proportions and polymer ratio, the density of GGBS concrete

was about 81% and 49% lower than that of the magnesium phosphate and cement based concrete, respectively.

11.2.2 Mechanical properties of proposed concretes

The experimental results show that manufacturing of concrete with EPLA aggregate causes significant changes in mechanical properties of concrete. Compared to EPS concrete, a remarkable reduction in compressive strength was observed with inclusion of EPLA beads due to the chemical reactivity of EPLA beads in the alkaline environment of cement. The compressive strength of EPLA and EPS concrete decrease with an increase in polymer ratio due to an increase in concrete porosity and internal voids created by the polymer beads along with close to zero strength of polymer aggregates.

The EPLA lost its strength and shrunk when subjected to the alkaline environment. The shrinkages of EPLA beads cause bond failure at the interfacial transition zone of paste-aggregate. In fact, the existence of large voids due to shrinkage and degradation of EPLA along with the conversion of hydration products due to alkaline reactivity results in the concrete to fail at much lower stresses. The maximum compressive strength of EPLA concrete having a density range of 300-400 kg/m³ was 64% lower than that of the corresponding EPS concrete with the same mix proportion. The failure modes of EPLA concrete were significantly different from the EPS concrete. It is worth noting that the EPLA samples cured in a moist condition showed an even lower compressive strength as moist curing causes an acceleration of EPLA degradation.

In the case of CEPLA concrete, an increase in CEPLA content results in a decrease in compressive strength, however, the rate of strength reduction was much lower than that of EPS and EPLA concrete. The compressive strength of CEPLA concrete was about 349% and 37% higher than that of EPLA and EPS concrete, respectively. A better interfacial bond strength was observed in CEPLA concrete due to the porous structure of the coating layer and penetration of cement paste into the layers of coating materials. In the case of magnesium phosphate concrete, a rapid hardening and high early strength were observed, but this trend starts to decrease after 7 days. The 28 days, 56 days and 90 days compressive strength of magnesium phosphate concrete was about 88%, 77% and 70% of the 7 days strength. It was also found that the compressive strength of concrete depends mostly on the w/c ratio and retarder content. The strength of magnesium

phosphate concrete increased with decreasing the water-cement ratio while increasing the amount of retarder content and magnesium oxide causes an improvement in strength development of concrete. In the case on GGBS concrete, the sample containing a larger amount of calcium carbonate shows the lowest compressive strength due to higher porosity and changes in hydration products of concrete as a results of EPLA degradation. The 28 days compressive strength of GGBS concrete was at the ranges of 0.44 to 0.19 MPa and 1.79 to 0.37 MPa for sample containing EPLA and EPS, respectively.

The tensile strength of concrete containing EPLA aggregate with a density range from 520 to 302 kg/m³ was 8 to 50% lower than that of the corresponding EPS concrete. The failure modes of EPLA concrete were significantly different from the control sample of 100% perlite. The lack of resisting components and the de-bonding of EPLA because of alkaline reactivity were the main reasons for changes in the failure modes of EPLA concrete. The elastic modulus of concrete containing polymer was about 3 times lower than that of the control samples at the polymer volume of 70% aggregate volume. The elastic moduli of perlite and vermiculite concrete were in a range from 900 to 1100 MPa for a corresponding density range of 400 to 500 kg/m³, which is much lower than that of normal concrete of 14 to 41 GPa. The substitution with polymer aggregate causes a significant reduction in the elastic modulus of concrete. Compared to the EPS concrete, the elastic modulus of EPLA concrete was about 30% lower.

There was a fundamental difference in the water absorption ratio of concrete containing EPLA and EPS aggregate. The water absorption of concrete is dependent upon the absorption ratio of lightweight aggregate and the matrix porosity. The initial (after 1 hour) water absorption of concrete containing EPLA and EPS aggregate was much lower than that of control samples without polymers mainly due to the presence of hydrophobic aggregate with a zero absorption ratio. At a later stage and compared to EPS concrete, the water absorption of EPLA concrete increased due to the chemical reactivity of EPLA. The EPLA beads lost their hydrophobicity, started to take up water and shrunk when subjected to the alkaline environment of cement. This trend leads to an increase in concrete porosity as a result of an increase in CO₂ concentration in the matrix.

11.2.3 Thermal properties of proposed concretes

The thermal conductivity of concrete is reduced by the incorporation of polymer aggregate, which is attributed to the thermal properties of the polymer and an increase in

concrete porosity. The difference between EPLA and EPS concrete in this respect is not significant, while this difference was increased slightly with the changes in curing conditions. It was found the curing condition of EPLA samples significantly affects the thermal properties of concrete. The chemical reactivity of EPLA leads to an increase in CO_2 concentration in the matrix and an increase in concrete porosity. In the case of EPLA concrete, the variation of thermal conductivity is mostly related to the changes in hydration products and the alkaline reactivity of EPLA.

The thermal conductivity of EPLA and EPS was about 20% lower than that of perlite and vermiculite concrete. In the case of CEPLA concrete, the thermal conductivity of CEPLA concrete was slightly higher than that of EPS and EPLA concrete. Larger differences were observed in a sample containing 70% polymers. The thermal conductivity of magnesium phosphate concrete was slightly higher than that of the EPLA and EPS concrete. The thermal conductivity of magnesium phosphate concrete was influenced by the borax content and P/M ratio, however, this trend was reversed in a sample containing a lower amount of magnesia. In the case of GGBS concrete, the alkaline reactivity of EPLA significantly affects the thermal conductivity of concrete. An increase in calcium content causes a decrease in thermal conductivity value mainly due to an increase in concrete porosity. The influence of the activator on thermal conductivity of EPS concrete was minimal. Overall, the lowest thermal conductivity was observed in cement based sample (PP4) with a relative thermal conductivity value of 0.0710 W/mK.

11.2.4 Electrical properties of proposed concretes

The parameters such as water-cement ratio, additives, aggregates, the degree of hydration, porosity, pore size distribution and cement paste microstructure significantly affect the electrical resistivity values of concrete. A significant decrease in electrical resistivity of vermiculite concrete was observed with an increase in EPLA volume, while the addition of EPS beads results in a sudden increase in electrical resistivity of concrete.

The decrease in electrical resistivity is associated with a decrease in concrete porosity. In fact, the coarser pore size distribution and higher ionic concentration leads to a lower electrical resistivity in concrete containing a high volume of EPLA. Also, the changes in electrical resistivity of EPLA concrete are related to the microstructural changes and its chemical reactivity. It can be found that the high water absorption value of vermiculite

and alkaline reactivity of EPLA beads results in the electrical resistivity to remain unchanged even after 7 days of curing. Surprisingly, the application of EPLA in perlite concrete results in an increase in electrical resistivity of concrete when a high volume of EPLA is used. In fact, the propagation and growth of calcium carbonate decreased the porosity of concrete and caused a higher electrical resistivity in the samples containing EPLA at the later ages. A significant change in setting time of concrete was observed when EPLA beads are used as lightweight aggregate.

In the case of CEPLA concrete, the electrical resistivity was much higher than that of EPLA concrete due to the lower percentages of porosity in the concrete matrix. It can be found that the coating of EPLA aggregate is a proper method to eliminate the chemical reactivity of EPLA at the initial stage of the hydration process which leads to a significant reduction in the alkaline reactivity of EPLA and limits the carbonation process at the layers of the coating materials. The difference between the exothermic reaction of EPLA and CEPLA was minimal, and both samples showed the same exothermic reaction patterns.

For magnesium phosphate concrete, the electrical resistivity was much higher than that of EPS and EPLA concrete at the initial stage of curing due to the fast reaction of magnesium phosphate concrete. It was found that the factors such as Borax and ammonium content significantly affect the electrical resistivity and exothermic reaction of magnesium phosphate concrete. An increase in Borax content causes a significant decrease in exothermic reaction, while an inverse effect was obtained with an increase in ammonium content.

11.2.5 Fire resistance of proposed concretes

EPLA concrete, CEPLA concrete, EPS concrete and perlite concrete failed a cone calorimeter test with some minor thermal cracks without losing the integrity when subjected to high temperatures. In contrast magnesium phosphate concrete lost its strength with explosive spalling and visible thermal cracks. The EPLA, CEPLA, and EPS concretes were evaluated as quasi-noncombustible materials, while magnesium phosphate concrete and perlite concrete were non-combustible materials. In the case of GGBS concrete containing EPLA and EPS, no visible thermal cracks and matrix degradation was observed.

The highest heat release rate was observed in concrete containing CEPLA due to the burning of the coating layers, while the lowest was observed in perlite concrete. In addition, no ignition point was recorded for magnesium phosphate concrete and perlite concrete and there was no contribution to the fire development. By contrast, the fastest ignition was observed in samples containing CEPLA. Ignition took longer in samples containing EPLA and EPS.

A sharp increase in CO₂ gas production was observed in CEPLA samples mainly due to the combustion process of coating layers as well with EPLA aggregate. The samples EPS concrete, magnesium phosphate concrete and perlite concrete produced lower amounts of CO₂ gas. A sudden increase of CO₂ gas production of concrete was observed in GGBS concrete containing EPLA. This increase happened for samples containing EPS at a lower level.

The CO gas production of magnesium phosphate concrete was slightly lower than that of EPLA, EPS and GGBS concrete. The highest and fastest growth in CO gas production were observed in CEPLA concrete ahead of EPLA concrete. The highest rate of mass reduction was observed in magnesium phosphate concrete followed by CEPLA concrete, EPLA concrete, EPS concrete, EPLA GGBS concrete and EPS GGBS concrete as well as perlite concrete.

Also, it was found the concentration of CO and its safety level categorized in safe mode (less than 70 ppm). The CO concentration of CEPLA, perlite, magnesium phosphate concrete containing EPLA, GGBS concrete containing EPLA, EPLA concrete and EPS concrete (as reference) were 50.41ppm, 8.84 ppm, 31.0 ppm, 72.0 ppm, 53.5 ppm and 41.0 ppm, respectively.

11.2.6 Phase analysis of proposed concretes

SEM, XRD and EDS analyses were used to assess the influence of EPLA aggregate on microstructures of concrete. The addition of EPLA beads changed the microstructure and hydration products of concrete. These changes can mainly be attributed to the concrete carbonation and EPLA degradation in the alkaline environment of cement. The formation of large amounts of calcium carbonate (CaCO₃) and calcium aluminium sulfate (AFt) shows that the degradation of EPLA leads to a chemical conversion of hydration products as no calcium silicate hydrate was found in the microstructure of the samples. The

conversion of C-S-H gel to calcium carbonate was the main cause for strength reduction in concrete containing EPLA. The presence of a large amount of calcium carbonate explains the interaction of EPLA with calcium and sodium. However, at the later stage of one year more calcium silicate hydrate gel was found in the microstructure of concrete. The phases identified in the EPS concrete samples are mostly calcium-silicate-hydrate (C-S-H), calcium hydroxide (portlandite) and calcium sulfoaluminate (ettringite), while Magnesium phosphate hydrate was present as the main hydration product of magnesium phosphate concrete. In addition, it was found that the existence of Cl and Ca elements at the later stages of curing leads to the formation of calcium chloride after 7 days of curing. The formation of calcium chloride was the main cause of strength reduction in magnesium phosphate concrete at the later stages of curing of 90 days.

11.2.7 Bond properties of proposed concretes

It was found that the parameters such as density, compressive strength, binder type and volume of polymer affects the bond mechanisms of concrete. The locking area, bearing area, cut feature, elastic and inelastic area of embedded members are the key factors that directly affect the bond mechanisms. The bond strength of concrete containing EPLA was found to be significantly different from that of EPS concrete due to an interfacial bond failure and microstructural changes at the paste-aggregate interface. The ultimate bond stress of EPS and EPLA concrete with a variation in locking patterns of embedded strips were in the ranges of 0.131 to 0.518 MPa and 0.045 to 0.277 MPa, respectively. The samples containing EPLA failed in a more brittle manner compared to EPS concrete. In addition, an increase in locking area at the inelastic region is a proper method for increasing the bond capacity. The same improvement was observed with a decrease in the angle of locking components. This means the bond strength of EPS concrete was about 42% to 476% higher than that of EPLA concrete.

Two failure modes of pullout and splitting crack were observed for concretes containing EPS and EPLA. A sudden splitting failure and visible cracks were formed on both sides of the embedded strips in EPLA concrete due to the bond strength between EPLA concrete and embedded strips being much higher than that of the tensile strength of about 0.025 MPa [140]. The failure mode of all EPS concretes were pullout failures without any noticeable cracks.

11.3 Design recommendations for proposed concretes

From the experimental results the following equations are proposed for mix design and to predict the engineering properties of ultra-lightweight concrete containing polymer aggregate.

1) The mix proportion of ultra-lightweight concrete can be obtained by the following mix design method.

- Selection of approximate water-cement ratio (w/c):

Perlite concrete:

$$\frac{w}{c} = a = \frac{0.76\gamma^{0.0001\gamma}}{0.0001\gamma \cdot \gamma^{0.5}}$$

Vermiculite concrete:

$$\frac{w}{c} = a = \frac{0.77\gamma^{0.0001\gamma}}{0.0001\gamma \cdot \gamma^{0.5}} + 0.25WA_r$$

- Required cement content:

$$\begin{cases} 1000 = \frac{(\frac{\gamma}{a})^{0.5}}{RD_c \cdot RD_p} C + \frac{Ka(\frac{a}{\gamma})^{0.5}}{RD_p} C + 10aV_p \\ \gamma = \gamma^{\frac{1}{10a}} C + aC + RD_p V_p \end{cases}$$

2) The tensile strength of concrete can be calculated from compressive strength by the following equations in different curing conditions.

$$\hat{f}_c = 4.6773 f_t - 0.3521 \text{ (EPLA concrete - air cured)}$$

$$\hat{f}_c = 6.0261 f_t - 0.8001 \text{ (EPLA concrete - water cured)}$$

$$\hat{f}_c = 4.8199 f_t - 0.4167 \text{ (EPS concrete - air cured)}$$

$$\hat{f}_c = 5.994 f_t - 0.8375 \text{ (EPS concrete - water cured)}$$

- 3) The thermal conductivity of vermiculite concrete containing EPLA aggregate can be calculated by the following equations.

$$\lambda = \left(\frac{\sqrt{\gamma_{\text{concrete}}}}{(\gamma_{\text{vermiculite}} \cdot R_{\text{vermiculite}}) + (\gamma_{\text{EPLA}} \cdot R_{\text{EPLA}})} \right)^{K + \frac{0.5R_{\text{EPLA}}}{R_{\text{vermiculite}}^{0.5}}}$$

$$K = 1.40 \text{ (for vermiculite concrete)}$$

$$K = 1.21 \text{ (for perlite concrete)}$$

- 4) The water absorption of vermiculite concrete can be calculated from the following equation.

$$WA_R = \frac{(A)^{0.1}(BC)}{\sqrt{RD_v}}$$

Where,

$$A = 60t^{0.6}$$

$$B = RD_v WA_v$$

$$C = R^{R + R \frac{t}{RD_v}}$$

- 5) The elastic modulus of concrete containing polymer aggregate can be calculated by the following equation.

$$E = K \left(\frac{\gamma}{\sqrt{(800 - \gamma)}} \right) (\sqrt{f_{cu}})$$

- 6) The compressive strength of concrete containing EPLA and EPS can be obtained from the following equations.

$$f_{cEPS} = 0.012e^{0.0088\gamma}$$

$$f_{cPLA} = 0.0017e^{0.0126\gamma}$$

7) The differences between the target density and actual density of foamed concrete containing EPS aggregate can be calculated with the following equations

$$\alpha = \frac{2B^2 \sqrt{B + \frac{E}{F}} \frac{F}{E\bar{B}}}{EF^{2.5}}$$

$$\begin{cases} \gamma_{AD} = \gamma_{TD} + \alpha & 100 \text{ kg/m}^3 < \gamma \leq 150 \text{ kg/m}^3 \\ \gamma_{AD} = \gamma_{TD} - \alpha & 150 \text{ kg/m}^3 < \gamma \leq 400 \text{ kg/m}^3 \end{cases}$$

8) The compressive strength of foamed and foamed concrete containing polymer aggregate can be obtained by the following equations.

$$f_c = 0.0034e^{0.0063\gamma} \quad (R^2 = 0.9803)$$

$$f_c = 0.0243e^{0.0083\gamma} \quad (R^2 = 0.8075)$$

9) The thermal conductivity of foamed concrete containing polymer aggregate can be calculated by the following equations.

$$\lambda = \frac{7.2 \frac{V_{EPS}}{V_{EPS}} \sqrt{\frac{\gamma}{V_{EPS} \cdot V_{Foam}}}}{V_{EPS} \frac{V_{EPS}}{\sqrt{\gamma \cdot V_{Foam}}}}$$

10) The following equation is developed to calculate the bond stress of embedded elements in foamed concrete.

$$\tau_b = \frac{4.2 \sqrt{f_c (A_e - A_h)}}{\gamma} + \frac{\sqrt{f_c A_h}}{2.4 \sqrt{(l_e - l_i)^{1.8} + (l_i^2 - l_e)}}$$

Where,

$$A_e = (l_e d_p)$$

$$A_h = \frac{\pi d_h^2}{4}$$

11) The bond stress-slip of embedded components of a composite section in foamed concrete can be obtained by the following equations.

$$\tau = \begin{cases} \frac{\mu\tau_u}{0.7\lambda\delta_u} \delta & 0 \leq \delta \leq \mu\delta_u \\ \frac{\tau_u}{1.1(1-\mu)} \left[\frac{(1-\mu)\delta}{\delta_u} + (1.4\mu - \lambda) \right] & \mu\delta_u < \delta \leq \delta_u \\ \tau_u - \frac{(\tau_u - \alpha\tau_u)(\delta_u - \delta)}{(\delta_u - \beta\delta_u)} & \delta_u < \delta \leq \beta\delta_u \\ K\tau_u \sqrt{2\delta - \beta\delta_u} & \delta > \beta\delta_u \end{cases}$$

Where,

$$\mu = \frac{\sqrt{L_e t_s^{0.2 + \frac{1}{t_s}}}}{2.2 \sqrt{(A_e - nA_h)}}$$

$$\lambda = \frac{2.5 \ln(L_e)}{\sqrt{(A_e - nA_h)}}$$

12) The tensile capacity of embedded components of a composite section in foamed concrete can be calculated with the following equations.

$$P_a = \frac{(L_e t_s)^{0.8}}{(A_e - nA_h)^{1+t_s}}$$

$$P_i = \frac{\ln(L_e n A_c t_s^{2.8})}{4.5 \sqrt{\ln(n A_h + n A_c) t_s}}$$

$$P_u = P_a + P_i$$

Where,

$$A_h = \pi R_h^2$$

$$A_c = \frac{2\pi R_h}{2}$$

13) The bond stress ratio of embedded elements in foamed concrete can be calculated by the following equations.

$$\tau_u = \frac{P_u}{2(d_s+t_s).L_e}$$

$$\frac{\tau_u}{\sqrt{f_c}} = \frac{\sqrt{(L_e^{1.2}-L_L)t_s}}{\gamma \ln(A_h)} + \frac{5.5t(A_e-A_h)^{0.5}}{\gamma} + \frac{\sqrt{A_h}}{2.4 [(L_e-L_L)^2+(L_L^2-L_e)]^{0.5}}$$

Where,

$$A_e = (L_e d_s)$$

$$A_h = \frac{\pi d_h^2}{4}$$

14) The elastic and inelastic length of embedded elements of a composite section can be calculated by the following equations.

$$l_{In.LWC} = \frac{l_{e.NC} \frac{(f_u-f_y)^{l_{in.NC}}}{2(b+t)u_{in}}}{2(b+t)u_{in}}$$

$$\text{Where } l_{in.NC} = \frac{(f_u-f_y)bt}{2(b+t)u_{in}}$$

$$l_{e.NC} = \frac{f_u bt}{2(b+t)u_e}$$

$$u_{e EPS} = 0.26\sqrt{f_c}$$

$$u_{in EPS} = 0.13\sqrt{f_c}$$

$$u_{in EPLA} = 0.07\sqrt{f_c}$$

$$u_{e EPLA} = 0.14\sqrt{f_c}$$

15) The bond stress-slip behaviour of embedded elements in concrete containing EPLA aggregate can be calculated by the following equations.

$$\tau_u = \begin{cases} \frac{5.2\tau_u\mu}{K\phi\delta_u} \delta, & 0 \leq \delta \leq \mu\delta_u \\ \frac{\tau_u}{1.1(1-\mu)} \left[\frac{(1-\mu)\delta^{0.5}}{\delta_u} + (1.11\mu - \phi)^{0.3} \right], & \mu\delta_u < \delta \leq \delta_u \\ \tau_u - \frac{(\tau_u - \alpha\tau_u)(\delta_u - \delta)}{(\delta_u - \beta\delta_u)}, & \delta_u < \delta \leq \beta\delta_u \\ K\tau_u \sqrt{2\delta - \beta\delta_u}, & \delta > \beta\delta_u \end{cases} \quad [5]$$

Where

$$\mu = \frac{\sqrt{L_e t_s^{0.2 + \frac{1}{t_s}}}}{2.2\sqrt{(A_e - A_c)}}$$

$$\phi = \frac{2.5\text{Ln}(L_e)}{\sqrt{(A_e - A_c)}}$$

16) The bond stress-slip behaviour of embedded elements in concrete containing EPS aggregate can be calculated by the following equations.

$$\tau_u = \begin{cases} \frac{0.3\tau_u\mu}{K\phi\delta_u} \delta, & 0 \leq \delta \leq \mu\delta_u \\ \frac{\tau_u}{1.1(1-\mu)} \left[\frac{(1-\mu)\delta^{1.3}}{\delta_u} + (1.11\mu - \phi)^{0.3} \right], & \mu\delta_u < \delta \leq \delta_u \\ \tau_u - \frac{(\tau_u - \alpha\tau_u)(\delta_u - \delta)}{(\delta_u - \beta\delta_u)}, & \delta_u < \delta \leq \beta\delta_u \\ K\tau_u (\delta^{0.1} - \beta\delta_u)^{0.1}, & \delta > \beta\delta_u \end{cases} \quad [6]$$

Where

$$\mu = \frac{\sqrt{L_e t_s^{0.2 + \frac{1}{t_s}}}}{2.2\sqrt{(A_e - A_c)}}$$

$$\phi = \frac{2.5\text{Ln}(L_e)}{\sqrt{(A_e - A_c)}}$$

17) The load-displacement behaviour of a cold formed channel and a box section filled ultra-lightweight concrete can be calculated as follows:

$$\beta = \text{Ln} (e^{\alpha f_c})$$

Where,

		Perlite concrete	EPS-perlite concrete	EPLA-perlite concrete
α	Channel section	1.40	4.0	11.6
	Box section	0.89	1.36	7.25

$$P = \frac{\text{Ln}(A_s)P_u}{\text{Ln}(f_c) + P_u^{2.02}} \delta, \quad (0 \leq \delta \leq \beta\delta_u) \quad (\text{Channel section})$$

$$P = \frac{\text{Ln}(A_s)P_u}{\text{Ln}(f_c) + P_u^{1.5}} \delta, \quad (0 \leq \delta \leq \beta\delta_u) \quad (\text{Box section})$$

$$P = \left(\frac{\text{Ln}(\delta^6 P_u)}{(2 - \text{Ln}(A_s))} \right) \left(\frac{\text{Ln}(P_u \delta)}{(1 - \text{Ln}(A_s))} \right), \quad (\beta\delta_u < \delta \leq \delta_u) \quad (\text{Channel section})$$

$$P = \left(\frac{\text{Ln}(\delta^{5.6} P_u)}{(2 - \text{Ln}(A_s))} \right) \left(\frac{\text{Ln}(P_u \delta^{5.6})}{(1 - \text{Ln}(A_s))} \right), \quad (\beta\delta_u < \delta \leq \delta_u) \quad (\text{Box section})$$

$$P = KP_u^{10 \left(\frac{\delta(1-1.1P_u)}{P_u} \right)}, \quad (\delta > \delta_u) \quad (\text{Channel section})$$

$$P = 15KP_u^{0.01 \left(\frac{\delta(2-0.9P_u)}{P_u} \right)}, \quad (\delta > \delta_u) \quad (\text{Box section})$$

		PC	PEC	PPC
K	Channel section	0.20	0.18	0.23
	Box section	21.5	19.5	17.5

11.4 Recommendations for further study

The following research topics can be developed further with regard to the application of expanded poly-lactic acid (EPLA) as a biopolymer lightweight aggregate.

- 1- Study on long term performance of concrete containing EPLA aggregate in terms of mechanical, thermal and electrical properties.
- 2- Modification of EPLA aggregate to be used as self-healing agent and air entraining agent and also surface modifications of EPLA aggregate for a high alkaline environment.
- 3- The corrosion and durability of concrete containing EPLA aggregate.
- 4- The impact resistance of concrete containing EPLA aggregate
- 5- The unrestrained and restrained shrinkages of lightweight concrete containing EPLA.
- 6- The creep and creep recovery of concrete containing EPLA aggregate.
- 7- The acoustic properties of concrete containing EPLA aggregate.
- 8- The relationship between concrete density and CO₂ content (due to the alkaline reactivity)
- 9- Further investigation on engineering properties of magnesium phosphate concrete and CEPLA concrete.
- 10- Further study on CO₂ emission and life-cycle cost analysis

References

1. Kockal NU, Ozturan T: Strength and elastic properties of structural lightweight concretes. *Materials & Design* 2011, 32(4):2396-2403.
2. Chen B, Liu J: Experimental application of mineral admixtures in lightweight concrete with high strength and workability. *Construction and Building Materials* 2008, 22(6):1108-1113.
3. Ünal O, Uygunoğlu T, Yildiz A: Investigation of properties of low-strength lightweight concrete for thermal insulation. *Building and Environment* 2007, 42(2):584-590.
4. Bagon C, Frondistou-Yannas S: Marine floating concrete made with polystyrene expanded beads. *Magazine of Concrete Research* 1976, 28(97):225-229.
5. Celik S, Family R, Menguc MP: Analysis of perlite and pumice based building insulation materials. *Journal of Building Engineering* 2016, 6(Supplement C):105-111.
6. Perry SH, Bischoff PH, Yamura K: Mix details and material behaviour of polystyrene aggregate concrete. *Magazine of Concrete Research* 1991, 43(154):71-76.
7. Sri Ravindrarajah R, Tuck AJ: Properties of hardened concrete containing treated expanded polystyrene beads. *Cement and Concrete Composites* 1994, 16(4):273-277.
8. Babu KG, Babu DS: Behaviour of lightweight expanded polystyrene concrete containing silica fume. *Cement and Concrete Research* 2003, 33(5):755-762.
9. Ferreira L, de Brito J, Saikia N: Influence of curing conditions on the mechanical performance of concrete containing recycled plastic aggregate. *Construction and Building Materials* 2012, 36:196-204.
10. Ismail ZZ, Al-Hashmi EA: Use of waste plastic in concrete mixture as aggregate replacement. *Waste Management* 2008, 28(11):2041-2047.
11. Durack JM, Weiqing L: The properties of foamed air cured fly ash based concrete for masonry production. *Proceedings of the Fifth Australasian Masonry Conference* 1998:129-138.
12. Carsana M, Tittarelli F, Bertolini L: Use of no-fines concrete as a building material: Strength, durability properties and corrosion protection of embedded steel. *Cement and Concrete Research* 2013, 48:64-73.

13. Tittarelli F, Carsana M, Ruello ML: Effect of hydrophobic admixture and recycled aggregate on physical–mechanical properties and durability aspects of no-fines concrete. *Construction and Building Materials* 2014, 66:30-37.
14. Abdulkadir Kan RD: Effect of cement and EPS beads ratios on compressive strength and density of lightweight concrete. *Indian Journal of Engineering and Materials Sciences (IJEMS)* 2007, 14(2):4.
15. Kotwica Ł, Pichór W, Kapeluszna E, Różycka A: Utilization of waste expanded perlite as new effective supplementary cementitious material. *Journal of Cleaner Production* 2017, 140(Part 3):1344-1352.
16. Hubertová M, Hela R: Durability of Lightweight Expanded Clay Aggregate Concrete. *Procedia Engineering* 2013, 65:2-6.
17. Gomathi P, Sivakumar A: Accelerated curing effects on the mechanical performance of cold bonded and sintered fly ash aggregate concrete. *Construction and Building Materials* 2015, 77:276-287.
18. Güneyisi E, Gesoğlu M, Pürsünlü Ö, Mermerdaş K: Durability aspect of concretes composed of cold bonded and sintered fly ash lightweight aggregates. *Composites Part B: Engineering* 2013, 53:258-266.
19. Lo TY, Cui H, Memon SA, Noguchi T: Manufacturing of sintered lightweight aggregate using high-carbon fly ash and its effect on the mechanical properties and microstructure of concrete. *Journal of Cleaner Production* 2016, 112:753-762.
20. Shafiqh P, Johnson Alengaram U, Mahmud HB, Jumaat MZ: Engineering properties of oil palm shell lightweight concrete containing fly ash. *Materials & Design* 2013, 49:613-621.
21. Abidi S, Nait-Ali B, Joliff Y, Favotto C: Impact of perlite, vermiculite and cement on the thermal conductivity of a plaster composite material: Experimental and numerical approaches. *Composites Part B: Engineering* 2015, 68:392-400.
22. Aliakbar Sayadi TN, Charles Clifton, Min Cheol Han: Assessment of Vermiculite Concrete Containing Bio-Polymer Aggregate. *International Journal of Civil, Environmental, Structural, Construction and Architectural Engineering* 2016, 10(6).
23. Fuat Köksal JJdCD, Osman Gencil, Felipe P. Alvarez Rabanal: Experimental and numerical analysis of new bricks made up of polymer modified-cement using expanded vermiculite. *Computers and Concrete* 2013, 12(3):16.

24. Koksall F, Gencil O, Kaya M: Combined effect of silica fume and expanded vermiculite on properties of lightweight mortars at ambient and elevated temperatures. *Construction and Building Materials* 2015, 88:175-187.
25. Martias C, Joliff Y, Favotto C: Effects of the addition of glass fibers, mica and vermiculite on the mechanical properties of a gypsum-based composite at room temperature and during a fire test. *Composites Part B: Engineering* 2014, 62:37-53.
26. Schackow A, Effting C, Folgueras MV, Güths S, Mendes GA: Mechanical and thermal properties of lightweight concretes with vermiculite and EPS using air-entraining agent. *Construction and Building Materials* 2014, 57(Supplement C):190-197.
27. Sutcu M: Influence of expanded vermiculite on physical properties and thermal conductivity of clay bricks. *Ceramics International* 2015, 41(2, Part B):2819-2827.
28. Sayadi AA, Tapia JV, Neitzert TR, Clifton GC: Effects of expanded polystyrene (EPS) particles on fire resistance, thermal conductivity and compressive strength of foamed concrete. *Construction and Building Materials* 2016, 112:716-724.
29. Schackow A, Effting C, Folgueras MV, Güths S, Mendes GA: Mechanical and thermal properties of lightweight concretes with vermiculite and EPS using air-entraining agent. *Construction and Building Materials* 2014, 57:190-197.
30. Anwar Hossain KM: Bond characteristics of plain and deformed bars in lightweight pumice concrete. *Construction and Building Materials* 2008, 22(7):1491-1499.
31. Ayhan M, Gönül H, Gönül İA, Karakuş A: Effect of basic pumice on morphologic properties of interfacial transition zone in load-bearing lightweight/semi-lightweight concretes. *Construction and Building Materials* 2011, 25(5):2507-2518.
32. Bideci A, Gültekin AH, Yıldırım H, Oymael S, Bideci ÖS: Internal structure examination of lightweight concrete produced with polymer-coated pumice aggregate. *Composites Part B: Engineering* 2013, 54:439-447.
33. Granata MF: Pumice powder as filler of self-compacting concrete. *Construction and Building Materials* 2015, 96:581-590.
34. Hossain KMA, Ahmed S, Lachemi M: Lightweight concrete incorporating pumice based blended cement and aggregate: Mechanical and durability characteristics. *Construction and Building Materials* 2011, 25(3):1186-1195.

35. Kabay N, Tufekci MM, Kizilkanat AB, Oktay D: Properties of concrete with pumice powder and fly ash as cement replacement materials. *Construction and Building Materials* 2015, 85:1-8.
36. Kurt MMG, ; Rustem Gul,; Abdulkadir Aydin,; Turkay Kotan: The Effect of Pumice Powder on the Self-Compactability of Pumice Aggregate Lightweight Concrete. *Construction and Building Materials Reed Business Information, Inc (US)* 2016 HighBeam Research 16 Jan 2016.
37. Libre NA, Shekarchi M, Mahoutian M, Soroushian P: Mechanical properties of hybrid fiber reinforced lightweight aggregate concrete made with natural pumice. *Construction and Building Materials* 2011, 25(5):2458-2464.
38. Onoue K, Tamai H, Suseno H: Shock-absorbing capability of lightweight concrete utilizing volcanic pumice aggregate. *Construction and Building Materials* 2015, 83:261-274.
39. Kotwica Ł, Pichór W, Nocuń-Wczelik W: Study of pozzolanic action of ground waste expanded perlite by means of thermal methods. *Journal of Thermal Analysis and Calorimetry* 2016, 123(1):607-613.
40. Su L, Ma B, Jian S, Zhao Z, Liu M: Hydration heat effect of cement pastes modified with hydroxypropyl methyl cellulose ether and expanded perlite. *Journal of Wuhan University of Technology-Mater Sci Ed* 2013, 28(1):122-126.
41. Kockal NU, Ozturan T: Durability of lightweight concretes with lightweight fly ash aggregates. *Construction and Building Materials* 2011, 25(3):1430-1438.
42. Kralj D: Experimental study of recycling lightweight concrete with aggregates containing expanded glass. *Process Safety and Environmental Protection* 2009, 87(4):267-273.
43. Chabannes M, Bénézet J-C, Clerc L, Garcia-Diaz E: Use of raw rice husk as natural aggregate in a lightweight insulating concrete: An innovative application. *Construction and Building Materials* 2014, 70:428-438.
44. Sadrumontazi A, Sobhani J, Mirgozar MA, Najimi M: Properties of multi-strength grade EPS concrete containing silica fume and rice husk ash. *Construction and Building Materials* 2012, 35(Supplement C):211-219.
45. Shafigh P, Mahmud HB, Jumaat MZ, Zargar M: Agricultural wastes as aggregate in concrete mixtures – A review. *Construction and Building Materials* 2014, 53:110-117.
46. Cook DJ: *Expanded Polystyrene Beads as Lightweight Aggregate for Concrete: School of Civil Engineering, University of New South Wales; 1972.*

47. Cook DJ: Expanded polystyrene concrete. *New Concrete Materials* 1983, 1:41-69.
48. Cook DJ: EXPANDED POLYSTYRENE BEADS AS LIGHTWEIGHT AGGREGATE FOR CONCRETE. *Precast Concr* 1973, 4(12):691-693.
49. Sin LT, Rahmat AR, Rahman WAWA: 2 - Synthesis and Production of Poly(lactic Acid). In: *Poly(lactic Acid)*. Oxford: William Andrew Publishing; 2013: 71-107.
50. Sin LT, Rahmat AR, Rahman WAWA: 4 - Chemical Properties of Poly(lactic Acid). In: *Poly(lactic Acid)*. Oxford: William Andrew Publishing; 2013: 143-176.
51. Garlotta D: A Literature Review of Poly(Lactic Acid). *Journal of Polymers and the Environment* 2001, 9(2):63-84.
52. Parker K, Garancher J-P, Shah S, Weal S, Fernyhough A: Poly(lactic Acid) (PLA) Foams for Packaging Applications. In: *Handbook of Bioplastics and Biocomposites Engineering Applications*. John Wiley & Sons, Inc.; 2011: 161-175.
53. Sin LT, Rahmat AR, Rahman WAWA: 8 - Applications of Poly(lactic Acid). In: *Poly(lactic Acid)*. Oxford: William Andrew Publishing; 2013: 301-327.
54. Kate Parker J-PG, Samir Shah , Alan Fernyhough: Expanded polylactic acid - an eco-friendly alternative to polystyrene foam. *Journal of Cellular Plastics* 2011, 47(3):10.
55. Parker K, Garancher, J.-P., Shah, S., Weal, S. and Fernyhough, A: Poly(lactic Acid) (PLA) Foams for Packaging Applications. *Handbook of Bioplastics and Biocomposites Engineering Applications* (ed S Pilla), John Wiley & Sons, Inc, Hoboken, NJ, USA 2011.
56. Jean-Philippe Garancher KP, Samir Shah, Alan Fernyhough: Expanded Polylactide (E-PLA): A Realistic Approach to Expanded Polystyrene. *Society of Plastics Engineers* 2010.
57. PRIYADHARSHINI P: A Review on Artificial Aggregates *International Journal of Earth Sciences and Engineering* 2012.
58. Celik AG, Kilic AM, Cakal GO: Expanded perlite aggregate characterization for use as a lightweight construction raw material. *Physicochemical Problems of Mineral Processing* 2013, 49(2):689-700.
59. Ardakani A, Yazdani M: The relation between particle density and static elastic moduli of lightweight expanded clay aggregates. *Applied Clay Science* 2014, 93-94:28-34.

60. Mo KH, Alengaram UJ, Jumaat MZ: Compressive behaviour of lightweight oil palm shell concrete incorporating slag. *Construction and Building Materials* 2015, 94(Supplement C):263-269.
61. Mo KH, Alengaram UJ, Jumaat MZ, Liu MYJ, Lim J: Assessing some durability properties of sustainable lightweight oil palm shell concrete incorporating slag and manufactured sand. *Journal of Cleaner Production* 2016, 112:763-770.
62. Yogesh Aggarwal SNC: Properties of Expanded Polystyrene Concrete Containing Ground Granulated Blast Furnace Slag. *NBM&CW* 2014.
63. Yuan X-h, Chen W, Lu Z-a, Chen H: Shrinkage compensation of alkali-activated slag concrete and microstructural analysis. *Construction and Building Materials* 2014, 66:422-428.
64. Ben Sabaa RSR: Engineering Properties of Lightweight Concrete Containing Crushed Expanded Polystyrene Waste. *Advances in Materials for Cementitious Composites* 2004.
65. Madandoust R, Ranjbar MM, Yasin Mousavi S: An investigation on the fresh properties of self-compacted lightweight concrete containing expanded polystyrene. *Construction and Building Materials* 2011, 25(9):3721-3731.
66. Saradhi Babu D, Ganesh Babu K, Wee TH: Properties of lightweight expanded polystyrene aggregate concretes containing fly ash. *Cement and Concrete Research* 2005, 35(6):1218-1223.
67. Sayadi AA, Tapia JV, Neitzert TR, Clifton GC: Effects of expanded polystyrene (EPS) particles on fire resistance, thermal conductivity and compressive strength of foamed concrete. *Construction and Building Materials* 2016, 112(Supplement C):716-724.
68. Chi JM, Huang R, Yang CC, Chang JJ: Effect of aggregate properties on the strength and stiffness of lightweight concrete. *Cement and Concrete Composites* 2003, 25(2):197-205.
69. Lo TY, Tang WC, Cui HZ: The effects of aggregate properties on lightweight concrete. *Building and Environment* 2007, 42(8):3025-3029.
70. Demirboga R, Kan A: Thermal conductivity and shrinkage properties of modified waste polystyrene aggregate concretes. *Construction and Building Materials* 2012, 35(Supplement C):730-734.
71. Demirboğa R, Gül R: Thermal conductivity and compressive strength of expanded perlite aggregate concrete with mineral admixtures. *Energy and Buildings* 2003, 35(11):1155-1159.

72. 302 A: Guide to concrete floor and slab construction. American concrete institute (ACI) 2004.
73. Lijiu W, Shuzhong Z, Guofan Z: Investigation of the mix ratio design of lightweight aggregate concrete. *Cement and Concrete Research* 2005, 35(5):931-935.
74. Mannan MA, Basri HB, Zain MFM, Islam MN: Effect of curing conditions on the properties of OPS-concrete. *Building and Environment* 2002, 37(11):1167-1171.
75. S. Chithra GD: Effect of hot water curing and hot air oven curing on admixed concrete. *International Journal of ChemTech Research* 2014, 6(2):7.
76. 211.2 A: Standard Practice for Selecting Proportions for Structural Lightweight Concrete ACI Committee 2004.
77. Ramazan Demirgoga AK: Design of specific gravity factor of artificial lightweight aggregate. *Indian Journal of Engineering & Materials Sciences* 2013, 20.
78. 213R-03 A: Guide for Structural Lightweight-Aggregate Concrete. American Concrete Institute 2003.
79. 318-14 A: Building Code Requirements for Structural Concrete and Commentary. American Concrete Institute 2014.
80. 3797 B: Specification for lightweight aggregates for masonry units and structural concrete. British Standard (BS) 1990.
81. 3600 A: AS 3600, concrete structures. Australian Standard (AS) 2009.
82. 51 J: Technical specification for lightweight aggregate concrete. Chinese Standard 2002.
83. Sengul O, Azizi S, Karaosmanoglu F, Tasdemir MA: Effect of expanded perlite on the mechanical properties and thermal conductivity of lightweight concrete. *Energy and Buildings* 2011, 43(2):671-676.
84. Topçu İB, Işıkdag B: Effect of expanded perlite aggregate on the properties of lightweight concrete. *Journal of Materials Processing Technology* 2008, 204(1):34-38.
85. C330/330M A: Standard specification for Lightweight Aggregates for structural concrete. ASTM International 2009.
86. C332 A: Standard Specification for lightweight aggregates for insulating concrete. ASTM International 2009.

87. Demirboğa R, Gül R: The effects of expanded perlite aggregate, silica fume and fly ash on the thermal conductivity of lightweight concrete. *Cement and Concrete Research* 2003, 33(5):723-727.
88. Gandage AS, Rao VRV, Sivakumar MVN, Vasan A, Venu M, Yaswanth AB: Effect of Perlite on Thermal Conductivity of Self Compacting Concrete. *Procedia - Social and Behavioral Sciences* 2013, 104(Supplement C):188-197.
89. Yu LH, Ou H, Lee LL: Investigation on pozzolanic effect of perlite powder in concrete. *Cement and Concrete Research* 2003, 33(1):73-76.
90. Türkmen İ, Kantarcı A: Effects of expanded perlite aggregate and different curing conditions on the physical and mechanical properties of self-compacting concrete. *Building and Environment* 2007, 42(6):2378-2383.
91. Silva LM, Ribeiro RA, Labrincha JA, Ferreira VM: Role of lightweight fillers on the properties of a mixed-binder mortar. *Cement and Concrete Composites* 2010, 32(1):19-24.
92. Ganesh Babu K, Saradhi Babu D: Performance of fly ash concretes containing lightweight EPS aggregates. *Cement and Concrete Composites* 2004, 26(6):605-611.
93. Chen B, Liu J: Properties of lightweight expanded polystyrene concrete reinforced with steel fiber. *Cement and Concrete Research* 2004, 34(7):1259-1263.
94. Amianti M, Botaro VR: Recycling of EPS: A new methodology for production of concrete impregnated with polystyrene (CIP). *Cement and Concrete Composites* 2008, 30(1):23-28.
95. Bouvard D, Chaix JM, Dendievel R, Fazekas A, Létang JM, Peix G, Quenard D: Characterization and simulation of microstructure and properties of EPS lightweight concrete. *Cement and Concrete Research* 2007, 37(12):1666-1673.
96. Chen B, Fang C: Contribution of fibres to the properties of EPS lightweight concrete. *Magazine of Concrete Research* 2009, 61(9):671-678.
97. Ling IH, Teo DCL: Properties of EPS RHA lightweight concrete bricks under different curing conditions. *Construction and Building Materials* 2011, 25(8):3648-3655.
98. Liu N, Chen B: Experimental study of the influence of EPS particle size on the mechanical properties of EPS lightweight concrete. *Construction and Building Materials* 2014, 68(Supplement C):227-232.

99. Miled K, Le Roy R, Sab K, Boulay C: Compressive behavior of an idealized EPS lightweight concrete: size effects and failure mode. *Mechanics of Materials* 2004, 36(11):1031-1046.
100. Miled K, Sab K, Le Roy R: Particle size effect on EPS lightweight concrete compressive strength: Experimental investigation and modelling. *Mechanics of Materials* 2007, 39(3):222-240.
101. Sadrmomtazi A, Sobhani J, Mirgozar MA: Modeling compressive strength of EPS lightweight concrete using regression, neural network and ANFIS. *Construction and Building Materials* 2013, 42(Supplement C):205-216.
102. Chen B, Liu N: A novel lightweight concrete-fabrication and its thermal and mechanical properties. *Construction and Building Materials* 2013, 44(Supplement C):691-698.
103. Xu Y, Jiang L, Xu J, Li Y: Mechanical properties of expanded polystyrene lightweight aggregate concrete and brick. *Construction and Building Materials* 2012, 27(1):32-38.
104. Tang WC, Cui HZ, Wu M: Creep and creep recovery properties of polystyrene aggregate concrete. *Construction and Building Materials* 2014, 51:338-343.
105. Sabaa BA: Engineering properties of polystyrene aggregate concrete. PhD Thesis, University of Technology, Sydney, Australia 1998.
106. Tang WC, Lo Y, Nadeem A: Mechanical and drying shrinkage properties of structural-graded polystyrene aggregate concrete. *Cement and Concrete Composites* 2008, 30(5):403-409.
107. Kan A, Demirboğa R: A new technique of processing for waste-expanded polystyrene foams as aggregates. *Journal of Materials Processing Technology* 2009, 209(6):2994-3000.
108. Kan A, Demirboğa R: A novel material for lightweight concrete production. *Cement and Concrete Composites* 2009, 31(7):489-495.
109. Chen B, Liu J: Mechanical properties of polymer-modified concretes containing expanded polystyrene beads. *Construction and Building Materials* 2007, 21(1):7-11.
110. Le Roy R, Parant E, Boulay C: Taking into account the inclusions' size in lightweight concrete compressive strength prediction. *Cement and Concrete Research* 2005, 35(4):770-775.

111. Babu DS, Ganesh Babu K, Tiong-Huan W: Effect of polystyrene aggregate size on strength and moisture migration characteristics of lightweight concrete. *Cement and Concrete Composites* 2006, 28(6):520-527.
112. Chen B, Liu J, Chen L-z: Experimental study of lightweight expanded polystyrene aggregate concrete containing silica fume and polypropylene fibers. *Journal of Shanghai Jiaotong University (Science)* 2010, 15(2):129-137.
113. Ferrándiz-Mas V, Bond T, García-Alcocel E, Cheeseman CR: Lightweight mortars containing expanded polystyrene and paper sludge ash. *Construction and Building Materials* 2014, 61:285-292.
114. Demirboga R, Kan A: Thermal conductivity and shrinkage properties of modified waste polystyrene aggregate concretes. *Construction and Building Materials* 2012, 35:730-734.
115. B.A. Herki JMKaEMN: Lightweight Concrete Made from Waste Polystyrene and Fly Ash. *World Applied Sciences Journal* 2013, 21(9):4.
116. K.-J Byun H-WS, S.-S Park, Y.-C Song: DEVELOPMENT OF STRUCTURAL LIGHTWEIGHT FOAMED CONCRETE USING POLYMER FOAM AGENT. *ICPIC* 1998.
117. Ramamurthy K, Kunhanandan Nambiar EK, Indu Siva Ranjani G: A classification of studies on properties of foam concrete. *Cement and Concrete Composites* 2009, 31(6):388-396.
118. Mustafa M: Fast set foamed concrete for same day reinstatement of openings in highways. *Proceedings of One Day Seminar on Foamed Concrete: Properties, Applications and Latest Technological Developments*, Loughborough University, Leicestershire, UK 2001:6.
119. Kearsley EP, Wainwright PJ: The effect of high fly ash content on the compressive strength of foamed concrete. *Cement and Concrete Research* 2001, 31(1):105-112.
120. Kearsley EP, Wainwright PJ: Ash content for optimum strength of foamed concrete. *Cement and Concrete Research* 2002, 32(2):241-246.
121. Wee TH, Babu DS, Tamilselvan T, Lim HS: Air-void system of foamed concrete and its effect on mechanical properties. *ACI Materials Journal* 2006, 103(1):45-52.
122. H. Fujiwara ES, Y. Ishikawa: Manufacturing of high strength aerated concrete containing silica fume. *Proceedings of the Fifth International Conference on Fly*

- Ash Silica Fume, Slag and Natural Pozzolana in Concrete, Milwaukee, WI, USA 1995:12.
123. The Influence of the Mix Design on the Properties of Micro-Cellular Concrete. In: Specialist Techniques and Materials for Concrete Construction. 185-197.
 124. E.P. Kearsley HFM: Designing Mix Composition of Foamed Concrete with High Fly Ash Contents. Use of Foamed Concrete in Construction. Thomas Telford, London 2005:7.
 125. Kearsley EP, Mostert HF: DESIGNING MIX COMPOSITION OF FOAMED CONCRETE WITH HIGH FLY ASH CONTENTS. In: Use of Foamed Concrete in Construction. 29-36.
 126. D AaAT: Foamed concrete: production and equipment design, properties, applications and potential. Proceedings of one day seminar on foamed concrete: properties, applications and latest technological developments Loughborough University 2001.
 127. Siddique R: Utilization of silica fume in concrete: Review of hardened properties. Resources, Conservation and Recycling 2011, 55(11):923-932.
 128. M.R. Jones AM, R.K. Dhir: Recycled and Secondary Aggregate in Foamed Concrete. WRAP Research Report, the Waste and Resources Action Programme. Banbury, Oxon 2005.
 129. Nambiar EKK, Ramamurthy K: Influence of filler type on the properties of foam concrete. Cement and Concrete Composites 2006, 28(5):475-480.
 130. C796-97 A: Standard Test Method for Foaming Agents for Use in Producing Cellular Concrete Using Preformed Foam. ASTM International 1997.
 131. 523 Ac: Guide for cellular concretes above 50 pcf, and for aggregate concretes above 50 pcf with compressive strengths less than 2500 psi. ACI J 1975, 72:16.
 132. Hilal AA, Thom NH, Dawson AR: On void structure and strength of foamed concrete made without/with additives. Construction and Building Materials 2015, 85:157-164.
 133. Kearsley EP, Wainwright PJ: Porosity and permeability of foamed concrete. Cement and Concrete Research 2001, 31(5):805-812.
 134. Kearsley EP, Wainwright PJ: The effect of porosity on the strength of foamed concrete. Cement and Concrete Research 2002, 32(2):233-239.
 135. Tiong-Huan Wee DSBTT, Hwee-Sin L: Air-Void System of Foamed Concrete and its Effect on Mechanical Properties. Materials Journal, 103(1).

136. Nambiar EKK, Ramamurthy K: Sorption characteristics of foam concrete. *Cement and Concrete Research* 2007, 37(9):1341-1347.
137. Pan Z, Li H, Liu W: Preparation and characterization of super low density foamed concrete from Portland cement and admixtures. *Construction and Building Materials* 2014, 72:256-261.
138. Kearsley EP, Mostert HF: Designing mix composition of foamed concrete with high fly ash contents. In: *Proceedings of the International Conference on the Use of Foamed Concrete in Construction: 2005; 2005: 29-36.*
139. Sayadi AA, Juan Vilches T, Neitzert TR, Charles Clifton G: Strength of bearing area and locking area of galvanized strips in foamed concrete. *Construction and Building Materials* 2016, 114(Supplement C):56-65.
140. Sayadi AA, Juan Vilches T, Neitzert TR, Charles Clifton G: Effectiveness of foamed concrete density and locking patterns on bond strength of galvanized strip. *Construction and Building Materials* 2016, 115(Supplement C):221-229.
141. S.J.A. HOSSEINI KK, A.B.A. RAHMAN, M. RAZAVI: The bond behaviour in reinforced concrete, state of the art. *Cement Wapno Beton* 2014.
142. Sayadi AA, Abd. Rahman AB, Sayadi A, Bahmani M, Shahryari L: Effective of elastic and inelastic zone on behavior of glass fiber reinforced polymer splice sleeve. *Construction and Building Materials* 2015, 80(Supplement C):38-47.
143. Sayadi AA, Rahman ABA, Jumaat MZB, Johnson Alengaram U, Ahmad S: The relationship between interlocking mechanism and bond strength in elastic and inelastic segment of splice sleeve. *Construction and Building Materials* 2014, 55(Supplement C):227-237.
144. 408 A: Bond and Development of Straight Reinforcing Bars in Tension (ACI408-03). ACI Committee 2003.
145. 408.2R-92 A: Bond under cyclic loads. ACI Committee 2014.
146. Treece RA, Jirsa JO: Bond Strength of Epoxy-Coated Reinforcing Bars. *Materials Journal*, 86(2).
147. Hussein L: Analytical Modelling of Bond Stress at Steel Concrete Interface Due to Corrosion. Ryerson University (Master thesis) 2011.
148. Orangun CO, Jirsa JO, Breen JE: A Reevaluation of Test Data on Development Length and Splices. *318Reference*, 12(9).
149. Tepfers R: A Theory of Bond Applied to Overlapping Tensile Reinforcement Splices for Deformed Bars. Chalmers University of Technology, Goteborg, Sweden, Division of concrete structures 1973.

150. C. Oan WC, Se Lee: Interfacial bond analysis of deformed bars to concrete. *ACI Struct J* 2002.
151. Clark AP: Bond of concrete reinforcing bars. *ACI J* 1949:23.
152. Darwin D, Graham EK: Effect of deformation height and spacing on bond strength of reinforcing bars. *ACI Materials Journal* 1993, 90(6):646-657.
153. Paul R. Jeanty DM, Mirza MS: Investigation of "Top Bar" Effects in Beams. *Structural Journal*, 85(3).
154. Robins PJ, Standish IG: The influence if lateral pressure upon anchorage bond. *Mag Of Concr Res* 1984, 36:129.
155. Hosseini SJA, Rahman ABA, Osman MH, Saim A, Adnan A: Bond behavior of spirally confined splice of deformed bars in grout. *Construction and Building Materials* 2015, 80:180-194.
156. Zuo J, Darwin D: Splice strength of conventional and high relative rib area bars in normal and high-strength concrete. *ACI Structural Journal* 2000, 97(4):630-641.
157. David D, Ebenezer KG: Effect of Deformation Height and Spacing on Bond Strength of Reinforcing Bars. *Structural Journal*, 90(6).
158. L.A. Lutz PG, G. Winter: Mechanics of Bond and Slip of Deformed Reinforcing Bars in Concrete. Research Report No. 324. Department of Civil Engineering, Cornell University, New York, USA 1966.
159. Clark AP: Bond of concrete reinforcing bars. *ACI J Proc* 1949, 46(11):161-184.
160. Seyed Jamal Aldin Hosseini ABAR: Effects of spiral diameter on the bond stress-slip relationship in grouted sleeve connector. *Malays Constr Res J* 2015.
161. Loo GK: Parametric Study Og Grout-Filled Splice Sleeve Integrated With Flexible Aluminum Tube for Precast Concrete Connection. *Universiti Teknologi Malaysia (Bsc)* 2009.
162. Soroushian P, Choi K-B, Park G-H, Aslani F: Bond of deformed bars to concrete. Effects of confinement and strength of concrete. *ACI Materials Journal* 1991, 88(3):227-232.
163. Simaan A, Pekoz TB: DIAPHRAGM BRACED MEMBERS AND DESIGN OF WALL STUDS. *ASCE J Struct Div* 1976, 102(1):77-92.
164. Hegyi P, Dunai L: Experimental study on ultra-lightweight-concrete encased cold-formed steel structures Part I: Stability behaviour of elements subjected to bending. *Thin-Walled Structures* 2016, 101:75-84.

165. Hegyi P, Dunai L: Experimental investigations on ultra-lightweight-concrete encased cold-formed steel structures: Part II: Stability behaviour of elements subjected to compression. *Thin-Walled Structures* 2016, 101:100-108.
166. Xu Z, Chen Z, Yang S: Seismic behavior of cold-formed steel high-strength foamed concrete shear walls with straw boards. *Thin-Walled Structures* 2018, 124:350-365.
167. Yousefi AM, Lim JBP, Charles Clifton G: Cold-formed ferritic stainless steel unlipped channels with web openings subjected to web crippling under interior-two-flange loading condition – Part I: Tests and finite element model validation. *Thin-Walled Structures* 2017, 116:333-341.
168. Manalo A: Structural behaviour of a prefabricated composite wall system made from rigid polyurethane foam and Magnesium Oxide board. *Construction and Building Materials* 2013, 41:642-653.
169. S100-07 A: North American Specification For The Design Of Cold-Formed Steel Structural Members, 2007 Edition With Supplement 2. AISI 2007.
170. 4600 AN: Cold-formed steel structures. AS/NZS 2005.
171. EC-EN1993-1-3: Cold-formed steel design. 1993.
172. Ye J, Hajirasouliha I, Becque J, Pilakoutas K: Development of more efficient cold-formed steel channel sections in bending. *Thin-Walled Structures* 2016, 101:1-13.
173. Pan C-L, Shan M-Y: Monotonic shear tests of cold-formed steel wall frames with sheathing. *Thin-Walled Structures* 2011, 49(2):363-370.
174. 3122 N: Specification for Portland and blended cements (General and special purpose). NZS 2009.
175. C143 A: Standard Test Method for Slump of Hydraulic-Cement Concrete. ASTM International 2015.
176. C567M-14 A: Standard Test Method for Determining Density of Structural Lightweight Concrete. ASTM International 2014.
177. C495M-12 AC: Standard Test Method for Compressive Strength of Lightweight Insulating Concrete. ASTM International 2012.
178. C496M AC: Standard Test Method for Splitting Tensile Strength of Cylindrical Concrete Specimens. ASTM International 2017.
179. Vilches J: The development of novel infill materials for composite structural assemblies. Master of Philosophy thesis; Auckland University of Technology 2014.

180. AASHTO: TP 95-11 - Standard Method of Test for Surface Resistivity Indication of Concrete's Ability to Resist Chloride Ion Penetration. American Association of State and Highway Transportation Officials 2011.
181. Degen T, Sadki M, Bron E, König U, Nénert G: The HighScore suite. Powder Diffraction 2014, 29(S2):S13-S18.
182. Gu K, Jin F, Al-Tabbaa A, Shi B, Liu J: Mechanical and hydration properties of ground granulated blastfurnace slag pastes activated with MgO–CaO mixtures. Construction and Building Materials 2014, 69:101-108.
183. E1354 A: Standard Test Method for Heat and Visible Smoke Release Rates for Materials and Products Using an Oxygen Consumption Calorimeter. ASTM International 2017.
184. Nadesan MS, Dinakar P: Mix design and properties of fly ash waste lightweight aggregates in structural lightweight concrete. Case Studies in Construction Materials 2017, 7(Supplement C):336-347.
185. ACI211.2: Standard Practice for Selecting Proportions for Structural Lightweight Concrete (ACI 211.2). Materials Journal 1990, 87(6).
186. Aliakbar Sayadi TN, Charles Clifton: Feasibility of a Biopolymer as Lightweight Aggregate in Perlite Concrete. International Journal of Civil, Environmental, Structural, Construction and Architectural Engineering 2016, 10(6).
187. ACI318-14: Building Code Requirements for Structural Concrete and Commentary. American Concrete Institute 2014.
188. C330M-17a A: Standard Specification for Lightweight Aggregates for Structural Concrete. ASTM International 2017.
189. Harmathy TZ: THERMAL PROPERTIES OF CONCRETE AT ELEVATED TEMPERATURES. American Society for Testing and Materials 1970, 5(1):18.
190. Kim HK, Jeon JH, Lee HK: Workability, and mechanical, acoustic and thermal properties of lightweight aggregate concrete with a high volume of entrained air. Construction and Building Materials 2012, 29(Supplement C):193-200.
191. Silva CARd, Reis RJP, Lameiras FS, Vasconcelos WL: Carbonation-Related Microstructural Changes in Long-Term Durability Concrete. Materials Research 2002, 5:287-293.
192. Šavija B, Luković M: Carbonation of cement paste: Understanding, challenges, and opportunities. Construction and Building Materials 2016, 117(Supplement C):285-301.

193. Tasdemir C, Sengul O, Tasdemir MA: A comparative study on the thermal conductivities and mechanical properties of lightweight concretes. *Energy and Buildings* 2017, 151(Supplement C):469-475.
194. Zhang SP, Zong L: Evaluation of Relationship between Water Absorption and Durability of Concrete Materials. *Advances in Materials Science and Engineering* 2014, 2014:8.
195. Ma G, Zhang Y, Li Z: Influencing Factors on the Interface Microhardness of Lightweight Aggregate Concrete Consisting of Glazed Hollow Bead. *Advances in Materials Science and Engineering* 2015, 2015:15.
196. Sobhnamayan F, Sahebi S, Alborzi A, Ghorbani S, Shojaee NS: Effect of Different pH Values on the Compressive Strength of Calcium-Enriched Mixture Cement. *Iranian Endodontic Journal* 2015, 10(1):26-29.
197. Morandeau A, Thiéry M, Dangla P: Investigation of the carbonation mechanism of CH and C-S-H in terms of kinetics, microstructure changes and moisture properties. *Cement and Concrete Research* 2014, 56(Supplement C):153-170.
198. Sin LT, Rahmat AR, Rahman WAWA: 7 - Degradation and Stability of Poly(lactic Acid). In: *Poly(lactic Acid)*. Oxford: William Andrew Publishing; 2013: 247-299.
199. Sin LT, Rahmat AR, Rahman WAWA: 6 - Rheological Properties of Poly(lactic Acid). In: *Poly(lactic Acid)*. Oxford: William Andrew Publishing; 2013: 221-245.
200. Khaliq W, Ehsan MB: Crack healing in concrete using various bio influenced self-healing techniques. *Construction and Building Materials* 2016, 102(Part 1):349-357.
201. Bernward Hölting WGC: *HYDROGEOLOGIE*. Spektrum Akademischer Verlag 2013.
202. Li Z, Xiao L, Wei X: Determination of Concrete Setting Time Using Electrical Resistivity Measurement. *Journal of Materials in Civil Engineering* 2007, 19(5):423-427.
203. Medeiros-Junior RA, Lima MG: Electrical resistivity of unsaturated concrete using different types of cement. *Construction and Building Materials* 2016, 107(Supplement C):11-16.
204. Xiao L, Li Z: New Understanding of Cement Hydration Mechanism through Electrical Resistivity Measurement and Microstructure Investigations. *Journal of Materials in Civil Engineering* 2009, 21(8):368-373.

205. XIAO L: Interpretation of hydration process of concrete based on electrical resistivity measurement. Thesis (PhD) - Hong Kong University of Science and Technology 2007.
206. Singh S, Khan S, Khandelwal R, Chugh A, Nagar R: Performance of sustainable concrete containing granite cutting waste. *Journal of Cleaner Production* 2016, 119(Supplement C):86-98.
207. Bullard JW, Jennings HM, Livingston RA, Nonat A, Scherer GW, Schweitzer JS, Scrivener KL, Thomas JJ: Mechanisms of cement hydration. *Cement and Concrete Research* 2011, 41(12):1208-1223.
208. Kim Y-Y, Lee K-M, Bang J-W, Kwon S-J: Effect of W/C Ratio on Durability and Porosity in Cement Mortar with Constant Cement Amount. *Advances in Materials Science and Engineering* 2014, 2014:11.
209. Kong Y, Wang P, Liu S, Zhao G, Peng Y: SEM Analysis of the Interfacial Transition Zone between Cement-Glass Powder Paste and Aggregate of Mortar under Microwave Curing. *Materials* 2016, 9(9):733.
210. Shafigh P, Mahmud HB, Jumaat MZB, Ahmmad R, Bahri S: Structural lightweight aggregate concrete using two types of waste from the palm oil industry as aggregate. *Journal of Cleaner Production* 2014, 80(Supplement C):187-196.
211. Marchon D, Flatt RJ: 8 - Mechanisms of cement hydration. In: *Science and Technology of Concrete Admixtures*. Woodhead Publishing; 2016: 129-145.
212. Rajaei M, Wang D-Y, Bhattacharyya D: Combined effects of ammonium polyphosphate and talc on the fire and mechanical properties of epoxy/glass fabric composites. *Composites Part B: Engineering* 2017, 113(Supplement C):381-390.
213. Ma C, Chen B: Experimental study on the preparation and properties of a novel foamed concrete based on magnesium phosphate cement. *Construction and Building Materials* 2017, 137:160-168.
214. Jiang Z, Qian C, Chen Q: Experimental investigation on the volume stability of magnesium phosphate cement with different types of mineral admixtures. *Construction and Building Materials* 2017, 157:10-17.
215. Fang Y, Cui P, Ding Z, Zhu J-X: Properties of a magnesium phosphate cement-based fire-retardant coating containing glass fiber or glass fiber powder. *Construction and Building Materials* 2018, 162:553-560.
216. Mo KH, Yeap KW, Alengaram UJ, Jumaat MZ, Bashar II: Bond strength evaluation of palm oil fuel ash-based geopolymer normal weight and lightweight

concretes with steel reinforcement. *Journal of Adhesion Science and Technology* 2018, 32(1):19-35.

217. Halil SEZEN JPM: Bond-slip behavior of reinforced concrete members. *Proceedings of Fib Symposium on Concrete Structures in Seismic Regions* 2003:10.
218. C78M AC: Standard Test Method for Flexural Strength of Concrete (Using Simple Beam with Third-Point Loading). ASTM International 2016.

List of publications resulting from this investigation

Peer reviewed journals:

- 1) Aliakbar Sayadi, Juan V. Tapia, Thomas Neitzert, Charles Clifton (2016), Effects of expanded polystyrene (EPS) particles on fire resistance, thermal conductivity and compressive strength of foamed concrete. *Construction and Building Materials - Elsevier*, Vol. 112: p. 716-724.
- 2) Aliakbar Sayadi, Juan V. Tapia, Thomas Neitzert, Charles Clifton (2016), Strength of bearing area and locking area of galvanized strips in foamed concrete. *Construction and Building Materials - Elsevier*, Vol. 114: p. 56-65.
- 3) Aliakbar Sayadi, Juan V. Tapia, Thomas Neitzert, Charles Clifton (2016), Effectiveness of foamed concrete density and locking patterns on bond strength of galvanized strip. *Construction and Building Materials - Elsevier*, Vol. 115: p. 221-229.
- 4) Aliakbar Sayadi, Thomas Neitzert, Charles Clifton, Min Cheol Han, Karnika De Silva, Ultra-lightweight Concrete Containing Expanded Poly-lactic Acid as Lightweight Aggregate. *KSCE Journal of Civil Engineering - Springer* (0000) 00(0):1-12, Accepted.
- 5) Aliakbar Sayadi, Thomas Neitzert, Charles Clifton, Investigation on bond stress-slip behavior of concrete containing poly-lactic acid aggregate. *KSCE Journal of Civil Engineering - Springer*, Accepted.
- 6) Aliakbar Sayadi, Thomas Neitzert, Charles Clifton, Influence of Poly-lactic Acid on the Properties of Perlite Concrete. *Construction and Building Materials - Elsevier*, Accepted.

- 7) Aliakbar Sayadi, Thomas Neitzert, Charles Clifton, “Magnesium Phosphate Concrete Containing Poly-lactic Acid”. *Journal of Cleaner Production – Elsevier*, Under Review.
- 8) Aliakbar Sayadi, Thomas Neitzert, Charles Clifton, “Experimental study on flexural behaviour of cold-formed steel structures filled with bio and petro-chemical polymer lightweight aggregate concrete”. *Journal of Thin-Walled Structures – Elsevier*, Under Review.

Conference Papers:

- 1) Aliakbar Sayadi, Thomas Neitzert., Charles Clifton, Min Cheol Han (2016), Assessment of Vermiculite Concrete Containing Bio-Polymer Aggregate. *International Journal of Civil, Environmental, Structural, Construction and Architectural Engineering*, 2016. 10(6).
- 2) Aliakbar Sayadi, Thomas Neitzert, Charles Clifton (2016), Feasibility of a Biopolymer as Lightweight Aggregate in Perlite Concrete. *International Journal of Civil, Environmental, Structural, Construction and Architectural Engineering*, 2016. 10(6).
- 3) Aliakbar Sayadi, Thomas Neitzert, Charles Clifton (2018), A Comparative Investigation of the Engineering Properties of Perlite Concrete Containing Petroleum and Bio-Polymer Aggregates. *International Conference on Architecture and Civil Engineering 2018*, New Law School Annexe, Sydney, NSW, Australia, January 10-12, 2018.